# An Exploration of the Redox Behavior and Higher Oxidation States of Diruthenium Paddlewheel Complexes

by

Michael D. Roy

A dissertation submitted in partial fulfillment of

the requirements for the degree of

Doctor of Philosophy

(Chemistry)

at the

University of Wisconsin–Madison

2021

Date of final oral examination: December 21, 2021.

The dissertation is approved by the following members of the Final Oral Committee:

John F. Berry, Professor, Chemistry

Thomas C. Brunold, Professor, Chemistry

Clark R. Landis, Professor, Chemistry

Samuel Pazicni, Assisstant Professor, Chemistry

# An Exploration of the Redox Behavior and Higher Oxidation States of Diruthenium Paddlewheel Complexes

Michael D. Roy

Under the Supervision of Professor John F. Berry

University of Wisconsin–Madison

## Abstract

This work describes several novel diruthenium paddlewheel complexes including structural and spectroscopic characterization, reactivity, and electronic structure modeling. Investigation into both the oxidation state of the $Ru_2$ core and the electron donating ability of the supporting equatorial ligands provides a framework for understanding the electronic structure of proposed reactive $Ru_2$ intermediates in high oxidation states ($Ru_2^{n+}$, n = 6-8). Chapter 3 presents aminopyridinate and related ligands and explores their use as supporting ligands for metal-metal bonded complex. Chapter 4 offers an extensive investigation into the electronic structure of intermediate spin ($S$ = 1) $Ru_2^{6+}$ complex. Chapter 5 describes preliminary evidence for $Ru_2^{6+}$-ligand radical complexes. These complexes are proposed as the product of one-electron oxidation of $Ru_2^{6+}$ complexes bearing *chloro* axial ligands. Chapter 6 explores a new ligand for supporting $Ru_2$ compounds: carbolinate. Finally, Chapter 7 outlines multiple routes to prepare $Ru_2$ compounds bearing terminal oxo or hydroxo ligands: a category of compounds which has been proposed several times but has never been definitively reported in the literature.

Acknowledgements

I offer my deepest gratitude to my advisor, Professor John Berry, for his unwavering support and enthusiastic teaching and mentorship over the last 11 semesters. John's love for chemistry is only rivaled by the proverbial kid in a candy store, and this passion helped me remain motivated despite the complexities of my research and the setbacks to my research caused by a global pandemic and a massive building construction project. Thank you, John, for sticking with me over the last several years.

The entire Berry group deserves thanks as well. While I have often joked over the year that we are a band of misfits, we are also a family. I have never felt as connected to a group of people as I have in the Berry group, and every single person means a lot to me. Past members, such as Dr. Jill Chipman and Prof. Christian Wallen were supportive friends as I struggled to figure out whether graduate school was right for me. Michael "Tren" Trenerry and Trey Pankratz are some of the best office and lab partners anyone could ask for. From the scientific and philosophical discussions in the office to the delights of lab cleanup and inventory checks, my fellow Berry group members have made the last 5.5 years possible. Thank you.

Just as the Berry group has become a second family to me, the entire department community has been like an extended family. From fellow graduate student friends across the department to faculty and staff, the list of people who have helped me through this journey is immense. I cannot possibly thank everyone who deserves it. So many people have had a positive impact on my life, and I am grateful for the chance to meet every single one of you.

My family has, of course, been incredibly supportive as well. From helping me move to Madison (thanks Dad) to the occasional Sunday dinner (thanks Steven), my family has been there

whenever I need them. I love you all and want you to know that you each deserve credit for the work I have been able to accomplish in my life.

Two friends outside of chemistry need to be mentioned: Sarah Zeichner and Romina Nemaei. The two of you have been so supportive and inspirational ever since college. As you both continue your own post-secondary education now, I can only hope that my efforts to support you come close to the support you have offered me. Thank you.

Finally, my entire journey in chemistry may not have started without the mentorship and inspiration of Ray Feldwick. As a retired chemical engineer, Ray volunteered at my high school to help set up lab experiments for the AP Chemistry course. But Ray did so much more than set up equipment and prepare reagents. He engaged with high school students as equals, and he shared his passion for every facet of chemistry. If I manage to inspire a single person the way that Ray inspired me, I will consider my entire life to be a resounding success. From the bottom of my heart, thank you Mr. Feldwick.

Table of Contents

**Chapter 4**

*Electronic Structure of $Ru_2^{6+}$ Complexes with Electron-Rich Anilinopyridinate Ligands*



**Chapter 5**

*Preliminary Evidence for a $Ru_2^{6+}$-Ligand Radical Complex.*

**Chapter 6**

*Enhanced Redox Sensitivity of $Ru_2$ Complexes Supported by Carbolinate Ligands.*



**Chapter 7**

*A New Route to Diruthenium Oxo Complexes: Activation of $O_2$*

# Chapter 1

*Wisconsin Initiative for Science Literacy: Introduction for a General Audience*

I often struggle to describe my thesis work to friends and family outside of chemistry. It feels very esoteric, and I often joke that I would need a weeklong lecture series to make sense of it all. Fortunately, that is not actually the case, and my research over the past several years can be described by considering a few key concepts I employ on a regular basis. I'll start this chapter off with a brief overview of my research goals, and then illustrate how the concepts of reaction intermediates, coordination compounds, and analytical methods explain what it is that I've done over the last five years.

The overarching goal of my work has been to prepare and study a diruthenium oxo compound. We'll build up to what this means over the course of this chapter, but suffice it to say that it has been a challenging project. In fact, the project is ongoing; it started with researchers before me and will continue after I graduate. In order to make progress toward this goal, I have repeatedly broken it down into smaller, simpler steps that I can accomplish to make incremental progress toward my ultimate goal.

The reason I was tasked with studying diruthenium oxo (pronounced "ox-oh ") compounds, and the reason I still find them so interesting after five years, is because they are unproven reaction intermediates. We'll talk about reaction intermediates shortly, but the "unproven" part is really important: researchers have repeatedly *proposed* diruthenium oxo compounds, but there is almost no published *evidence* to support their existence. This is what I have been working to resolve over the course of my thesis work.

**1.1 Reaction intermediates.**

At some point in your life, whether you remember it or not, you have surely seen a chemical equation. Chemical equations are fundamental tools for chemists and other scientists to describe a chemical reaction. On one side of an arrow, we list the starting chemicals, or reactants. On the other side of the arrow, we list all of the chemicals produced by the reaction, or products. Sometimes, we put annotations above or below the arrow to indicate some of the conditions under which the reaction took place. Scheme 1.1 lists several common chemical reactions that you may have encountered.

A) $2H_2 + O_2 \longrightarrow 2H_2O$

B) $2H_2O_2 \longrightarrow 2H_2O + O_2$

C) $C_6H_{12}O_6 + 6O_2 \longrightarrow 6CO_2 + 6H_2O$

*Scheme 1.1. Everyday chemical reactions. A) The reaction of hydrogen ($H_2$) and oxygen ($O_2$) to make water. This reaction can be done by igniting hydrogen in the presence of oxygen, or in a hydrogen fuel cell to generate electricity without making carbon dioxide. B) The decomposition of hydrogen peroxide ($H_2O_2$) into water ($H_2O$) and oxygen ($O_2$), which explains why bottles of hydrogen peroxide from the drug store have an expiration date. This reaction is harnessed in classic science demonstrations like "elephant toothpaste." C) Reaction of glucose ($C_6H_{12}O_6$) and oxygen ($O_2$) to produce carbon dioxide ($CO_2$) and water ($H_2O$). Your body is doing this right now to turn food into energy.*

What a chemical equation doesn't tell you about a chemical reaction, however, is *how* it takes place. Consider the last reaction from Scheme 1.1: the combustion of glucose. If you take a sample of glucose, a white powder, and leave it in air, which is about 21% oxygen, nothing happens. But if you sprinkle that glucose into a flame, it burns, rapidly reacting with oxygen to form carbon dioxide and water. In your body, however, glucose undergoes the same *net* reaction - reacting with 6 molecules of oxygen to produce carbon dioxide, which you exhale, and water. Clearly, though, you don't have a combustion engine inside of your body. The reaction *mechanism*,

or series of individual steps along the way from reactants to products, is different. When I took biology in high school, I was forced to memorize the Krebs cycle, also known as the citric acid cycle. The Krebs cycle is just one part of the mechanism by which your body converts glucose into carbon dioxide and water, and it involves several *intermediates*, or chemicals derived from the reagents that are not yet the products, as well as several other molecules, including enzymes, which act as *catalysts* to facilitate the reaction (remember, glucose and oxygen at room temperature don't do anything on their own).

When we study a chemical reaction mechanism and the intermediates involved, we learn far more than we could from just studying the reactants and products. Different mechanisms for metabolizing glucose explain why yeast can generate alcohol when fermenting for bread or beer, but you don't become inebriated when you work out. As chemists, we seek to understand reaction mechanisms both as a fundamental pillar of knowledge, and for the practical benefits that come from such knowledge. If we know how a reaction works, perhaps we can apply that mechanism to a different set of reactants, generating new products. This is routinely done in pharmaceutical work to design and prepare new potential drugs. I also mentioned catalysts earlier, which are molecules that facilitate a chemical reaction, but are not used up in the process. Think of slicing tomatoes in your kitchen: the whole tomato is the reactant, the slices are the products, and the knife is the catalyst that makes the process happen. A huge aspect of chemistry is discovering and studying new catalysts so that we can control chemical reactions.

Often, a catalyst molecule will temporarily react with a reactant, forming an intermediate that undergoes further chemical transformations to form the product while giving back the catalyst. The diruthenium oxo compounds that I mentioned earlier are proposed intermediates in a variety of chemical reactions, often as catalytic intermediates (those intermediates formed by a catalyst).

If we can verify that diruthenium oxo compounds are indeed intermediates in these reactions, or if we can disprove that, we will significantly advance our understanding of these reaction mechanisms. With that knowledge, we can work to design new catalysts or establish new mechanisms for preparing valuable products, such as those relevant for pharmaceuticals or renewable energy. Given that the study of a single type of reaction intermediate is the focus of my entire PhD work, you might guess that it isn't as straightforward as it may seem on paper. Studying highly reactive compounds requires creativity, hard work, and a wide variety of analytical techniques. We'll learn about some of the techniques I use in my research in section 1.3.

**1.2 Coordination compounds.**

Chemists organize compounds into several different categories. Coordination compounds make up a diverse subset of molecules (discrete collections of atoms that can be written down with a formula like those in Scheme 1.1) that also contain individual metal atoms. The portions of the molecule that bind to the metal atoms are known as ligands. This motif is how you have iron in your blood; it's not little flecks of iron metal, but individual atoms incorporated as part of hemoglobin protein molecules. Most frequently, coordination compounds contain a single transition metal atom (transition metals are the ones in the big middle chunk of the periodic table, Figure 1.1).

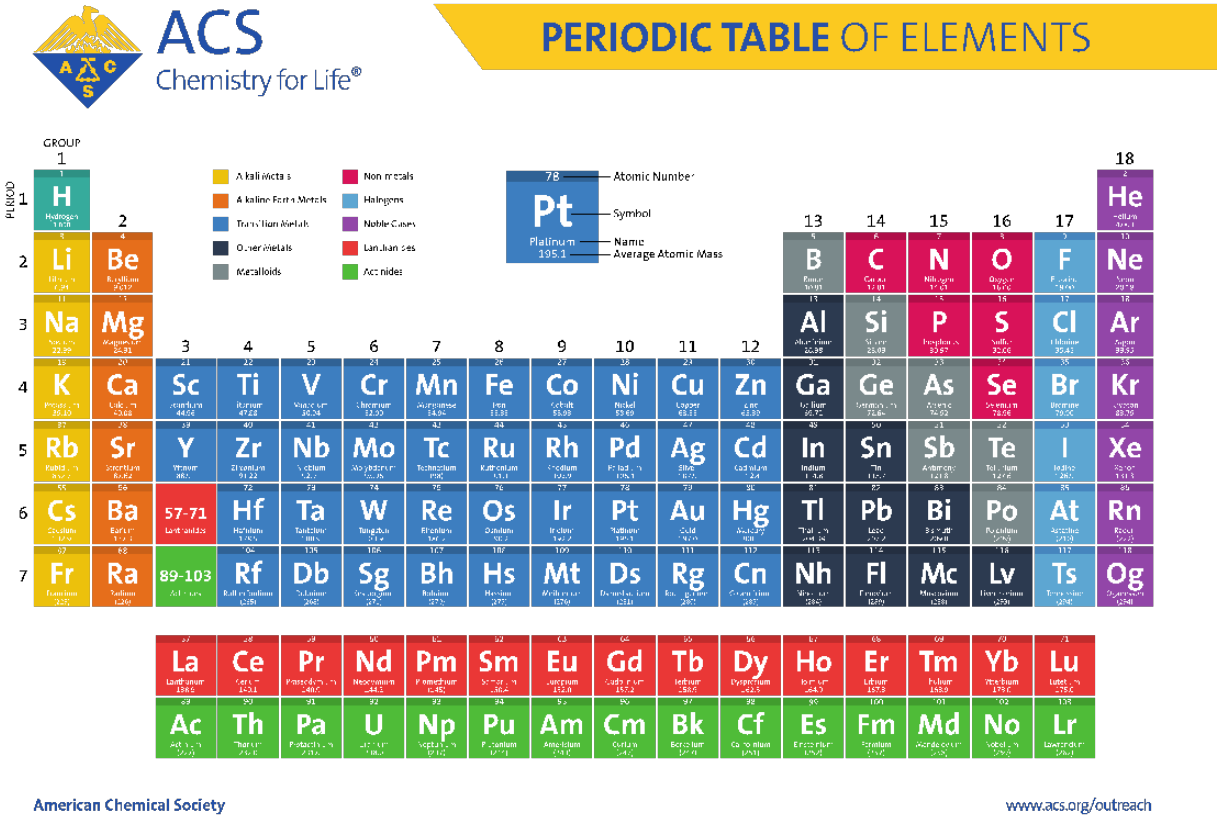


***Figure 1.1*** *The periodic table of the elements, with transition metals in dark blue. Ruthenium, the transition metal I work with, is right in the middle, in group 8, period 5. Image from the American Chemical Society, https://www.acs.org/content/acs/en/education/whatischemistry/periodictable.html accessed Nov. 23, 2011.*

The presence of a metal imparts all sorts of interesting properties on coordination compounds, and the wide variety of metals available for making coordination compounds means that this field of chemistry has an incredible list of applications in addition to the wide variety of naturally occurring coordination compounds in biology. Cisplatin, a common chemotherapy medication, is a simple coordination compound containing platinum (group 10, period 6); many extraction processes for refining metals from ores rely on the formation of coordination compounds of those metals; and a whole host of coordination compounds are employed as

catalysts to facilitate all manners of chemical reactions, from drug synthesis to plastic manufacturing.

With this definition, we can now break down what I mean when I say that I study diruthenium oxo compounds. Starting with diruthenium, this simply means two ruthenium atoms are present in the molecule. Oxo refers to oxygen, and more specifically describes an oxygen atom bound to a metal atom and nothing else. Beyond two ruthenium atoms and an oxygen atom, the compounds I study are commonly known as paddlewheel complexes due to the general shape: the two ruthenium atoms are bound together like an axle, and there are four ligands arranged like the fins of a paddleboat's paddlewheel. You can see this in Figure 1.2. With the particular ligands I use, only one side of the diruthenium axis is available to bind to another element. When the X, which is used to indicate a variety of possible ligands, is an oxygen atom, we have a diruthenium oxo paddlewheel complex.

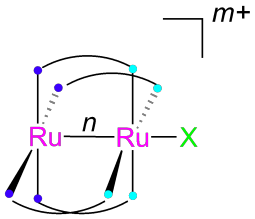


***Figure 1.2*** *Schematic drawing of a diruthenium paddlewheel complex. Imagine the axle through the Ru–Ru–X axis. The connected blue dots represent the bridging ligands, which look like the fans of a paddlewheel. My work in this thesis involves changing the charge of the complex ($m^+$), the Ru–Ru bond order (n), as well as the identity of the ligands, both X, the axial ligand, and the blue dots, which represent the equatorial ligands.*

### 1.3 Techniques I use in my research.

Trying to prepare and study reactive intermediates can be extremely difficult. Since the goal is to study something reactive, the trick is to keep it from reacting long enough to study it. While many of the compounds that I have synthesized are indefinitely stable, many others are

unstable, decomposing in minutes even when chilled with dry ice to –78 °C. Over the course of my studies, I have had the opportunity to learn and use a wide variety of fascinating instruments and techniques, and I would like to share a few of my favorites here.

**Single-Crystal X-Ray Diffraction**. I hope you are familiar with Rosalind Franklin, who was an X-ray crystallographer involved in determining the structure of DNA. In the time since Franklin's work, X-ray crystallography has come a long way. Today, analysis of the diffraction pattern of X-rays from a small crystal, often less than 1 mm in any dimension, provides enough information to determine the identity of and distance between each atom in a molecule. To achieve this, crystals must be carefully grown in the lab; the large crystals of minerals that may come to mind are actually made up of many crystals in different orientations, all growing into each other. Once high-quality single-crystals are obtained, they can be mounted inside an X-ray diffractometer. After the diffractometer is closed, the crystal is exposed to a tightly focused beam of X-ray irradiation and a digital detector records the intensity and location of diffracted X-rays around the crystal. Computer software then allows us to model this diffraction pattern, determining the identity and arrangement of the atoms that make up the crystal. The instruments available in the Department of Chemistry at UW-Madison are able to achieve length measurements of chemical bonds, which are often 1-2 Å (Å is the symbol for angstrom, a unit of distance equal to $10^{-10}$ m, or one ten-billionth of a meter), with a precision greater than 0.01 Å, or 0.000000000001 m. While this technique is excellent for many compounds, some of my research compounds are too reactive to grow crystals suitable for X-ray diffraction.

**Electron Paramagnetic Resonance (EPR) Spectroscopy.** It may surprise you to learn that individual electrons behave like little tiny bar magnets. While the explanation for this behavior is quantum mechanical in nature, the result is pretty straightforward: an individual electron acts like an exceedingly small yet powerful magnet. In most molecules, though, there is an even number of electrons and they pair up so that each electron cancels out the magnetic field of its partner electron. With coordination compounds, however, the metal atom can support one or more unpaired electrons, giving the compound magnetic behavior, known as paramagnetism. In EPR spectroscopy, we exploit these unpaired electrons by placing a paramagnetic sample in a strong magnetic field. We can then expose the sample to microwave radiation (the same as your kitchen microwave, Wi-Fi, or 5G cellular). This can cause the electron's magnetic field to flip between being aligned with the strong applied field to being aligned against it. By measuring the strength of the applied magnetic field and the frequency where the electron flips, we can learn about the number of unpaired electrons as well as the shape and distribution of the paramagnetic compound's magnetic field. Many compounds have very low sensitivity for EPR, so we run the experiments at very low temperatures (around 10 K, or –263 °C / –442 °F). This is also beneficial for extremely reactive compounds, as the low temperature prevents decomposition. Therefore, this technique is suitable for many paramagnetic compounds, whether they are stable or not.

**SQUID Magnetometry.**

Another technique for measuring paramagnetic compounds is SQUID magnetometry. SQUID is an acronym standing for Superconducting QUantum Interference Device, which ultimately just means that the device uses very low temperature (around 4 K, –269 °C, –452 °F) superconducting components to detect the magnetic field of paramagnetic materials. A typical SQUID

magnetometer is designed to operate over a wide temperature range, cooling the sample from room temperature down all the way to 2 K, just a few degrees above absolute zero. (Absolute zero is the lowest possible temperature, –459.67 °F. At absolute zero, there is no heat energy left in a material.) By measuring the magnetic properties of a sample over a wide range of temperatures and in different strengths of magnetic fields applied by the magnetometer, we can gain insight into the nature of the unpaired electrons in the compound. The biggest drawback to SQUID magnetometry, however, is that it measures the average of the entire sample, so you need a very pure sample. This makes it very difficult to collect data for reactive compounds, which may decompose as you attempt to purify them.

Since I have mentioned two methods for studying magnetism, it is important to discuss why we need multiple techniques for this. EPR generally works for coordination compounds only if they have an odd number of unpaired electrons, while SQUID magnetometry works for any number of unpaired electrons. As I mentioned above, however, EPR is more suitable for highly reactive compounds where you cannot isolate a large, pure sample for SQUID. Moreover, the specific information you can obtain from each technique is a bit different. SQUID is particularly effective for measuring properties such as coupling (when different magnetic systems, either in different parts of a molecule or between neighboring molecules interact) and zero-field splitting (a particular favorite of mine where multiple magnetic states have different energies due to the quirks of how unpaired electrons interact with each other quantum mechanically). EPR, on the other hand, can give very precise measurements of how strongly the unpaired electrons interact with a magnetic field. This is measured with a *g*-value, and how it differs from 2.0 (the value for a free electron, or an electron that is not a part of a molecule) can tell us a lot about the arrangement of all the electrons in the molecule. SQUID magnetometry can provide estimates of *g*-values, and

EPR can give approximate measures of coupling and zero-field splitting, but when possible, collecting both types of measurements allows for the most accurate description of what is going on with a compound's unpaired electrons.

**1.4 What comes next?**

Over the last five years, I have learned a wide variety of synthetic (making things), analytical (studying the things that I made), and computational (using computer models to predict measurable properties) techniques in order to address a highly specific question: are diruthenium oxo compounds actually the reactive intermediates in the reactions where they are predicted to be? While I don't have a definitive answer to this question, I have made significant advances in our understanding of this class of compound. However, it is time for me to hand that question to other researchers, as I will be taking the skills and knowledge I've accumulated at UW-Madison to Georgia Tech, where I will be working as a postdoctoral researcher for Prof. La Pierre. I will apply what I know to a new class of compounds: coordination compounds containing f-block metals (the f-block consists of the lanthanides and actinides and is often drawn below the rest of the table, Figure 1.1.). F-block coordination compounds can have fascinating magnetic and electronic properties, and I look forward to diving deep into the subject while also mentoring the PhD students who will soon be writing theses of their own.

# Chapter 2.

*Introduction, Background, and Outline*

## 2.1 The prevalence of Ru–Ru-L complexes

Since the first description of a multiple bond between Ru atoms,[1, 2] $Ru_2$ complexes have proven to be interesting for potential applications in magnetism,[3-12] materials,[13-15] molecular electronics,[16-22] and reactivity and catalysis.[23-28] Stemming from the prototypical $Ru_2(OAc)_4Cl$, the vast majority of well-characterized metal-metal bonded $Ru_2$ complexes exist in the $Ru_2^{5+}$ oxidation state.[29] The Ru–Ru bond order is readily changed via reduction to $Ru_2^{4+}$ or oxidation to $Ru_2^{6+}$, and the exact electronic structure is dependent on both the equatorial bridging ligands and the axial ligand or ligands. As a result, a wide variety of both paramagnetic and diamagnetic Ru–Ru units have been incorporated into discrete molecules,[30, 31] dimeric $Ru_2$–$Ru_2$[32] or $Ru_2$–L–$Ru_2$[16, 21] units, and even extended metal-organic frameworks[14] (see Figure 2.1 for select examples). The Berry group is interested in these compounds for both explorations of electronic structure and for applications in chemical reactivity and catalysis, with examples ranging from spontaneous $N_2$ formation via oxidation of $NH_3$[33] to C–H functionalization.[26] In the latter case, high-valent $Ru_2^{n+}$ (n = 6-8) have been routinely invoked,[14, 23, 24, 26, 27, 34] but very little evidence has been provided to confirm their intermediacy in these reactions. While the most spectacular examples, including direct crystallographic observation of a $Ru_2$ nitrido compound produced via single-crystal photolysis of the $Ru_2$ azido precursor,[25] are compelling, the general lack of evidence leaves considerable room for additional exploration.

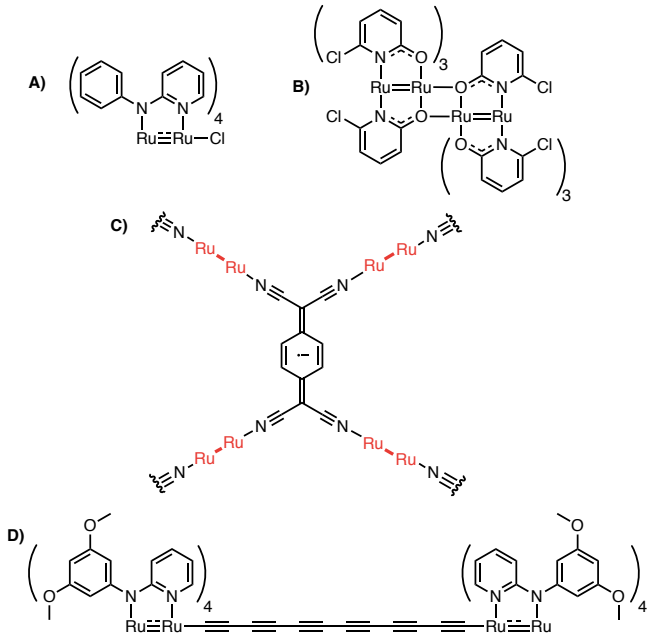


***Figure 2.1*** *Selected examples of Ru–Ru containing structures. A) discrete monomeric complex.[35] B) Dimeric $Ru_2$/$Ru_2$ unit.[32] C) Metal-organic framework incorporating $Ru_2$ units as links between nodes.[14] D) $Ru_2$–L–$Ru_2$ complex where $Ru_2$ units act as capping groups for a proposed molecular wire.[16]*

## 2.2 The M–M multiple bond

Critical to the chemistry of metal-metal bonded $Ru_2$ complexes is the nature of the Ru–Ru bond, or bonds between transition metals in general. In all the chemistry I have done over the course of this thesis, the derivation of the molecular orbital diagram for transition metal–transition metal bonds is perhaps the most satisfying. Starting from fundamentals of Ligand Field Theory taught to every undergraduate chemist, one can arrive at this fascinating and robust model via simple perturbation analysis.

To begin, we consider the 4-fold M–M paddlewheel complex to be the result of two discrete square-planar metal centers brought together. (As an aside, analysis for 3-fold paddlewheel complexes is equivalent by starting from a trigonal planar ligand field splitting.) As the two metal centers approach along the *z*-axis, we consider the overlap of the metal *d*-orbitals. The $d_{z^2}$ orbitals

overlap in a σ fashion, so we derive a σ-bonding and σ-antibonding pair with large splitting. Both the $d_{xz}$ and $d_{yz}$ orbital pairs overlap with π symmetry, giving two π-bonding and two π-antibonding orbitals with moderate splitting. Finally, the $d_{xy}$ and $d_{x^2-y^2}$ orbital pairs overlap with δ symmetry, giving rise to δ-bonding and δ-antibonding orbital pairs with only weak splitting. This process is visualized in Figure 2.2. All that remains is to count the number of *d* electrons and fill the orbitals in accordance with the *aufbau* principle. In the case of $Ru_2$, the $d_{x^2-y^2}$ orbitals are sufficiently high in energy, due to the M–L antibonding interaction, that they can be omitted from the diagram entirely. (This assumption works well for most M–M bonding systems, though important exceptions, such as $Cu_2$, are known.) A particularly interesting consequence of these interactions for $Ru_2$ is the near degeneracy of the $\pi^*$ and $\delta^*$ orbitals, which are often the frontier orbitals.[29] As a result, high spin configurations are available, despite the proclivity for second and third -row transition metals to adopt low spin configurations. In fact, quintet $Ru_2^{6+}$ complexes have even been reported by use of weak-field equatorial ligands.[36]

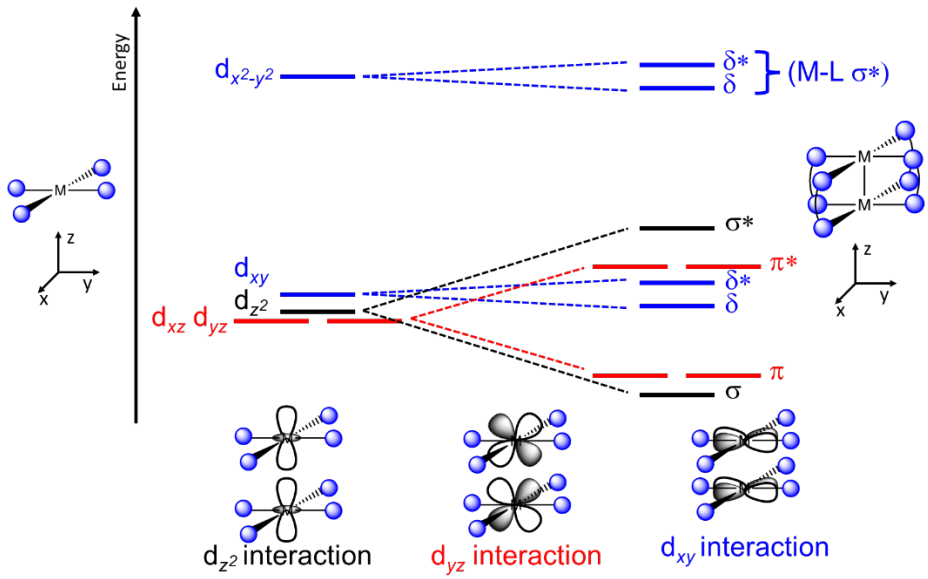


***Figure 2.2*** *Qualitative molecular orbital energy level diagram for a M–M bonded complex. σ-type interactions are presented in black, π-type in red, and δ-type in blue. Representative orbital sketches for each interaction are provided at the bottom.*

## 2.3 The supporting ligand

The exact energy difference between the frontier orbitals is determined primarily by the nature of the ligands. *p* orbitals or conjugated π systems on the binding atoms of the equatorial ligands have the correct molecular symmetry to overlap with the δ and $\delta^*$ M–M bonding orbitals (see Figure 2.3), meaning that stronger π donor ligands (e.g., N compared to O) have a more destabilizing effect on these metal-centered orbitals. The axial ligand or ligands, however, have π overlap with the π and $\pi^*$ M–M bonding orbitals, meaning that more strongly π donating ligands in the axial position will result in enhanced destabilization of the M–M π system. This allows the energy, and indeed the relative ordering, of the $\pi^*$ and $\delta^*$ orbitals, to be tuned by careful selection of equatorial and axial ligands.

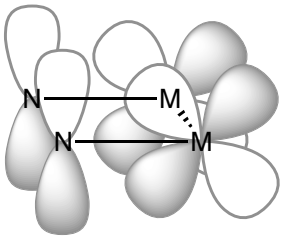


***Figure 2.3*** *Atomic orbital depiction showing the overlap of* p*-orbitals on equatorial N-atoms overlapping with the δ combination of the metal* d*-orbitals.*

The work presented here focuses on N, N-donor equatorial ligands. The strongly π basic nature of these ligands results in a particularly high energy M–M $\delta^*$ orbital.[37] In fact, the anilinopyridinate and carbolinate ligands (Figure 2.4) are so electron-rich that they actually pose unique challenges for achieving high oxidation states at $Ru_2$, namely that the highest occupied ligand orbitals are interposed among the frontier Ru-based orbitals. This is discussed extensively in Chapters 4 and 5 and is one of the key contributions from this work to the field.

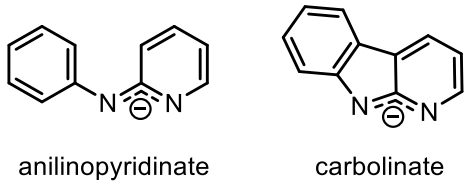


***Figure 2.4*** *Structure of anilinopyridinate and carbolinate ligands.*

## 2.4 Outline of subsequent chapters

Chapter 3[38] provides context on the type of N, N-donor ligands used in this work. This chapter takes the form of a survey of ligands based around the 2-aminopyridinate core and their use in supporting M–M bonds. The chapter begins with anilinopyridinate ligands, which are featured in Chapters 4, 5, and 7. Structurally similar ligands with different binding atoms are then discussed. Finally, extended ligands used to support complexes with three or more linearly bonded metal atoms are described.

Chapter 4 describes an extensive investigation of the electronic structure of $Ru_2^{6+}$ complexes with triplet electron configurations. This work is particularly noteworthy because of the dearth of triplet $Ru_2^{6+}$ complexes in the literature. The majority of $Ru_2^{6+}$ compounds comes from the work of Ren and coworkers. These compounds bear strongly σ-donating organometallic ligands and are therefore diamagnetic.[39] In contrast, this chapter lays a foundation from which to consider the electronic structure of highly oxidized paramagnetic $Ru_2$ compounds.

Chapter 5 picks up where Chapter 4 leaves off. As discussed above, ligand-centered orbitals of anilinopyridinate ligands are interposed with the metal-based frontier orbitals. In fact, the $Ru_2^{6+}$ complexes featured in Chapter 4 are all expected to have ligand-based highest occupied molecular orbitals. Chapter 5 therefore explores the attempted one-electron oxidation of these compounds and the description of the resulting complexes as $Ru_2^{6+}$-ligand radical systems.

Chapter 6 features a quite unexplored ligand: carbolinate. While the proteo α-carboline has been known for nearly a century, there are only two published works describing carbolinate as a ligand, and only one in which it supports a M–M bond. This chapter begins with predictions from density functional theory (DFT) about the enhanced redox sensitivity of these compounds due to the extended conjugation of the ligand. Preliminary synthetic efforts are then outlined. While incomplete, this work is quite promising for expanding the frontiers of $Ru_2$ chemistry.

Chapter 7 hearkens back to the progenitor of this entire thesis: the desire to observe, characterize, and even isolate a terminal $Ru_2$ oxo complex. Earlier efforts focused on the use of an O-atom transfer agent, such as *m*CPBA (*meta*-chloroperoxybenzoic acid) or PhIO (iodosylbenzene) to prepare an $Ru_2^{7+}$ oxo. While EPR spectroscopy suggests successful formation of an $Ru_2^{7+}$ compound, said compound is so reactive that a more comprehensive study has not been possible. Using the insights gained in the previous chapters, Chapter 7 discusses three potential routes to the successful isolation of a terminal $Ru_2$ oxo in either the $Ru_2^{6+}$ or $Ru_2^{7+}$ oxidation state. Most interesting of these is the direct reaction of an axially accessible $Ru_2^{5+}$ compound with $O_2$, with preliminary work suggesting successful cleavage of the O=O bond and H-atom transfer from the solvent to form a $Ru_2^{6+}$ hydroxo compound.

**2.5 References**

1. Stephenson, T. A.; Wilkinson, G., New ruthenium carboxylate complexes. *J. Inorg. Nuc. Chem.* **1966,** *28* (10), 2285-2291.

2. Bennett, M. J.; Caulton, K. G.; Cotton, F. A., Structure of tetra-n-butyratodiruthenium chloride, a compound with a strong metal-metal bond. *Inorg. Chem.* **1969,** *8* (1), 1-6.

3. Chiarella, G. M.; Cotton, F. A.; Murillo, C. A.; Ventura, K.; Villagrán, D.; Wang, X., Manipulating Magnetism: $Ru_2^{5+}$ Paddlewheels Devoid of Axial Interactions. *J. Am. Chem. Soc.* **2014,** *136* (27), 9580-9589.

4. Mikuriya, M.; Yoshioka, D.; Handa, M., Magnetic interactions in one-, two-, and three-dimensional assemblies of dinuclear ruthenium carboxylates. *Coord. Chem. Rev.* **2006,** *250* (17), 2194-2211.

5. Miyasaka, H.; Clérac, R.; Campos-Fernández, C. S.; Dunbar, K. R., The first crystal structure of a one-dimensional chain of linked $Ru^{II}$=$Ru^{II}$ units. *J. Chem. Soc. Dalton Trans.* **2001,** (6), 858-861.

6. O'Neal, K. R.; Liu, Z.; Miller, J. S.; Fishman, R. S.; Musfeldt, J. L., Pressure-driven high-to-low spin transition in the bimetallic quantum magnet $[Ru_2(O_2CMe)_4][Cr(CN)_6]$. *Phys. Rev. B* **2014,** *90* (10), 104301.

7. Opperwall, S. R.; Liu, B.; Pilo, A. L.; Cao, Z.; Fanwick, P. E.; Ren, T., Synthesis and characterization of $Ru_2(\eta^2$-D*m*AniF$)_2(\mu$-D*m*AniF$)_2(\mu$-OAc$)(\mu$-O). *Polyhedron* **2016,** *103*, 126-130.

8. Raghavan, A.; Yuan, F.; Ren, T., Drastic Tuning of the Electronic Structures of Diruthenium Aryl Complexes by Isoelectronic Axial Ligands. *Inorg. Chem.* **2020,** *59* (13), 8663-8666.

9. Su, S.-D.; Zhu, X.-Q.; Wen, Y.-H.; Zhang, L.-T.; Yang, Y.-Y.; Lin, C.-S.; Wu, X.-T.; Sheng, T.-L., A Diruthenium-Based Mixed Spin Complex $Ru_2^{5+}$(*S*=1/2)-CN-$Ru_2^{5+}$(*S*=3/2). *Angew. Chem. Int. Ed.* **2019,** *58* (43), 15344-15348.

10. Uemura, K.; Uesugi, N.; Matsuyama, A.; Ebihara, M.; Yoshikawa, H.; Awaga, K., Integration of Paramagnetic Diruthenium Complexes into an Extended Chain by Heterometallic Metal–Metal Bonds with Diplatinum Complexes. *Inorg. Chem.* **2016,** *55* (14), 7003-7011.

11. Yang, B.-B.; Feng, L.-N.; Fan, X.-M.; Zhang, K.-X.; Yang, J.-H.; Liu, B., Towards a new type of heterometallic system based on a paddle-wheel $Ru_2$ dimer: first results derived from the use of a high spin diruthenium(III,III) building block. *Inorg. Chem. Front.* **2017,** *4* (6), 1061-1065.

12. Zhang, J.; Kosaka, W.; Sugimoto, K.; Miyasaka, H., Magnetic Sponge Behavior via Electronic State Modulations. *J. Am. Chem. Soc.* **2018,** *140* (16), 5644-5652.

13. Miyasaka, H., Control of Charge Transfer in Donor/Acceptor Metal–Organic Frameworks. *Acc. Chem. Res.* **2013,** *46* (2), 248-257.

14. Miyasaka, H.; Motokawa, N.; Matsunaga, S.; Yamashita, M.; Sugimoto, K.; Mori, T.; Toyota, N.; Dunbar, K. R., Control of Charge Transfer in a Series of $Ru_2^{II,II}$/TCNQ Two-Dimensional Networks by Tuning the Electron Affinity of TCNQ Units: A Route to Synergistic Magnetic/Conducting Materials. *J. Am. Chem. Soc.* **2010,** *132* (5), 1532-1544.

15. Wang, C.-H.; Gao, W.-Y.; Powers, D. C., Measuring and Modulating Substrate Confinement during Nitrogen-Atom Transfer in a $Ru_2$-Based Metal-Organic Framework. *J. Am. Chem. Soc.* **2019,** *141* (49), 19203-19207.

16. Cao, Z.; Xi, B.; Jodoin, D. S.; Zhang, L.; Cummings, S. P.; Gao, Y.; Tyler, S. F.; Fanwick, P. E.; Crutchley, R. J.; Ren, T., Diruthenium–Polyyn-diyl–Diruthenium Wires: Electronic Coupling in the Long Distance Regime. *J. Am. Chem. Soc.* **2014,** *136* (34), 12174-12183.

17. Delgado-Martínez, P.; González-Prieto, R.; Gómez-García, C. J.; Jiménez-Aparicio, R.; Priego, J. L.; Torres, M. R., Structural, magnetic and electrical properties of one-dimensional tetraamidatodiruthenium compounds. *Dalton Trans.* **2014,** *43* (8), 3227-3237.

18. Jiang, K.; Pookpanratana, S. J.; Ren, T.; Natoli, S. N.; Sperling, B. A.; Robertson, J.; Richter, C. A.; Yu, S.; Li, Q., Nonvolatile memory based on redox-active ruthenium molecular monolayers. *Appl. Phys. Lett.* **2019,** *115* (16), 162102.

19. Pookpanratana, S.; Zhu, H.; Bittle, E. G.; Natoli, S. N.; Ren, T.; Richter, C. A.; Li, Q.; Hacker, C. A., Non-volatile memory devices with redox-active diruthenium molecular compound. *J. Phys. Condens. Matter* **2016,** *28* (9), 094009.

20. Ren, T., Diruthenium *σ*-Alkynyl Compounds: A New Class of Conjugated Organometallics. *Organometallics* **2005,** *24* (21), 4854-4870.

21. Ren, T.; Zou, G.; Alvarez, J. C., Facile electronic communication between bimetallic termini bridged by elemental carbon chains. *Chem. Commun.* **2000,** (13), 1197-1198.

22. Ying, J.-W.; Cao, Z.; Campana, C.; Song, Y.; Zuo, J.-L.; Tyler, S. F.; Ren, T., Linear trimers of diruthenium linked by polyyndiyl or phenylenediethynyl bridges: A family of unique electronic wires. *Polyhedron* **2015,** *86*, 76-80.

23. Corcos, A. R.; Long, A. K. M.; Guzei, I. A.; Berry, J. F., A Synthetic Cycle for Nitrogen Atom Transfer Featuring a Diruthenium Nitride Intermediate. *Eur. J. Inorg. Chem.* **2013,** *2013* (22-23), 3808-3811.

24. Corcos, A. R.; Pap, J. S.; Yang, T.; Berry, J. F., A Synthetic Oxygen Atom Transfer Photocycle from a Diruthenium Oxyanion Complex. *J. Am. Chem. Soc.* **2016,** *138* (31), 10032-10040.

25. Das, A.; Reibenspies, J. H.; Chen, Y.-S.; Powers, D. C., Direct Characterization of a Reactive Lattice-Confined $Ru_2$ Nitride by Photocrystallography. *J. Am. Chem. Soc.* **2017,** *139* (8), 2912-2915.

26. Harvey, M. E.; Musaev, D. G.; Du Bois, J., A Diruthenium Catalyst for Selective, Intramolecular Allylic C–H Amination: Reaction Development and Mechanistic Insight Gained through Experiment and Theory. *J. Am. Chem. Soc.* **2011,** *133* (43), 17207-17216.

27. Musch Long, A. K.; Timmer, G. H.; Pap, J. S.; Snyder, J. L.; Yu, R. P.; Berry, J. F., Aryl C–H Amination by Diruthenium Nitrides in the Solid State and in Solution at Room Temperature: Experimental and Computational Study of the Reaction Mechanism. *J. Am. Chem. Soc.* **2011,** *133* (33), 13138-13150.

28. Musch Long, A. K.; Yu, R. P.; Timmer, G. H.; Berry, J. F., Aryl C−H Bond Amination by an Electrophilic Diruthenium Nitride. *J. Am. Chem. Soc.* **2010,** *132* (35), 12228-12230.

29. Angaridis, P., Ruthenium Compounds. In *Multiple Bonds Between Metal Atoms*, Cotton, F. A.; Murillo, C. A.; Walton, R. A., Eds. Springer: Boston, MA, 2005.

30. Bear, J. L.; Li, Y.; Han, B.; Kadish, K. M., Synthesis, Molecular Structure, and Electrochemistry of a Paramagnetic Diruthenium(III) Complex. Characterization of $Ru_2(hpp)_4Cl_2$, Where hpp Is the 1,3,4,6,7,8- Hexahydro-2H-pyrimido[1,2-a]pyrimidinate Ion. *Inorg. Chem.* **1996,** *35* (5), 1395-1398.

31. Corcos, A. R.; Berry, J. F., Anilinopyridinate-supported $Ru_2^{x+}$ (x = 5 or 6) paddlewheel complexes with labile axial ligands. *Dalton Trans.* **2017,** *46* (17), 5532-5539.

32. Brown, T. R.; Dolinar, B. S.; Hillard, E. A.; Clérac, R.; Berry, J. F., Electronic Structure of $Ru_2$(II,II) Oxypyridinates: Synthetic, Structural, and Theoretical Insights into Axial Ligand Binding. *Inorg. Chem.* **2015,** *54* (17), 8571-8589.

33. Trenerry, M. J.; Wallen, C. M.; Brown, T. R.; Park, S. V.; Berry, J. F., Spontaneous $N_2$ formation by a diruthenium complex enables electrocatalytic and aerobic oxidation of ammonia. *Nature Chem.* **2021,** *13* (12), 1221-1227.

34. Goberna-Ferrón, S.; Peña, B.; Soriano-López, J.; Carbó, J. J.; Zhao, H.; Poblet, J. M.; Dunbar, K. R.; Galán-Mascarós, J. R., A fast metal–metal bonded water oxidation catalyst. *J. Catal.* **2014,** *315*, 25-32.

35. Chakravarty, A. R.; Cotton, F. A.; Tocher, D. A., Syntheses, molecular structures, and properties of two polar diruthenium(II,III) complexes of 2-hydroxypyridine and 2-anilinopyridine. *Inorg. Chem.* **1985,** *24* (2), 172-177.

36. Liu, B.; Ding, T.; Hua, W.-J.; Liu, X.-M.; Hu, H.-M.; Li, S.-H.; Zheng, L.-M., Diruthenium(III,III) diphosphonate with a spin ground state $S = 2$. *Dalton Trans.* **2013,** *42* (10), 3429-3433.

37. Corcos, A. R.; Roy, M. D.; Killian, M. M.; Dillon, S.; Brunold, T. C.; Berry, J. F., Electronic Structure of Anilinopyridinate-Supported $Ru_2^{5+}$ Paddlewheel Compounds. *Inorg. Chem.* **2017,** *56* (23), 14662-14670.

38. Berry, J. F.; Roy, M., 2-Aminopyridine and Related Ligands to Support Metal-Metal Bonded Compounds. In *Comprehensive Coordination Chemistry III*, Constable, E. C.; Parkin, G.; Que Jr, L., Eds. Elsevier: Oxford, 2021; pp 406-427.

39. Raghavan, A.; Ren, T., Bisaryl Diruthenium(III) Paddlewheel Complexes: Synthesis and Characterization. *Organometallics* **2019,** *38* (19), 3888-3896.

# Chapter 3

*2-Aminopyridine and Related Ligands to Support Metal-Metal Bonded Compounds*

This chapter has been published:

Reprinted with permission from Berry, J. F.; Roy, M. D, 2-Aminopyridine and Related Ligands to Support Metal-Metal Bonded Compounds. In *Comprehensive Coordination Chemistry III*, Constable, E. C.; Parkin, G.; Que Jr, L., Eds. Elsevier: Oxford, 2021; pp 406-427.

## 3.1 Abstract

Compounds derived from 2-aminopyridine are versatile ligands for supporting metal-metal bonded complexes. Prominent examples that support bimetallic paddlewheel complexes include 2-anilinopyridines, 2-pyridones, and 2-mercaptopyridines. Trimetallic complexes are well known with dipyridylamine ligands, and extended polypyridylamine ligands and naphthyridine- and pyridine-derivative -containing ligands are able to support metal-metal bonded compounds with up to 11 metal atoms. This chapter discusses creative advances in the use of these ligand classes to support metal-metal bonded compounds since 2003.

## 3.2 Introduction

Derivatives of 2-aminopyridine (Hampy, Figure 3.1) are exceptionally versatile ligands for supporting metal-metal bonded compounds. Deprotonation at the $NH_2$ group to form the ampy anion allows for the two N atoms to bind to two metal atoms with a three-atom N–C–N bridge. An arrangement of up to four ampy ligands around two metals is possible, as in the tetragonal paddlewheel structure shown at the top right of Figure 3.1. Bimetallic tetragonal paddlewheel compounds are known with metal-metal bond orders ranging from zero to four,[1] and related compounds having fewer bridging ligands can reach a metal-metal bond order of five.[2] A key

feature of the ampy ligand is the π delocalization in the N–C–N bridge via the N and C *p* orbitals that are normal to the ligand plane. There are many classes of ligands with three-atom π systems that also support metal-metal bonded compounds. Notable are carboxylate ligands (O–C–O), carboxamidates (O–C–N), and formamidinates (N–C–N).[1] In this chapter, we focus on ligands in which one N atom and the central C atom of the three-atom bridge are part of a pyridine ring, and thus display π conjugation that extends beyond the three-atom bridge. The incorporation of the pyridine ring into the π system increases the π-donating character of the ligands, as exemplified by the ~ 200 mV cathodic shift in reduction potentials between $Ru_2$ complexes supported by N,N'-diphenylformamidinate (DPhF) vs. anilinopyridinate (ap) ligands (Table 1).

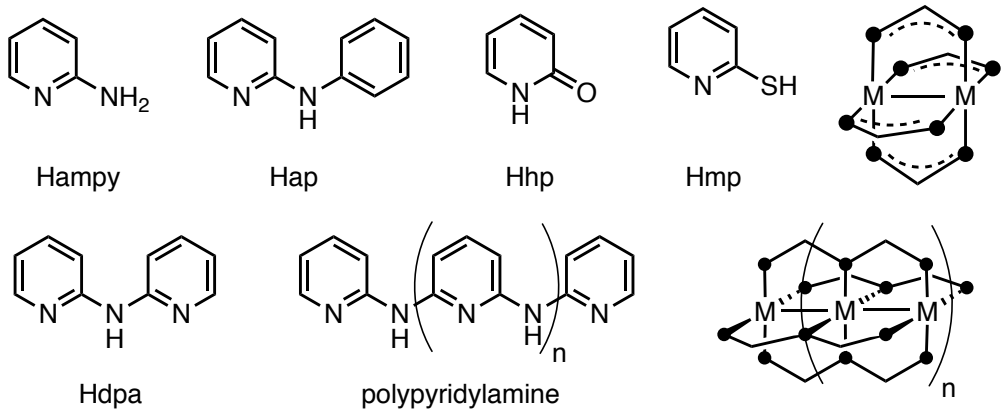


*Figure 3.1 Types of ligands discussed in this chapter. Top: Ligands that support discrete bimetallic structures. Bottom: Ligands that support chains of three or more metal atoms.*

| Compound: | $Ru_2^{4+/5+}$ (V vs. SCE in $CH_2Cl_2$) | $Ru_2^{5+/6+}$ (V vs. SCE in $CH_2Cl_2$) | Ref. |
|---|---|---|---|
| 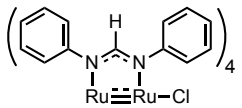 | –0.64 | 0.54 | 3 |
| 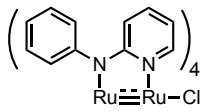 | –0.86 | 0.37 | 4 |

*Table 3.1 Reduction and Oxidation Potentials for $Ru_2(DPhF)_4Cl$ and $Ru_2(ap)_4Cl$.*

The ligands discussed here fall into two major classes: those that support bimetallic complexes, and those that support chains of three or more metal atoms. The first class using the ligands shown in the top of Figure 3.1 contain the archetypical Hampy ligand, though this un-derivatized ligand itself is seldom utilized. More commonly used are anilinopyridine and its derivatives, and derivatives of Hampy in which the $–NH_2$ group is substituted for either an –OH group (2-hydroxypyridine, Hhp, which is more stable in the 2-pyridone tautomer shown in Chart 3.1), or an –SH group (2-mercaptopyridine, Hmp).

The ligand 2,2'-dipyridylamine (Hdpa) is the prototype ligand for the class of metal-metal bonded compounds called *extended metal atom chains* (EMACs). Upon deprotonation of the NH group, the dpa ligand is able to support trimetallic compounds in a linear array, extending the paddlewheel structure laterally along the metal-metal axis. As demonstrated by the polypyridylamine structure shown in Chart 3.1, this ligand-design concept can be extended potentially ad infinitum, as synthetic methods to access the ligands allow. Solubility is another important challenge that has limited structural characterization of very long EMACs. To date, the largest complex that has been crystallographically characterized contains a linear chain of eleven metal atoms.[5]

The purpose of this chapter is to highlight the creative use of 2-aminopyridine derivatives in the coordination chemistry of metal-metal bonded compounds since ca. 2003, with special focus on ligand design. We discuss first the ligands that support bimetallic structures, followed by the ligands that support the larger EMAC structures.

### 3.3 2-Anilinopyridine Ligands for Bimetallic Complexes

2-Anilinopyridinate ligands have been employed to support metal-metal bonded compounds for a wide variety of metals. While Rh,[6-8] V,[9] Mo,[10] and W,[10] have received considerable attention before 2003, this chapter focuses on more recent developments involving ap ligands that support bimetallic complexes. In the past two decades, the majority of this work has focused on Ru and Cr, with additional efforts involving Re, Os, Pd, and several first row transition metals. This section describes these advances in greater detail.

A major feature of ap ligands is the facile synthesis of substituted derivatives from the reaction of the corresponding aniline with 2-bromopyridine (Scheme 3.1). Nucleophilic aromatic substitution occurs readily at elevated temperatures without solvent, affording the desired 2-anilinopyridine in high yield and purity. This modular ligand design allows for the ability to tune solubility[11] as well as electronic[12, 13] and steric[14, 15] properties, making ap ligands robust scaffolds for a variety of metal-metal bonded compounds.

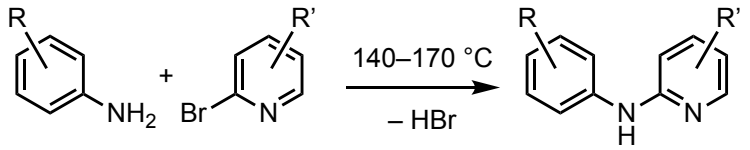


*Scheme 3.1 Synthesis of substituted 2-anilinopyridine ligands. Two equivalents of the aniline are frequently used in the reaction, with chromatographic or crystallographic separation of the product from residual aniline.*

The most common motif for metal-metal bonded compounds supported by ap ligands is the $M_2L_4$ paddlewheel compound. Due to the unsymmetric nature of the two ligand N atoms, multiple geometric isomers about a given $M_2$ core are possible. Of the four possible isomers (Figure 3.2), the (4,0) and (3,1) isomers are by far the most common for ap ligands.

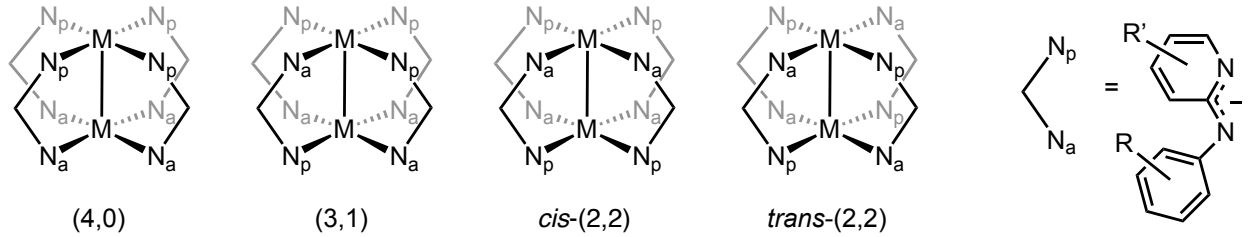


*Figure 3.2 Geometric isomers of $M_2L_4$ paddlewheel complexes with ap ligands.*

### *3.3.1 Paddlewheel Complexes with 4 Equatorial Ligands*

Paddlewheel complexes with ap ligands are most numerous with a diruthenium core. The mixed-valent diruthenium tetraacetate chloride, $Ru_2(OAc)_4Cl$, serves as the precursor for all such compounds, and the most common oxidation states are $Ru_2^{5+}$ and $Ru_2^{6+}$.

#### *3.3.1.1 $Ru_2$ Compounds with the (4,0) Arrangement of Ligands*

Synthesis of $Ru_2(ap)_4$ compounds is generally performed in one of two ways: a melt reaction or a Soxhlet reaction. In the case of the prototypical $Ru_2(ap)_4Cl$, first reported by Cotton and coworkers in 1985, $Ru_2(OAc)_4Cl$ is heated in a large excess of molten Hap. Following the reaction, excess ligand is removed by vacuum sublimation.[16] Alternatively, $Ru_2(OAc)_4Cl$ and the Hap ligand are heated to reflux, frequently in toluene, with an excess of LiCl present, and a Soxhlet apparatus filled with $K_2CO_3$ is used to remove the evolved acetic acid (this technique was originally employed by Doyle and coworkers for the synthesis of dirhodium carboxamidate complexes).[17, 18] It is hypothesized that the excess chloride present in the reaction mixture prevents the axial chloride from dissociating from the $Ru_2$ core, and the steric influence of the axial chloride may help impose the (4,0) geometry in the product. With either the unsubstituted anilinopyridine or various substituted ap ligands, the resulting $Ru_2(Xap)_4Cl$ complex serves as a robust core for further chemistry at the axial position. Using silver or thallium salt metathesis, the Berry group has prepared a variety of complexes bearing labile axial ligands, rather than strongly bound chloride.[19] The Ren group has demonstrated extensively the ability to install selectively one or two

alkynyl groups to the $Ru_2$ core using alkynyl-lithium reagents.[20-23] Two $Ru_2(ap)_4$ units have also been bridged by polyyn-diyl ligands with as many as 12 carbon atoms between the $Ru_2$ termini (Figure 3.3).[24] Extensive studies have been conducted on the electronic structure of these compounds, from the bimetallic[25] to the bridged tetrametallic complexes with various electronic and geometric bridging groups.[24, 26, 27]

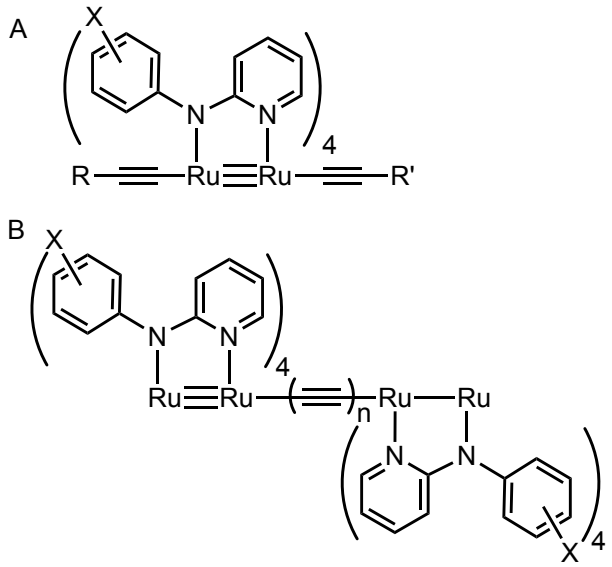


*Figure 3.3 Dialkynyl (A) and alkynyl-bridged (B) compounds from Ren and coworkers.*

$Ru_2(ap)_4X$ complexes can be readily oxidized to the $Ru_2^{6+}$ state. While treatment with one equivalent of a silver salt results in axial ligand metathesis, an excess of silver in $CH_2Cl_2$ or THF results in rapid oxidation to $Ru_2^{6+}$.[19, 28] Due to the strong electron-donating nature of the alkynyl ligands, the dialkynyl complexes prepared by Ren and coworkers are isolated in the $Ru_2^{6+}$ state after exposure to oxygen.[23, 29, 30]

In contrast to the oxidative chemistry examined by the Ren group, Bear, Kadish, and coworkers have studied reductive chemistry of $Ru_2(Xap)_4$ compounds under a CO atmosphere. While $Ru_2(Xap)_4Cl$ compounds were found not to bind CO in the axial position, irreversible electrochemical reduction to $Ru_2(Xap)_4$ results in binding of one axial CO ligand, and subsequent

irreversible electrochemical reduction to $[Ru_2(ap)_4(CO)]^-$ allows for a second axial CO ligand to coordinate. This trend is observed across 11 $Ru_2$ compounds, 6 (4,0) isomers and 5 (3,1) isomers, as summarized in Scheme 3.2.[31]

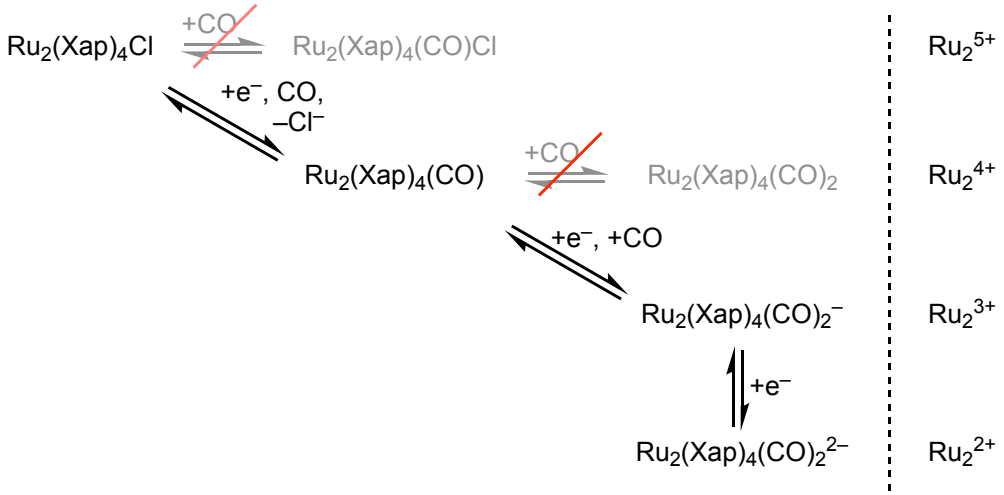


*Scheme 3.2 Electrochemical reduction and binding of CO observed for $Ru_2(Xap)_4$ compounds.*

*3.3.1.2 $Ru_2$ Compounds with the (3,1) Arrangement of Ligands.*

While (4,0) isomers are the most frequently studied, the (3,1) isomers are also relevant. In an investigation of anilinomethylpyridine ligands, Bear, Kadish, and coworkers found that 2-anilino-4-methylpyridinate (amp) binds selectively in a (3,1) geometry when $Ru_2(amp)_4Cl$ is prepared both by melt and Soxhlet reaction. Interestingly, reaction of $Ru_2(OAc)_4Cl$ with 2-anilino-6-methylpyridine resulted in a monoruthenium complex, again regardless of synthetic method.[14] Bear and coworkers also discovered that certain compounds can interconvert between (4,0) and (3,1) upon metathesis of the axial ligand. It was found that $Ru_2(ap)_4Cl$, which had previously only been observed as the (4,0) isomer, converts to the (3,1) isomer upon ligation with two 4-ethynyl pyridine ligands and oxidation with air at ambient temperature. Conversely, (3,1) $Ru_2(F_3ap)_4Cl$ ($F_3ap$ = 2-(2, 4, 6-trifluoroanilino)pyridinate) converts to the (4,0) isomer upon treatment with a large excess of tetrabutylammonium chloride at ambient temperature.[32] This observation lends

support to the hypothesis that excess chloride favors a (4,0) isomer during synthesis. Given the general difficulty of predicting and controlling the ligand arrangement in these complexes, procedures for post-synthetic isomerization are particularly valuable.

*3.3.1.3 Heteroleptic $Ru_2L_nL'_{4-n}$ Compounds*

A variety of paddlewheel complexes are known with a combination of two different bridging ligands. With the 2-(2-fluoroanilino)pyridine, Bear, Kadish, and coworkers were able to isolate $Ru_2(OAc)_n(Fap)_{4-n}Cl$ compounds with n = 0–3 from a single reaction in refluxing methanol. Increased reaction time resulted in greater quantities of $Ru_2(Fap)_4Cl$ and $Ru_2(OAc)(Fap)_3Cl$,[33] the former having been previously prepared by melt reaction.[34] With the ligand 2,4,6-$(CH_3)_3$ap, Bear, Kadish, and coworkers were able to isolate $Ru_2(OAc)(2,4,6\text{-}(CH_3)ap)_3Cl$ from a melt reaction.[35] This product is notable for two reasons: first, it is a rare example of only partial substitution of the original acetate ligands in a melt reaction where tetrasubstitution is expected, and second, it was the first compound of the type $Ru_2(OAc)L_3$ with a (2,1) arrangement of L, all previously characterized compounds having the (3,0) arrangement.

In a rather different manner, Bear, Kadish, and coworkers observed ligand oxidation upon reaction of $Ru_2(F_3ap)_4Cl$ with NaSCN in THF. With freshly distilled THF, the reaction proceeded as expected, with only substitution of the axial chloro ligand for NCS. However, when using THF distilled one day prior to the reaction, oxidation of an equatorial ligand was observed, resulting in the $Ru_2^{6+}$ compound $Ru_2(F_3ap)_3(F_2Oap)NCS$ ($F_2Oap$ = 2-oxo-4,6-difluoropyridinate), with the oxygen atom of $F_2Oap$ binding to the axial site opposite the isothiocyanate ligand (Figure 3.4).[36]

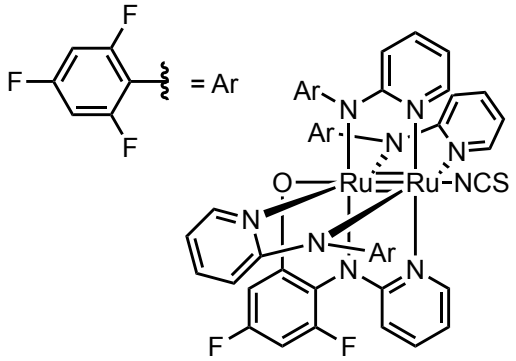


*Figure 3.4 Molecular structure of $Ru_2(F_3ap)_3(F_2Oap)NCS$.*

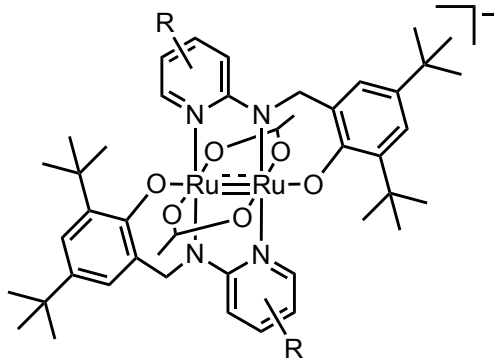


*Figure 3.5 Molecular structure of $Ru_2(OAc)_2$(t-Busal-R'Py)$_2^-$.*

The ligand Rsalpy, employed by Miyasaka and coworkers, supports heteroleptic $Ru_2$ paddlewheel complexes, as shown in Figure 3.5. When fully deprotonated, this ligand binds in a *trans*-(1,1) arrangement, with a phenolic O atom serving as an axial ligand to each Ru. Two bridging acetate ligands are also present. [37]

*3.3.1.4 Non-$Ru_2$ Paddlewheel-TypeCompounds (Re, Os)*

Despite the prevalence of $Ru_2(ap)_4$ compounds, other metals have been found to form paddlewheel complexes supported by ap ligands. Osmium, as a congener of Ru, provides a natural extension of the rich chemistry of $Ru_2(ap)_4$ compounds. Indeed, the Ren group prepared $Os_2(ap)_4Cl_2$ from $Os_2(OAc)_4Cl_2$ using the same Soxhlet reaction technique employed in the Ru chemistry. Interestingly, different crystallization solvents selectively produced different isomers: $CH_3OH/CH_2Cl_2$ yielding the *cis*-(2,2) isomer and hexanes/$CH_2Cl_2$ yielding the (3,1) isomer. Powder X-ray diffraction and NMR studies indicate the presence of both isomers in solution, with the same behavior noted for the bis-alkynyl analogs prepared by axial ligand metathesis with $LiC_2Ph$.[38]

The Ren group also obtained a variety of isomers when exploring the chemistry of Re with ap ligands. From melt reactions of $Re_2(OAc)_4Cl_2$ with Xap ligands, $Re_2(ap)_4Cl_2$ was isolated as a *trans*-(2,2) isomer; $Re_2(3,5\text{-}(CH_3)_2ap)_4Cl_2$, and $Re_2(3\text{-}Clap)_4Cl_2$ were isolated as *cis*-(2,2) isomers, and $Re_2(3,5\text{-}Cl_2ap)_4Cl_2$ was isolated as a 3,1 isomer. $Re_2(3\text{-}(OCH_3)ap)_4Cl_2$ was also isolated, though characterization sufficient to determine the molecular structure was not reported. While the electrochemical potentials of the five compounds correlate well with the Hammett parameters of

the aniline substituents, there is no apparent correlation between the steric or electronic properties of the ligand and the geometry of the complex.[39]

## 3.4 Non-paddlewheel Complexes with ap Ligands

### *3.4.1 Bulky Ligands and the Cr-Cr Quintuple Bond*

Anilinopyridine ligands with bulky substitution at the 6 position are particularly noteworthy. In 2006, Kempe and coworkers reported a $Pd_2^{2+}$ compound with only two ap-type ligands bridging the metal centers.[40] While a third neutral Hap ligand capped the axial site on one Pd atom, the steric bulk of the ligand prevented additional bridging ligands from supporting the metal-metal bond. An even bulkier ligand, 2-(2',6'-diisopropylanilino)-6-(2",6"-dimethylphenyl)-pyridine, Hdadp, was prepared by Grignard reaction of 2,6-dimethylphenylmagnesium bromide with 2,6-dibromopyridine to afford the functionalized pyridine, followed by Buchwald-Hartwig Pd-catalyzed amination with 2,6-diisopropylaniline to afford the neutral ligand.[41] The dadp ligand was used in 2008 to support a digonal $Cr_2^{2+}$ quintuple-bonded complex.[15]

The preparation of the Cr≣Cr compound differs significantly from the preparation of the previously discussed paddlewheel compounds. Deprotonation of Hdadp followed by metallation results in either a monomeric species $(dadp)Cr(thf)_2(Cl)_2$ from $CrCl_3(THF)_3$ or a bis-μ-Cl dimer $[(dadp)Cr(thf)Cl]_2$ from $CrCl_2$. The metal-metal bond is then formed in either case by reductive coupling with $KC_8$ to afford $Cr_2(dadp)_2$ (Scheme 3.3).

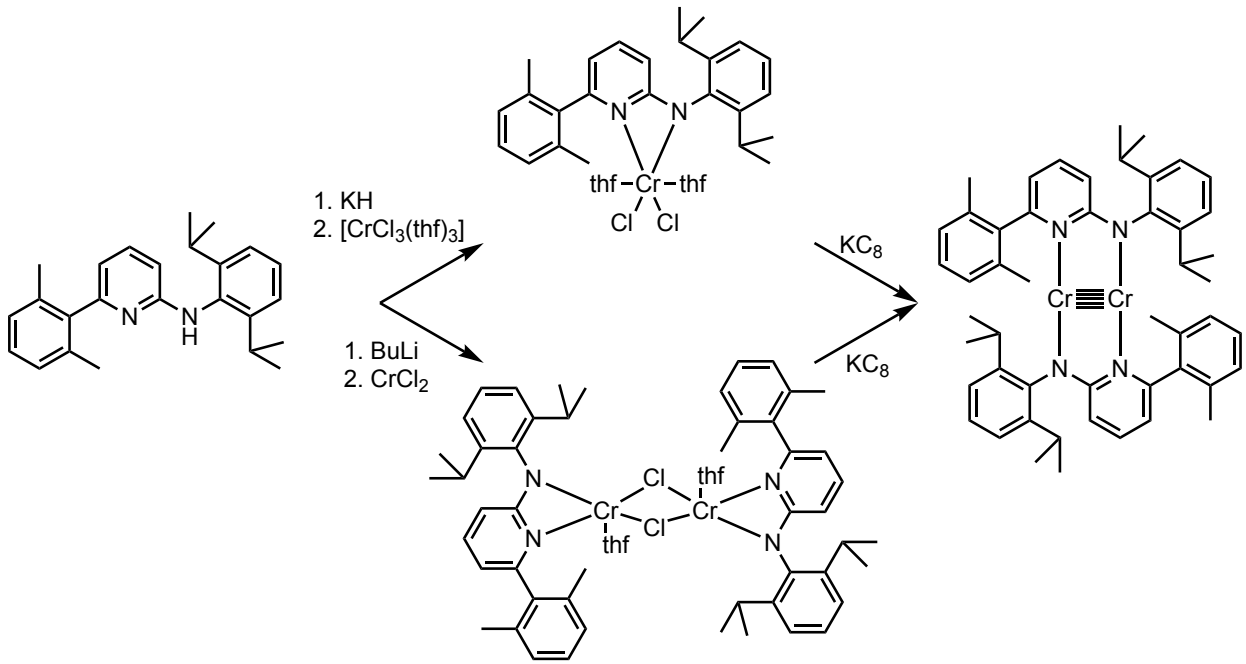


*Scheme 3.3 Synthesis of a $Cr_2(dadp)_2$.*

$Cr_2(dadp)_2$ has since proven to be a rich compound for research, with several types of reactivity afforded by activation of the quintuple bond with formal oxidation to a quadruple-bonded $Cr_2^{4+}$ core. Much of the reactivity of Kempe and coworkers' Cr≣Cr compound can be described as either insertion, addition, or cycloaddition, as shown in Scheme 4. For example, reaction of $Cr_2(dadp)_2$ with $Al(CH_3)_3$ results in the insertion product with *trans* bridging $CH_3$ and $Al(CH_3)_2$ ligands.[42] Similarly, reaction with methyl iodide[43] or halogens ($Cl_2$, $Br_2$, and $I_2$)[44] results in insertion of Cr≣Cr to form *trans* bridging complexes (Scheme 4A).

$Cr_2(dadp)_2$ also undergoes addition reactions with tetrahedral $P_4$, as well as $As_4$ and $AsP_3$, to form side-on adducts of cyclo-$E_4^{2-}$ anions (Scheme 3.4C).[45] Similar addition occurs upon reaction with $S_8$, $Se_8$, or Te, with formation of the side-on adduct of an $E_2^{2-}$ anion (Scheme 3.4E). Reaction with $O_2$, unlike reaction with other chalcogens, results in oxidation all the way to Cr(V) and the formation of both bridging and terminal oxo ligands (Scheme 3.4D).[44] Cycloaddition occurs when $Cr_2(dadp)_2$ reacts with substituted alkynes or with dienes (Scheme 3.4G, H).[46] When

butadiene coordinates to $Cr_2(dadp)_4$, the C–C bond lengths are more consistent with an $\eta^2$, $\eta^2$ diene; however, reaction with isoprene results in a shorter inner C–C distance and longer outer C–C distances, consistent with a Diels-Alder like reaction. In all of these addition reactions, the anilinopyridine ligands take on a *cis* geometry, in contrast to the *trans* geometry afforded by insertion reactions.

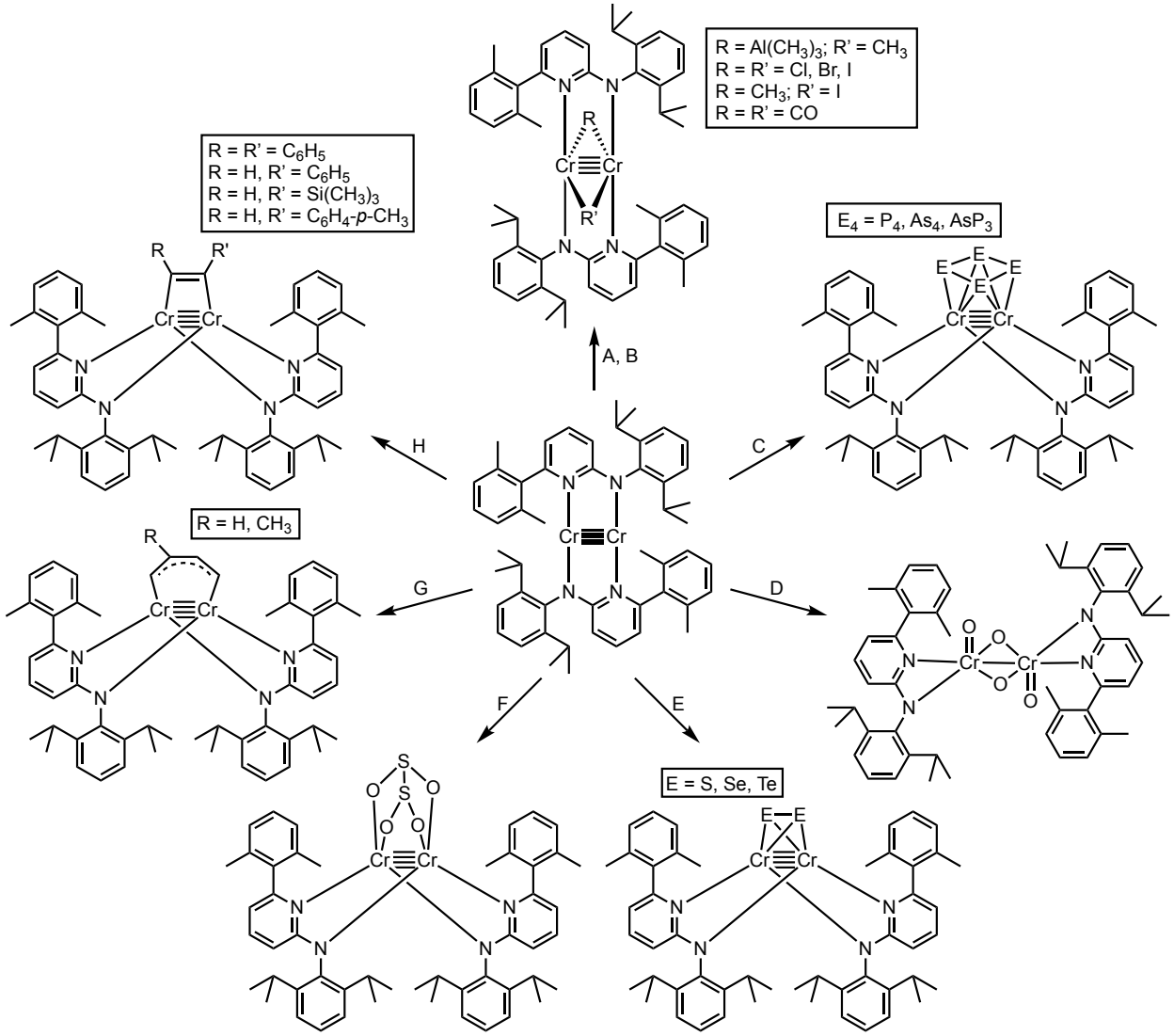


*Scheme 3.4 Reactivity of $Cr_2(dadp)_2$. A) Insertion into $Al(CH_3)_3$ in hexane, $CH_3I$, $Cl_2$, $Br_2$ in toluene, and $I_2$ in $C_6D_6$. B) Binding of CO or reaction with $CO_2$ in toluene, which also generates Cr-oxo byproducts. C) Addition to $P_4$, $As_4$, or $AsP_3$ in THF. D) Reaction with $O_2$ in hexanes. E) Reaction with $S_8$, $Se_8$, or Te in THF. F) Reaction with $SO_2$ in toluene. G) Reaction with dienes in toluene. H) Reaction with alkynes in toluene.*

$Cr_2(dadp)_2$ reacts with $SO_2$, $CO_2$, and CO. Upon reaction with $SO_2$, reductive coupling results in the formation of a dithionite ($S_2O_4^{2-}$) ligand (Scheme 3.4F). Reaction with both CO and $CO_2$ result in *trans* bridging CO complexes (Scheme 3.4B), with additional Cr-oxo byproducts formed in the reaction with $CO_2$.[47]

Using similar bulky ligands, the Carmona group has synthesized heteroleptic Mo≡Mo compounds bearing two acetate ligands and two ap-type ligands in an *anti-trans* conformation.[48] Substitution of the acetate ligands using MeLi resulted in bridging methyl complexes, with isomerization to a *syn* orientation and retention of one acetate for the more sterically-demanding dadp ligand (Figure 3.6).[49]

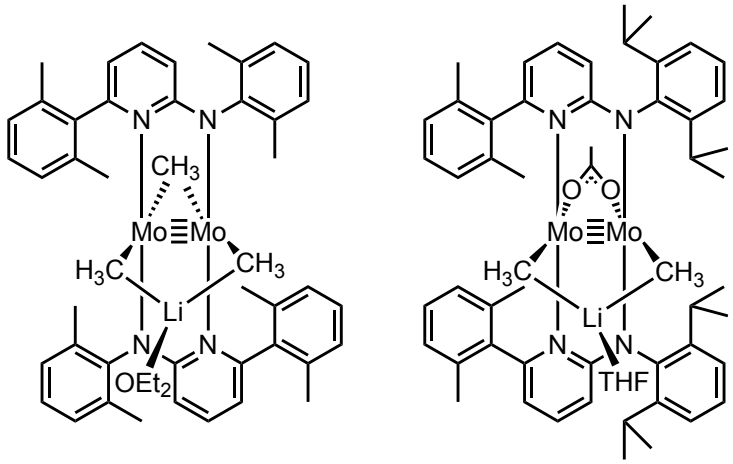


*Figure 3.6 Molecular structures of methylated $Mo_2$ complexes.*

*3.4.2 Tripodal Ligands Supporting First-row Transition Metals with M-M Bonds*

In stark contrast to the bidentate bridging ligands discussed above is the chelating, so-called "double-decker," ligand N,N,N-tris(2-(2-pyridylamino)ethyl)amine ($py_3tren$) used by Lu and coworkers to support metal-metal bonds between first-row transition metals. Several homo- and heterometallic compounds have been made, with $M_A$ = Fe and $M_B$ = Mn and Fe[50] or $M_A$ = Co and $M_B$ = Co, Fe, Mn[50], Ni[51], and Cu.[52] The accessibility of first-row metal-metal bonds is particularly

noteworthy, as coordination compounds with heterometallic multiple bonds between first-row transition metals were not known prior to 2013.[51]

Despite the topological differences between $py_3tren$ and the bidentate ap ligands, the synthetic routes are essentially the same. Tris(2-aminoethyl)amine is heated with 2-bromopyridine in the presence of $K_2CO_3$ to afford the desired tripodal ligand. Metallation, however, is distinct from paddlewheel routes, as metal-metal bonded precursors are not available for most first row transition metals. With this class of compounds, a metalloligand approach is employed, where the ligand is first deprotonated with benzylpotassium (KBn) and bound to $M_A$ (Fe(II) or Co(II)) to yield an isolable anionic mononuclear complex as a potassium salt. Subsequent metallation with an $M_BCl_2$ salt furnishes the bimetallic product, as shown in Scheme 3.5.[50] Interestingly, the isomer of $CoFeCl(py_3tren)$ where Fe is bound in the amido nitrogen pocket is not observed even when $CoCl_2$ is added to $K[Fe(py_3tren)]$. Instead, a mixture of $CoFeCl(py_3tren)$ and $Co_2Cl(py_3tren)$ is obtained.[50]

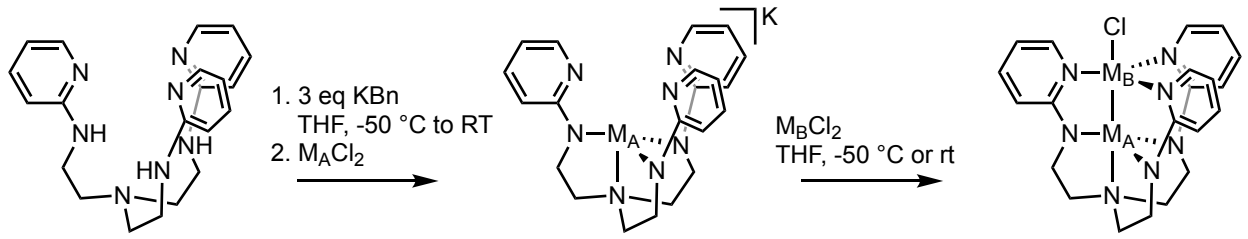


*Scheme 3.5 Synthesis of bimetallic complexes with the double-decker $py_3tren$ ligand.*

## 3.5 2-Hydroxypyridine Ligands

### *3.5.1 (4,0) Paddlewheel Complexes of Xhp Ligands*

Related to aminopyridines, 2-hydroxypyridine (or 2-pyridone) ligands have a rich history[53-55] and continue to be relevant to this day. Both 2-hydroxypyridine (hp) and 6-chloro-2-hydroxypyridine (chp) form (4,0) paddlewheel complexes with a $Ru_2^{n+}$ core. In 2011, Du Bois and

coworkers reported intramolecular allylic C-H amination with sulfamate esters catalyzed by $Ru_2(hp)_4Cl{\cdot}DMSO$.[56] The Berry group has employed the chp ligand to support $Ru_2^{n+}$ compounds in a variety of oxidation states. Starting from the stable $Ru_2(chp)_4X$ compounds, photolysis when X = nitrate[57] or azide[58] results in a putative $Ru_2^{6+}$ oxo or $Ru_2^{7+}$ nitrido intermediate, which can undergo group transfer reactions to nucleophilic substrates such as $PPh_3$. Furthermore, hydroxypyridine ligands are less electron-donating than aminopyridine ligands, which facilitates study of the reduced $Ru_2(Xhp)_4$ compounds. Facile reduction of $Ru_2(chp)_4Cl$ with Zn results in a neutral $Ru_2^{4+}$ complex that can bind a variety of axial ligands, including THF, DMSO, triphenylphosphine, and pyridine. DFT analysis indicates a linear relationship between binding strength and σ-donor ability, while no trend was observed between binding strength and π-donor ability.[59] An interesting feature of reduced $Ru_2(chp)_4$ compounds is dimerization in the absence of a strongly coordinating axial ligand to form a tetrametallic complex, with one O-atom from an equatorial chp ligand binding axially to the Ru-atom of the next paddlewheel unit (Figure 3.7). This interaction results in an insoluble compound that can only reenter solution when an axial ligand strong enough to displace the second $Ru_2$ unit is present.

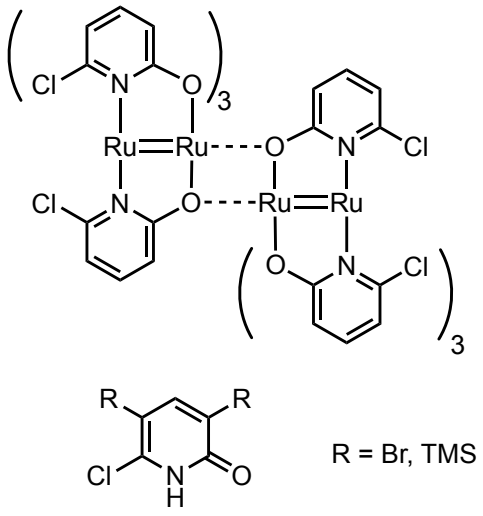


*Figure 3.7 Tetrametallic dimer $[Ru_2(chp)_4]_2$ (top) and sterically-enhanced ligands (bottom).*

To disfavor the formation of insoluble tetrametallic dimers, new ligands were developed through substitution of the pyridine ring at the 3 and 5 position (Figure 3.7). Bromination of Hchp with two equivalents of N-bromosuccinimide affords 3,5-dibromo-6-chloro-2-pyridone ($HBr_2chp$), while lithiation of chp with excess lithium diisopropylamide (LDA) followed by quenching with trimethylsilyl chloride results in 3,5-bis(trimethylsilyl)-6-chloro-2-pyridone ($HSi_2chp$). Both ligands prevent formation of the tetrametallic dimer by preventing the O atom lone pair from being able to bind to another $Ru_2$ unit. A Soxhlet reaction of $Ru_2(OAc)_4Cl$ with eight equivalents of $HBr_2chp$ results in the reduced $Ru_2^{4+}$ compound $Ru_2(Br_2chp)_4$. The analogous reaction with $HSi_2chp$ results in a mixture of $Ru_2^{4+}$ and $Ru_2^{5+}$ compounds. Decreasing the quantity of $HSi_2chp$ to only four equivalents affords the $Ru_2^{5+}$ complex $Ru_2(Si_2chp)_4Cl$ as the major product in approximately 50% yield. Subsequent reduction of this complex with Zn in $CH_2Cl_2$ affords a monomeric paddlewheel complex $Ru_2(Si_2chp)_4(CH_2Cl_2)$ having a coordinating $CH_2Cl_2$ ligand. Heating this $CH_2Cl_2$ adduct in benzene results in the axially free $Ru_2(Si_2chp)_4 \cdot C_6H_6$.[60]

*3.5.2 (2,2) Paddlewheel Complexes with Pendant Phosphines: Tetrametallic Chains*

While the ligands previously discussed have supported bimetallic complexes, hydroxypyridine can be functionalized with phosphines at the 6 position, resulting in the tridentate ligand pyphos (6-diphenyl-phosphanyl-2-pyridone, Figure 3.8). This ligand binds to a $Mo_2^{4+}$ quadruple-bonded core in a *trans*-(2,2) orientation, which then allows for two additional metal atoms to bind at either axial end of the $Mo_2$ core. Mashima and coworkers

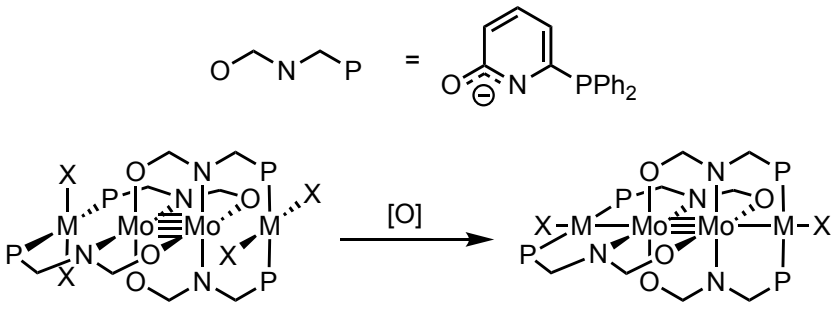


*Figure 3.8 Tetrametallic compounds supported by the pyphos ligand.*

have demonstrated this addition reaction with a number of $d^8$ metals, including Pd(II),[61] Rh(I),[62] and Ir(I).[63] The $d^8$ metal is formally non-bonding with respect to $Mo_2$, but oxidation by two electrons results in M–Mo≡Mo–M complexes (Figure 3.8). Similar metal-metal interactions and oxidative bond formation are observed when Pt(0) is added to $Mo_2(pyphos)_4$.[64] It has also been demonstrated that the pyphos ligands can rearrange about a Cu–Mo≡Mo–Cu core, with the *trans*-(2,2) isomer rearranging to the *cis*-(2,2) isomer in acetonitrile. The reverse reaction of *cis*-(2,2) to *trans*-(2,2) was not observed.[65]

*3.5.3 Partial Paddlewheel Complexes*

A large variety of compounds exist in which Xhp ligands support metal-metal bonds with other, monodentate ligands also occupying some equatorial ligand positions. These "partial paddlewheel" complexes can exist in a variety of isomeric forms, similar to the (4,0), (3,1), and (2,2) isomers described above for homoleptic $M_2L_4$ paddlewheel complexes. Maas and coworkers have examined partial paddlewheel complexes of Ru supported by 2 Xhp and 4 CO ligands, $Ru_2(Xap)_2(CO)_4$, prepared by the reaction of $Ru_2(CO)_{12}$ with HXap in refluxing toluene or methanol. The two Xhp ligands are found in a *cis*-(2,0) arrangement, and both bimetallic monomers and tetrametallic dimers are found, similar to the (4,0) $Ru_2(chp)_4$ compounds described earlier.[66] Depending on the axial ligand, either the (2,0) or (1,1) *cis* isomers are found in the solid state, though a solvent- and temperature- dependent equilibrium exists in solution.[67] The facile conversion between isomers at room temperature indicates that the bridging ligands in these complexes are much more labile than those in tetragonal paddlewheel complexes. Maas and coworkers note a trend in the equilibria that correlates with the identity of the axial halide ligand: (1,0) to (2,0) rearrangement is more favorable for Br > Cl > F, indicating a steric contribution. The

presence of strong *trans* effect ligands, namely CO and phosphines, may also contribute to the lability of the bridging Xap ligands.

Partial paddlewheel complexes of Rh have been studied by Dunbar and coworkers. Reaction of $Rh_2(Xhp)_4$ with 3-4 equivalents of $Et_3OBF_4$ in acetonitrile results in *cis*-$Rh_2(Xhp)_2(NCCH_3)_n^{2+}$ complexes, with the (2,0) or (1,1) orientation depending on the ligand. 6-methyl-2-hydroxypyridine (mhp) gives the (1,1) isomer, 6-fluoro-2-hydroxypyridine (fhp) gives the (2,0) isomer, and chp gives a mixture of both.[68]

The heteroleptic partial paddlewheel complex $Ir_2(OAc)_2Cl_2(CO)_2$ can undergo ligand substitution reactions to form partial paddlewheel complexes with Xhp ligands. Reaction with 4-mhp gives a (3,0) heteroleptic complex, $Ir_2(mhp)_3(CO)_2Cl(Hmhp)$, where the neutral Hmhp ligand is bound axially via the N-atom and is stabilized by hydrogen bonding of the -OH group with one of the anionic mhp ligands. Reaction of the same starting material with 1-hydroxyisoquinoline (hiq) only adds two ligands, resulting in the *cis*-(1,1) $Ir_2(hiq)_2Cl_2(CO)_2$.[69]

Partial paddlewheel complexes of Ir can also be prepared by reaction of the dimer $[(cod)Ir(hp)]_2$ (cod = 1,5-cyclooctadiene), prepared by treatment of $[(cod)IrCl]_2$ with Na(hp) in THF, with CO to afford $Ir_2(hp)_2(CO)_4$, where the hp ligands have a *cis*-(2,0) geometry. While the two $d^8$ Ir centers have no formal metal-metal bond, oxidation with substoichiometric iodine results in tetra-Ir and hexa-Ir chains, as shown in Scheme 3.6. These extended chain compounds are stabilized by the 2-electron/2n-center σ bond delocalized over the Ir atoms. Interestingly, the hp ligands are labile and both the *cis*-(2,0) and *cis*-(1,1) isomers are accessible. Indeed, when solid $I_2$ is added to a solution of $Ir_2(hp)_2(CO)_4$, the resulting $I[Ir_2(hp)_2(CO)_4]_nI$ chain exhibits a mixture of (1,1) and (2,0) isomers. Conversely, addition of solid $Ir_2(hp)_2(CO)_4$ to a solution of $I_2$ results in a dimer of (2,0) isomers (Scheme 3.6).[70] When a ferrocenium oxidant is used in acetonitrile, the

head-on (2,0)-(2,0) dimer is isolated, and it can be functionalized with an alkyne, similar to the aforementioned work by Ren and coworkers on $Ru_2$ compounds.[71]

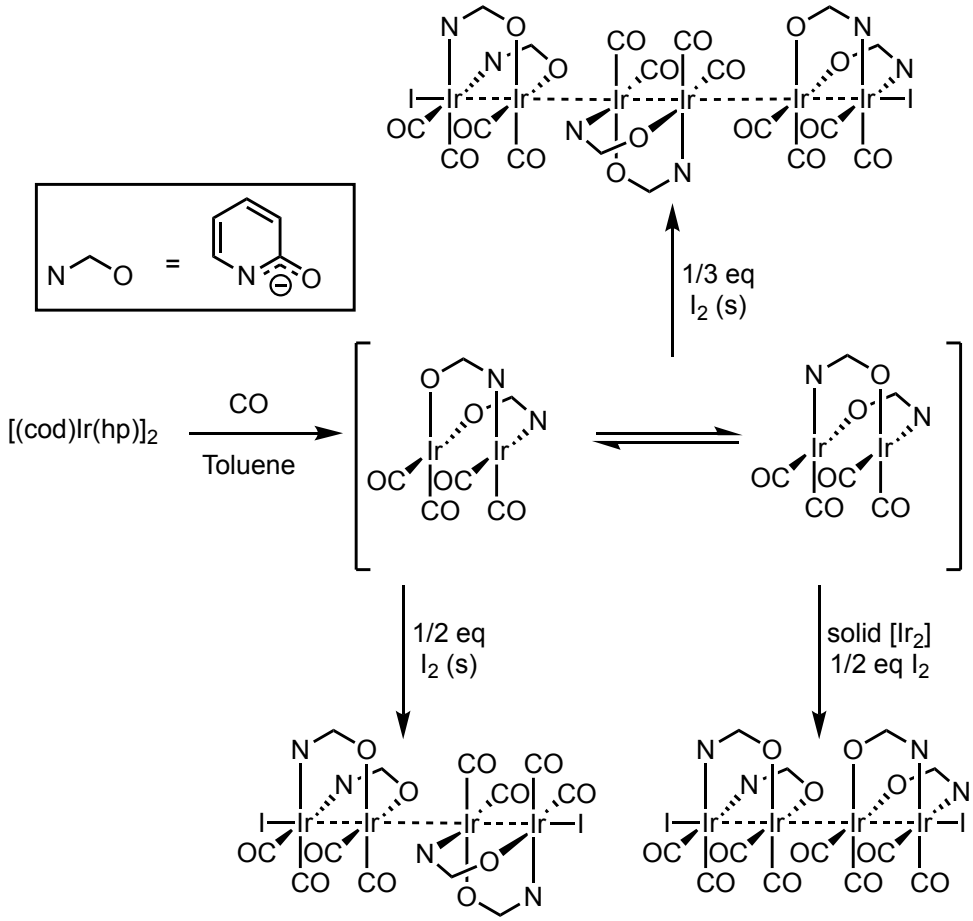


*Scheme 3.6 Synthesis of $Ir_2(hp)_2(CO)_2$ and oxidation to afford isomers of tetra-iridium and hexa-iridium extended chains.*

## 3.6 2-Mercaptopyridine Ligands

### *3.6.1 Bimetallic Paddlewheel Complexes*

Bimetallic paddlewheel complexes supported by mercaptopyridine ligands were first reported by Kinoshita, Ooi, and coworkers. The first homometallic compounds featured $Pd_2^{4+}$, $Pt_2^{4+}$, and $Pt_2^{6+}$ cores supported by the *cis*-(2,2) arrangement of mp ligands.[72, 73] Subsequent heterometallic paddlewheel complexes were prepared exhibiting the (4,0) geometry. In these complexes, Pt(II) is bound to the four S atoms, in accordance with hard/soft acid/base theory, and a first row transition metal (V, Cr, Co, or Ni) is bound to the N atoms. However, metal-metal

bonding in the heterometallic complexes was either not considered or ruled out based on the magnetic moment of the compounds.[74-76] More recently, Zhou and coworkers reexamined the Pt-Cr complex supported by four mp ligands. Upon oxidation by one electron, the Pt-Cr distance decreased from 2.65 Å to 2.50 Å, indicative of a bonding interaction between Pt(II) and Cr(III).[77]

The Berry group recently reported an analogous paddlewheel complex of Pd and Fe supported by four mp ligands.[78] The stepwise synthesis begins with ligation of Pd(II) with four neutral Hmp ligands. Treatment with a source of Fe(II) and triethylamine, to deprotonate the pyridinium N atoms of the monometallic complex, in acetonitrile affords the (4,0) heterobimetallic complex $PdFe(mp)_4(NCCH_3)$ in a high-spin $S = 2$ state with a formal Pd-Fe bond order of ½.

*3.6.2 Partial Paddlewheel Complexes of $Pd_2$ and $Pt_2$*

While there are very few reports of $M_2(mp)_4$ paddlewheel complexes, the mp ligand can support metal-metal bonded partial paddlewheel compounds in a number of other binding modes. With a soft S-atom, this ligand is perfectly suited for binding to soft metals such as Pt and Pd, and the mp ligand can be used to support $Pt_2^{4+}$ and singly-bonded $Pt_2^{6+}$ compounds. The mp ligand

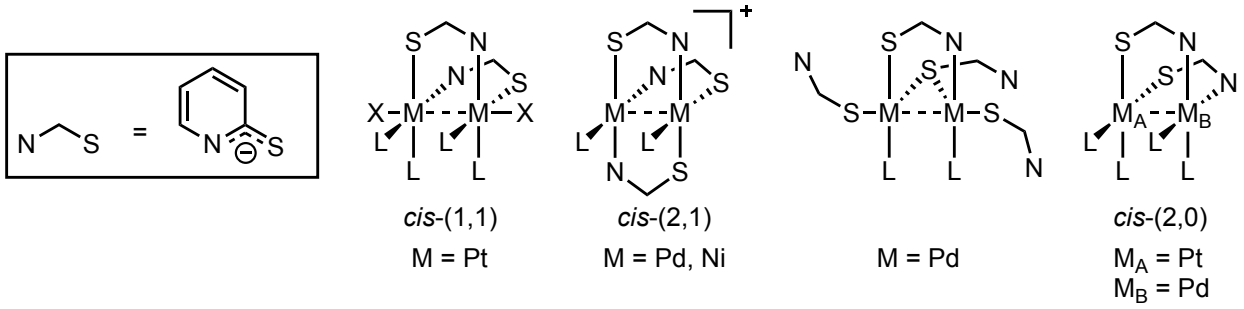


*Figure 3.9 Binding modes of 2-mercaptopyridine.*

binds in a variety of geometries, including *cis*-(1,1)[79] and *cis*-(2,1) N,S bridging modes, S-only bridging, and terminal S binding.[80] When the mixed Pd/Pt complex $[(bpy)_2PtPd(mp)_2]^{2+}$ is prepared from addition of $Pd^{2+}$ to $[(bpy)Pt(mp)_2]$, the hard/soft acid/base preference results in a

*cis*-(2,0) geometry with both N atoms bound to Pd and both S atoms bound to Pt.[81] These binding modes are shown in Figure 3.9.

In $Pt_2^{4+}$ compounds, no formal bonding is expected between the Pt centers. However, short Pt–Pt distances of < 2.9 Å indicate weak bonding interactions for $Pt_2^{4+}$ compounds.[79] In contrast, $Pt_2^{6+}$ compounds have a definitive Pt-Pt bond with Pt-Pt distances of ~ 2.6 Å. With Pd, a similar bonding pattern is observed: a weak bonding interaction in $Pd_2^{4+}$ compounds (Pd–Pd distance ~ 2.7–2.8 Å) and a strong Pd–Pd bond in $Pd_2^{6+}$ compounds (~ 2.6 Å).[82] In the related compound $[Ni_2(mp)_3(dppe)][BF_4]$, no net bonding is assigned in the $Ni_2^{4+}$ core.[83]

Kato and coworkers have also employed 2,6-dimercaptopyridine (dmp) to support $Pt_3$ partial paddlewheel complexes.[84] Each Pt atom is supported by a bpy ligand, with two *cis* dmp ligands bridging the three metal centers. The $[Pt_3(bpy)_3(dmp)_2]^{2+}$ dication undergoes reversible two-electron oxidation in the presence of coordinating anions (chloride, bromide, thiocyanate) to form $[Pt_3(bpy)_3(dmp)_2X_2]^{2+}$ dications. Short Pt–Pt distances (2.86 and 2.91 Å) in the $Pt_3^{6+}$ complex are indicative of weak Pt–Pt bonding interactions, similar to the $Pt_2^{4+}$ complexes described above. While the $Pt_3^{8+}$ compounds were not isolated, it is likely that the Pt–Pt distances decrease due to the predicted 3-center/2-electron σ bond delocalized over the three Pt atoms.

### 3.7. 2,2'-Dipyridylamine and Related Ligands for Supporting Trimetallic Metal Atom Chains

The ligand 2,2'-dipyridylamine (Hdpa) has played a central and founding role for the field of extended metal atom chains (EMACs),[85] and for more recent developments using mixed-metal heterometallic extended metal atom chains (HEMACs).[86, 87] Recently, the coordination chemistry of the Hdpa ligand was reviewed, and nine distinct coordination modes were identified.[88] Those

coordination modes that support metal-metal bonds are shown in Figure 3.10; all of them involve the deprotonated form of the ligand. There are many coordination modes that support bimetallic compounds, and these will be discussed first before discussing coordination mode **V**, which supports EMACs and HEMACs.

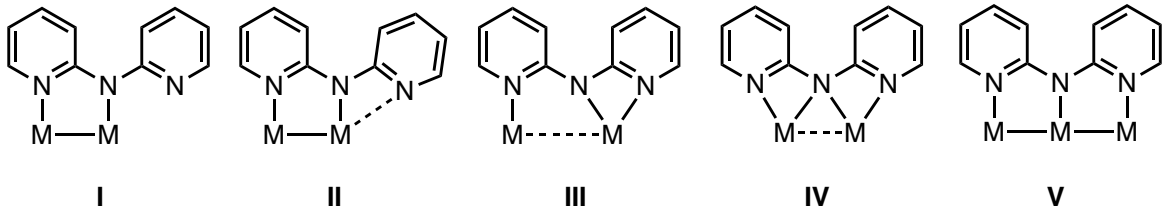


*Figure 3.10 Coordination modes of the dpa ligand that support metal-metal bonds.*

*3.7.1. Bimetallic Compounds Supported by the dpa Ligand*

Coordination modes **I** – **IV** shown in Figure 3.10 support bimetallic compounds. Each of these modes is fairly distinct, though the difference between modes **I** and **II** is somewhat subtle, as it revolves around whether or not the third N atom coordinates to one of the metal centers. Because of the geometry, such an interaction is necessarily weak. To quantify this effect, in addition to the M···N distances, Cotton and coworkers advanced the idea that M–N–C–N torsion angles will be close to zero when the pyridine rings are directed toward the axial site.[89]

Thus, in molecules that truly adopt coordination mode **I**, such as the $M_2(dpa)_4$ compounds with M = Cr, Mo, or W and their monocations, relatively long M···N distances of ~ 2.7 to 3.1 Å and large torsion angles of ~ 25° indicate minimal interactions of the dangling pyridine group to the $M_2$ core.[90] On the other hand, the analogous $Rh_2$ complex, $Rh_2(dpa)_4$, contains two dpa ligands in which the Rh···N distance is 3.2 Å with torsion angles of ~ 50°, but the other two ligands clearly show coordination to the Rh axial site with Rh–N distances of 2.39 Å and torsion angles of 4°.[91] In this respect, the bimetallic compound $Ru_2(dpa)_4Cl$ is also notable in that three of the dpa ligands adopt coordination mode **I**, while the fourth dpa ligand binds to the axial site at an Ru···N distance of 2.49 Å and a torsion angle of 9°, clearly indicating coordination mode **II**.[92]

There are two general strategies for the preparation of $M_2(dpa)_4$ compounds. These compounds may be prepared from a reaction of Hdpa or Li(dpa) with a suitable metal precursor. $Mo_2(dpa)_4$ is formed by reaction of Li(dpa) with $Mo_2(OAc)_4$,[93] though a more recent method using Kdpa is more convenient.[94] $W_2(dpa)_4$ and $Rh_2(dpa)_4$ are prepared by reaction of Hdpa with $W(CO)_6$ in naphthalene, or with $Rh_2(OAc)_4$ in neat Hdpa, respectively.[90, 91]

The second synthetic strategy for $M_2(dpa)_4$ compounds is extraction of a metal atom from trimetallic EMAC compounds (cf. sections 6.2, 6.3). Thus, treatment of $Cr_3(dpa)_4Cl_2$ with excess NaCN in methanol results in extraction of one "$CrCl_2$" equivalent to yield $Cr_2(dpa)_4$.[95] $Ru_2(dpa)_4Cl$ is prepared in a multi-step sequence. First, $Co_3(dpa)_4Cl_2$ reacts with $Ru_2(OAc)_4Cl$ to yield $Ru_2Co(dpa)_4Cl_2$, and treatment of this heterotrimetallic complex with aqueous ammonia results in the isolation of $Ru_2(dpa)_4Cl$.[92]

In 2011, Berry and coworkers reported that $W_2(dpa)_4$ could be oxidized by two electrons to yield the $[W_2(dpa)_4]^{2+}$ dication, which in turn could be further oxidized by two electrons to the $[W_2O(dpa)_4]^{2+}$ dication, as shown in Scheme 3.7.[96] The dications both display coordination of the dpa ligand through coordination mode **III**. For the $[W_2(dpa)_4]^{2+}$ cation, as well as its $Mo_2$ and heterometallic MoW analogs,[97] each metal atom achieves a coordination number of six with respect to the dpa N atoms. This chelation of the metal atoms pulls them apart from each other, elongating the metal-metal bond by > 0.5 Å. Despite the long distances, calculations indicate a $\sigma^2\pi^2\delta^2$ metal-metal triple bond, with the triple-bonded configuration contributing more to the electronic structure across the series from $Mo_2$ to MoW to $W_2$. The terminal oxo complexes $[M_2O(dpa)_4]^{2+}$ have even longer metal-metal distances and show minimal metal-metal bonding. Further one-electron oxidation of $[W_2O(dpa)_4]^{2+}$ to the $[W_2O(dpa)_4]^{3+}$ trication causes the W–W distance to become shorter by ~ 0.1 Å, consistent with a dative interaction between the filled $d_{z^2}$

orbital of the eight-coordinate W(IV) ion with the empty $d_{z^2}$ orbital of the square-pyramidal W(V)≡O group.[98]

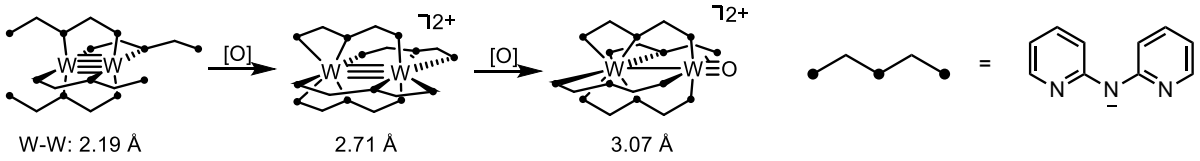


*Scheme 3.7 Structures of $W_2(dpa)_4$, $[W_2(dpa)_4]^{2+}$, and $[W_2O(dpa)_4]^{2+}$.*

Another class of bimetallic compounds supported by the dpa ligand contains a mix of coordination modes **III** and **IV**. The cationic, diamagnetic $[W_2(dpa)_3Cl_2]^+$ ion (Figure 3.11) was obtained upon two electron oxidation of $W_2(dpa)_4$ with $SO_2Cl_2$ and is described as having a long W–W bond order of three or less.[90] The analogous $Ru_2(dpa)_3(Cl)_x(OAc)_{2-x}$ compound with x = 1.36 was described as not having an Ru–Ru bond.[99]

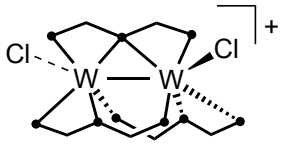


*Figure 3.11 Core structure of the $[W_2(dpa)_3Cl_2]^+$ cation.*

*3.7.2. Homotrimetallic Compounds Supported by the dpa Ligand.*

The rest of the dpa-supported compounds described here adopt the coordination mode **V**, with three metals held into a linear array by four doubly-bridging dpa ligands. The trimetallic compounds fall into two main categories: homometallic (EMAC) and heterometallic (HEMAC). The former category will be discussed in this section, and it was reviewed comprehensively in 2005;[85] this chapter will focus on work since that time.

The range of metal atoms that are known to form homometallic $M_3(dpa)_4Cl_2$ compounds encompass Cr, Co, Ni, Cu, Ru, and Rh – all of which were known prior to 2003.[85] Two of these compounds ($Cr_3$ and $Co_3$) have been subjected to high-level crystallographic analysis, providing

new details on the nature of metal-metal bonding within the compounds. For both compounds, persistent questions about structural distortions to $C_4$ symmetry (Scheme 3.8) were present from earlier literature. These distortions are of particular importance for understanding the degree of electron delocalization/localization throughout the $M_3$ chain.

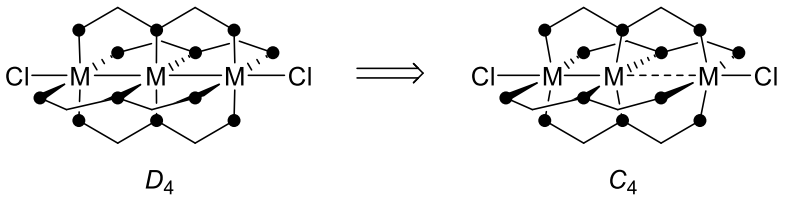


*Scheme 3.8 Axial distortion in $M_3(dpa)_4Cl_2$ compounds with M = Cr, Co.*

In the case of $Cr_3(dpa)_4Cl_2$, crystallographic studies at 213 K showed disorder of the central metal atom position that was modeled as a $C_4$-symmetric structure disordered in two oppositely-facing orientations.[100] Crystal structures at 100 K and 15 K also show this disorder; however, the difference in Cr mean square displacement amplitudes between the central Cr atom and the outer two becomes dramatically smaller at 15 K, indicating that the crystallographic disorder is dynamic in nature rather than static. These data, combined with a charge density model for the electronic structure, indicate that $Cr_3(dpa)_4Cl_2$ is best described as having $D_4$ symmetry, with a very shallow potential energy well towards $C_4$ distortion.[101] Despite the symmetric structure, electronic structure indicators point to localized Cr–Cr bonds in the structure rather than a delocalized three-center $Cr_3$ bonding interaction.[101]

The compound $Co_3(dpa)_4Cl_2$ forms two types of crystals upon crystallization from $CH_2Cl_2$, one containing $Co_3(dpa)_4Cl_2{\cdot}CH_2Cl_2$ and the other containing $Co_3(dpa)_4Cl_2{\cdot}2CH_2Cl_2$.[102] The intermolecular interactions with $CH_2Cl_2$ solvate molecules drastically affect the molecular structure of the compound, as the $Co_3$ molecule in the mono-$CH_2Cl_2$ solvate has $D_4$ symmetry while that in the bis-$CH_2Cl_2$ solvate has $C_4$ symmetry.[102] Further variable-temperature

crystallographic studies and electron density measurements have been performed for the $C_4$-symmetric bis-$CH_2Cl_2$ solvate.[103] These measurements have clarified that there is Co–Co bonding over both the short and long Co–Co vectors, and that the "isolated" Co ion has more ionic Co–N bonds and is involved in thermally-induced spin crossover.[103] High-pressure crystallographic studies on the $D_4$-symmetric mono-$CH_2Cl_2$ solvate show variations in the Co–Co and Co–Cl distances consistent with those seen in variable temperature measurements, suggesting a similar traversal of excited states upon applied pressure.[104]

Substitution of the axial chloro ligands in $M_3(dpa)_4Cl_2$ compounds has been successful with a variety of different ligands. Other halides,[100] pseudohalides,[100, 105, 106] oxyanions,[100, 107] carboxylates,[108-111] and acetylides[100, 112-114] have been effective ligands, as well as hexafluorometallate dianions, which have been used as bidentate axial ligands to link the EMAC molecules into one-dimensional coordination polymers.[115]

The dpa ligands wrap around the $M_3$ chains in a helical fashion, giving rise to Λ and Δ enantiomers, which can be resolved by selective crystallization of the $[Co_3(dpa)_4(NCCH_3)_2]^{2+}$ cation with either Λ- or Δ-$[As_2(tartrate)_2]^{2-}$ anions.[116] Once resolved, the EMAC molecules do not racemize in solution, as confirmed by oppositely-signed circular dichroism spectra. Magnetic X-ray dichroism spectra did not show signals at the Co K edge, and this absence of signal was attributed to delocalization of the spins across the $Co_3$ chain.[116]

Prior to 2005, one-electron oxidation of the $M_3(dpa)_4Cl_2$ compounds had been achieved for M = Cr, Co, Ni, and Cu.[85] New examples of $Cr_3^{7+}$ compounds have since been described, which show the characteristic, unsymmetrical, and localized $Cr^{II}\equiv Cr^{II}\cdots Cr^{III}$ geometric and electronic structure.[100, 117, 118] New examples of $M_3^{7+}$ compounds include $[Ru_3(dpa)_4X_2]^+$ cations with X = Cl,[105] CN,[105] and NCS,[106] as well as $[Rh_3(dpa)_4Cl_2]^+$.[119] Both the $Ru_3^{7+}$ and $Rh_3^{7+}$ species are low-

spin with $S = ½$ and $S = 0$, respectively. The $[Ru_3(dpa)_4Cl_2]^+$ complex can be further oxidized to the diamagnetic $[Ru_3(dpa)_4Cl_2]^{2+}$ diaction.[105] All of the Ru and Rh cationic structures show symmetric M–M distances; several show distinct non-linearity as shown in Scheme 3.9. For example, the Rh–Rh–Rh angle in the $[Rh_3(dpa)_4Cl_2]^+$ ion is 168°.[119] The nature and consequences of the $C_2$-symmetric distortion in $Ru_2^{6+}$ species have been discussed from an electronic structure standpoint by McGrady and coworkers.[120, 121] In short, the near-degeneracy of $\sigma_{nb}$ and $\pi^*$ orbitals creates a situation where, in perfect $D_4$ symmetry, a high-spin $S = 2$ state is favored with the $\sigma_{nb}$ and $\pi^*$ orbitals (and also the lower energy $\delta^*$) singly occupied. However, a distortion to $C_2$ symmetry allows mixing of the $\sigma_{nb}$ and $\pi^*$ orbitals and favors the $S = 0$ state.

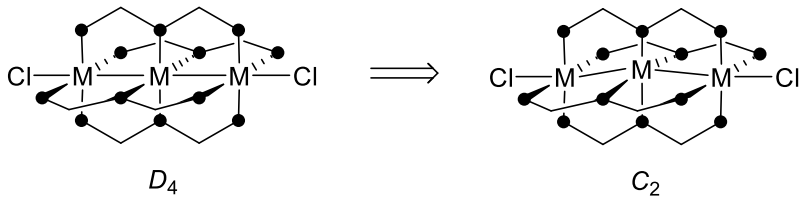


*Scheme 3.9 Rhombic distortion in $M_3(dpa)_4Cl_2$ compounds with $M_3 = Ru_3^{6+}$, $Ru_3^{7+}$, $Rh_3^{7+}$.*

*3.7.3. Heterotrimetallic Compounds Supported by the dpa Ligand*

In addition to the homotrimetallic chain compounds described above, the dpa ligand has been utilized to support a wide array of heterotrimetallic compounds.[122] There are three general categories of these, depending on the heterometal arrangement. When there are two types of metal atoms in the chain, $M_A$ and $M_B$, there are both $C_4$-symmetric ($M_A$–$M_A$–$M_B$) and $D_4$-symmetric ($M_A$–$M_B$–$M_A$) arrangements possible. It is also possible to construct $C_4$-symmetric chains that contain three different metals, $M_A$–$M_B$–$M_C$.

For the $M_A$–$M_A$–$M_B$ chains, these have generally been constructed via a metalloligand approach in which a distinct bimetallic $(M_A)_2(dpa)_4$ molecular precursor (discussed in section 3.7.1) is prepared and $M_B$ is added as a dihalide salt in a subsequent step. Thus,

$(M_A)_2(M_B)(dpa)_4Cl_2$ compounds are known for nearly all of the metal combinations with $M_A$ = Cr,[86, 88, 93, 95, 123-125] Mo,[86, 88, 93, 94, 123, 126-128] W,[88, 123, 127] or Ru[92, 129] and $M_B$ = Cr,[88, 125] Mn,[86, 92, 125, 126] Fe,[86, 92, 95, 125, 126] Co,[92, 93, 125, 126] Ni,[94, 124, 128, 129] Cu,[92, 129] Zn,[92, 123] Ag[92] and Ru.[127] When $M_A$ = Ru, the precursor compound $Ru_2(dpa)_4Cl$ is a $Ru_2^{5+}$ mixed-valent species and the resulting trimetallic complexes are therefore monocationic. Besides compounds in which $M_B$ is a first-row transition metal, $[Ru_2(M_B)(dpa)_4Cl_2]^+$ compounds with $M_B$ = Rh, Pd, Cd, and Ir are known.[92]

Symmetric $M_A$–$M_B$–$M_A$ compounds are currently limited to those with a group 10 metal, Ni, Pd, or Pt, in the $M_B$ site. Compounds in which $M_A$ = Mn, Fe, and Co are known, and are generally prepared by heating mixtures of $M_ACl_2$ and $M_BCl_2$ precursors with Hdpa and $KO^tBu$ in naphthalene .[92, 130, 131] Truly heterotrimetallic $M_A$–$M_B$–$M_C$ compounds require clever synthetic design. Two such molecules are known. The first was prepared starting from the heterobimetallic $MoW(dpa)_4$ starting material; addition of $CrCl_2$ yielded $MoWCr(dpa)_4Cl_2$, formed selectively with no trace of the other possible WMoCr isomer.[132] The compound $NiCoRh(dpa)_4Cl_2$ was also prepared in a stepwise manner, but starting with $Co_2Rh(dpa)_4Cl_2$, synthesized from a mixture of $CoCl_2$ and $RhCl_3$ with the Hdpa ligand. Heating $Co_2Rh(dpa)_4Cl_2$ with $Ni(OAc)_2$ resulted in the selective replacement of the terminal Co atom with a Ni atom in a metal atom exchange reaction.[133]

*3.7.4. Other New Ligands that Support Trimetallic Chains.*

The dpa ligand is able to support linear trimetallic chains via its central amido N atom flanked by two pyridine groups. It is also possible to flip these functional groups such that a central pyridine group has flanking amido groups in the 2 and 6 positions. The resulting pyridine-di-amide (pda) ligands, shown in Figure 3.12, stabilize linear chain compounds as dianionic ligands rather than monoanionic like dpa. The first use of a pyridine-di-amide ligand was in 2001, when the diphenyl variant, 2,6-bis(phenylamino)pyridine ($H_2BPAP$), was used to prepare a dianionic

trinickel(II) complex.[134] In contrast to $Ni_3(dpa)_4Cl_2$, the $[Ni_3(BPAP)_4]^{2-}$ dianion contains no axial ligands and thus all three Ni(II) ions are diamagnetic with square planar coordination geometry. In 2006, Peng and coworkers reported heteroleptic trinickel compounds bearing two dpa ligands and two pda ligands oriented in the *trans* geometry, as shown in Figure 3.12.[135] These neutral trinickel compounds are formed selectively upon heating three equivalents of $Ni(OAc)_2$ with two equivalents each of Hdpa and $H_2$pda in molten naphthalene.

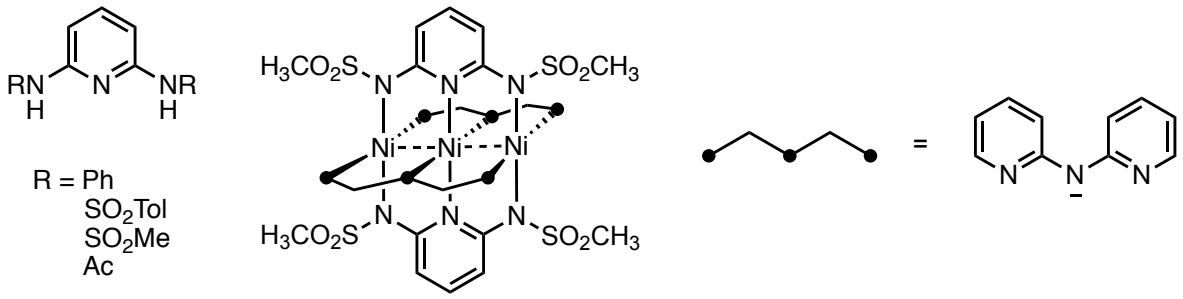


*Figure 3.12 (left) Pyridine-di-amine ligands. (right) Structure of a neutral $Ni_3$ mixed-ligand compound.*

Other modified ligands for the stabilization of linear trimetallic complexes include 1,9-diazaphenoxazine (Hdzp) and 4-methylpyridyl-thiazolylamine (Hmpta), both shown in Figure 3.13. The Hdzp ligand was prepared by double condensation of 2-amino-3-hydroxypyridine and 2-chloro-3-nitropyridine in refluxing DMSO. $Co_3$ and $Ni_3$ complexes of the dzp anion were characterized and found to have a somewhat smaller helical twist (N–Ni–Ni–N torsion angle of 14-18°) than in the corresponding dpa complexes (~ 23° torsion). The smaller torsion angles are enforced by the central O atom of the dzp ligand effectively tying together the two pyridyl rings. Magnetic properties of the dzp complexes are similar to the dpa analogs with partially occupied high-spin states being slightly lower in energy for the former.[136] The Hmpta ligand was prepared by reaction of 2-amino-4-methylpyridine with 2-bromothiazole. Its $Ni_3$ complexes with axial CN and NCS ligands have been characterized and found to adopt the *cis*-(2,2) geometry, with similar propreties to the corresponding dpa compounds.[137]

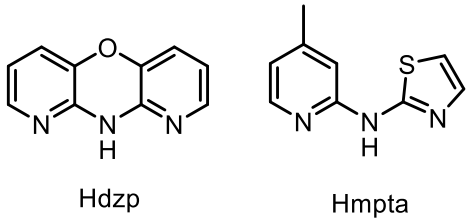


*Figure 3.13 Molecular structures of the Hdzp and Hmpta ligands.*

As will be discussed further in section 7.3, a large class of new ligands for supporting EMACs has been prepared that incorporate naphthyridine groups. Two particular naphthyridine-derived ligands have been used to support linear trimetallic complexes: 2-naphthyridylphenylamine (Hnpa) and 1,8-naphthyridin-2(1*H*)-one (Hnpo). The structures are given in Figure 3.14. The Hnpa ligand was prepared by Buchwald-Hartwig amination of 2-chloronaphthyridine with aniline. The triruthenium complex $[Ru_3(npa)_4(NCS)_2]^+$ was prepared by reaction of $Ru_2(OAc)_4Cl$ with Hnpa and KO$^t$Bu in naphthalene. The complex adopts the (3,1) geometry and has an $S = 1/2$ ground spin state.[138] The Hnpo ligand, accessible via hydrolysis of 2-naphthyridylamine, has been used to support a family of *trans*-(2,2) heterometallic $Mo_2M$ complexes with M = Fe, Co, and Ni. The $Mo_2Fe$ complex is prepared first by reaction of Hnpo, $Mo_2(OAc)_4$, and $FeCl_2$ in molten naphthalene. The Fe(II) ion is then subsequently replaced by heating the $Mo_2Fe$ complex with $CoCl_2$ or $Ni(OAc)_2$ to yield the $Mo_2Co$ or $Mo_2Ni$ complexes.[139]

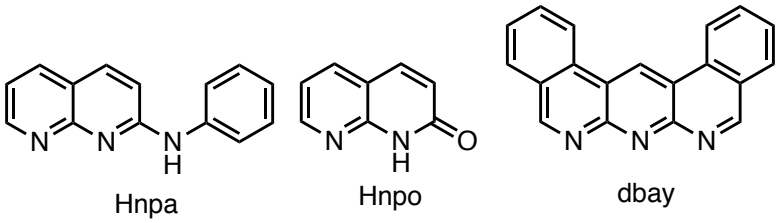


*Figure 3.14 Molecular structures of the Hnpa, Hnpo, and dbay ligands.*

Very recently, Peng and coworkers reported an anthyridine-based ligand, 1,13,14-triaza-dibenz[*a*,*j*]anthracene (dbay, also shown in Figure 3.14).[140] Though no synthetic information is provided, the authors note that dbay is synthesized by a double Suzuki coupling reaction. A

trinickel complex of this ligand was prepared and characterized, $[Ni_3(dbay)_4Cl_2]^{3+}$. Since the dbay ligand is neutral, the charge indicates a mix of two Ni(II) ions and one Ni(I) center in the complex. The magnetic properties are consistent with this formulation, with the Ni(I) ion occupying the central position.

One additional approach to the stabilization of linear trimetallic structures has been to use heptadentate ligands that can wrap around the $M_3$ chain binding to six equatorial sites and one axial site, as shown for the dimethyl-pentapyridyl-tetramine (mpeptea) ligand in Figure 3.15. $Ni_3$ and $Co_3$ complexes have been reported with this type of ligand, and are similar to the dpa compounds but cannot undergo axial ligand substitution reactions.[135, 141, 142] The multi-step ligand synthesis is built off of successive 2-pyridylamine/2-bromopyridine couplings.[141]

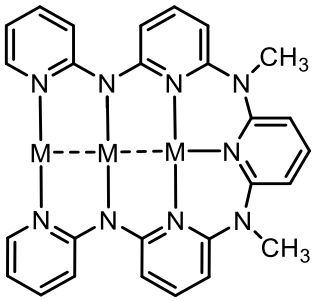


*Figure 3.15 Heptadentate coordination mode of the mpeptea ligand.*

### 3.8 Extended Ligands for Supporting Chains of Metal Atoms with *n* > 3

The expansion of the field of EMACs and HEMACs beyond linear trimetallic compounds relies heavily on new ligand design. The expansion of the polypyridylamine ligand platform in Figure 3.16 from Hdpa (2,2'-dipyridylamine) to $H_2$tpda (tripyridyldiamine) to $H_3$teptra (tetrapyridyltriamine) to $H_4$peptea (pentapyridyltetramine) was achieved by 2003 with the peptea ligand being shown to support a linear chain of 9 Ni atoms.[143] Some additional work since 2003 has focused on pentametallic complexes supported by the tpda ligand, but a greater focus has been on the design of new ligands to achieve syntheses of longer chains, also not just odd-

numbered chains but ones with even numbers of metal atoms as well. The incorporation of naphthyridine units into the ligand structures has greatly expanded these possibilities.

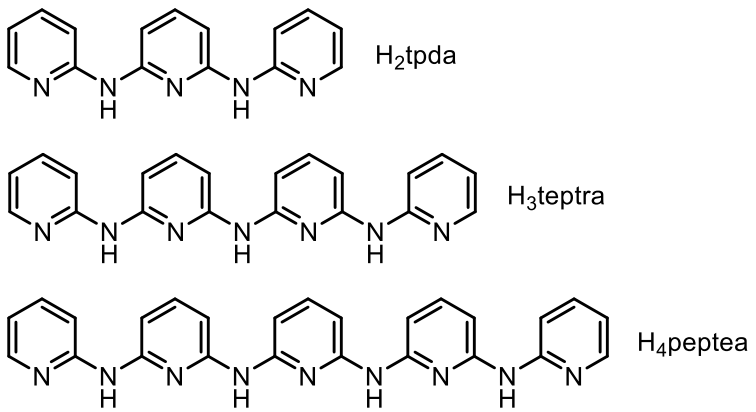


*Figure 3.16 Molecular structures of the extended polypyridylamine ligands $H_2$tpda, $H_3$teptra, and $H_4$peptea. These ligands have been shown to support pentametallic, heptametallic, and nonametallic linear chain compounds, respectively.*

*3.8.1. Pentametallic Compounds Supported by the tpda Ligand.*

The $M_5(tpda)_4X_2$ and $[M_5(tpda)_4X_2]^+$ compounds that were known prior to 2003 were those containing $Cr_5$, $Co_5$, and $Ni_5$ chains. Electron transport measurements of these compounds were examined by scanning-tunneling microscopy in 2004, finding that the effective heights of the molecules (and therefore their ability to transport charge) decreased from Cr to Co to Ni.[144] Pentaruthenium complexes supported by the tpda ligand were reported in 2008. In terms of molecular conductance, the $Ru_5(tpda)_4(NCS)_2$ molecule falls between its $Cr_5$ and $Co_5$ analogs.[145]

A major new direction in the chemistry of pentametallic complexes has been the preparation of heterometallic complexes. The tpda ligand has served as the most important testing ground for this new area. To date, two heteropentametallic chain compounds have been reported: $Ni_3Ru_2(tpda)_4(NCS)_2$ and $NiMo_4(tpda)_4(NCS)_2$. The first compound, $Ni_3Ru_2(tpda)_4(NCS)_2$, was prepared by heating a mixture of $H_2$tpda with a 1:2 mole ratio of $Ni(OAc)_2$ and $Ru_2(OAc)_4Cl$ in molten naphthalene. The resulting pentametallic complex has an unsymmetrical array of metal

atoms: Ni–Ru–Ru–Ni–Ni. Furthermore, the complex is proposed to contain mixed-valency with a terminal Ni(I) ion and an internal $Ru_2^{5+}$ unit. The complex shows an unusual spike in its I/V curve described as negative differential resistance.[146]

By changing the starting material from $Ru_2(OAc)_4Cl$ to $Mo_2(OAc)_4$ but otherwise keeping the conditions the same, the $NiMo_4(tpda)_4(NCS)_2$ complex is formed. This time, the metal atom ordering is more symmetric: Mo–Mo–Ni–Mo–Mo. Moreover, the complex is more symmetric than other tpda complexes as well in that it is achiral. Generally, EMACs are chiral due to a helical twist of the ligands around the metal atom core. In $NiMo_4(tpda)_4(NCS)_2$, the twist of the ligand is bent in such a way to preserve a mirror plane perpendicular to the metal atom chain, passing through the central high-spin Ni(II) ion and its N ligands.[147]

*3.8.2. New Ligands that Incorporate Pyridine Derivatives*

The prototypical polypyridylamido ligands shown in Figure 3.16 allowed for extensive new chemistry to be discovered, but also provided some significant limitations. The demanding synthetic methods for EMAC synthesis (molten naphthalene) do not always work for every metal, and in the hands of the authors can even give widely variable yields from batch to batch. Solubility is another limitation that hinders the preparation of very long chains. Exploration of new polypyridylamine ligands that incorporate derivatives of pyridine, or other N-containing heterocycles, has therefore been of interest with the goals of achieving reproducible syntheses, soluble compounds, and redox tunability.

The first and simplest derivatization of the tpda ligand was the addition of ethyl groups in the 4-position of the two terminal pyridine rings to yield the ligand $H_2$etpda (Figure 3.17). $Cr_5$, $Co_5$, and $Ni_5$ complexes of the etpda ligand were prepared and found to be structurally similar to the tpda compounds, but with more accessible potentials for one-electron oxidation, consistent

with the addition of eight electron donating groups to the periphery of the molecules.[89, 148, 149] For example, the reversible $Ni_5^{10+/11+}$ redox events were found to be at 0.409 V and 0.517 V vs Ag/AgCl for $CH_2Cl_2$ solutions of $Ni_5(etpda)_4Cl_2$ and $Ni_5(tpda)_4Cl_2$, respectively.[148]

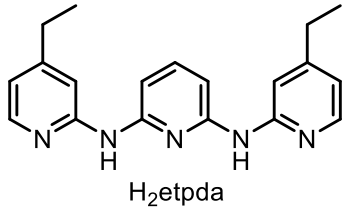


*Figure 3.17 Molecular structure of the $H_2$etpda ligand.*

A series of new ligands has been prepared that incorporates pyrazine rings into the polypyridylamine structures, Figure 3.18. The inclusion of these pyrazine groups has generally led to improved yields of the EMAC compounds that are less prone to air oxidation than their polypyridylamido analogs. These ligands are generally accessible via multi-step cross-coupling chemistry. We will discuss the compounds in order of increasing nuclearity.

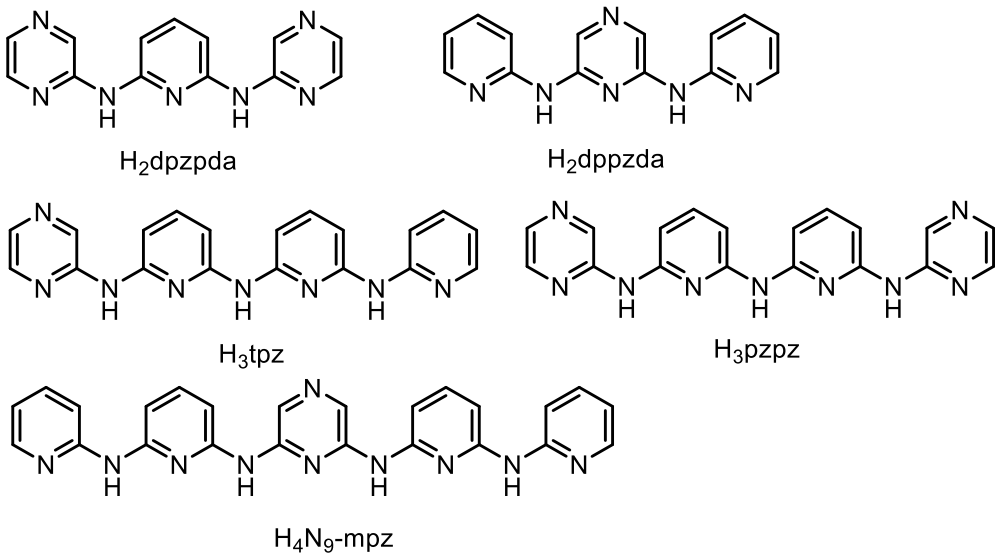


*Figure 3.18 New EMAC ligands containing pyrazine rings.*

The pyrazine-derived ligands dpzpda and dppzda have both been used to support $Cr_5$ EMACs.[150] Much like the corresponding tpda compounds, these compounds contain an

unsymmetrical Cr≡Cr···Cr≡Cr···Cr structure with alternating long and short Cr–Cr distances. The inclusion of pyrazine rings in the ligand strongly affects the redox potentials of the corresponding EMACs. As compared to $Cr_5(tpda)_4Cl_2$, the $Cr_5^{10+/11+}$ redox event is +0.3 V higher for the dppzda analog and +0.44 V higher for the dpzpda analog, indicating an overall electron-withdrawing effect of the pyrazine groups.

A similar effect on redox potentials is seen for $Co_5$ complexes supported by the dpzpda ligand. The redox potentials are raised such that a one-electron reduction from $Co_5^{10+}$ to $Co_5^{9+}$ becomes accessible. The $Co_5^{9+}$ complexes bearing axial Cl and NCS ligands were obtained by reduction of the $Co_5^{10+}$ species with hydrazine.[151] There is little variation in Co–Co distances upon reduction, and the spin state changes from $S = 1/2$ for the $Co_5^{10+}$ species to an apparent diamagnetic ground state for $Co_5^{9+}$ species. A $Ni_5^{10+}$ complex was also prepared using a modification of the dppzda ligand having 4-methyl substituents on the pyridine rings.[152] Properties of this complex are not substantively different from those of the tpda complex.

The tpz and pzpz ligands have been used to prepare linear heptanuclear EMACs with Cr, Ni, and Co. The latter metal is most notable as $Co_7$ complexes were not accessible with the teptra ligand, though the $Co_7$ tpz and pzpz compounds are consistently obtained in only 1% yield.[153] In contrast, the $Cr_7$ and $Ni_7$ complexes are obtained in more useful yields of 30-40%.[154] As in the corresponding teptra compounds, the $Cr_7$ complexes have an unsymmetrical distribution of alternating long and short Cr–Cr distances, Cr≡Cr···Cr≡Cr···Cr≡Cr···Cr, and an $S = 2$ ground state attributable to the terminal high-spin Cr(II) ion. The $Ni_7$ complexes contain high-spin Ni(II) ions at the chain termini with five square-planar, diamagnetic Ni(II) ions in between.

The $N_9$-mpz ligand has been used to prepare two linear $Cr_9$ complexes,[155] adding to the only other known nonametallic EMAC, $Ni_9(peptea)_4Cl_2$.[143] The yield for EMAC synthesis is low,

~ 1%. As in the other $Cr_n$ structures discussed here with $n$ >3, the structures contain an alternating array of long and short Cr–Cr distances: Cr≡Cr···Cr≡Cr···Cr≡Cr···Cr≡Cr···Cr. The longer distances are as long as 2.45 Å and the shortest distances are 1.97 Å, within the quadruple bond range. The terminal Cr(II) ion is again high-spin, giving rise to an $S$ = 2 ground spin state. Both complexes, with axial Cl or NCS ligands, display three quasi-reversible oxidations to $Cr_9^{19+}$, $Cr_9^{20+}$, and $Cr_9^{21+}$ species.

One new ligand has been reported that utilizes a pyrimidine ring in the backbone, the $H_2$pppmda ligand shown in Figure 3.19.[156] A $Ni_5$ complex was prepared with this ligand, and was shown to have a $Ni_5^{10+/11+}$ redox couple 0.1 V higher than in $Ni_5(tpda)_4Cl_2$, indicating that, like the pyrazine groups described above, pyrimidines are also electron withdrawing and can help to provide oxidative stability to EMACs.

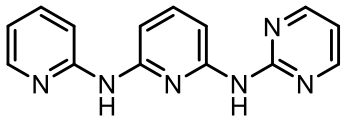


$H_2$pppmda

*Figure 3.19 Molecular structure of the $H_2$pppmda ligand.*

*3.8.3. New Ligands that Incorporate Naphthyridines.*

In addition to the issues of oxidative stability and solubility discussed above, the polypyridylamine ligand family in Figure 3.16 has another major limitation: only odd-numbered EMACs can be produced. In order to achieve the fullest possible synthetic flexibility, ligands should be developed that can also stabilize linear chains of even numbers of metal atoms. Ligands containing naphthyridine units have provided this necessary breakthrough and have led to new ligand classes for both odd-numbered and even-numbered chains. Additionally, naphthyridines, like the pyrazine and pyrimidine ligands discussed above, are electron withdrawing and provide oxidative stability to new classes of EMACs. In addition to the even- and odd-numbered chains,

naphthyridine-based ligands have also given rise to a new phenomenon: defective chains. Each of these types of compounds will be discussed below.

*3.8.3.1. Ligands Supporting Even-Numbered Metal Atom Chains.*

Several ligands, shown in Figure 3.20, have been developed to support tetrametallic EMACs. One notable pyridylamine-derived ligand has been used, but there is a larger number of naphthyridine-derived ligands that support tetrametallic chains. Both homoleptic and heteroleptic complexes have been studied, but with only Ni as the metal. In terms of the homoleptic complexes, $Ni_4^{8+}$ species $Ni_4(DAniDANy)_4$, $Ni_4(Tsdpda)_4(OH_2)_2$, $[Ni_4(Phpyany)_4Cl_2]^{2+}$, and $[Ni_4(Phpyany)_4(NCS)_2]^{2+}$ have been crystallographically characterized as well as one-electron oxidized $Ni_4^{9+}$ complexes $[Ni_4(DAniDANy)_4]^+$ and $[Ni_4(Tsdpda)_4]^+$, and one-electron reduced $Ni_4^{7+}$ complexes $[Ni_4(Phpyany)_4Cl_2]^+$ and $[Ni_4(Phpyany)_4(NCS)_2]^+$.[157-159] Heteroleptic compounds (having exclusively a *trans*-(2,2) geometry) have been prepared in two different charge states.[160] The $Ni_4^{8+}$ species *trans*-(2,2)-$[Ni_4(pyany)_2(tsdpda)_2(H_2O)Cl]^+$ and *trans*-(2,2)-$Ni_4(pyany)_2(tsdpda)_2(NCS)_2$ are obtained by one-electron oxidation of *trans*-(2,2)-$Ni_4(pyany)_2(tsdpda)_2Cl$ and ligand substitution, respectively. Reduction of $Ni_4(pyany)_2(tsdpda)_2(NCS)_2$ with hydrazine yields *trans*-(2,2)-$Ni_4(pyany)_2(tsdpda)_2(NCS)$. Interestingly, it is the $Ni_4^{7+}$ species *trans*-(2,2)-$Ni_4(pyany)_2(tsdpda)_2Cl$ that is formed in relatively high yield (67%) under the molten naphthalene EMAC synthesis conditions with two equivalents of each equatorial ligand, despite starting with a Ni source, $NiCl_2$, solely in the Ni(II) oxidation state.

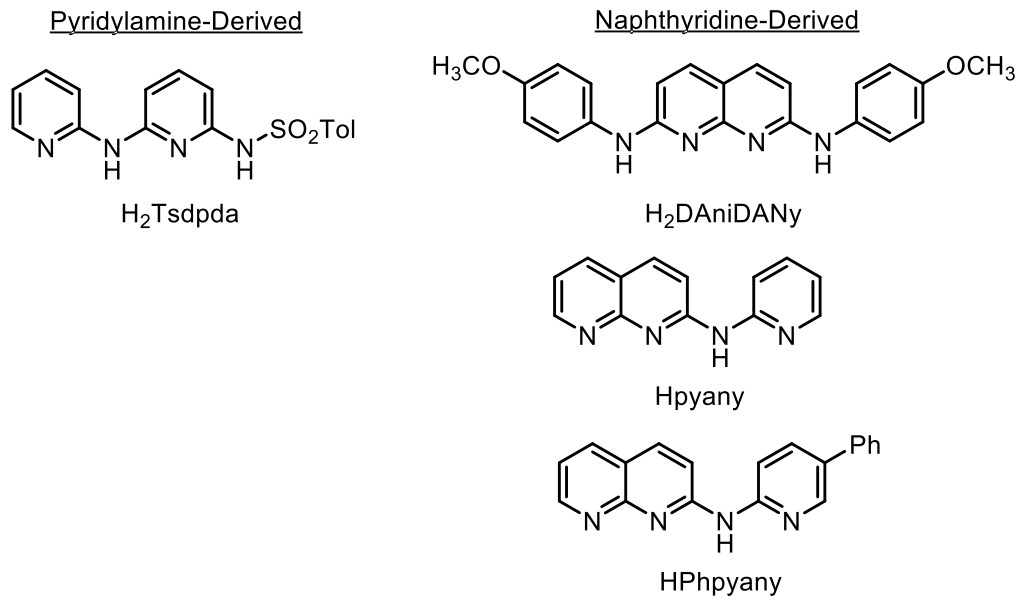


*Figure 3.20 Ligands used to stabilize linear tetrametallic chain compounds.*

Several useful trends in the magnetic properties may be gleaned from this series of $Ni_4$ complexes.[157-160] (1) Ni(II) ions in square coordination geometry are diamagnetic. (2) Axial ligands, when present, cause the terminal Ni(II) ions to which they are bound to become high-spin ($S = 1$). (3) One-electron oxidized $Ni_4^{9+}$ species contain a single unpaired electron in a delocalized σ-symmetry orbital. (4) Reduced $Ni_4^{7+}$ species have a localized, Ni–Ni-bonded $Ni_2^{3+}$ unit stabilized by naphthyridine ligands; this $Ni_2^{3+}$ unit is high-spin with $S = 3/2$ due to double exchange (electron delocalization via the Ni–Ni bond).

Two new naphthyridine-derived ligands shown in Figure 3.21 have been designed to support linear, hexametallic complexes: $H_2$bpyany and $H_2$napany. As with many of the other ligands discussed in this section, these hexadentate ligands are prepared using a sequence of Pd-catalyzed cross coupling reactions. The bpyany ligand has been used to prepare $Co_6$ complexes. Interestingly, the initial reaction product is the $Co_6^{11+}$ species $[Co_6(bpyany)_4(NCS)_2]^+$. One-electron oxidation yields the corresponding $Co_6^{12+}$ complexes.[161] A $Ni_6^{11+}$ complex has been prepared using the napany ligand, with the unsymmetrical ligands binding the $Ni_6$ chain in a (4,0)

orientation. The complex contains a terminal $[Ni_2\ (naphthyridine)_4]^{3+}$ group giving the complex an $S = 3/2$ ground spin state.[162]

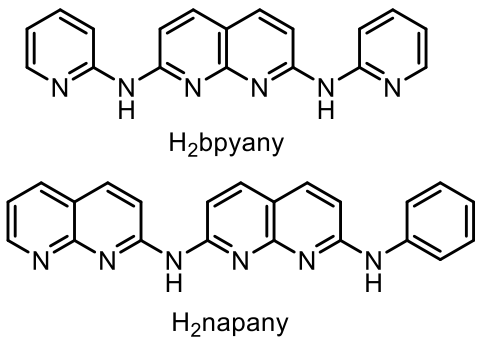


*Figure 3.21 Molecular structures of the ligands $H_2$bpyany and $H_2$napany.*

A linear, decanuclear Ni complex supported by the bdpdany ligand is the longest even-numbered EMAC reported to date, $[Ni_{10}(bdpdany)_4(NCS)_2]^{2+}$ (Figure 3.22).[163] The $Ni_{10}^{20+}$ complex contains antiferromagnetically coupled high-spin Ni(II) termini, and displays four quasi-reversible redox events: one reduction and three oxidations.

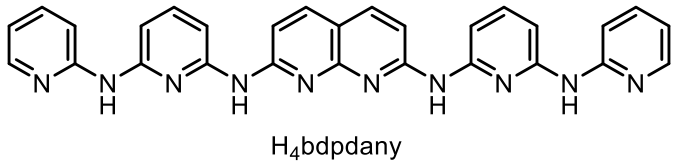


*Figure 3.22 Molecular structure of the $H_4$bdpdany ligand.*

*3.8.3.2 Ligands Supporting Odd-Numbered Metal Atom Chains.*

Naphthyridine ligands have also been designed that can support odd-numbered chains with five, seven, or up to eleven metal atoms in a linear array. The ligand bis-naphthyridylamine (Hbna, Figure 3.23) has been used to support $Ni_5$ chains in two oxidation states, both $Ni_5^{8+}$ and $Ni_5^{10+}$. The $Ni_5^{8+}$ ion $[Ni_5(bna)_4Cl_2]^{2+}$ contains two terminal antiferromagnetically coupled $S = 3/2$ $Ni_2^{3+}$ units, whereas the $Ni_5^{10+}$ species $[Ni_5(bna)_4Cl_2]^{4+}$ contains two terminal $S = 1$ high-spin Ni(II) ions.[164]

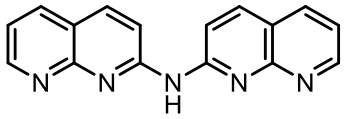


*Figure 3.23 Molecular structure of the Hbna ligand.*

The $H_3$phdptrany ligand (Figure 3.24) was designed to support linear, heptametallic chains. The complex ion (4,0)-$[Ni_7(phdptrany)_4Cl]^+$ was prepared by reaction of $H_3$phdtrany with KO$^t$Bu and $NiCl_2$ and contains a $Ni_7^{14+}$ core.[165] Interestingly, the magnetic susceptibility data indicate that, rather than containing a $\{Ni(II)\}_7$ charge distribution, the $Ni_7$ chain is mixed-valent. The complex is proposed to contain an $S$ = 3/2 $[Ni_2(naphthyridine)_4]^{3+}$ group at one terminus, and an $S$ = 1/2 $Ni_3^{7+}$ unit at the other terminus. These groups couple antiferromagnetically to yield an $S$ = 1 ground spin state.

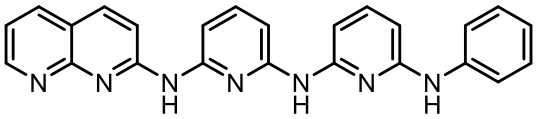


*Figure 3.24 Molecular structure of $H_3$phdptrany.*

The longest EMACs, containing chains of 11 nickel atoms, have been obtained through the use of the ligands $H_3$tentra and $H_4$bnatpya (Figure 3.25). The $[Ni_{11}(tentra)_4Cl_2]^{4+}$ and $[Ni_{11}(tentra)_4(NCS)_2]^{4+}$ ions contain a $Ni_{11}^{18+}$ core, four redox equivalents reduced from a full Ni(II) set. These four reduced equivalents occur as metal-metal bonded $Ni_2^{3+}$ units at the four sites in the chain that incorporate naphthyridine groups in the backbone.[166] The $H_4$bnatpya ligand yields the $Ni_{11}^{22+}$ complex $[Ni_{11}(bnatpya)_4Cl_2]^{4+}$, obtained in 1% yield. Ligand exchange yields $[Ni_{11}(bnatpya)_4(NCS)_2]^{4+}$ while hydrazine reduction yields $[Ni_{11}(bnatpya)_4Cl_2]^{2+}$.[5] The $Ni_{11}^{22+}$ complexes feature antiferromagnetic coupling between two terminal $S$ = 1 Ni(II) ions, and the $Ni_{11}^{20+}$ complex has two antiferromagnetically coupled $S$ = 3/2 $Ni_2^{3+}$ units.

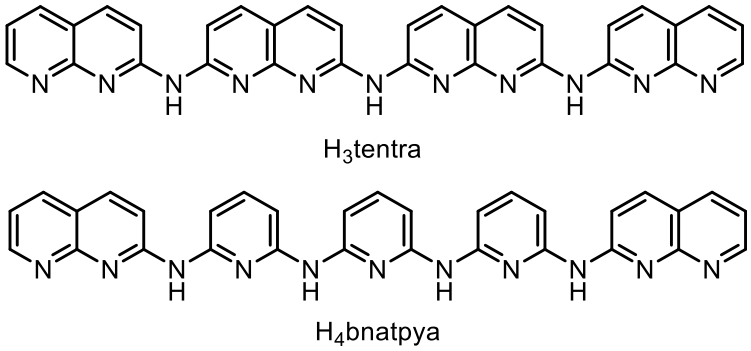


*Figure 3.25 Molecular structures of the undecadentate $H_3$tentra and $H_4$bnatpya ligands.*

*3.8.3.3. "Defective" Metal Atom Chains.*

One of the interesting things that can occur during the harsh conditions of the EMAC synthesis reactions is the formation of "defective" chains. These are compounds with one metal atom short of a full EMAC. The ligands $H_2$dpzndа and $H_2$bphpzany, although designed to support hexametallic EMACs consistently yield pentametallic EMACs with Cr, Co, or Ni, having a vacancy at one of the internal positions (Figures 3.26 and 3.27).[167-169] Interestingly, reaction of the $H_2$bphpzany ligand with $CoCl_2$ yields a mixture of $Co_6$ and defective $Co_5$ complexes.[170]

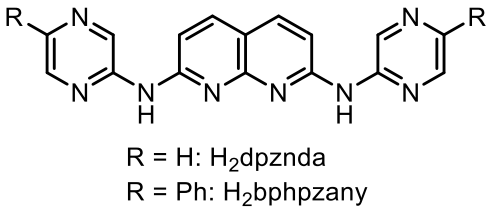


*Figure 3.26 Molecular structures of the $H_2$dpzndа and $H_2$bphpzany ligands.*

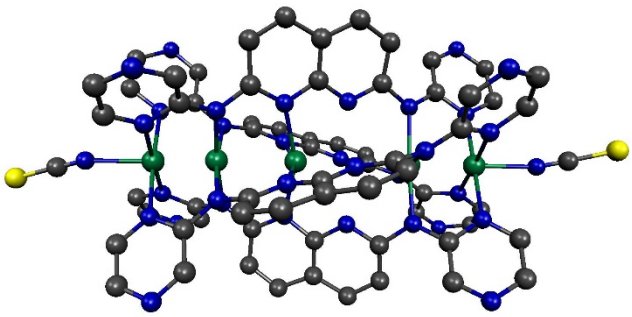

*Figure 3.27 Molecular structure of $Cr_5(dpzndа)_4(NCS)_2$.*

Defects can also occur in longer chains. Though the $H_3N_9$-2pm ligand (Figure 3.28) was designed to support a nonametallic chain, the resulting Ni complex contains only 8.33 Ni atoms. One of the internal Ni atoms shows an occupancy of 0.33, or a two-thirds vacancy.[171]

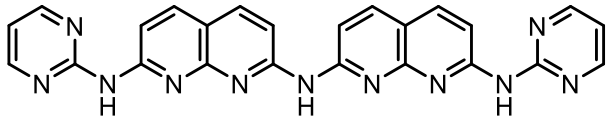


$H_3N_9$-2pm

*Figure 3.28 Molecular structure of $H_3N_9$-2pm.*

### 3.9 Summary and Outlook

Pyridylamines and related ligands are versatile and utilitarian ligands for a broad array of coordination compounds that contain metal-metal bonds. The chemistry of bimetallic compounds supported by these ligands is reaching new avenues of reactivity, including small molecule activation and catalysis. Oligomerization of pyridylamine ligands gives rise to the field of EMACs, extended metal atom chains, that present fascinating 1D chain structures with interesting magnetic and conductivity properties. These are all fruitful directions for further study, and, especially with the ease of modern Buchwald-Hartwig synthetic methods, we may anticipate the current explosion of work on pyridylamine ligands to continue into the future.

### 3.10 Acknowledgement

We are grateful to the US National Science Foundation (CHE-1700982 and CHE-1664999) and the US Department of Energy (DE-SC0016442) for support of research in our laboratory.

**3.11 References**

1. Cotton, F. A.; Murillo, C. A.; Walton, R. A., *Multiple Bonds Between Metal Atoms*. Third ed.; Springer Science and Business Media, Inc.: New York, 2005.

2. Wagner, F. R.; Noor, A.; Kempe, R., *Nat. Chem.* **2009,** *1* (7), 529-536.

3. Bear, J. L.; Han, B.; Huang, S.; Kadish, K. M., *Inorg. Chem.* **1996,** *35* (10), 3012-3021.

4. Kadish, K. M.; Wang, L.-L.; Thuriere, A.; Van Caemelbecke, E.; Bear, J. L., *Inorg. Chem.* **2003,** *42* (3), 834-843.

5. Chen, P.-J.; Sigrist, M.; Horng, E.-C.; Lin, G.-M.; Lee, G.-H.; Chen, C.-h.; Peng, S.-M., *Chem. Commun.* **2017,** *53* (34), 4673-4676.

6. Bear, J. L.; Han, B.; Wu, Z.; Van Caemelbecke, E.; Kadish, K. M., *Inorg. Chem.* **2001,** *40* (10), 2275-2281.

7. Bear, J. L.; Yao, C.-L.; Liu, L.-M.; Capdevielle, F. J.; Korp, J. D.; Albright, T. A.; Kang, S.-K.; Kadish, K. M., *Inorg. Chem.* **1989,** *28* (7), 1254-1262.

8. Kadish, K. M.; Phan, T. D.; Giribabu, L.; Van Caemelbecke, E.; Bear, J. L., *Inorg. Chem.* **2003,** *42* (26), 8663-8673.

9. Cotton, F. A.; Hillard, E. A.; Murillo, C. A.; Wang, X., *Inorg. Chem.* **2003,** *42* (19), 6063-6070.

10. Chakravarty, A. R.; Cotton, F. A.; Shamshoum, E. S., *Inorg. Chem.* **1984,** *23* (25), 4216-4221.

11. Zhang, L.; Xi, B.; Liu, I. P.-C.; Choudhuri, M. M.; Crutchley, R. J.; Updegraff, J. B.; Protasiewicz, J. D.; Ren, T., *Inorg. Chem.* **2009,** *48* (12), 5187-94.

12. Xi, B.; Xu, G.-L.; Ying, J.-W.; Han, H.-L.; Cordova, A.; Ren, T., *J. Organomet. Chem.* **2008,** *693* (8-9), 1656-1663.

13. Xu, G.-L.; Cordova, A.; Ren, T., *J. Cluster Sci.* **2004,** *15* (4), 413-424.

14. Kadish, K. M.; Nguyen, M.; Van Caemelbecke, E.; Bear, J. L., *Inorg. Chem.* **2006,** *45* (15), 5996-6003.

15. Noor, A.; Wagner, F. R.; Kempe, R., *Angew. Chem. Int. Ed.* **2008,** *47* (38), 7246-7249.

16. Chakravarty, A. R.; Cotton, F. A.; Tocher, D. A., *Inorg. Chem.* **1985,** *24* (2), 172-177.

17. Doyle, M. P.; Bagheri, V.; Wandless, T. J.; Harn, N. K.; Brinker, D. A.; Eagle, C. T.; Loh, K. L., *J. Am. Chem. Soc.* **1990,** *112* (5), 1906-1912.

18. Doyle, M. P.; Winchester, W. R.; Hoorn, J. A. A.; Lynch, V.; Simonsen, S. H.; Ghosh, R., *J. Am. Chem. Soc.* **1993,** *115* (22), 9968-9978.

19. Corcos, A. R.; Berry, J. F., *Dalton Trans.* **2017,** *46* (17), 5532-5539.

20. Xu, G.-L.; Wang, C.-Y.; Ni, Y.-H.; Goodson, T. G.; Ren, T., *Organometallics* **2005,** *24* (13), 3247-3254.

21. Fan, Y.; Liu, I. P.-C.; Fanwick, P. E.; Ren, T., *Organometallics* **2009,** *28* (13), 3959-3962.

22. Blum, A. S.; Ren, T.; Parish, D. A.; Trammell, S. A.; Moore, M. H.; Kushmerick, J. G.; Xu, G.-L.; Deschamps, J. R.; Pollack, S. K.; Shashidhar, R., *J. Am. Chem. Soc.* **2005,** *127* (28), 10010-10011.

23. Cummings, S. P.; Savchenko, J.; Fanwick, P. E.; Kharlamova, A.; Ren, T., *Organometallics* **2013,** *32* (4), 1129-1132.

24. Cao, Z.; Xi, B.; Jodoin, D. S.; Zhang, L.; Cummings, S. P.; Gao, Y.; Tyler, S. F.; Fanwick, P. E.; Crutchley, R. J.; Ren, T., *J. Am. Chem. Soc.* **2014,** *136* (34), 12174-12183.

25. Corcos, A. R.; Roy, M. D.; Killian, M. M.; Dillon, S.; Brunold, T. C.; Berry, J. F., *Inorg. Chem.* **2017,** *56* (23), 14662-14670.

26. Xi, B.; Liu, I. P.-C.; Xu, G.-L.; Choudhuri, M. M. R.; DeRosa, M. C.; Crutchley, R. J.; Ren, T., *J. Am. Chem. Soc.* **2011,** *133* (38), 15094-15104.

27. Forrest, W. P.; Choudhuri, M. M. R.; Kilyanek, S. M.; Natoli, S. N.; Prentice, B. M.; Fanwick, P. E.; Crutchley, R. J.; Ren, T., *Inorg. Chem.* **2015,** *54* (15), 7645-7652.

28. Corcos, A. R.; Berry, J. F., *Dalton Trans.* **2016,** *45* (6), 2386-2389.

29. Ren, T.; Parish, D. A.; Xu, G.-L.; Moore, M. H.; Deschamps, J. R.; Ying, J.-W.; Pollack, S. K.; Schull, T. L.; Shashidhar, R., *J. Organomet. Chem.* **2005,** *690* (21-22), 4734-4739.

30. Savchenko, J.; Cao, Z.; Natoli, S. N.; Cummings, S. P.; Prentice, B. M.; Fanwick, P. E.; Ren, T., *Organometallics* **2013,** *32* (21), 6461-6467.

31. Kadish, K. M.; Phan, T. D.; Giribabu, L.; Shao, J. G.; Wang, L.-L.; Thuriere, A.; Van Caemelbecke, E.; Bear, J. L., *Inorg. Chem.* **2004,** *43* (3), 1012-1020.

32. Nguyen, M.; Phan, T.; Van Caemelbecke, E.; Kajonkijya, W.; Bear, J. L.; Kadish, K. M., *Inorg. Chem.* **2008,** *47* (17), 7775-7783.

33. Kadish, K. M.; Garcia, R.; Phan, T.; Wellhoff, J.; Van Caemelbecke, E.; Bear, J. L., *Inorg. Chem.* **2008,** *47* (23), 11423-11428.

34. Bear, J. L.; Wellhoff, J.; Royal, G.; Caemelbecke, E. V.; Eapen, S.; Kadish, K. M., *Inorg. Chem.* **2001,** *40* (10), 2282-2286.

35. Ngubane, S.; Kadish, K. M.; Bear, J. L.; Van Caemelbecke, E.; Thuriere, A.; Ramirez, K. P., *Dalton Trans.* **2013,** *42* (10), 3571-3580.

36. Nguyen, M.; Phan, T.; Van Caemelbecke, E.; Wei, X.; Bear, J. L.; Kadish, K. M., *Inorg. Chem.* **2008,** *47* (10), 4392-4400.

37. Miyasaka, H.; Izawa, T.; Takaishi, S.; Sugimoto, K.; Sugiura, K.; Yamashita, M., *Bull. Chem. Soc. Jpn.* **2006,** *79* (4), 612-620.

38. Shi, Y.-H.; Chen, W.-Z.; John, K. D.; Da Re, R. E.; Cohn, J. L.; Xu, G.-L.; Eglin, J. L.; Sattelberger, A. P.; Hare, C. R.; Ren, T., *Inorg. Chem.* **2005,** *44* (16), 5719-5727.

39. Dequeant, M. Q.; Ren, T., *J. Cluster Sci.* **2006,** *17* (3), 479-494.

40. Deeken, S.; Motz, G.; Bezugly, V.; Borrmann, H.; Wagner, F. R.; Kempe, R., *Inorg. Chem.* **2006,** *45* (23), 9160-9162.

41. Scott, Natalie M.; Schareina, T.; Tok, O.; Kempe, R., *Eur. J. Inorg. Chem.* **2004,** *2004* (16), 3297-3304.

42. Noor, A.; Glatz, G.; Müller, R.; Kaupp, M.; Demeshko, S.; Kempe, R., *Nat. Chem.* **2009,** *1* (4), 322-325.

43. Noor, A.; Schwarz, S.; Kempe, R., *Organometallics* **2015,** *34* (11), 2122-2125.

44. Tamne, E. S.; Noor, A.; Qayyum, S.; Bauer, T.; Kempe, R., *Inorg. Chem.* **2013,** *52* (1), 329-336.

45. Schwarzmaier, C.; Noor, A.; Glatz, G.; Zabel, M.; Timoshkin, A. Y.; Cossairt, B. M.; Cummins, C. C.; Kempe, R.; Scheer, M., *Angew. Chem. Int. Ed.* **2011,** *50* (32), 7283-7286.

46. Noor, A.; Tamne, E. S.; Qayyum, S.; Bauer, T.; Kempe, R., *Chem. Eur. J.* **2011,** *17* (25), 6900-6903.

47. Noor, A.; Qayyum, S.; Bauer, T.; Schwarz, S.; Weber, B.; Kempe, R., *Chem. Commun.* **2014,** *50* (86), 13127-13130.

48. Mendoza, I.; Curado, N.; Carrasco, M.; Álvarez, E.; Peloso, R.; Rodríguez, A.; Carmona, E., *Inorg. Chim. Acta* **2015,** *424*, 120-128.

49. Curado, N.; Carrasco, M.; Álvarez, E.; Maya, C.; Peloso, R.; Rodriguez, A.; Lopez-Serrano, J.; Carmona, E., *J. Am. Chem. Soc.* **2015,** *137* (38), 12378-12387.

50. Tereniak, S. J.; Carlson, R. K.; Clouston, L. J.; Young, V. G.; Bill, E.; Maurice, R.; Chen, Y.-S.; Kim, H. J.; Gagliardi, L.; Lu, C. C., *J. Am. Chem. Soc.* **2014,** *136* (5), 1842-1855.

51. Eisenhart, R. J.; Clouston, L. J.; Lu, C. C., *Acc. Chem. Res.* **2015,** *48* (11), 2885-2894.

52. Eisenhart, R. J.; Carlson, R. K.; Clouston, L. J.; Young, V. G.; Chen, Y.-S.; Bill, E.; Gagliardi, L.; Lu, C. C., *Inorg. Chem.* **2015,** *54* (23), 11330-11338.

53. Cotton, F. A.; Kim, Y.; Yokochi, A., *Inorg. Chim. Acta* **1995,** *236* (1), 55-61.

54. Cotton, F. A.; Ren, T.; Eglin, J. L., *J. Am. Chem. Soc.* **1990,** *112* (9), 3439-3445.

55. Chakravarty, A. R.; Cotton, F. A.; Schwotzer, W., *Polyhedron* **1986,** *5* (11), 1821-1827.

56. Harvey, M. E.; Musaev, D. G.; Du Bois, J., *J. Am. Chem. Soc.* **2011,** *133* (43), 17207-17216.

57. Corcos, A. R.; Pap, J. S.; Yang, T.; Berry, J. F., *J. Am. Chem. Soc.* **2016,** *138* (31), 10032-10040.

58. Corcos, A. R.; Long, A. K. M.; Guzei, I. A.; Berry, J. F., *Eur. J. Inorg. Chem.* **2013,** *2013* (22-23), 3808-3811.

59. Brown, T. R.; Dolinar, B. S.; Hillard, E. A.; Clérac, R.; Berry, J. F., *Inorg. Chem.* **2015,** *54* (17), 8571-8589.

60. Brown, T. R.; Lange, J. P.; Mortimer, M. J.; Berry, J. F., *Inorg. Chem.* **2018,** *57* (16), 10331-10340.

61. Mashima, K.; Nakano, H.; Nakamura, A., *J. Am. Chem. Soc.* **1996,** *118* (38), 9083-9095.

62. Rüffer, T.; Ohashi, M.; Shima, A.; Mizomoto, H.; Kaneda, Y.; Mashima, K., *J. Am. Chem. Soc.* **2004,** *126* (39), 12244-12245.

63. Ohashi, M.; Shima, A.; Rüffer, T.; Mizomoto, H.; Kaneda, Y.; Mashima, K., *Inorg. Chem.* **2007,** *46* (16), 6702-6714.

64. Mashima, K.; Shimoyama, Y.; Kusumi, Y.; Fukumoto, A.; Yamagata, T.; Ohashi, M., *Eur. J. Inorg. Chem.* **2007,** (2), 235-238.

65. Pal, K.; Nakao, K.; Mashima, K., *Eur. J. Inorg. Chem.* **2010,** (36), 5668-5674.

66. Schäffler, L.; Mäller, B.; Maas, G., *Inorg. Chim. Acta* **2006,** *359* (3), 970-977.

67. Schäffler, L.; Buck, S.; Maas, G., *Inorg. Chim. Acta* **2008,** *361* (1), 109-122.

68. Li, Z. Y.; David, A.; Albani, B. A.; Pellois, J.-P.; Turro, C.; Dunbar, K. R., *J. Am. Chem. Soc.* **2014,** *136* (49), 17058-17070.

69. Ebihara, M.; Kanematsu, N.; Sakuma, T.; Noritake, S.; Kawamura, T., *Inorg. Chim. Acta* **2005,** *358* (7), 2174-2182.

70. Villarroya, B. E.; Tejel, C.; Rohmer, M.-M.; Oro, L. A.; Ciriano, M. A.; Bénard, M., *Inorg. Chem.* **2005,** *44* (19), 6536-6544.

71. del Río, M. P.; López, J. A.; Ciriano, M. A.; Tejel, C., *Chem. Eur. J.* **2013,** *19* (15), 4707-4711.

72. Umakoshi, K.; Kinoshita, I.; Ooi, S., *Inorg. Chim. Acta* **1987,** *127* (2), L41-L42.

73. Umakoshi, K.; Kinoshita, I.; Ichimura, A.; Ooi, S., *Inorg. Chem.* **1987,** *26* (21), 3551-3556.

74. Kitano, K.; Tanaka, K.; Nishioka, T.; Ichimura, A.; Kinoshita, I.; Isobe, K.; Ooi, S., *J. Chem. Soc., Dalton Trans.* **1998,** (19), 3177-3182.

75. Nishioka, T.; Kinoshita, I.; Kitano, K.; Ooi, S., *Chem. Lett.* **1992,** *21* (5), 883-886.

76. Kitano, K.; Tanaka, R.; Kimura, T.; Tsuda, T.; Shimizu, S.; Takagi, H.; Nishioka, T.; Shiomi, D.; Ichimura, A.; Kinoshita, I.; Isobe, K.; Ooi, S., *J. Chem. Soc., Dalton Trans.* **2000,** (6), 995-1000.

77. Scott, T. A.; Abbaoui, B.; Zhou, H.-C., *Inorg. Chem.* **2004,** *43* (8), 2459-2461.

78. Halder, P.; SantaLucia, D. J.; Park, S. V.; Berry, J. F., *Inorg. Chem.* **2019,** *58* (4), 2270-2274.

79. Koshiyama, T.; Omura, A.; Kato, M., *Chem. Lett.* **2004,** *33* (10), 1386-1387.

80. Mendía, A.; Cerrada, E.; Arnáiz, F. J.; Laguna, M., *Dalton Trans.* **2006,** (4), 609-616.

81. Ohba, T.; Kobayashi, A.; Chang, H.-C.; Kato, M., *Dalton Trans.* **2013,** *42* (15), 5514-5523.

82. Ibáñez, S.; Vrečko, D. N.; Estevan, F.; Hirva, P.; Sanaú, M.; Úbeda, M. A., *Dalton Trans.* **2014,** *43* (7), 2961-2970.

83. Hamaguchi, T.; Shimazaki, R.; Ando, I., *J. Mol. Struct.* **2018,** *1173*, 345-348.

84. Yoshida, M.; Shitama, H.; Sameera, W. M. C.; Kobayashi, A.; Kato, M., *Chem. Eur. J.* **2019,** *25* (32), 7669-7678.

85. Berry, J. F., Extended Metal Atom Chains. In *Multiple Bonds Between Metal Atoms*, Third ed.; Cotton, F. A.; Murillo, C. A.; Walton, R. A., Eds. Springer Science and Business Media, Inc.: New York, 2005.

86. Nippe, M.; Wang, J. F.; Bill, E.; Hope, H.; Dalal, N. S.; Berry, J. F., *J. Am. Chem. Soc.* **2010,** *132* (40), 14261-14272.

87. Hua, S.-A.; Cheng, M.-C.; Chen, C.-h.; Peng, S.-M., *Eur. J. Inorg. Chem.* **2015,** (15), 2510-2523.

88. Brogden, D. W.; Christian, J. H.; Dalal, N. S.; Berry, J. F., *Inorg. Chim. Acta* **2015,** *424*, 241-247.

89. Berry, J. F.; Cotton, F. A.; Fewox, C. S.; Lu, T.; Murillo, C. A.; Wang, X. P., *Dalton Trans.* **2004,** (15), 2297-2302.

90. Nippe, M.; Victor, E.; Berry, J. F., *Inorg. Chem.* **2009,** *48* (24), 11889-11895.

91. Berry, J. F.; Cotton, F. A.; Lin, C.; Murillo, C. A., *J. Cluster Sci.* **2004,** *15* (4), 531-541.

92. Cheng, M.-C.; Hua, S.-A.; Lv, Q. Y.; Sigrist, M.; Lee, G.-H.; Liu, Y.-C.; Chiang, M.-H.; Peng, S.-M., *Dalton Trans.* **2018,** *47* (5), 1422-1434.

93. Nippe, M.; Victor, E.; Berry, J. F., *Eur. J. Inorg. Chem.* **2008,** (36), 5569-5572.

94. Chipman, J. A.; Berry, J. F., *Inorg. Chem.* **2018,** *57* (15), 9354-9363.

95. Nippe, M.; Berry, J. F., *J. Am. Chem. Soc.* **2007,** *129* (42), 12684-12685.

96. Nippe, M.; Goodman, S. M.; Fry, C. G.; Berry, J. F., *J. Am. Chem. Soc.* **2011,** *133* (9), 2856-2859.

97. Brogden, D. W.; Turov, Y.; Nippe, M.; Li Manni, G.; Hillard, E. A.; Clérac, R.; Gagliardi, L.; Berry, J. F., *Inorg. Chem.* **2014,** *53* (9), 4777-4790.

98. Brogden, D. W.; Berry, J. F., *Chem. Commun.* **2015,** *51* (44), 9153-9156.

99. Berry, J. F.; Cotton, F. A.; Murillo, C. A., *Inorg. Chim. Acta* **2004,** *357* (13), 3847-3853.

100. Berry, J. F.; Cotton, F. A.; Lu, T.; Murillo, C. A.; Roberts, B. K.; Wang, X., *J. Am. Chem. Soc.* **2004,** *126* (22), 7082-7096.

101. Wu, L.-C.; Thomsen, M. K.; Madsen, S. R.; Schmoekel, M.; Jørgensen, M. R. V.; Cheng, M.-C.; Peng, S.-M.; Chen, Y.-S.; Overgaard, J.; Iversen, B. B., *Inorg. Chem.* **2014,** *53* (23), 12489-12498.

102. Clérac, R.; Cotton, F. A.; Daniels, L. M.; Dunbar, K. R.; Kirschbaum, K.; Murillo, C. A.; Pinkerton, A. A.; Schultz, A. J.; Wang, X., *J. Am. Chem. Soc.* **2000,** *122* (26), 6226-6236.

103. Poulsen, R. D.; Overgaard, J.; Schulman, A.; Østergaard, C.; Murillo, C. A.; Spackman, M. A.; Iversen, B. B., *J. Am. Chem. Soc.* **2009,** *131* (22), 7580-7591.

104. Madsen, S. R.; Thomsen, M. K.; Scheins, S.; Chen, Y. S.; Finkelmeier, N.; Stalke, D.; Overgaard, J.; Iversen, B. B., *Dalton Trans.* **2014,** *43* (3), 1313-1320.

105. Kuo, C.-K.; Liu, I. P.-C.; Yeh, C.-Y.; Chou, C.-H.; Tsao, T.-B.; Lee, G.-H.; Peng, S.-M., *Chem. Eur. J.* **2007,** *13* (5), 1442-1451.

106. Shih, K.-N.; Huang, M.-J.; Lu, H.-C.; Fu, M.-D.; Kuo, C.-K.; Huang, G.-C.; Lee, G.-H.; Chen, C.-h.; Peng, S.-M., *Chem. Commun.* **2010,** *46* (8), 1338-1340.

107. Miao, X.-H.; Zhu, L.-G., *Z. Anorg. Allg. Chem.* **2010,** *636* (5), 878-881.

108. Zhang, J.; Zhu, L.-G., *Z. Kristallogr. - New Cryst. Struct.* **2010,** *225* (3), 478-480.

109. Zhang, J.; Zhu, L. G., *Russ. J. Coord. Chem.* **2011,** *37* (9), 660-663.

110. Zheng, X.-F.; Zhu, L.-G., *Crystals* **2011,** *1* (3), 120-127.

111. Zhang, J.; Zhu, L.-G., *Crystengcomm* **2011,** *13* (2), 553-560.

112. Berry, J. F.; Cotton, F. A.; Murillo, C. A.; Roberts, B. K., *Inorg. Chem.* **2004,** *43* (7), 2277-2283.

113. Berry, J. F.; Cotton, F. A.; Murillo, C. A., *Organometallics* **2004,** *23* (10), 2503-2506.

114. Kuo, C.-K.; Chang, J.-C.; Yeh, C.-Y.; Lee, G.-H.; Wang, C.-C.; Peng, S.-M., *Dalton Trans.* **2005,** (22), 3696-3701.

115. Cortijo, M.; Bulicanu, V.; Pedersen, K. S.; Rouzières, M.; Bendix, J.; Clérac, R.; Hillard, E. A., *Eur. J. Inorg. Chem.* **2018,** (3-4), 320-325.

116. Srinivasan, A.; Cortijo, M.; Bulicanu, V.; Naim, A.; Clérac, R.; Sainctavit, P.; Rogalev, A.; Wilhelm, F.; Rosa, P.; Hillard, E. A., *Chem. Sci.* **2018,** *9* (5), 1136-1143.

117. Li, H.; Lee, G.-H.; Peng, S.-M., *J. Mol. Struct.* **2004,** *707* (1-3), 179-186.

118. Aydin-Canturk, D.; Nuss, H., *Z. Naturforsch., B: Chem. Sci.* **2012,** *67* (8), 759-764.

119. Huang, G.-C.; Liu, I. P.-C.; Kuo, J.-H.; Huang, Y.-L.; Yeh, C.-Y.; Lee, G.-H.; Peng, S.-M., *Dalton Trans.* **2009,** (14), 2623-2629.

120. Mohan, P. J.; Georgiev, V. P.; McGrady, J. E., *Chem. Sci.* **2012,** *3* (4), 1319-1329.

121. Georgiev, V. P.; Mohan, P. J.; DeBrincat, D.; McGrady, J. E., *Coord. Chem. Rev.* **2013,** *257* (1), 290-298.

122. Chipman, J. A.; Berry, J. F., *Chem. Rev.*, In press.

123. Nippe, M.; Bill, E.; Berry, J. F., *Inorg. Chem.* **2011,** *50* (16), 7650-7661.

124. Aydin-Canturk, D.; Nuss, H., *Z. Anorg. Allg. Chem.* **2011,** *637* (5), 543-546.

125. Turov, Y.; Berry, J. F., *Dalton Trans.* **2012,** *41* (26), 8153-8161.

126. Nippe, M.; Turov, Y.; Berry, J. F., *Inorg. Chem.* **2011,** *50* (21), 10592-10599.

127. Brogden, D. W.; Berry, J. F., *Inorg. Chem.* **2014,** *53* (21), 11354-11356.

128. Chipman, J. A.; Berry, J. F., *Chem. Eur. J.* **2018,** *24* (7), 1494-1499.

129. Huang, G.-C.; Bénard, M.; Rohmer, M.-M.; Li, L.-A.; Chiu, M.-J.; Yeh, C.-Y.; Lee, G.-H.; Peng, S.-M., *Eur. J. Inorg. Chem.* **2008,** (11), 1767-1777.

130. Rohmer, M.-M.; Liu, I. P.-C.; Lin, J.-C.; Chiu, M.-J.; Lee, C.-H.; Lee, G.-H.; Bénard, M.; López, X.; Peng, S.-M., *Angew. Chem. Int. Ed.* **2007,** *46* (19), 3533-3536.

131. Yu, L.-C.; Lee, G.-H.; Sigrist, M.; Lin, T.-S.; Peng, S.-M., *Eur. J. Inorg. Chem.* **2016,** (26), 4250-4256.

132. Nippe, M.; Timmer, G. H.; Berry, J. F., *Chem. Commun.* **2009,** (29), 4357-4359.

133. Cheng, M.-C.; Mai, C.-L.; Yeh, C.-Y.; Lee, G.-H.; Peng, S.-M., *Chem. Commun.* **2013,** *49* (72), 7938-7940.

134. Cotton, F. A.; Daniels, L. M.; Lei, P.; Murillo, C. A.; Wang, X., *Inorg. Chem.* **2001,** *40* (12), 2778-2784.

135. Huang, M.-Y.; Yeh, C.-Y.; Lee, G.-H.; Peng, S.-M., *Dalton Trans.* **2006,** (48), 5683-5690.

136. Cheng, M.-C.; Liu, I. P.-C.; Hsu, C.-H.; Lee, G.-H.; Chen, C.-h.; Peng, S.-M., *Dalton Trans.* **2012,** *41* (11), 3166-3173.

137. Yang, C.-C.; Liu, I. P.-C.; Hsu, Y.-J.; Lee, G.-H.; Chen, C.-h.; Peng, S.-M., *Eur. J. Inorg. Chem.* **2013,** (2), 263-268.

138. Tsai, C.-S.; Liu, I. P.-C.; Tien, F.-W.; Lee, G.-H.; Yeh, C.-Y.; Chen, C.-h.; Peng, S.-M., *Inorg. Chem. Commun.* **2013,** *38*, 152-155.

139. Chang, W.-C.; Chang, C.-W.; Sigrist, M.; Hua, S.-A.; Liu, T.-J.; Lee, G.-H.; Jin, B.-Y.; Chen, C.-h.; Peng, S.-M., *Chem. Commun.* **2017,** *53* (63), 8886-8889.

140. Hsieh, C.-L.; Liu, T.-J.; Song, Y.; Lee, G.-H.; Jin, B.-Y.; Lin, T.-S.; Peng, S.-M., *Dalton Trans.* **2019,** *48* (27), 9912-9915.

141. Cotton, F. A.; Chao, H.; Murillo, C. A.; Wang, Q., *Dalton Trans.* **2006,** (45), 5416-5422.

142. Cotton, F. A.; Murillo, C. A.; Wang, Q., *Inorg. Chim. Acta* **2010,** *363* (15), 4175-4180.

143. Peng, S.-M.; Wang, C.-C.; Jang, Y.-L.; Chen, Y.-H.; Li, F.-Y.; Mou, C.-Y.; Leung, M.-K., *J. Magn. Magn. Mater.* **2000,** *209* (1), 80-83.

144. Lin, S.-Y.; Chen, I.-W. P.; Chen, C.-h.; Hsieh, M.-H.; Yeh, C.-Y.; Lin, T.-W.; Chen, Y.-H.; Peng, S.-M., *J. Phys. Chem. B* **2004,** *108* (3), 959-964.

145. Yin, C. X.; Huang, G.-C.; Kuo, C.-K.; Fu, M.-D.; Lu, H.-C.; Ke, J.-H.; Shih, K.-N.; Huang, Y.-L.; Lee, G.-H.; Yeh, C.-Y.; Chen, C.-h.; Peng, S.-M., *J. Am. Chem. Soc.* **2008,** *130* (31), 10090-+.

146. Huang, M.-J.; Hua, S.-A.; Fu, M.-D.; Huang, G.-C.; Yin, C.; Ko, C.-H.; Kuo, C.-K.; Hsu, C.-H.; Lee, G.-H.; Ho, K.-Y.; Wang, C.-H.; Yang, Y.-W.; Chen, I.-C.; Peng, S.-M.; Chen, C.-h., *Chem. Eur. J.* **2014,** *20* (16), 4526-4531.

147. Hung, W.-C.; Sigrist, M.; Hua, S.-A.; Wu, L.-C.; Liu, T.-J.; Jin, B.-Y.; Lee, G.-H.; Peng, S.-M., *Chem. Commun.* **2016,** *52* (83), 12380-12382.

148. Berry, J. F.; Cotton, F. A.; Lei, P.; Lu, T.; Murillo, C. A., *Inorg. Chem.* **2003,** *42* (11), 3534-3539.

149. Berry, J. F.; Cotton, F. A.; Lu, T.; Murillo, C. A., *Inorg. Chem.* **2003,** *42* (14), 4425-4430.

150. Wang, W.-Z.; Ismayilov, R. H.; Lee, G.-H.; Huang, Y.-L.; Yeh, C.-Y.; Fu, M.-D.; Chen, C.-h.; Peng, S.-M., *New J. Chem.* **2012,** *36* (3), 632-637.

151. Wang, W.-Z.; Ismayilov, R. H.; Wang, R.-R.; Huang, Y.-L.; Yeh, C.-Y.; Lee, G.-H.; Peng, S.-M., *Dalton Trans.* **2008,** (47), 6808-6816.

152. Yin, C. X.; Huo, F.-J.; Wang, W.-Z.; Ismayiloy, R. H.; Lee, G.; Yeh, C.-Y.; Peng, S.-M.; Yang, P., *Chin. J. Chem* . **2009,** *27* (7), 1295-1299.

153. Wang, W.-Z.; Ismayilov, R. H.; Lee, G.-H.; Liu, I. P.-C.; Yeh, C.-Y.; Peng, S.-M., *Dalton Trans.* **2007,** (8), 830-839.

154. Ismayilov, R. H.; Wang, W.-Z.; Lee, G.-H.; Chien, C.-H.; Jiang, C.-H.; Chiu, C.-L.; Yeh, C.-Y.; Peng, S.-M., *Eur. J. Inorg. Chem.* **2009,** (14), 2110-2120.

155. Ismayilov, R. H.; Wang, W.-Z.; Wang, R.-R.; Yeh, C.-Y.; Lee, G.-H.; Peng, S.-M., *Chem. Commun.* **2007,** (11), 1121-1123.

156. Ismayilov, R. H.; Wang, W.-Z.; Lee, G.-H.; Peng, S.-M.; Suleimanov, B. A., *Polyhedron* **2017,** *122*, 203-209.

157. Huang, G.-C.; Hua, S.-A.; Liu, I. P.-C.; Chien, C.-H.; Kuo, J.-H.; Lee, G.-H.; Peng, S.-M., *C. R. Chim.* **2012,** *15* (2-3), 159-162.

158. López, X.; Huang, M.-Y.; Huang, G.-C.; Peng, S.-M.; Li, F.-Y.; Bénard, M.; Rohmer, M.-M., *Inorg. Chem.* **2006,** *45* (22), 9075-9084.

159. Tsou, L.-H.; Sigrist, M.; Chiang, M.-H.; Horng, E.-C.; Chen, C.-h.; Huang, S.-L.; Lee, G.-H.; Peng, S.-M., *Dalton Trans.* **2016,** *45* (43), 17281-17289.

160. Yeh, C.-W.; Liu, I. P.-C.; Wang, R.-R.; Yeh, C.-Y.; Lee, G.-H.; Peng, S.-M., *Eur. J. Inorg. Chem.* **2010,** (20), 3153-3159.

161. Chien, C.-H.; Chang, J.-C.; Yeh, C.-Y.; Lee, G.-H.; Fang, J.-M.; Peng, S.-M., *Dalton Trans.* **2006,** (17), 2106-2113.

162. Liu, I. P.-C.; Chen, C.-F.; Hua, S.-A.; Chen, C.-H.; Wang, H.-T.; Lee, G.-H.; Peng, S.-M., *Dalton Trans.* **2009,** (18), 3571-3573.

163. Kuo, J.-H.; Tsao, T.-B.; Lee, G.-H.; Lee, H.-W.; Yeh, C.-Y.; Peng, S.-M., *Eur. J. Inorg. Chem.* **2011,** (13), 2025-2028.

164. Liu, I. P.-C.; Bénard, M.; Hasanov, H.; Chen, I.-W. P.; Tseng, W.-H.; Fu, M.-D.; Rohmer, M.-M.; Chen, C.-h.; Lee, G.-H.; Peng, S.-M., *Chem. Eur. J.* **2007,** *13* (31), 8667-8677.

165. Hua, S.-A.; Huang, G.-C.; Liu, I. P.-C.; Kuo, J.-H.; Jiang, C.-H.; Chiu, C.-L.; Yeh, C.-Y.; Lee, G.-H.; Peng, S.-M., *Chem. Commun.* **2010,** *46* (27), 5018-5020.

166. Ismayilov, R. H.; Wang, W.-Z.; Lee, G.-H.; Yeh, C.-Y.; Hua, S.-A.; Song, Y.; Rohmer, M.-M.; Bénard, M.; Peng, S.-M., *Angew. Chem. Int. Ed.* **2011,** *50* (9), 2045-2048.

167. Wang, W.-Z.; Wu, Y.; Ismayilov, R. H.; Kuo, J.-H.; Yeh, C.-Y.; Lee, H.-W.; Fu, M.-D.; Chen, C.-h.; Lee, G.-H.; Peng, S.-M., *Dalton Trans.* **2014,** *43* (16), 6229-6235.

168. Wang, W.-Z.; Zhao, D.; Tsao, T.-B.; Ismayilov, R.; Lee, G.-H.; Peng, S.-M., *Eur. J. Inorg. Chem.* **2015,** (26), 4329-4334.

169. Wang, W.-Z.; Geng, S.-B.; Liu, S.; Zhao, D.; Jia, X.-G.; Wei, H.-L.; Ismayilov, R. H.; Yeh, C.-Y.; Lee, G.-H.; Peng, S.-M., *J. Mol. Struct.* **2017,** *1138*, 222-226.

170. Lin, G.-M.; Sigrist, M.; Horng, E.-C.; Chen, C.-h.; Yeh, C.-Y.; Lee, G.-H.; Peng, S.-M., *Z. Anorg. Allg. Chem.* **2015,** *641* (12-13), 2258-2265.

171. Ismayilov, R. H.; Valiyev, F. F.; Israfilov, N. V.; Wang, W.-Z.; Lee, G.-H.; Peng, S.-M.; Suleimanov, B. A., *J. Mol. Struct.* **2020,** *1200*, 126998.

# Chapter 4

*Electronic Structure of $Ru_2^{6+}$ Complexes with Electron-Rich Anilinopyridinate Ligands*

This article has been submitted for publication in *Inorganic Chemistry*

Michael D. Roy,[1] Michael J. Trenerry,[1] Biswash Thakuri,[2] Samantha N. MacMillan,[3] Matthew D. Liptak,[2] Kyle M. Lancaster,[3] and John F. Berry[1,*]

[1] Department of Chemistry, University of Wisconsin-Madison, 1101 University Ave., Madison, Wisconsin 53706, United States
[2] Department of Chemistry, University of Vermont, Burlington, Vermont 05405, United States
[3] Department of Chemistry & Chemical Biology, Baker Laboratory, Cornell University, Ithaca, New York 14853, United States

Contributions: Michael D. Roy synthesized all compounds, performed all calculations, and collected all experimental data except as noted. Michael J. Trenerry performed all electrochemical measurements. Biswash Thakuri acquired MCD spectral data. Samantha N. MacMillan collected X-ray absorbance spectral data and performed XAS modeling.

## 4.1 Abstract

Diruthenium paddlewheel complexes supported by electron rich anilinopyridinate (Xap) ligands were synthesized in order to allow for the first in-depth structural and spectroscopic interrogation of monocationic $[Ru_2(Xap)_4Cl]^+$ species in the $Ru_2^{6+}$ oxidation state. Despite paramagnetism of the compounds, $^1H$ NMR spectroscopy proved highly informative for determining the isomerism of the $Ru_2^{5+}$ and $Ru_2^{6+}$ compounds. While most compounds are found to have the polar (4,0) geometry, with all four Xap ligands in the same orientation, some synthetic procedures resulted in a mixture of (4,0) and (3,1) isomers, most notably in the case of the parent compound $Ru_2(ap)_4Cl$. The isomerism of this compound has been overlooked in previous reports. Electrochemical studies demonstrate that oxidation potentials can be tuned by the installation of electron donating groups to the ligands, increasing accessibility of the $Ru_2^{6+}$ oxidation state. The resulting $Ru_2^{6+}$ monocations were found to have the expected $(\pi^*)^2$ ground state, and an in-depth

study of the electronic transitions by Vis/NIR absorption and MCD spectroscopy with the aid of TD-DFT allowed for the assignment of the electronic spectra. The empty δ* orbital is the major acceptor orbital for the most prominent electronic transitions. Both $Ru_2^{5+}$ and $Ru_2^{6+}$ compounds were studied by Ru K-edge X-ray absorption spectroscopy; however, the rising edge energy insensitive to redox changes in the compounds studied due to the broad lineshape observed for 4d transition metal K-edges. DFT calculations indicate the presence of ligand orbitals at the frontier level, suggesting that further oxidation beyond $Ru_2^{6+}$ will be ligand-centered rather than metal-centered.

## 4.2 Introduction

Diruthenium paddlewheel complexes with metal-metal multiple bonds are of interest for their applications in magnetism,[1-10] materials,[11-13] medicine,[14-20] molecular electronics,[21-27] and reactivity/catalysis.[28-33] The vast majority of these compounds contain the mixed-valent $Ru_2^{5+}$ core supported by four monoanionic bridging ligands and one or two axial ligands. While these $Ru_2^{5+}$ compounds are abundant and well-studied,[34, 35] we and others have recently explored the chemistry of diruthenium compounds in more oxidized states, to provide a foundation for applications in O- and N-atom transfer,[30-32, 36] sulfide oxidation,[37, 38] water oxidation,[39] and catalytic C-H amination reactions.[29]

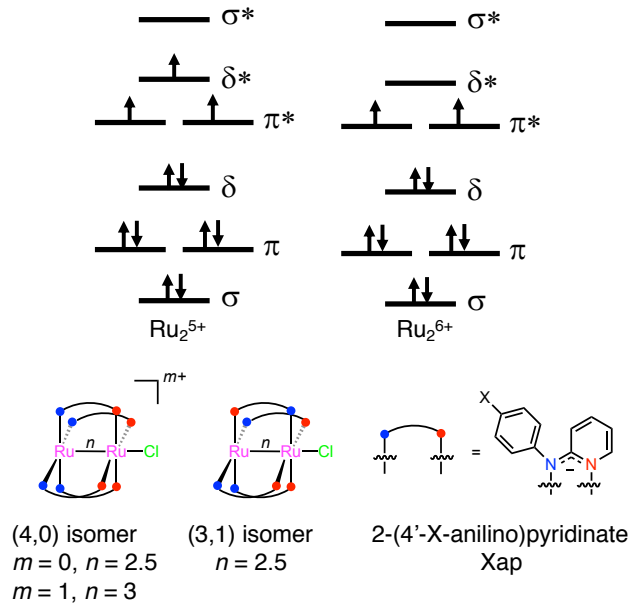


*Figure 4.1 Top: Generic representation of $Ru_2^{5+}$ (left) and $Ru_2^{6+}$ (right) orbital energy level diagrams for complexes with equatorial N-atom donors. In contrast, carboxylate ligands typically have less donation from ligand π orbitals into the δ-symmetry metal orbitals, resulting in the metal δ* orbitals being lower in energy than the π* orbitals. Bottom: Representation of $Ru_2(Xap)_4Cl$ compounds discussed in this work.*

Isolated $Ru_2^{6+}$ compounds nearly uniformly bear strongly σ-donating organometallic axial ligands, resulting in a diamagnetic $S = 0$ ground electronic state.[8, 40-42] However, in the case of weak-field ligands relevant to catalysis, the paramagnetic $S = 1$ ground electronic state is expected (Figure 4.1). Representative examples include $Ru_2(hpp)_4Cl_2$ (hpp = 1,3,4,6,7,8-hexahydro-2*H*-pyrimido[1,2-*a*]pyrimidinate), the first $S = 1$ $Ru_2^{6+}$ compound;[43, 44] Ren and coworkers' dimethylbenzamidinate (DMBA)-supported complex $Ru_2(DMBA)_4(NO_3)_2$ with labile nitrato axial ligands;[45] and $Ru_2(ap)_4Cl^+$, first reported by Cotton and Yokochi but without a definitive magnetic assignment due to the paramagnetic $FeCl_4^-$ counterion.[46] While catalytic intermediates invoke high-spin $Ru_2^{6+}$ as well as $Ru_2^{7+}$ and even $Ru_2^{8+}$,[32, 36, 39] there are exceedingly few reports of crystallographically characterized high-spin $Ru_2^{6+}$ compounds,[34] and the only crystallographically characterized $Ru_2^{7+}$ compound, a terminal nitrido compound, was prepared and studied by X-ray photocrystallography starting from a $Ru_2^{5+}$ azido compound.[28] To expand the field of high-spin, high-valent $Ru_2$ compounds, we set out to synthesize and study a systematic series of $Ru_2^{6+}$ compounds supported by modifications of the well-known 2-anilinopyridinate (ap) ligand (Figure 4.1).

While the parent compound, $Ru_2(ap)_4Cl$, **1**, and its monocation $\mathbf{1}^+$ were first reported decades ago,[46, 47] only more recently has interest in this and related compounds as potential

catalysts grown.[29, 33] Bear, Kadish, and coworkers explored the effect of electron withdrawing modifications of the ap ligand on the reduction potentials of $Ru_2(Xap)_4Cl$ compounds.[48-51] Our work emphasizes ap ligands having electron donating groups, which allows for facile structural characterization of ap-supported compounds in both the $Ru_2^{5+}$ and $Ru_2^{6+}$ oxidation states. The electronic structure of these $Ru_2^{6+}$ compounds has been examined in detail with information obtained using SQUID magnetometry, electronic absorption and magnetic-circular dichroism (MCD) spectroscopies, and X-ray absorption spectroscopy. These data, along with computational models from density functional theory (DFT) were used to probe the nature of the Ru–Ru triple bond and the energies of the π* and δ* orbitals (Fig. 4.1). Ultimately, we contextualize our results in predictions from ligand field theory, including the nature of the features in the electronic spectra and the magnitude and sign of the zero field splitting. We further demonstrate that the oxidations beyond the $Ru_2^{6+}$ level are likely to be ligand centered.

## 4.3 Results/Discussion

### *4.3.1 Synthesis, NMR Spectroscopy, and X-ray Crystallography*

Derivatives of 2-anilinopyridine were prepared in 60-80% yield by solvent-free condensation of 2-bromopyridine or 2-bromo-5-methylpyridine with the corresponding 4-substituted aniline (Figure 4.2A).[52] Following the procedure established for the synthesis of **1**,[47] an excess of molten ligand was used to prepare, in good isomeric specificity, the (4,0) isomer of $Ru_2(Meap)_4Cl$ (**3**, >90% yield), $Ru_2(OMeap)_4Cl$ (**4**, >70% yield), and $Ru_2(a(Me)p)_4Cl$ (**5**, 64% yield), from diruthenium tetraacetate chloride ($Ru_2(OAc)_4Cl$) and 2-(4'-methylanilino)pyridine (H-Meap), 2-(4'-methoxylanilino)pyridine (H-OMeap), and 2-anilino-5-methylpyridine (H-a(Me)p),

respectively (Figure 4.2B). Interestingly, when 2-(4'-chloroanilino)pyridine (H-Clap) and $Ru_2(OAc)_4Cl$ react under the same conditions, the result is an inseparable mixture of the (3,1) and (4,0) isomers of $Ru_2(Clap)_4Cl$ (**2'** and **2**, respectively), in low yield (26%, Figure 4.2C)). However, when H-Clap and $Ru_2(OAc)_4Cl$ react in refluxing toluene with an excess of LiCl present and a Soxhlet extractor charged with calcium carbonate,[53] the (4,0) isomer of $Ru_2(Clap)_4Cl$ (**2**) is exclusively obtained, though in low yield (35%, Figure 4.2D).

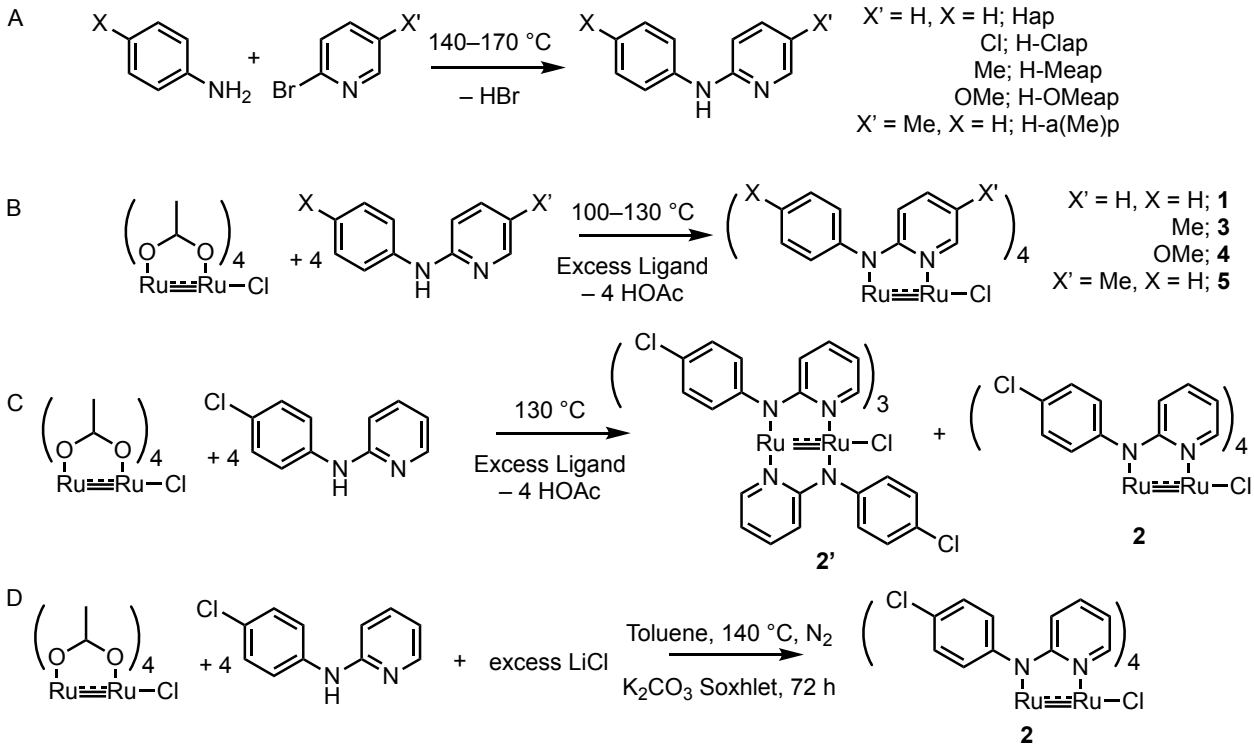


*Figure 4.2 A) Synthesis of anilinopyridine ligands; B) Reaction of $Ru_2(OAc)_4Cl$ with excess molten ligand; C) Synthesis of **2'** D) Preparation of **2**.*

The commercially available oxidant magic blue, tris(4-bromophenyl)ammoniumyl hexachloroantimonate, was found to oxidize readily all five $Ru_2^{5+}$ compounds (**1**-**5**), and the $Ru_2^{6+}$ products [**1**-**5**][$SbCl_6$] were isolated by precipitation from the $CH_2Cl_2$ reaction mixture upon addition of diethyl ether, separating the product from the soluble tris(4-bromophenyl)amine.

Analogous reactions with tris(4-bromophenyl)ammoniumyl hexafluorophosphate[54] proceed in an identical manner to give the analogous salts with alternate counterions.

Despite the paramagnetism of the compounds, $^1$H NMR spectroscopy was found to be extremely helpful in assessing both geometry and purity in both the $Ru_2^{5+}$ and $Ru_2^{6+}$ states. Notably, the NMR spectrum of the known compound **1** has never been published previously. All the $Ru_2^{5+}$ compounds have three strongly paramagnetically shifted singlet resonances at 35 – 37, -32 – -34, and -77 – -81 ppm, which have been assigned to the 3-5 positions on the pyridine, with the 6 position proton not being observed (Figure 4.3). Assignments were made through a combination of $^1$H COSY and the preparation of **5**, which has a methyl-substituted pyridine ring (Figure 4.S1, 4.S2). In the NMR spectrum of **1**, a fourth resonance with equal integration value is detected at -1 ppm and assigned to the 4-position of the aryl ring, while the $CH_3$ group in **3** is observed at -6.74 ppm. Other aryl H atoms are not observed. Compound **4** is not sufficiently soluble for NMR analysis.

Upon oxidation, there are still three strongly paramagnetically shifted proton resonances observable, assigned to pyridine H atoms. These peaks at 24 – 27, 10 – 14, and -12 – -14 ppm are assigned as the H atoms at the 3, 5, and 6 positions, respectively, with the H atom in the 5 position appearing in the diamagnetic region of the spectrum between 6 and 7 ppm. More resonances are also observed for the aryl ring compared to the $Ru_2^{5+}$ compounds, with the *para* H atom appearing at 5.98 ppm in $\mathbf{1}^+$ and the *meta* H atoms becoming detectable as a broad peak between 2 and 4

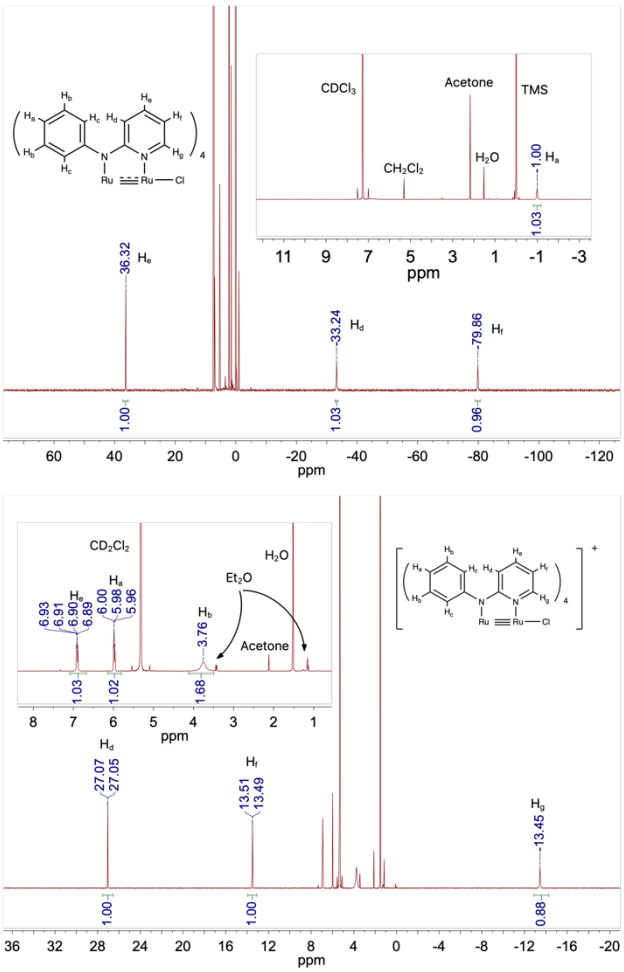


*Figure 4.3 $^1$H NMR spectra of **1** (top) and [**1**][$SbCl_6$] (bottom).*

ppm. Only the *ortho* H atoms are not observed for $Ru_2^{6+}$ compounds. Assignments were again made through a combination of $^1$H COSY and comparison with [**5**][$SbCl_6$] (Figure 4.S3, 4.S4).

The geometry of the (3,1) isomer results in two equivalent and two electronically distinct ligands, causing the singlets each to split into a 2:1:1 pattern, which is observed for **2'**. Interestingly, preparations of **1** were found to contain a similar pattern of resonances (Figure 4.S5), with crude material containing as much as 20% of the (3,1) isomer, which has previously not been recognized.[34, 55] Investigation into the crude material obtained using the published preparation of **1** revealed that both (3,1) and (4,0) isomers are obtained, but that the (3,1) isomer is significantly more soluble than the (4,0) isomer in methanol. Analytically pure (4,0)-**1** can therefore be obtained by sufficient washing. Beyond validating the usefulness of $^1$H NMR spectroscopy for these compounds, this finding also indicates that (3,1)-**1** is an isolable product, and deliberate synthesis is likely possible.

Single crystals suitable for X-ray diffraction of **2**, **2'**, and **3** were grown by slow evaporation of dichloromethane solutions, while crystals of **4** were obtained from slow evaporation of a trifluoroethanol solution. As with the parent compound,[47] **2** and **3** also crystallize in the *C*2/*c* space

group with the Ru–Ru axis oriented along the two-fold crystallographic rotation axis. Compound **2'** also crystallizes in the *C*2/*c* space group, but the molecule does not reside on a special position. Compound **4** crystallizes in the tetragonal space group *P*4*nc*, with the molecule residing on the crystallographic four-fold rotation axis. For **1-4**, the molecules pack along the major rotation axis; however, in **4**, the packing is much closer, with the Ru–Cl distance elongated by ~0.1 Å and a much shorter intermolecular Cl···Ru distance to the terminal Ru of the adjacent molecule (~3 Å for **4** and ~5 Å for **1-3**) (Fig 4.4). This intermolecular interaction likely explains the significantly decreased solubility of **4** compared to **1-3**.

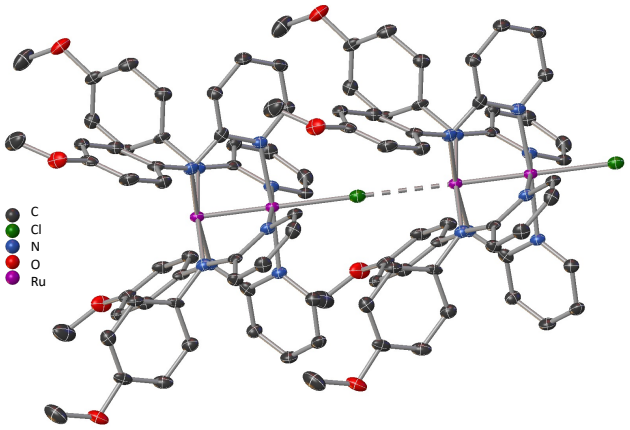


*Figure 4.4 Two molecules (eight asymmetric units) of **4** highlighting the intermolecular Cl···Ru interaction. H-atoms and individual atom labels omitted for clarity. Thermal ellipsoids drawn at 50% probability.*

Single crystals of [**1-4**][$SbCl_6$] were grown by vapor diffusion of diethyl ether into a saturated dichloromethane solution. Compounds [**1-3**][$SbCl_6$] crystallize in the monoclinic space group *P*2/*c* with both the complex and counterion positioned on adjacent crystallographic two-fold axes. Compound [**4**][$SbCl_6$] crystallizes in the tetragonal space group *I*4 with the complex and counterion alternating along the same crystallographic four-fold axis.

The key bond lengths across **2**-**4** are all similar to the parent **1**, aside from the Ru–Cl distances in **4** discussed above. In [**1**-**4**][$SbCl_6$], consistent bonding metrics are again observed. As expected for the increase in charge, the metal-ligand bond lengths decrease by ~ 0.02-0.03 Å. While the increase in Ru–Ru bond length (~0.03 Å) may be surprising, given that the formal bond order increases from 2.5 to 3 upon oxidation, this behavior is seen in other $Ru_2$ compounds and is attributed to the increased electrostatic repulsion between the two cationic Ru atoms, counterbalancing the small Ru–Ru contraction that would result from removing an electron from a δ* orbital.[34, 46]

*Table 4.1 Key bonding metrics for all compounds.*

| Compound: | Ru–Ru (Å) | Ru–$N_{py}$ (Å) | Ru–$N_{an}$ (Å) | Ru–Cl (Å) | Reference |
|---|---|---|---|---|---|
| **1** | 2.275(3)[a] | 2.10[2] | 2.03[2] | 2.437(7) | [47] |
| **2'** | 2.284(1) | 2.100(3), 2.108(3), 2.089(3), 2.040(3)[b] | 2.053(3), 2.020(3), 2.026(3), 2.086(3)[b] | 2.474(2) | This work |
| **2** | 2.276(1) | 2.104[6] | 2.033[6] | 2.471(2) | This work |
| **3** | 2.2781(9) | 2.100[3] | 2.030[3] | 2.465(1) | This work |
| **4** | 2.284(1) | 2.078(5) | 2.069(5) | 2.586(6) | This work |
| [**1**][$FeCl_4$] | 2.301(1) | 2.09[1] | 2.01[1] | 2.419(2) | [46] |
| [**1**][$SbCl_6$] | 2.3022(6) | 2.081[2] | 2.005[2] | 2.4248(7) | This work |
| [**2**][$SbCl_6$] | 2.2964(7) | 2.089[2] | 2.002[2] | 2.4430(8) | This work |
| [**3**][$SbCl_6$] | 2.302(1) | 2.084[4] | 1.999[4] | 2.444(2) | This work |
| [**4**][$SbCl_6$] | 2.296(1) | 2.077(4) | 2.009(3) | 2.452(3) | This work |

[a] Digits in curved brackets are ESDs for a single measured value, while digits in square brackets are ESDs which have been propagated for multiple averaged measured values.
[b] In **2'**, the Ru–N distance depends on which Ru atom is involved rather than the nature of the N atom, as indicated by the Ru–N distances of the ligand with the minority orientation.

*Table 4.1 Crystallographic experimental data for all compounds.*

| Compound | **2'** | **2** | **3** | **4** | **[1][SbCl$_6$]** | **[2][SbCl$_6$]** | **[3][SbCl$_6$]** | **[4][SbCl$_6$]** |
|---|---|---|---|---|---|---|---|---|
| Formula | $C_{44}H_{32}Cl_5N_8Ru_2$ | $C_{44}H_{32}Cl_5N_8Ru_2$ | $C_{48}H_{44}ClN_8Ru_2$ | $C_{48}H_{44}ClN_8O_4Ru_2$ | $C_{44}H_{36}Cl7N_8Ru_2Sb$ • 0.95 $CH_2Cl_2$ | $C_{44}H_{32}Cl_{11}N_8Ru_2Sb$ • 0.97 $CH_2Cl_2$ | $C_{48}H_{44}Cl_7N_8Ru_2Sb$ | $C_{48}H_{44}Cl_7N_8O_4Ru_2Sb$ |
| Formula weight | 1052.16 | 1052.16 | 970.50 | 1034.50 | 1329.53 | 1469.17 | 1304.95 | 1368.95 |
| Temperature/K | 100.01 | 100.01 | 100 | 100.01 | 100.0 | 100.0 | 99.99 | 100.01 |
| Crystal system | Monoclinic | Monoclinic | Monoclinic | Tetragonal | Monoclinic | Monoclinic | Monoclinic | Tetragonal |
| Space group | *C*2/c | *C*2/c | *C*2/c | *P*4nc | *P*2/c | *P*2/c | *P*2/c | *I*4 |
| a/Å | 24.098(9) | 24.016(8) | 24.204(8) | 16.000(1) | 12.706(3) | 12.722(3) | 12.030(4) | 10.330(3) |
| b/Å | 9.742(4) | 10.203(4) | 10.080(3) | 16.000(1) | 9.559(2) | 10.507(3) | 10.327(5) | 10.330(3) |
| c/Å | 35.90(2) | 20.428(8) | 20.79(1) | 7.8460(9) | 20.288(6) | 20.169(5) | 21.603(8) | 25.049(7) |
| α/° | 90 | 90 | 90 | 90 | 90 | 90 | 90 | 90 |
| β/° | 96.42(2) | 123.74(2) | 124.33(1) | 90 | 99.171(4) | 98.19(1) | 98.20(2) | 90 |
| γ/° | 90 | 90 | 90 | 90 | 90 | 90 | 90 | 90 |
| Volume/Å$^3$ | 8376(6) | 4162(3) | 4188(3) | 2008.6(4) | 2433(1) | 2669(1) | 2657(2) | 2673(2) |
| Z | 8 | 4 | 4 | 2 | 2 | 2 | 2 | 2 |
| $\rho_{calc}$g/cm$^3$ | 1.669 | 1.679 | 1.539 | 1.710 | 1.815 | 1.828 | 1.631 | 1.701 |
| μ/mm$^{-1}$ | 1.084 | 1.091 | 0.830 | 7.187 | 1.696 | 1.752 | 1.459 | 1.460 |
| Radiation | MoKα (λ = 0.71073) | MoKα (λ = 0.71073) | MoKα (λ = 0.71073) | CuKα (λ = 1.54178) | MoKα (λ = 0.71073) | MoKα (λ = 0.71073) | MoKα (λ = 0.71073) | Mo Kα (λ = 0.71073) |
| $R_{int}$ | 0.1165 | 0.1237 | 0.0765 | 0.1029 | 0.0353 | 0.0367 | 0.1061 | 0.0704 |
| Data/restraints/parameters | 8591/0/532 | 3833/0/268 | 6146/0/270 | 1846/1/146 | 9270/0/308 | 10168/0/326 | 6592/0/303 | 4111/1/164 |
| Goodness-of-fit on F$^2$ | 1.015 | 1.013 | 1.024 | 1.066 | 1.043 | 1.028 | 0.998 | 1.051 |
| Final R indexes | $R_1$ = 0.0435 | $R_1$ = 0.0408 | $R_1$ = 0.0362 | $R_1$ = 0.0325 | $R_1$ = 0.0211 | $R_1$ = 0.0198 | $R_1$ = 0.0420 | $R_1$ = 0.0297 |
| [I>=2σ (I)][a, b] | $wR_2$ = 0.0751 | $wR_2$ = 0.0750 | $wR_2$ = 0.0750 | $wR_2$ = 0.0733 | $wR_2$ = 0.0484 | $wR_2$ = 0.0450 | $wR_2$ = 0.0657 | $wR_2$ = 0.0649 |
| Final R indexes | $R_1$ = 0.0806 | $R_1$ = 0.0730 | $R_1$ = 0.0582 | $R_1$ = 0.0506 | $R_1$ = 0.0258 | $R_1$ = 0.0260 | $R_1$ = 0.0908 | $R_1$ = 0.0380 |
| [all data] | $wR_2$ = 0.0853 | $wR_2$ = 0.0843 | $wR_2$ = 0.0819 | $wR_2$ = 0.0803 | $wR_2$ = 0.0499 | $wR_2$ = 0.0471 | $wR_2$ = 0.0778 | $wR_2$ = 0.0675 |

[a] $R_1 = \sum||F_o| - |F_c||/\sum|F_o|$. [b] $wR_2 = [\sum[w(F_o^2 - F_c^2)^2]/\sum[w(F_o^2)^2]]^{1/2}$, $w = [(\sigma_{F_o^2})^2 + a^2[(1/3)F_o^2 + (2/3)F_c^2]^2]$

*4.3.2 Electrochemical Studies*

The low solubilities of **2**-**4** prevented electrochemical analysis on the $Ru_2^{5+}$ compounds directly. Therefore, the more soluble [**1**-**4**][$PF_6$] were used as analytes. Half-wave potentials ($E_{1/2}$ in V vs $Fc^{0/+}$ in $CH_2Cl_2$) of the $Ru_2^{4+/5+}$, $Ru^{5+/6+}$, and $Ru^{6+/7+}$ redox couples are plotted for complexes [**1**-**4**]$PF_6$ as functions of the sum of the Hammett parameters for the ligands' aryl functional groups (Figure 4.5; $\sum \sigma = 4\sigma_{Ar}$). For all three redox events, novel compounds [**2**-**4**][$PF_6$] match the linear free energy relationships previously observed for other (4,0) diruthenium complexes with methyl and fluoro-substituted anilinopyridinate ligands,[48, 56] demonstrating that these trends continue in the cathodic direction for complexes bearing more electron-donating substituents such as -OMe and -Me. As a point of comparison, the slope for the relationship $\Delta E_{1/2} = E_{1/2}(X) - E_{1/2}(H) = \rho(4\sigma)$, where ρ is the slope and σ is the Hammett parameter for the ligand substituent, is 0.116 V for the $Ru_2^{5+/6+}$ redox couple, while the well-studied diarylformamidinate (DArF) complexes exhibit a smaller slope of ρ = 0.085 V[57] for the $Ru_2^{5+/6+}$ redox couple of $Ru_2(DArF)_4Cl$[58] and ρ = 0.087 V for the $Mo_2^{4+/5+}$ redox couple of $Mo_2(DArF)_4$,[59, 60] though these compounds exhibit wider overall redox ranges due to the eight total substituents.

To assess the chemical reversibility of individual redox couples, we collected voltammograms of isolated redox features at multiple scan rates (Figures 4.S6-4.S9). The $Ru_2^{4+/5+}$ redox couples showed generally poor chemical reversibility in all four complexes, presumably due to the loss of the axial -Cl ligand upon reduction to the $Ru_2^{4+}$ oxidation state. By contrast, the $Ru_2^{5+/6+}$ and $Ru_2^{6+/7+}$ redox couples displayed quasireversible to fully reversible features. The $Ru_2^{6+/7+}$ features of compound [**2**][$PF_6$] uniquely showed two distinct redox events and we report both $E_{1/2}$ values, resolved by differential pulse voltammetry (Figure 4.S10), in our Hammett

analysis. Further discussion of oxidations beyond the $Ru_2^{6+}$ oxidation state is provided in the *Computational Studies* section.

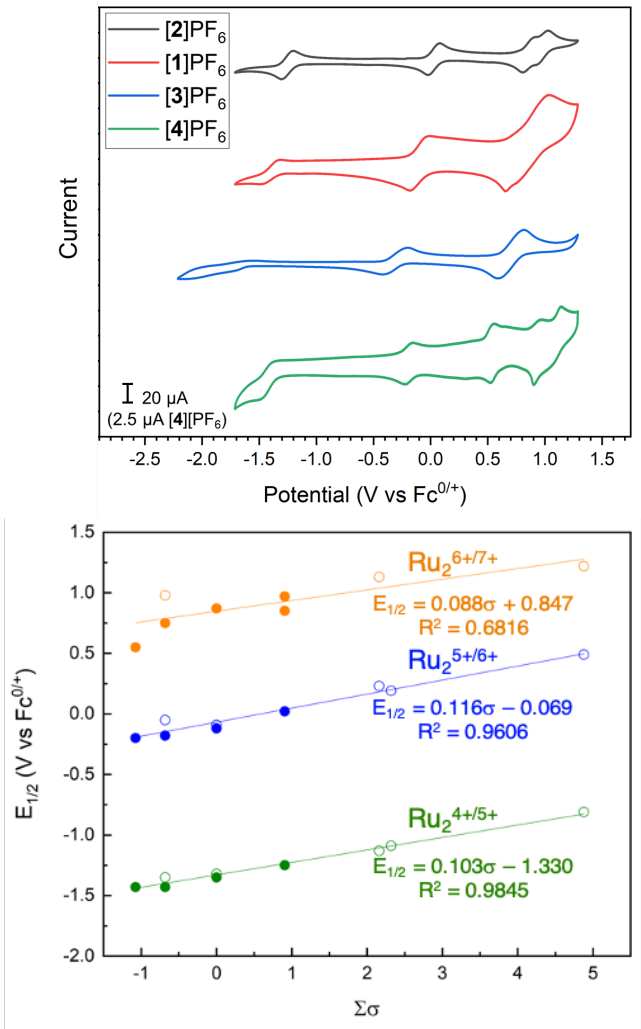


*Figure 4.5 Top: Representative cyclic voltammograms of [**1-4**][$PF_6$], collected for 1 mM [$Ru_2$] and 100 mM $Bu_4NPF_6$ solutions in $CH_2Cl_2$ at a 100 mV/s scan rate. Bottom: Linear free energy relationships for the redox reactions of (4,0) $Ru_2(L)_4Cl$ complexes examined by this work (●= [**1-4**][$SbCl_6$]) and in previous work by Bear and Kadish[48] (o, L = 2-$CH_3$ap, ap, 2-Fap, 2,6-$F_2$ap, 2,5-$F_2$ap, 2,4,6-$F_3$ap, or $F_5$ap). Half-wave potentials are shown for the $Ru_2^{4+/5+}$ (green trace), $Ru^{5+/6+}$ (blue trace), and $Ru^{6+/7+}$ (orange trace) redox couples and are reported versus the $Fc^{0/+}$ redox couple in $CH_2Cl_2$. Half-wave potentials originally reported by Bear and Kadish versus SCE in $CH_2Cl_2$ have been converted to the $Fc^{0/+}$ reference according to Ref.61.*

*4.3.3 X-ray Absorption Spectroscopy*

Ru K-edge XAS data obtained for **1**, [**1**][$PF_6$] and [**1**][$SbCl_6$] are shown in Figure 4.6. None of the spectra exhibit resolved pre-edge (1s → 4d) features; these features are generally absent in conventionally-measured 4d transition metal K-edges due to core-hole lifetime broadening.[62-64] The position of the rising edge for all three compounds is invariant (22,111 eV), despite oxidation from $Ru_2^{5+}$ to $Ru_2^{6+}$. In a prior report of $Ru_2$ XAS, a 1eV shift was observed upon oxidation from $Ru_2^{5+}$ to $Ru_2^{7+}$ (Table 4.3).[65] Given this precedent, a 0.5 eV shift is predicted for the present redox pair, which is presumably unresolved due to the aforementioned line broadening.

The EXAFS region for **1** (Figure 4.S11 and Table 4.S1) was fitted using a model featuring 4 inner-sphere N scatterers with Ru−N = 2.075 Å, 1 Ru scatterer with Ru−Ru = 2.278 Å, 0.5 Cl scatterer with Ru−Cl = 2.735 Å and 4 distal N scatterers with Ru−N = 3.004 Å. The Ru−Ru distance is in excellent agreement with the reported crystal structure (2.278(5) Å and 2.276(4) Å for EXAFS and X-ray, respectively). Fitting of the EXAFS region for the monocations (Figure 4.S12-4.S13 and Tables 4.S2-4.S3) was accomplished with the similar scattering paths. The elongation of the Ru−Ru distance upon oxidation observed in the crystal structure of [**1**][$SbCl_6$] is borne out in the EXAFS analysis, at 2.313(6) Å for [**1**][$PF_6$] and 2.307(8) Å for [**1**][$SbCl_6$], indicating that the effectively superimposable XANES correspond to unique compounds.

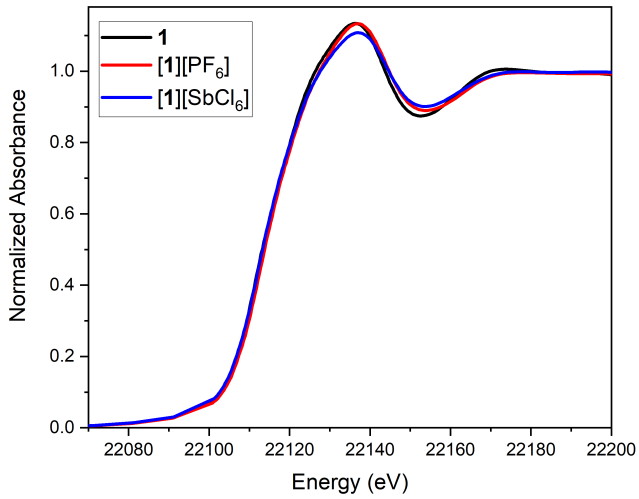


*Figure 4.6 Ru K-edge XANES data obtained for **1**, [**1**][$PF_6$] and [**1**][$SbCl_6$].*

*Table 4.3 Rising K-edge energies for $Ru_2$ complexes (dPhf = N,N'-diphenylformamidinate).*

| Compound | $Ru_2$ Oxidation State | Rising Edge (eV) | Reference |
|---|---|---|---|
| **1** | $Ru_2^{5+}$ | 22,111 | This work |
| [**1**][$PF_6$] | $Ru_2^{6+}$ | 22,111 | This work |
| [**1**][$SbCl_6$] | $Ru_2^{6+}$ | 22,111 | This work |
| $Ru_2(dPhf)_4N_3$ | $Ru_2^{5+}$ | 22,116.5 | [65] |
| $Ru_2(dPhf)_4N$ | $Ru_2^{7+}$ | 22,117.9 | [65] |

### *4.3.4 Electronic Absorption and MCD Spectroscopies*

Compounds **1**-**3** are green solids, while **4** is brown (Figure 4.S14). However, when dissolved in $CH_2Cl_2$, all **1**-**4** are green with nearly identical visible light absorption spectra (Figure 4.S15). In previous work, we were able to assign the lowest energy electronic transition as mainly having LMCT character, with partial $\delta \rightarrow \pi^*$ character.[35] Upon oxidation, [**1**-**4**][$SbCl_6$] are dark red solids, and [**1**-**3**][$SbCl_6$] are red in solution while [**4**][$SblCl_6$] is purple (Figure 4.S16).

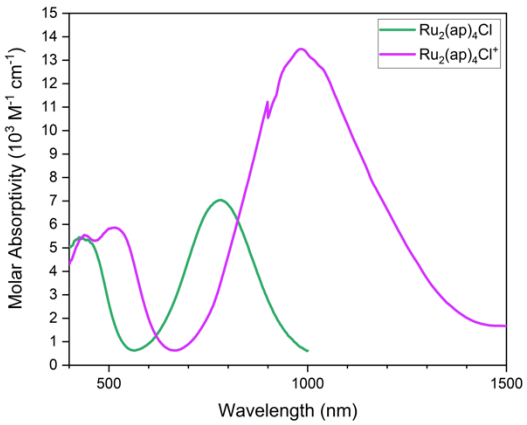


*Figure 4.7 Vis-NIR electronic spectra of **1** and [**1**][$SbCl_6$] in $CH_2Cl_2$. The discontinuity in the spectrum of [**1**][$SbCl_6$] at 900 nm is due to a change from a UV-Vis to a NIR detector.*

Spectroscopically, the two features in the $Ru_2^{5+}$ spectrum shift to lower energy and the lower energy band increases in intensity, with the higher energy feature splitting into two (Figure 4.7). To better understand the electronic transitions contributing to the spectrum, MCD spectroscopy was employed. The MCD selection rules are such that d-d transitions are comparatively more intense than charge transfer transitions. The absorption and MCD spectra were iteratively fitted with Gaussian peaks, and those peaks correlated to transitions predicted *via* time-dependent density functional theory (see *Computational Studies* below). Figure 4.8 shows that the low-energy absorption band can be modeled as a single transition with negligible MCD intensity, and the low energy transitions primarily involve excitation to the δ* orbitals. The lower energy and greater intensity of these transitions compared to those in **1** are consistent with removal of the single δ* electron in **1**, and significantly more LMCT character in $\mathbf{1}^+$. Of the higher energy bands, the red-shifted band at ~550 nm also involves excitation to the now empty δ* orbital, while the band at ~450 nm, which is unshifted relative to **1**, involves excitation from and to orbitals orthogonal to the δ*.

*Table 4.4 Transition assignments for experimental and calculated spectra.*

| **Observed Band** | **Observed Energy ($cm^{-1}$)** | **Observed ε ($M^{-1}$ $cm^{-1}$)** | **Calculated Band** | **Calculated Energy ($cm^{-1}$)** | **Calculated ε[a] ($M^{-1}$ $cm^{-1}$)** | **Assignment** |
|---|---|---|---|---|---|---|
| I | 5836 | 1414 | i[b] | 5056 | 887 | *e*(N) → δ*($Ru_2$) |
| II | 7403 | 0 | ii[b] | 10014 | 2020 | *e/a*(N) → δ*/π* ($Ru_2$) |
| III | 7800 | 0 | iii[b] | 10308 | 892 | *a*(N) → π*($Ru_2$) |
| IV | 10175 | 13069 | iv[b] | 11907 | 14734 | *e*(N)/π*($Ru_2$) → δ*($Ru_2$) |
| V | 13049 | 760 | v[b] | 15622 | 555 | Ligand aryl → δ*($Ru_2$) |
| VI | 16118 | 0 | vi[b] | 17513 | 1052 | Ligand aryl → δ*($Ru_2$) |
| VII | 18679 | 2753 | vii[b] | 18228 | 8047 | Ligand aryl/$\pi_{nb}$($Ru_2Cl$) → δ*($Ru_2$) |
| VIII | 19082 | 2464 | viii | 18916 | 5052 | Ligand aryl/δ($Ru_2$) → δ*($Ru_2$) |
| IX | 21660 | 2820 | $ix_a$[b] | 19521 | 1155 | Ligand aryl → δ*($Ru_2$) |
| | | | $ix_b$[b] | 19739 | 2969 | *e*(N) → σ*($Ru_2$) |
| X | 23439 | 3267 | $x_a$[b] | 22382 | 1289 | $\sigma_{nb}$($Ru_2Cl$)/Ligand → π*($Ru_2$) |
| | | | $x_b$[b] | 22891 | 2991 | *e*(N)/π*($Ru_2$) → σ*($Ru_2$) |
| XI | 26058 | 2135 | xi | 25220 | 1749 | $\pi_{nb}$($Ru_2Cl$) → π*($Ru_2$) |
| XII | 28007 | 3351 | xii | 31027 | 3367 | Ligand pyr → π*($Ru_2$) |

[a]ε calculated using Gaussian line width of 2000 $cm^{-1}$. [b]Two near-degenerate transitions are averaged to calculate energy and ε.

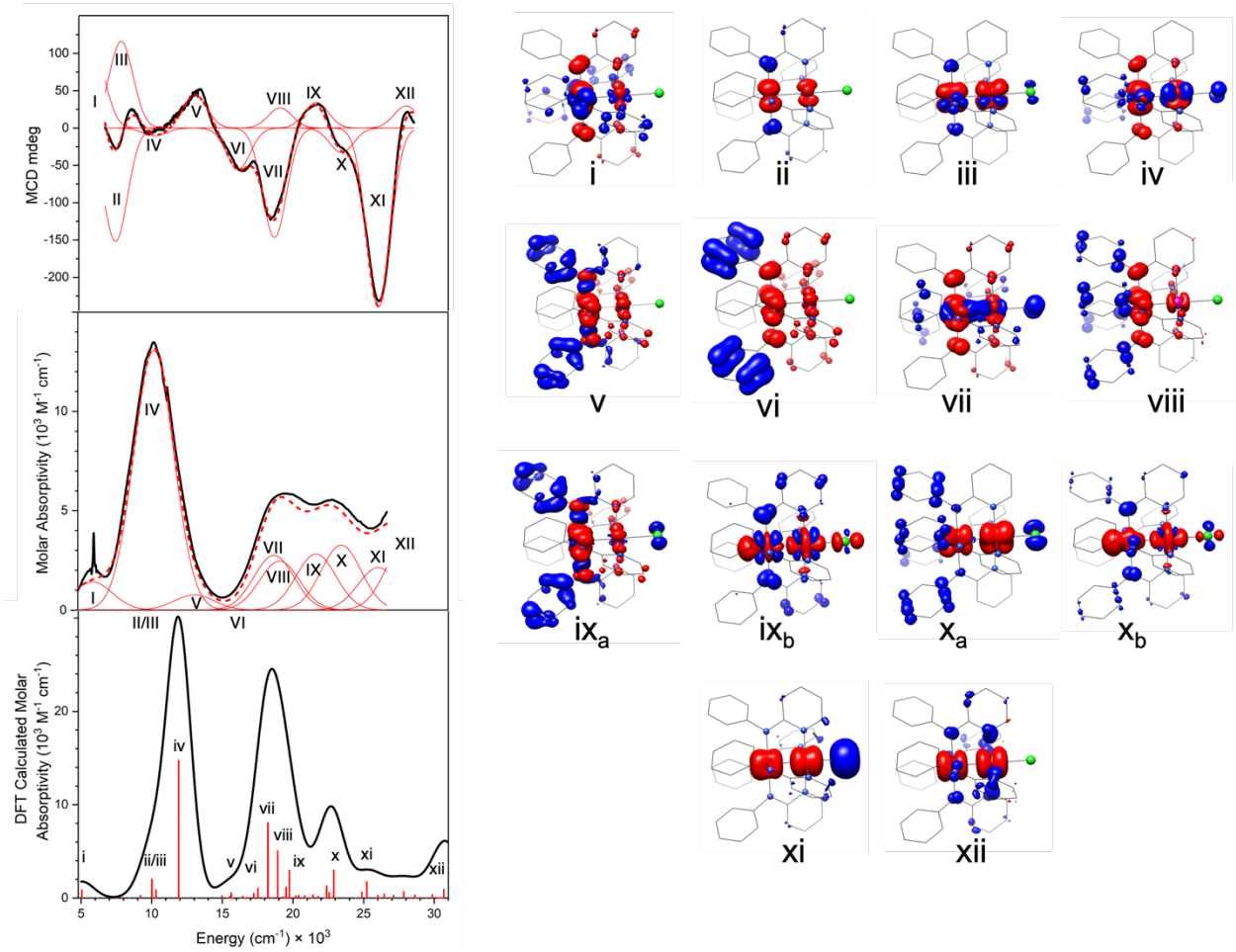


Figure 4.8 MCD (top), Vis-NIR (middle), and TD-DFT transitions (bottom) of [**1**]$SbCl_6$ in $CH_2Cl_2$ with electron density difference maps plotted to the right, where blue and red indicate the loss and gain of electron density, respectively. MCD data was acquired at 4.5 K on a mull of [**1**]$SbCl_6$ with poly(dimethylsiloxane). Vis-NIR data was collected at room temperature from a solution of [**1**]$SbCl_6$ in $CH_2Cl_2$. TD-DFT calculations are for 298 K with $CH_2Cl_2$ solvation.

### *4.3.5 Magnetometry*

The electronic structure of **1** has been studied previously, and the $S = 3/2$ ground electronic state is evident from EPR spectroscopy and SQUID magnetometry.[35] Based on the nearly identical spectroscopic features of **1**–**4**, we assign $S = 3/2$ as the ground electronic state for all of the $Ru_2^{5+}$ compounds discussed herein.

In comparison, $Ru_2^{6+}$ compounds can exhibit $S = 0$, 1, or 2 ground electronic states. The cation [**1**]$^+$ was previously studied as a salt with the $FeCl_4^-$ counterion; due to the paramagnetism

of the anion, magnetic susceptibility measurements of [**1**][$FeCl_4$] were not performed. Nevertheless, an $S$ = 1 ground state was inferred from structural arguments.[46] While the paramagnetic shifting of the $^1$H NMR spectra reported here are suggestive of an $S$ = 1 ground state, variable temperature magnetic susceptibility of [**1**][$SbCl_6$] was measured to confirm this assignment (Figure 4.9). At room temperature, a $\chi \cdot T$ value of ~ 1.3 emu·K/mol is observed, somewhat higher than the spin-only value expected for $S$ = 1 (1.0 emu·K/mol), but nowhere near as high as expected for $S$ = 2 (3.0 emu·K/mol). As temperature is lowered, the $\chi \cdot T$ data show a dramatic decrease, reaching ~ 0 emu·K/mol at the lowest temperature recorded. This behavior is consistent with an extraordinarily large zero-field splitting of the $S$ = 1 state, as has been documented for other $Ru_2^{6+}$ compounds.[66, 67] The data were modelled as an $S$ = 1 system using a fixed isotropic $g$ factor of 2.00 and large, positive axial zero-field splitting ($D$ = 196 cm$^{-1}$). Free refinement of isotropic or anisotropic $g$ factors did not meaningfully improve the quality of the model. Though few other $S$ = 1 $Ru_2^{6+}$ examples are known, reported values of $D$ range from 168 to 261 cm$^{-1}$.[66, 67] A large temperature-independent paramagnetism term (1.34 10$^{-3}$ emu/mol) was included to account for the larger-than-expected value for the room temperature magnetic susceptibility.

The trend in the $\chi$T plot toward zero at low temperatures indicates that the lowest energy $m_s$ state is the $m_s$ = 0 term of the $S$ = 1 multiplet. This allows for unambiguous assignment of the sign of the zero field splitting as positive. Due to the large zero field splitting and $m_s$ = 0 ground state, no saturation behavior is observed in low temperature magnetization measurements up to 7 T (Figure 4.S17). As a result, the VT magnetic susceptibility data cannot be simultaneously fitted with reduced magnetization data, preventing the rhombic component of the zero field splitting, $E$, from being modeled, as the fit of the susceptibility data alone is insensitive to $E$.

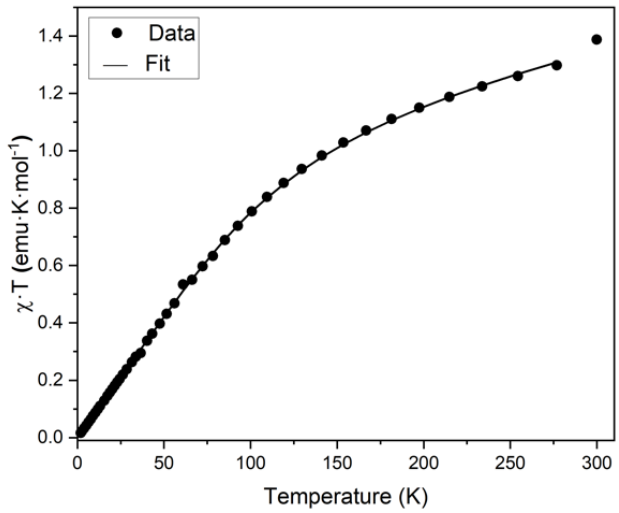


*Figure 4.9 Variable temperature SQUID magnetometry data for [**1**]SbCl$_6$.*

*Table 4.5 Fitting parameters for magnetic data.*

| | *g* | *D* (cm$^{-1}$) | *E* (cm$^{-1}$) | z*J* (cm$^{-1}$) | TIP (emu/mol) | Residual | Reference |
|---|---|---|---|---|---|---|---|
| **1** | 2.00 (fixed) | 56.9(8) | 15(1) | –0.188(4) | $1.59(2) \times 10^{-3}$ | $1.8 \times 10^{-3}$ | [35] |
| [**1**][SbCl$_6$] | 2.00 (fixed) | 195.8(8) | Not Fitted | Not Fitted | $1.34(1) \times 10^{-3}$ | $1.4 \times 10^{-3}$ | This work |

*Residuals calculated as the sum of squares between experimental and calculated data points.[68]

### *4.3.6 Resonance Raman Spectroscopy*

To probe the Ru–Ru bond stretching frequency as a function of Ru$_2$ oxidation state, resonance Raman spectroscopy was performed on a frozen $CH_2Cl_2$ solution of [**1**][PF$_6$] using 514 nm excitation (Figure 4.10). A stretch at 334 cm$^{-1}$ in the spectrum matches well with the calculated Ru–Ru stretching frequency of 334 cm$^{-1}$ (see below). In **1**, the Ru–Ru stretch is coupled with a rocking motion of the pyridine, giving a Fermi pair of vibrations at 345 and 421 cm$^{-1}$.[35] As indicated by the crystallographic data, the Ru-Ru bond length is longer for the Ru$_2^{6+}$ compound than the Ru$_2^{5+}$ compound, despite the increase in formal bond order. This change is consistent with

the decrease in bond stretching frequency. These data can be compared to the $[Ru(OEP)]_2^{n+}$ (OEP = octaethylporphyrin, $n$ = 0, 1, 2) series, where the Ru–Ru stretching frequency increases from 301 to 310 $cm^{-1}$ upon oxidation from $Ru_2^{5+}$ to $Ru_2^{6+}$ (Table 4.6).[69] In this system, however, the Ru–Ru bond length is estimated to decrease from 2.33 to 2.30 Å. Despite similar Ru–Ru bond lengths in the $Ru_2^{6+}$ examples, the higher stretching frequency for [**1**][$PF_6$] clearly indicates that the anilinopyridinate-supported Ru–Ru bond is stronger. Furthermore, the electrostatic repulsion between the Ru cations contributes more to the observed Ru–Ru distance in the anilinopyridinate compounds than the removal of antibonding electrons, contrary to the OEP system studied earlier.

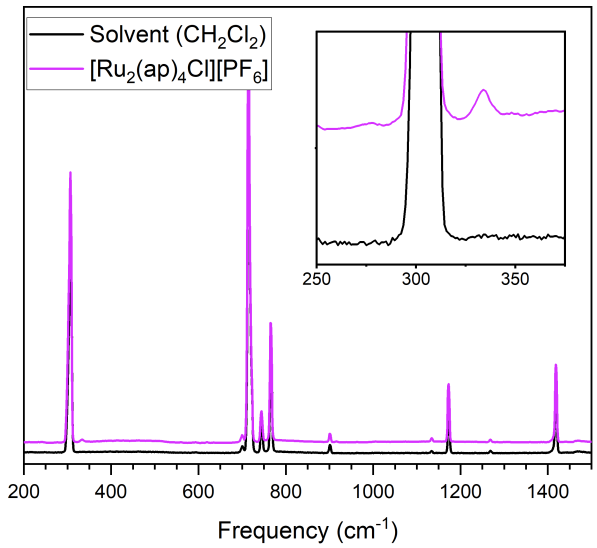


*Figure 4.10 Resonance Raman spectra of [**1**][$PF_6$] in frozen $CH_2Cl_2$ (purple) and pure frozen $CH_2Cl_2$ (black).*

*Table 4.6 Ru–Ru bond distances and stretching frequencies for $Ru_2(ap)_4Cl^{0/+}$ and $[Ru(OEP)]_2^{+/2+}$.*

| Compound | Ru–Ru distance (Å) | Ru–Ru stretching frequency ($cm^{-1}$) | Reference |
|---|---|---|---|
| **1** | 2.275(3) | 345 and 421 (Fermi) | [35, 47] |
| **1**$^{+\,a}$ | 2.3022(6) | 334 | This work |
| $[Ru(OEP)]_2^{+\,b}$ | 2.33$^c$ | 301 | [69] |
| $[Ru(OEP)]_2^{2+\,b}$ | 2.30$^c$ | 310 | [69] |

[a] Crystallographic distance reported for [**1**][$SbCl_6$] while resonance Raman reported for [**1**][$PF_6$].
[b] All data reported with $BF_4^-$ counterions.
[c] Bond distances estimated from empirical bond distance / force constant correlations.

*4.3.7 Computational Studies*

DFT calculations, including predictions of the physical properties discussed above, were performed to provide a detailed electronic structure consistent with experimental measurements. Optimized geometries for **1**-**4** and [**1**-**4**]$^+$ were calculated based on initial crystal structure coordinates. The calculated bond distances were in good agreement with experimental values, with Ru–Ru distances overestimated by only ~0.03 Å, and Ru–Cl and Ru–N distances overestimated by ~ 0.06 Å, with **4** having the Ru–Cl distance underestimated due to the aforementioned elongation caused by intermolecular interactions observed in the crystal structure. The calculated redox potentials for the $Ru_2^{5+/6+}$ couple correlate well with experimental values, though a constant offset is observed, consistent with other B3LYP calculations of redox potentials.[70] Importantly, the slope of the calculated redox potentials as a function of Hammett parameters, 0.13 V/σ, is in good agreement with the experimental slope, 0.12 V/σ (Figures 4.5, 4.S18). As noted above, the calculated vibrational frequency of the Ru–Ru stretch and electronic transitions modeled *via* TD-DFT matched well with experiment, leading further credence to the validity of the computational model.

The electronic ground state of **1** is known to be $(\pi^*)^2(\delta^*)^1$, and the electronic ground state of the $Ru_2^{6+}$ $S = 1$ compounds investigated here is expected to be $(\pi^*)^2$. DFT calculations support these ground states for [**1**-**4**] and [**1**-**4**]$^+$, though careful analysis reveals filled ligand-based orbitals intermingled with these singly-occupied metal-centered orbitals (Figure 4.11). The HOMO of the anilinopyridinate ligands has a dominant contribution from the *p* orbital on the anilino nitrogen atom, and the combination of four of these orbitals in $C_4$ symmetry result in *a*, *b*, and *e* combinations. The *b* combination shares symmetry with the $Ru_2$ δ bonding and antibonding orbitals, and is responsible for the raising of the δ* orbital energy above that of the π* orbitals.

However, the *a* and *e* combinations of ap orbitals are also higher in energy than the singly occupied π* orbitals, though spin polarization causes the vacant π* orbitals to be higher in energy. The interloping ligand orbitals have profound implications for higher oxidation state compounds, as oxidation beyond $Ru_2^{6+}$ would likely result in formation of a complex with a ligand radical rather than a formally $Ru_2^{7+}$ core, despite the common practice of labeling the electrochemical feature as $Ru_2^{6+/7+}$. This dicationic compound could have either an $S = 1/2$ or $S = 3/2$ ground electronic state, depending on the nature and magnitude of coupling between the $Ru_2$ $(\pi^*)^2$ electrons and the ligand radical. While such ligand-based radicals have been invoked for oxidation of $Ni_2^{4+}$ and $Pd_2^{4+}$ paddlewheel-type compounds, further analysis ultimately concluded that oxidation took place from metal-centered orbitals, resulting in $Ni_2^{5+}$ and $Pd_2^{5+}$ species.[71-73] Based on the robust computational methods and strong agreement with experimental measures, we are confident in the orbital assignments depicted here. One further prediction that can be made on the basis of this electronic structure is that true $Ru_2^{7+}$ species will only be accessible if they are supported by π-donor axial ligands strongly donating enough to raise the π* orbitals above the ligand orbitals, as would be expected for the oxo or nitrido complexes postulated as important intermediates in previous studies.[30-32, 36-39]

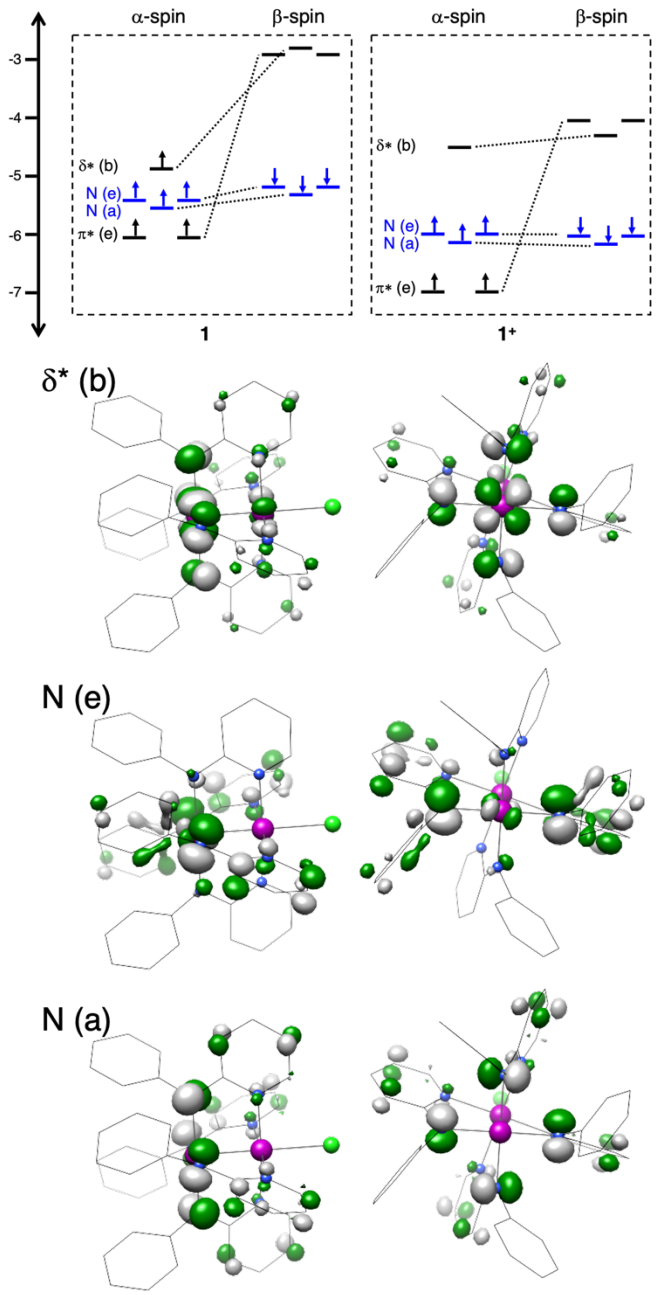


*Figure 4.11 Calculated orbital energy level diagram for **1** (top left) and **1**$^+$ (top right) with ligand-based orbitals highlighted in blue. Boundary surface plots of the δ*, N (e), and N(a) α-spin orbitals for **1**$^+$ from top to bottom, viewed along two different axes (left, right). Full 3D models of these orbitals are available in the Supporting Information.*

## 4.4 Conclusions

We present here synthesis and characterization for several novel $Ru_2$ paddlewheel complexes in both the $Ru_2^{5+}$ and $Ru_2^{6+}$ oxidation states, with $^1$H NMR analysis offering a

previously untapped wealth of information. Trends in reduction potential based on ligand substitution extend previous work for new electron-rich ligands. Comprehensive analysis of the $Ru_2^{6+}$ oxidation state confirms the expected $(\pi^*)^2$ ground electronic state, and the DFT calculated electronic structure indicates that the actual highest occupied molecular orbitals are ligand-based, explaining why attempts to isolate more oxidized diruthenium compounds have been largely unsuccessful in the past.

## 4.5 Methods

### *4.5.1 Physical Measurements*

Electrospray ionization mass spectrometry was performed with a Thermo Q Exactive Plus mass spectrometer. IR spectra were recorded with a Bruker Tensor 27 spectrometer using an ATR adapter. Vis/NIR spectra were obtained using a StellarNet tungsten halogen source, a BLACK-Comet UV/Vis spectrometer, and a DWARF-Star NIR spectrometer equipped with a 10 mm path length dip probe tip. Elemental analysis was performed by Midwest Microlab, LLC in Indianapolis, IN, USA. $^1$H NMR spectra were recorded on 400 MHz and 500 MHz Bruker Avance III spectrometers.

### *4.5.2 Crystallography*

Crystallographc data were collected at the Molecular Structure Laboratory of the Chemistry Department of the University of Wisconsin-Madison. Suitable single crystals of **2**-**4**, **2'**, and [**1**-**4**][$SbCl_6$] were selected under oil and ambient conditions. The crystals were attached to the tip of a MiTeGen MicroMount©, mounted in a stream of cold nitrogen at 100(1) K, and centered in the X-ray beam using a video monitoring system. Crystal evaluation and data collection were performed on a Bruker Quazar SMART APEX-II diffractometer with Mo K$\alpha$ ($\lambda$ = 0.71073 Å)

radiation. The data were collected using a routine to survey reciprocal space and were indexed by the APEX program.[74] The structures were solved *via* intrinsic phasing and refined by iterative cycles of least-squares refinement on $F^2$ followed by difference Fourier synthesis. All hydrogen atoms were included in the final structure factor calculation at idealized positions and were allowed to ride on the neighboring atoms with relative isotropic displacement coefficients. Absorption corrections were based on a fitted function to the empirical transmission surface as sampled by multiple equivalent measurements.[75] A highly disordered $CH_2Cl_2$ molecule was present in the structure of [**4**][$SbCl_6$]. The dataset was treated with SQUEEZE and approximately 43 electrons (c.f., $CH_2Cl_2$ contains 42 electrons) were accounted for in the solvent accessible void.[76] Crystallographic solution and refinement parameters are given in Table 2.

*4.5.3 Electrochemistry*

Electrochemical experiments were performed in a nitrogen-filled glovebox using a BioLogic SP-200 potentiostat in dry, degassed $CH_2Cl_2$ (Fisher, HPLC-grade, non-stabilized) containing 100 mM $Bu_4NPF_6$ (tetrabutylammonium hexafluorophosphate, Aldrich, 98%) as the supporting electrolyte. $Bu_4NPF_6$ was purified by thermal recrystallization from ethyl acetate prior to use. A three-electrode setup was employed in all cyclic voltammetry and differential pulse voltammetry experiments, using a glassy carbon disk working electrode (3 mm diameter, CH Instruments), a platinum wire counter electrode (CH Instruments), and a silver wire reference electrode and capillary (Pine Research). The glassy carbon working electrode was polished with an alumina and water slurry (0.05 μm particle size, BASi Research Products), rinsed with methanol, and dried before use. All working electrode potentials were measured versus a $Ag/AgNO_3$ reference electrode containing an internal solution of 100 mM $Bu_4NPF_6$ and 10 mM $AgNO_3$ in $CH_3CN$. The Ag electrode was lightly polished with 600 grit sandpaper to remove any surface corrosion before

use. Solid ferrocene was dissolved in analyte solution at the end of each experiment to provide an internal reference for calibrating potentials to the $Fc^{0/+}$ redox couple in $CH_2Cl_2$.

*4.5.4 X-ray Absorption Spectroscopy*

Solid samples were diluted in BN, finely ground in an agate mortar, pressed into 1 mm Al spacers, and sealed with 38 μm Kapton tape. Ru K-edge XAS spectra were collected at the Stanford Synchrotron Radiation Lightsource (SSRL) at beamline 9-3. Beamline 9-3 is equipped with a 16-pole, 2-Tesla wiggler source. Incident X-ray radiation was monochromated using a double Si(220) crystal monochromator; samples were maintained at 10 K in a liquid He cryostat during data collection. Spectra were collected in fluorescence mode, with X-rays detected by a passivated implanted planar silicon (PIPS) detector placed at a 90° angle to the sample. Inelastic scatter was attenuated using Soller slits fitted with a Mo filter. Ru foil and a third ionization chamber upstream of the sample were used for internal energy calibration, setting the first inflection point of the Ru foil scan to 22117.0 eV. Data were collected from 21890 to 23111 eV ($k = 16$ Å$^{-1}$). Two to four scans were averaged and processed using the program Athena of the Demeter package.[77] A smooth pre-edge background was removed from each averaged spectrum by fitting a second-order polynomial to the pre-edge region and subtracting this polynomial from the entire spectrum. A polynomial spline was subtracted above $E_0 = 22130$ eV and the data were normalized in the post-edge absorption to 1.0. Extended X-ray absorption fine structure (EXAFS) fitting was performed using FEFF6 calculations as implemented in the program Artemis, also part of the Demeter package. Scattering paths were initially determined from FEFF calculations using input coordinates based on the X-ray crystal structure of **1**. Paths were optimized by least-squares fitting, where floated parameters included the interatomic scattering distances (R), and the Debye-Waller thermal factors ($\sigma^2$).

*4.5.5 Magnetometry*

SQUID data were collected on a powder sample of **1**[$SbCl_6$] contained in a gel capsule using a Quantum Design MPMS 3 SQUID magnetometer. Magnetic susceptibility data were collected in an externally applied magnetic field of 0.1 T (1000 G) from 2 to 300 K. Magnetization data were collected at 2, 4, 8, and 12 K from 0–7 T, but saturation behavior was not observed at any temperature and these data were not fitted. Magnetic susceptibility data were fitted using the software program PHI.[78] A range of different fitting models were examined, including ones in which the *g* tensor was refined isotropically or anisotropically, and with either both axial and rhombic ZFS tensor components or just an axial component. Ultimately, we selected a model that provided the best fit to the data with the smallest number of unique parameters that gave well-defined and physically reasonable results. In the final model, the *g* value was fixed at 2.00 and the rhombic ZFS component (*E*) was omitted as it had no impact on the fit.

*4.5.6 Magnetic Circular Dichroism (MCD)*

A mull of **1**[$SbCl_6$] was prepared by grinding a powder sample with poly(dimthylsiloxane). The mull was pressed between quartz windows and mounted in an MCD cell before being flash frozen with liquid nitrogen. MCD spectra were collected at 4.5 K and 3, 5, and 7 T using a Jasco J-1700 spectropolarimeter and an Oxford SM4000-8T Spectromag controlled by a Mercuty iTC temperature controller and a Mercury iPS power supply.

*4.5.7 Resonance Raman Spectroscopy*

Resonance Raman data were collected on a frozen solution sample of **1**[$PF_6$] dissolved in $CH_2Cl_2$ mounted in a quartz finger dewar filled with liquid nitrogen. A Coherent I-305 $Ar^+$ ion laser (514.5 nm) was used as the excitation source, and ~135° backscattered light was dispersed by an Acton Research triple monochromator equipped with 1200 and 2400 grooves/mm gratings. Dispersed

light was analyzed by a Princeton Instruments Spec X:100BR deep depletion, back-thinned CCD camera. Data were collected with a laser power of 40 mW at the sample, an integration time of 25 seconds, and averaged over 5 scans.

*4.5.8 Computational Methods*

Initial coordinates for **1**-**4** and [**1**-**4**]$^+$ were taken from the corresponding crystallographic data. All calculations were carried out with the ORCA (version 4.0.0.2 for geometry and frequency calculations, 4.2.1 for time-dependent DFT) software package.[79] Calculations were performed by unrestricted Kohn-Sham DFT using the B3LYP hybrid functional with the RIJCOSX chain of spheres approximation.[80-83] Ruthenium atoms were modeled with the TZVP basis set. All other atoms were modeled with the def2-SVP basis set.[84] Relativistic effects were treated using the zero-order relativistic approximation (ZORA) Hamiltonian with the SARC/J auxiliary basis set for coulomb fitting.[85, 86] These methods were used to perform geometry optimizations and numerical vibrational frequency analysis on relevant structures. The conductor-like polarizable continuum model (CPCM) was also implemented to model the solvent effects of dichloromethane in all calculations.[87] The Avogadro program[88,89] was used to edit .xyz files, the Jmol program[90] was used to visualize vibrational frequencies, the MultiWFN program[91] was used to visualize molecular orbitals, and final orbital images were generated with the UCSF Chimera package.[92] Calculations were also attempted using the BP86 functional,[93, 94] but calculated reduction potentials did not agree well with experimental measures. Iterative Gaussian multi-peak fitting of the Abs and MCD spectra was conducting using IGOR Pro 8.[95] Abs transitions were modeled as gaussian bands with linewidths of 2000 cm$^{-1}$ and MCD transitions were modeled as gaussian bands with linewidths of 1200 cm$^{-1}$.

*4.5.9 General Methods*

Hap was purchased from Accela ChemBio Inc. and sublimed prior to use. Tris(4-bromophenyl)ammoniumyl hexachloroantimonate (magic blue) was purchased from Sigma-Aldrich and used as received. $Ru_2(OAc)_4Cl$ was synthesized following a literature procedure[96] with important modifications.[97] 2-(4-chloroanilino)pyridine, 2-(4-methylanilino)pyridine, 2(-4-methoxyanilino)pyridine, and 2-anilino-5-methylpyridine were prepared by a modified literature procedure.[52] $Ru_2(Xap)_4Cl$ (X = H, Me, OMe) and $Ru_2(a(Me)p)_4Cl$ were prepared according to the literature procedure for $Ru_2(ap)_4Cl$.[47] The hexafluorophosphate analog of magic blue was prepared according to a literature procedure.[54] Inhibitor-free dichloromethane was purchased from Fisher Scientific, distilled from $CaH_2$ under $N_2$, stored over molecular sieves, and filtered before use. Inhibitor-free anhydrous diethyl ether was purchased from Sigma-Aldrich, stored over molecular sieves, and filtered before use.

Synthesis of substituted anilinopyridine ligands.[52] 2-Bromopyridine (1 eq) and the substituted aniline (2 eq) were added to an oven-dried Schlenk flask. The flask was evacuated and refilled with nitrogen three times. The reaction mixture was then heated to 140–170 °C and stirred for 3 hours. The crude mixture was cooled and extracted into diethyl ether or dichloromethane and neutralized with saturated aqueous sodium bicarbonate. The organic layer was washed with additional bicarbonate solution until the aqueous layer remained basic, and the combined aqueous portions were then extracted with additional diethyl ether or dichloromethane. The combined organic fractions were dried with brine and $MgSO_4$. The solvent was removed under vacuum to afford a mixture of product and residual aniline. For H-Clap, H-Meap, and H-a(Me)p, the crude product was recrystallized from boiling hexanes. For H-OMeap, the crude product was purified by

column chromatography (1:1 ethyl acetate and hexanes on silica). All ligands were then sublimed under dynamic vacuum at 110 °C to afford the colorless product in high purity as determined by $^1$H NMR.

H-Clap 66% yield. $^1$H NMR ($CDCl_3$): 8.21 (d 1H), 7.51 (t 1H), 7.31 (m 4H), 6.78 (m 2H), 6.50 (s, b, 1H).

H-Meap 66% yield. $^1$H NMR ($CDCl_3$): 8.18 (d 1H), 7.46 (t 1H), 7.17 (m 4H), 6.81 (d 1H), 6.70 (t 1H), 6.45 (s, b, 1H), 2.33 (s 3H).

H-OMeap 81% yield. $^1$H NMR ($CDCl_3$): 8.16 (d 1H), 7.44 (t 1H), 7.24 (d 2H), 6.90 (d 2H), 6.67 (m 2H), 6.31 (s, b, 1H), 3.81 (s 3H).

H-a(Me)p 63% yield. $^1$H NMR ($CDCl_3$): 8.04 (d 1H), 7.31 (m 5H), 7.01 (t 1H), 6.83 (d 1H), 6.39 (s, b, 1H), 2.23 (s 3H).

General synthesis for $Ru_2(ap)_4Cl$ and analogous complexes. $Ru_2(OAc)_4Cl$ and protio-ligand (~10 mass equivalents; >20 molar equivalents) were added to an oven-dried sublimator. The sublimator was closed without a cold finger, evacuated and refilled with nitrogen three times, then evacuated to a static vacuum. The reaction mixture was then heated to 100-130 °C for 90 minutes. Upon melting of the ligand, the reaction rapidly changed in color from brown to green *via* a blue intermediate. Over the course of the reaction, liberated HOAc condensed on the flask above the reaction mixture. Upon completion of the reaction, the mixture was cooled until it solidified, then the sides of the flask were cleaned to remove HOAc and deposited ligand. A cold finger was fitted to the sublimator, and the system was again evacuated and refilled three times before being evacuated to a dynamic vacuum. The crude mixture was then heated to 100 °C overnight to completely sublime away all excess ligand. The remaining green solid was transferred to a fritted

filter and washed with methanol until the filtrate was nearly colorless. The product was then extracted into $CH_2Cl_2$ and evaporated to dryness to give analytically pure material. Yields: **1** 80-90%; **3** 81-94%; **4** 46-48%; **5** 64%.

Characterization information:

**2'** could not be isolated from a mixture of **2** and **2'**. However, a characteristic 1:2:1 pattern is observed by $^1$H NMR, which is most evident with peaks at 42.53, 40.40, and 32.18 ppm, compared to the corresponding peak at 35.96 ppm for **2** (see below). Crystals suitable for X-ray diffraction were grown by slow evaporation from a $CH_2Cl_2$ solution.

**3** MW: 970.52 g mol$^{-1}$. ESI (*m*/*z*): ([M-Cl]$^+$) 936.18. IR (ATR): 1600, 1539, 1503, 1470, 1433, 1362, 1289, 1256, 1220, 1157, 1109, 1017, 942, 883, 810, 785, 753, 735, 713, 670, 660, 651, 633 cm$^{-1}$. UV/vis in $CH_2Cl_2$ $\lambda_{max}$ ($\varepsilon$) = 433 (5400), 780 nm (6400 mol$^{-1}$ L cm$^{-1}$). $^1$H NMR ($CDCl_3$): 36.33 (1H), 6.74 ($CH_3$), -33.11 (1H), -81.12 (1H). [$C_{48}H_{44}ClN_8Ru_2$]: Calcd C 59.40, H 4.57, N 11.55, found C 59.22, H 4.81, N 11.04. Crystals suitable for X-ray diffraction were grown by slow evaporation from a $CH_2Cl_2$ solution.

**4** MW: 1034.52 g mol$^{-1}$. ESI (*m*/*z*): ([M-Cl]$^+$) 1000.16. IR (ATR): 1591, 1536, 1502, 1465, 1434, 1355, 1292, 1261, 1239, 1218, 1175, 1165, 1151, 1103, 1027, 961, 878, 841, 822, 782, 756, 733, 722, 652 cm$^{-1}$. UV/Vis in $CH_2Cl_2$ $\lambda_{max}$ ($\varepsilon$) = 425 (5800), 788 nm (5900 mol$^{-1}$ L cm$^{-1}$). **4** was not sufficiently soluble for acquisition of $^1$H NMR data. [$C_{48}H_{44}ClN_8O_4Ru_2$] Calcd C 55.73, H 4.29, N 10.83, found C 55.86, H 4.31, N 10.70. Crystals suitable for X-ray diffraction were grown by slow evaporation from a trifluoroethanol solution.

**5** MW: 970.52 g mol$^{-1}$. ESI ([M-Cl]$^+$) 936.18. IR (ATR): 1617, 1590, 1538, 1483, 1447, 1395, 1379, 1350, 1291, 1231, 1207, 1143, 1072, 1041, 920, 866, 814, 750, 730, 696, 677 cm$^{-1}$. $^1$H NMR

($CDCl_3$): 37.33 (1H), 4.71 ($CH_3$), -2.29 (1H), -33.98 (1H). [$C_{48}H_{44}ClN_8Ru_2$]: Calcd C 59.40, H 4.57, N 11.55, found C 58.81, H 4.75, N 11.75.

Synthesis of (4,0) $Ru_2(Clap)_4Cl$ (**2**). Attempted synthesis of **2** by the same method as other $Ru_2(Xap)_4Cl$ compounds resulted in a (3,1) isomer, where one of the Clap ligands was oriented opposite the other three. To prepare the (4,0) isomer, $Ru_2(OAc)_4Cl$ (300.0 mg, 0.6330 mmol), H-Clap (1.109 g, 5.416 mmol), and LiCl (343.6 mg, 8.106 mmol) were added to an oven-dried 100 mL Schlenk flask. The flask was evacuated and refilled with $N_2$ three times, and the solids were then dried under active vacuum at 80 °C for one hour. The Schlenk flask was fitted with a reflux condenser and Soxhlet extractor with a cellulose thimble containing $K_2CO_3$. 50 mL anhydrous toluene was added, and the mixture was brought to reflux at 140 °C for 3 days. The solvent was then removed under vacuum and the solid residue was extracted through a medium fritted filter with $CH_2Cl_2$ (> 3 L). The $CH_2Cl_2$ was removed under vacuum and the solid was placed in a sublimator. Excess ligand was removed by sublimation under active vacuum at 110 °C overnight. The remaining solid was redissolved in $CH_2Cl_2$, filtered through a medium fritted filter, and dried under vacuum. Yield: 235.5 mg, 35% (up to 44% in other trials). MW: 1052.19 g $mol^{-1}$. ESI (*m*/*z*): ($[M-Cl]^+$) 1017.96. IR (ATR): 1600, 1483, 1468, 1434, 1361, 1289, 1283, 1217, 1159, 1090, 1018, 900, 884, 802, 757, 736, 725, 697 $cm^{-1}$. UV/vis in $CH_2Cl_2$ $\lambda_{max}$ ($\varepsilon$) = 421 (5900), 785 nm (6300 $mol^{-1}$ L $cm^{-1}$). $^1H$ NMR ($CDCl_3$): 35.96 (1H), -32.84 (1H), -76.84 (1H). [$C_{44}H_{32}Cl_5N_8$-$Ru_2$•$2CH_2Cl_2$] Calcd C 45.21, H 2.97, N 9.17, found C 45.01, H 2.86, N 9.17. Crystals suitable for X-ray diffraction were grown by slow evaporation from a $CH_2Cl_2$ solution.

Oxidation of $Ru_2(Xap)_4Cl$ with MB-$SbCl_6$ or MB-$PF_6$ [MB = Magic Blue, tris(4-bromophenyl)ammoniumyl cation]. In a glovebox with a dry $N_2$ atmosphere, $Ru_2(Xap)_4Cl$ and one equivalent of the desired MB salt were added to a Schlenk flask and dissolved in $CH_2Cl_2$ at roughly 6 mg $Ru_2(Xap)_4Cl$ / 1 mL $CH_2Cl_2$ concentration. An immediate color change to red/purple was noticed. The solution was stirred for 30-60 minutes before 3 volume equivalents of diethyl ether was added. The solid product was then collected by filtration in air. Yield: 71-86%.

Characterization information:

[**1**][$SbCl_6$] MW: 1248.88 g $mol^{-1}$; [**1**][$PF_6$] MW: 1059.37 g $mol^{-1}$. ESI (*m*/*z*): ([$M_{cat}$]$^+$) 915.09. IR (ATR): 1597, 1478, 1462, 1429, 1336, 1292, 1257, 1208, 1162, 1115, 1073, 1053, 1018, 1001, 923, 871, 766, 734, 696, 676, 649 $cm^{-1}$; 833 $cm^{-1}$ ($PF_6^-$) for [**1**][$PF_6$], but the expected peak for $SbCl_6^-$ is too low in energy to be detected (expected ~ 353[98]). UV/vis in $CH_2Cl_2$ $\lambda_{max}$ (ε) = 439 (5500), 516 (5900), 981 nm (13000 $mol^{-1}$ L $cm^{-1}$). $^1$H NMR (**1**[$SbCl_6$] in $CDCl_3$): 27.06 (d 1H), 13.50 (d 1H), 6.91 (t 1H), 5.98 (t 1H), 3.76 (b 2H), -13.45 (1H); (**1**[$PF_6$] in $CD_2Cl_2$): 27.15 (d 1H), 13.35 (d 1H), 6.93 (t 1H), 5.99 (t 1H), 3.76 (b 2H), -13.43 (1H). [$C_{44}H_{36}Cl_7N_8Ru_2Sb$•$CH_2Cl_2$]: Calcd C 40.52, H 2.87, N 8.40, found C 40.38, H 2.85, N 8.35. Crystals suitable for X-ray diffraction were grown by vapor diffusion of diethyl ether to a saturated $CH_2Cl_2$ solution.

[**2**][$SbCl_6$] MW: 1386.66 g $mol^{-1}$; [**1**][$PF_6$] MW: 1197.15 g $mol^{-1}$. ESI (*m*/*z*): ([$M_{cat}$-Cl]$^+$) 1017.96. IR (ATR): 1597, 1482, 1463, 1432, 1400, 1340, 1292, 1253, 1208, 1162, 1093, 1011, 942, 899, 887, 812, 765, 734, 699, 649 $cm^{-1}$; 839 $cm^{-1}$ ($PF_6^-$) for [**1**][$PF_6$]. UV/vis in $CH_2Cl_2$ $\lambda_{max}$ (ε) = 450 (5200), 520 (5000), 994 nm (11000 $mol^{-1}$ L $cm^{-1}$). $^1$H NMR (**2**[$SbCl_6$] in $CD_2Cl_2$): 25.91 (1H), 13.80 (d 1H), 7.12 (t 1H), 4.26 (b 2H), -13.24 (1H). [$C_{44}H_{32}Cl_{11}N_8Ru_2Sb$] Calcd C 38.11, H 2.33, N 8.08, found C 37.93, H 2.38, N 7.87. Crystals suitable for X-ray diffraction were grown by vapor diffusion of diethyl ether to a saturated $CH_2Cl_2$ solution.

[**3**][$SbCl_6$] MW: 1304.99 g $mol^{-1}$; [**1**][$PF_6$] MW: 1179.47 g $mol^{-1}$. ESI (*m*/*z*): ([$M_{cat}$]$^+$) 971.15. IR (ATR): 1597, 1500, 1461, 1424, 1343, 1290, 1254, 1211, 1177, 1160, 1113, 1050, 1016, 942, 885, 808, 785, 772, 738, 712, 666, 647, 638 $cm^{-1}$; 835 $cm^{-1}$ ($PF_6^-$) for [**1**][$PF_6$]. UV/vis in $CH_2Cl_2$ $\lambda_{max}$ ($\varepsilon$) = 452 (5400), 529 (5500), 989 nm (12000 $mol^{-1}$ L $cm^{-1}$). $^1$H NMR (**3**[$SbCl_6$] in $CDCl_3$): 27.26 (1H), 12.54 (1H), 6.80 (t 1H), 3.63 (b 2H), 0.98 ($CH_3$), -13.03 (1H); (**3**[$PF_6$] in $CD_2Cl_2$): 27.04 (1H), 12.56 (1H), 6.83 (t 1H), 3.64 (b 2H), 0.95 ($CH_3$), -13.01 (1H). [$C_{48}H_{44}Cl_7N_8Ru_2Sb$] Calcd C 44.18, H 3.40, N 8.59, found C 44.20, H 3.62, N 8.06. Crystals suitable for X-ray diffraction were grown by vapor diffusion of diethyl ether to a saturated $CH_2Cl_2$ solution.

[**4**][$SbCl_6$] MW: 1368.98 g $mol^{-1}$; [**1**][$PF_6$] MW: 1115.47 g $mol^{-1}$. ESI (*m*/*z*): ([$M_{cat}$]$^+$) 1035.13. IR (ATR): 1597, 1575, 1500, 1460, 1427, 1335, 1302, 1292, 1248, 1212, 1185, 1167, 1107, 1035, 937, 882, 824, 809, 786, 772, 759, 736, 717, 661, 649, 633 $cm^{-1}$; 840 $cm^{-1}$ ($PF_6^-$) for [**1**][$PF_6$]. UV/vis in $CH_2Cl_2$ $\lambda_{max}$ ($\varepsilon$) = 450 (6000), 549 (7400), 1018 nm (13000 $mol^{-1}$ L $cm^{-1}$). $^1$H NMR (**4**[$SbCl_6$] in $CDCl_3$): 26.16 (1H), 10.55 (1H), 6.46 (1H), 4.10 (b 2H), -2.59 ($OCH_3$), -12.60 (1H). [$C_{48}H_{44}Cl_7N_8O_4Ru_2Sb$] Calcd C 42.11, H 3.24, N 8.19, found C 41.74, H 3.30, N 7.91. Crystals suitable for X-ray diffraction were grown by vapor diffusion of diethyl ether to a saturated $CH_2Cl_2$ solution.

[**5**][$SbCl_6$] MW: 1304.99 g $mol^{-1}$. ESI (*m*/*z*): ([$M_{cat}$]$^+$) 971.15. IR (ATR): 1472, 1376, 1328, 1257, 1203, 924, 876, 814, 756, 736, 695, 667, 644 $cm^{-1}$. $^1$H NMR (**5**[$SbCl_6$] in $CDCl_3$): 24.38 (1H), 8.09 (d 1H), 5.48 (1H) 4.22 (b 2H), -2.73 ($CH_3$), -14.34 (1H). [$C_{48}H_{44}Cl_7N_8Ru_2Sb$•$2CH_2Cl_2$] Calcd C 40.72, H 3.28, N 7.60, found C 40.50, H 3.36, N 7.61.

## 4.6 Supplemental Content

*4.6.1 Supplemental Magnetometry Information*. A thorough discussion of the mathematical expressions used in fitting the magnetic susceptibility and magnetization data are available in the Phi User Manual.

Samples were measured in gelatin capsules, with sample holder diamagnetic corrections obtained as a function of temperature by measuring the magnetic moment of an empty sample holder from 2-300 K in an applied field of 0.1 T (1000 G).

$M_{capsule}$ = (0.000023718/T)-0.000015494-(0.0000000012331*T)

Diamagnetic corrections for samples were calculated from tabulated Pascal's constants.

[**1**][$SbCl_6$]: -0.00062984 emu/mol

*4.6.2 Supplemental Figures.*

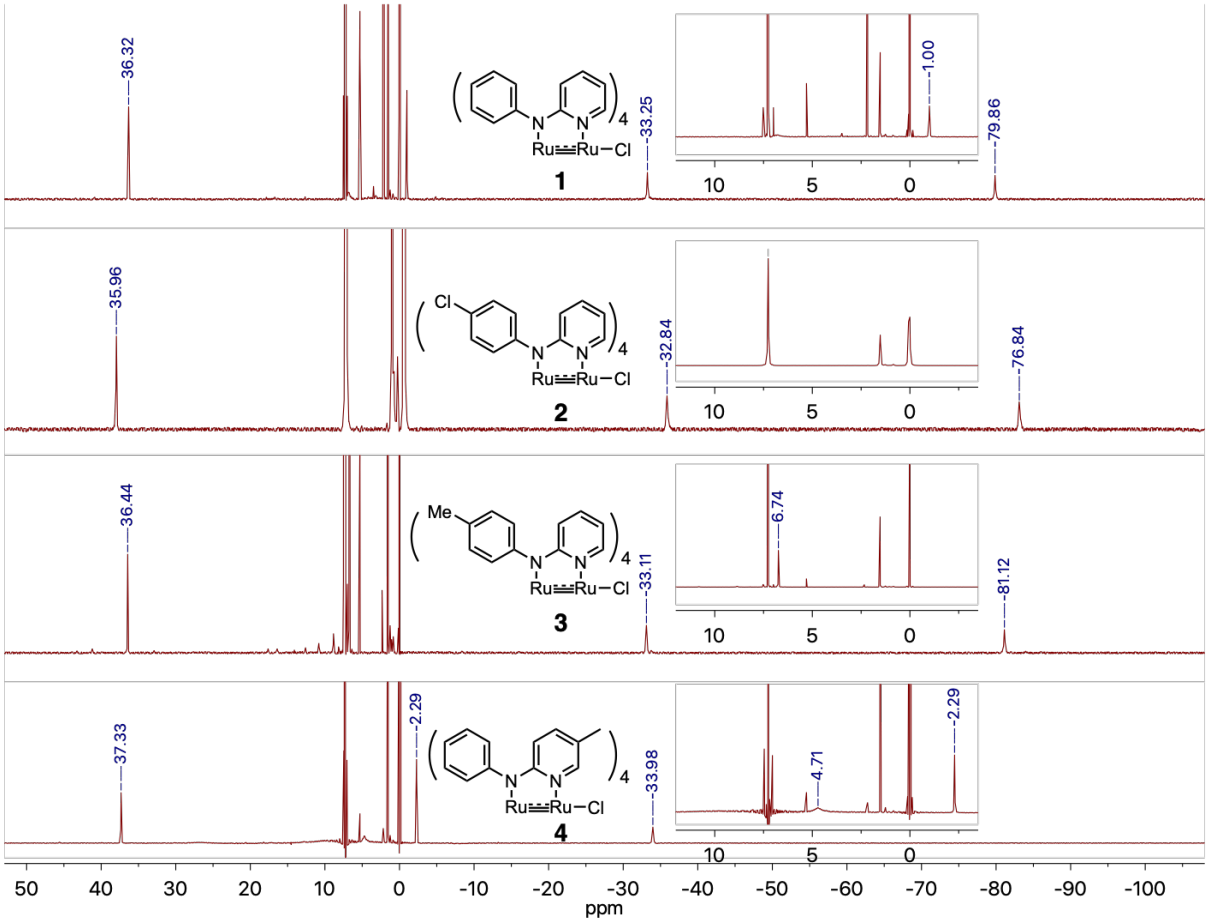


Figure 4.S1 $^{1}$H NMR spectra of **1-3** and **5** in $CDCl_3$.

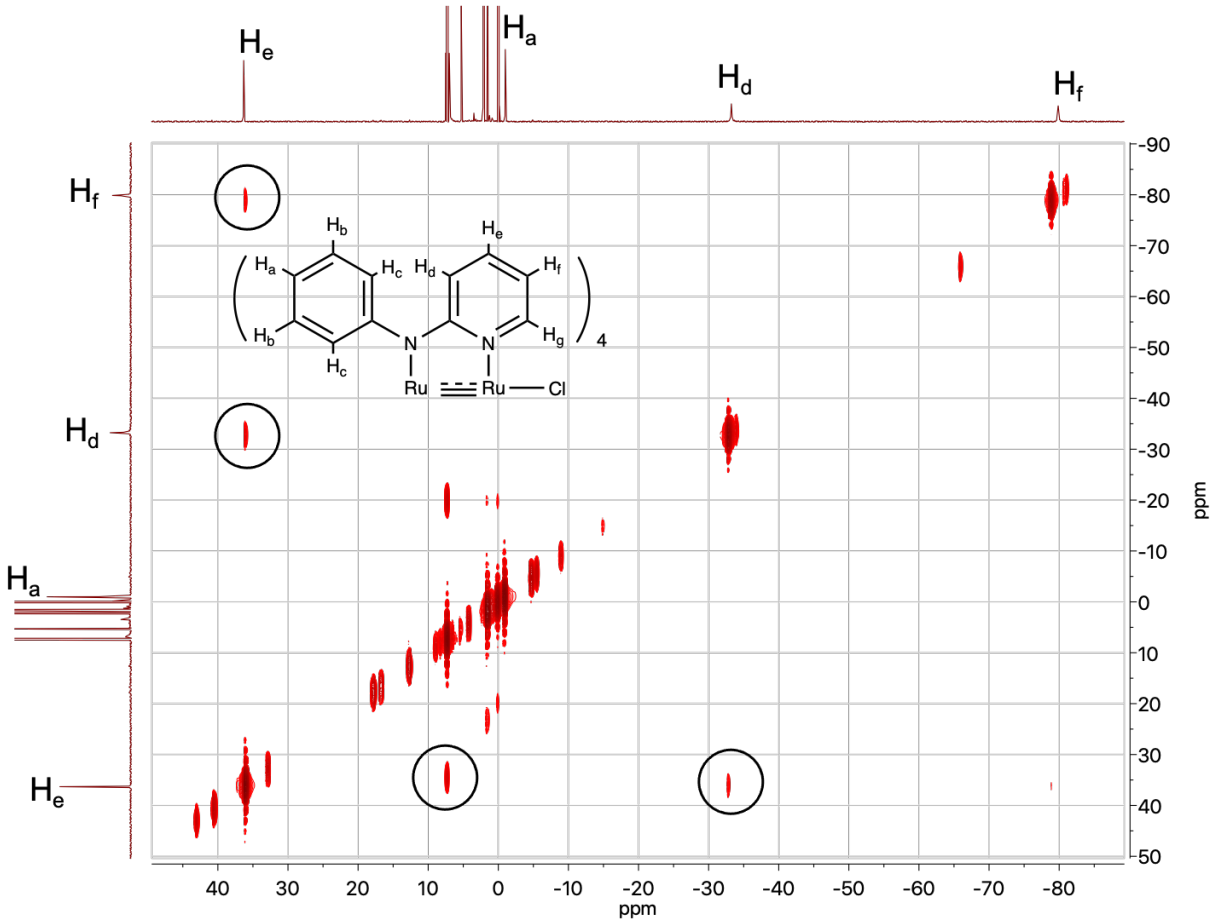


Figure 4.S2 $^{1}$H COSY spectrum of **1** in $CDCl_3$.

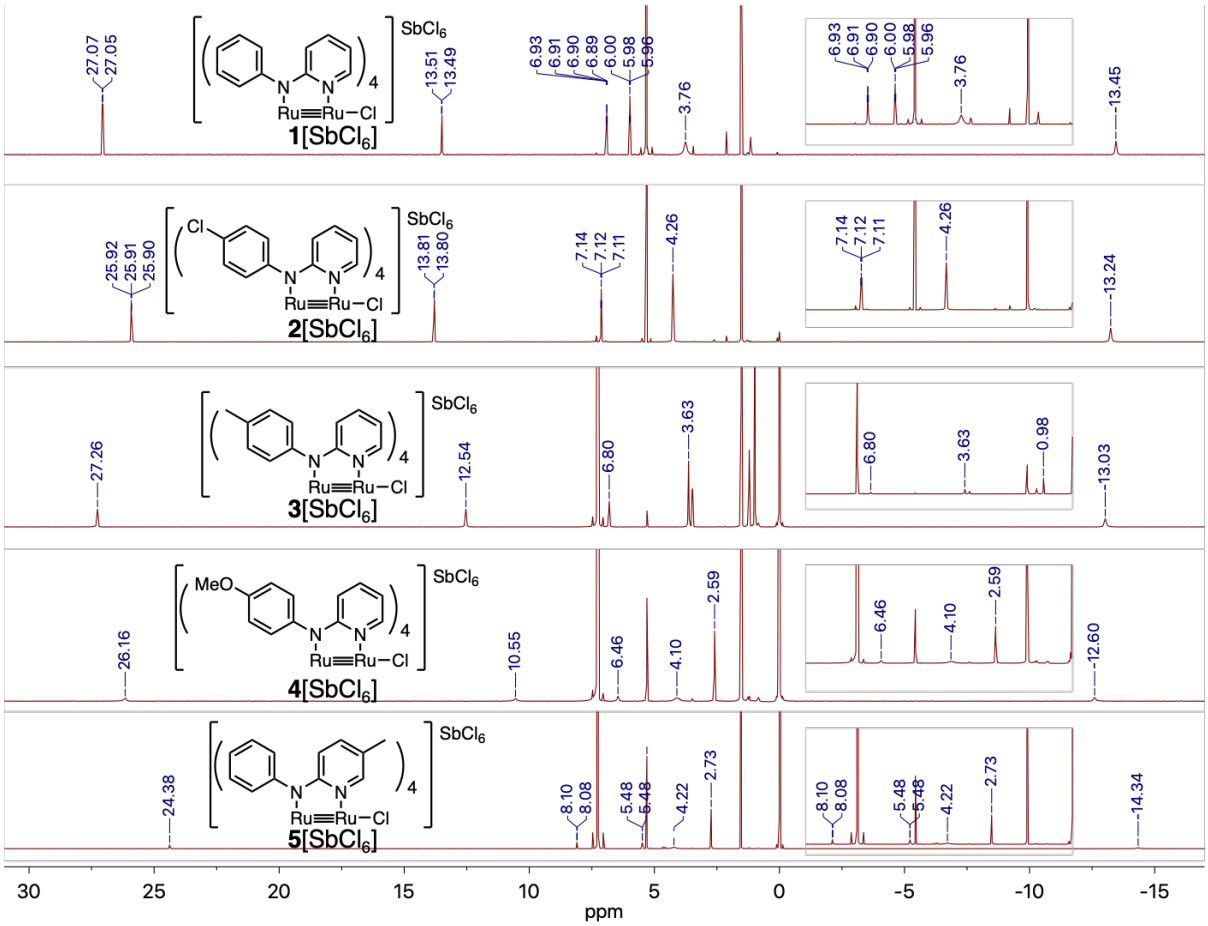


Figure 4.S3 $^{1}$H NMR spectra of [**1**-**2**][$SbCl_6$] in $CD_2Cl_2$ and [**3**-**5**][$SbCl_6$] in $CDCl_3$.

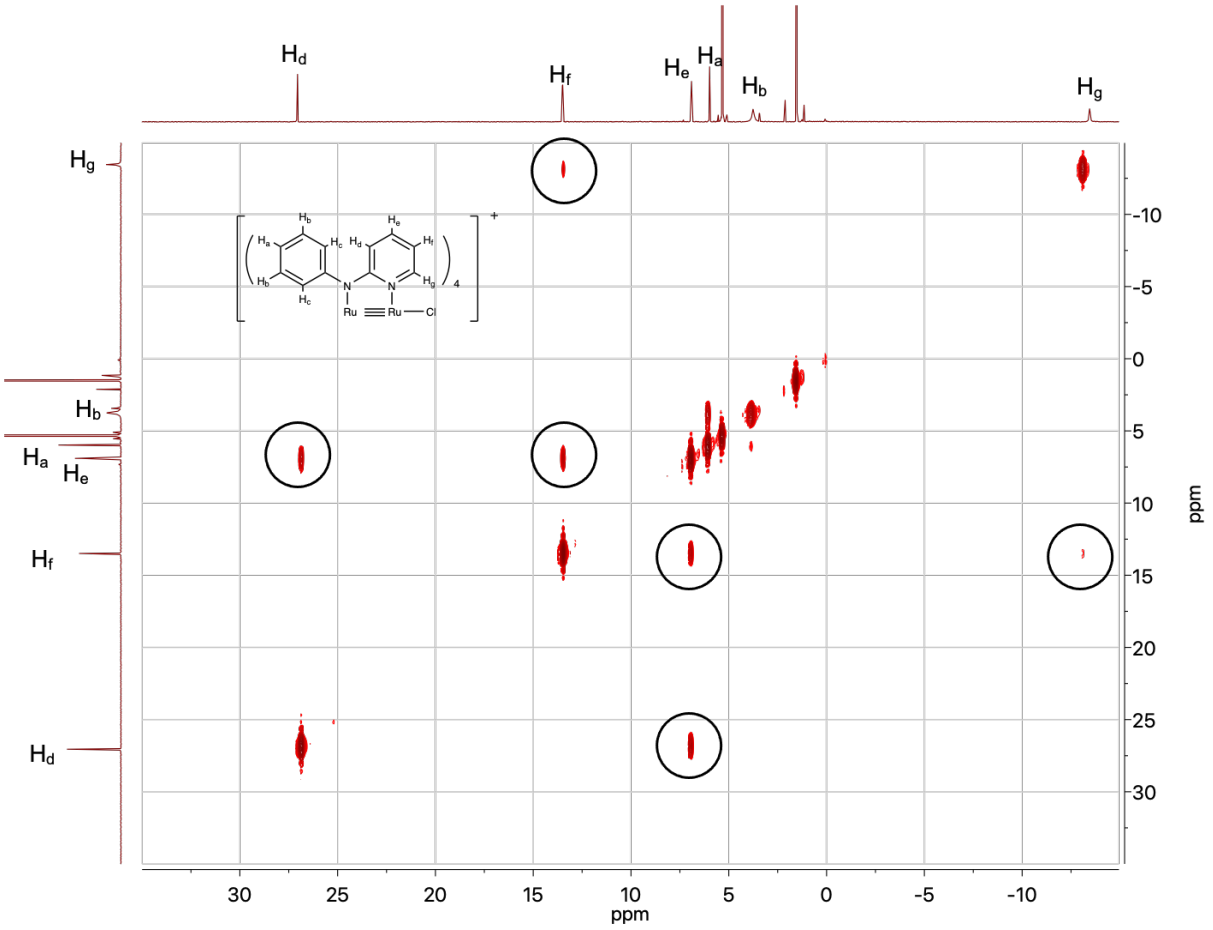


Figure 4.S4 $^{1}$H COSY spectrum of [**1**][$SbCl_6$] in $CD_2Cl_2$.

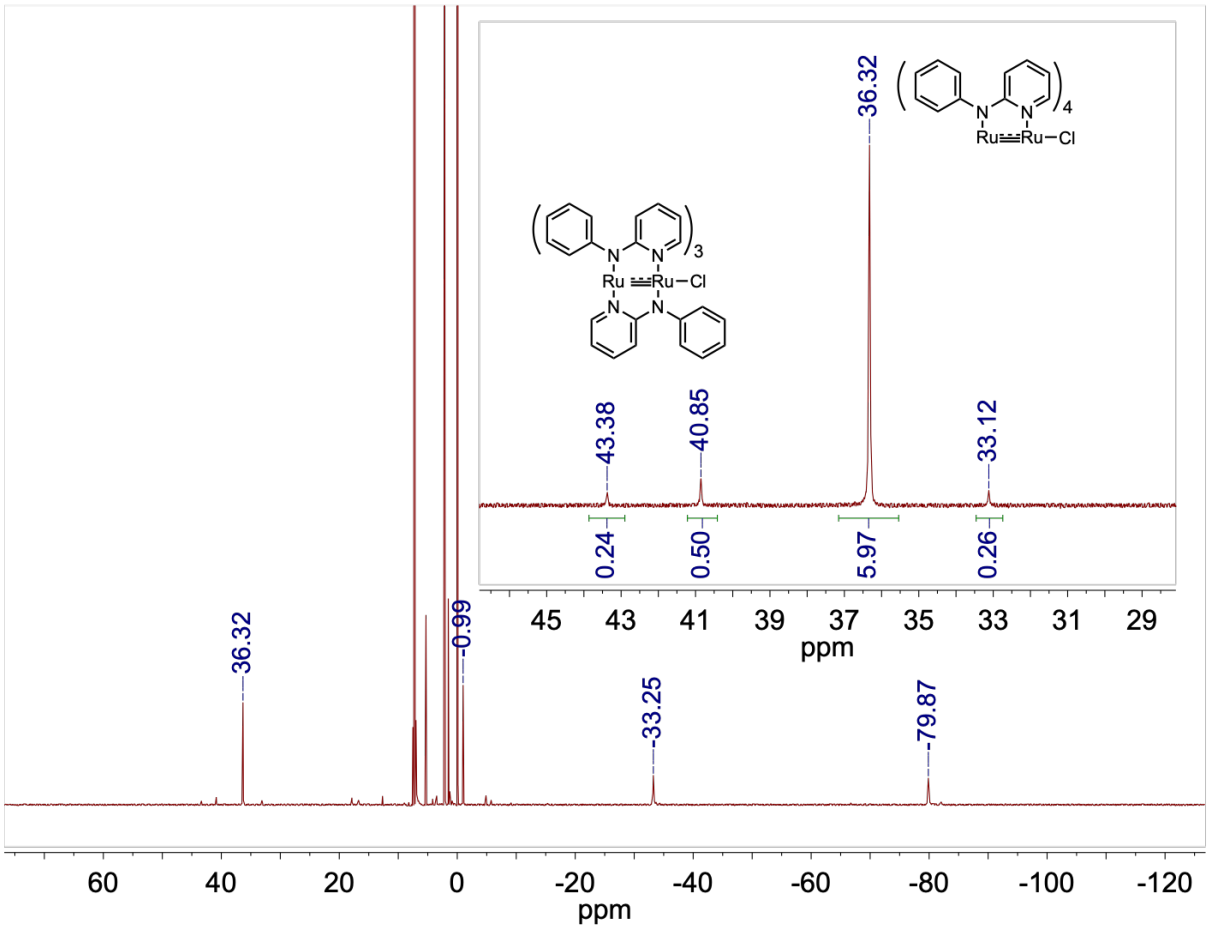


Figure 4.S5 $^{1}$H NMR spectrum in $CDCl_3$ showing the (3,1) isomer as a 1:6 impurity in **1**.

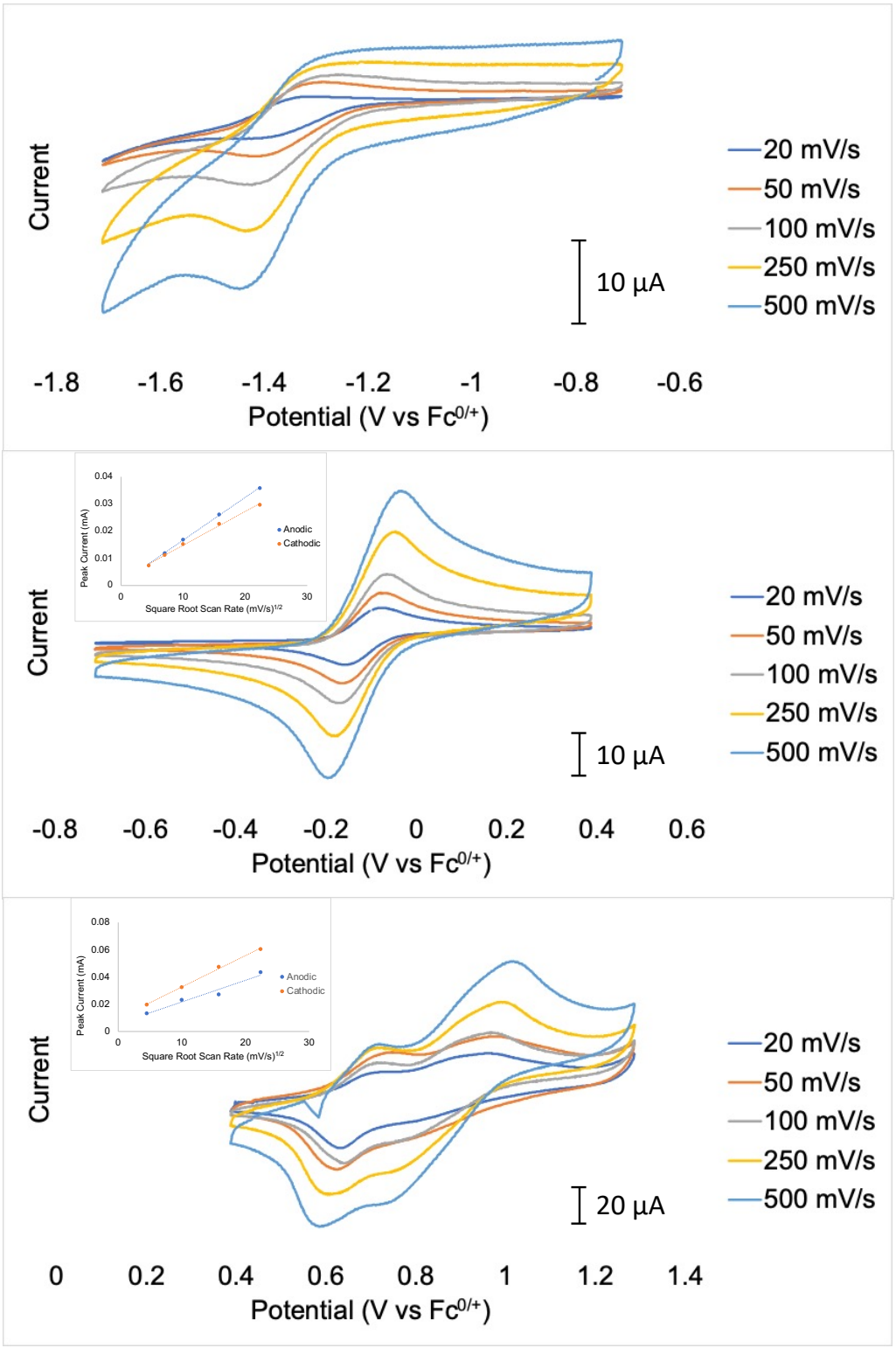


Figure 4.S6 Cyclic voltammograms of isolated redox events for [**1**][$PF_6$]. Top: $Ru_2^{4+/5+}$, middle: $Ru_2^{5+/6+}$, bottom: $Ru_2^{6+/7+}$. Insets: plots of peak current vs square root of scan rate.

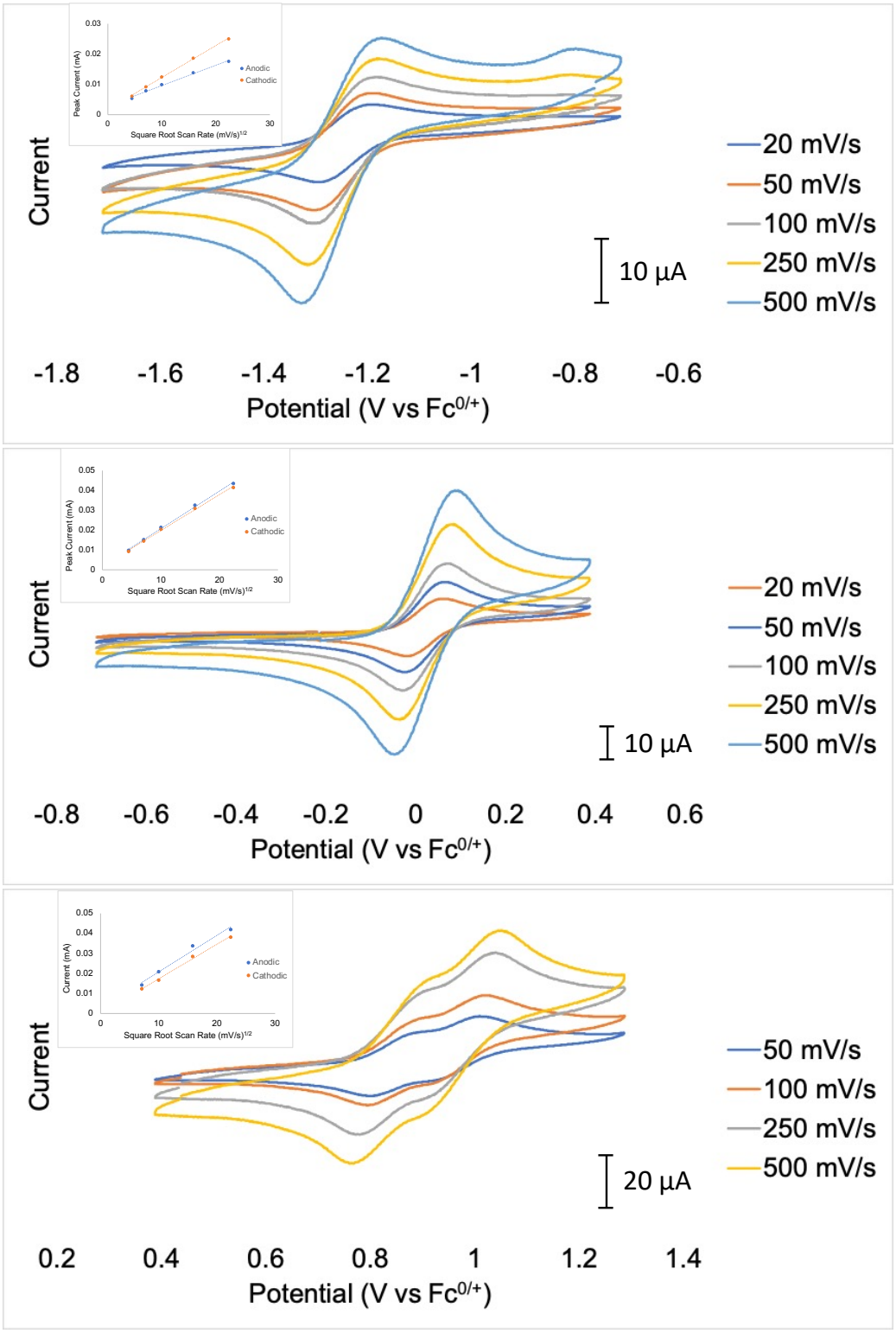


Figure 4.S7 Cyclic voltammograms of isolated redox events for [**2**][$PF_6$]. Top: $Ru_2^{4+/5+}$, middle: $Ru_2^{5+/6+}$, bottom: $Ru_2^{6+/7+}$. Insets: plots of peak current vs square root of scan rate.

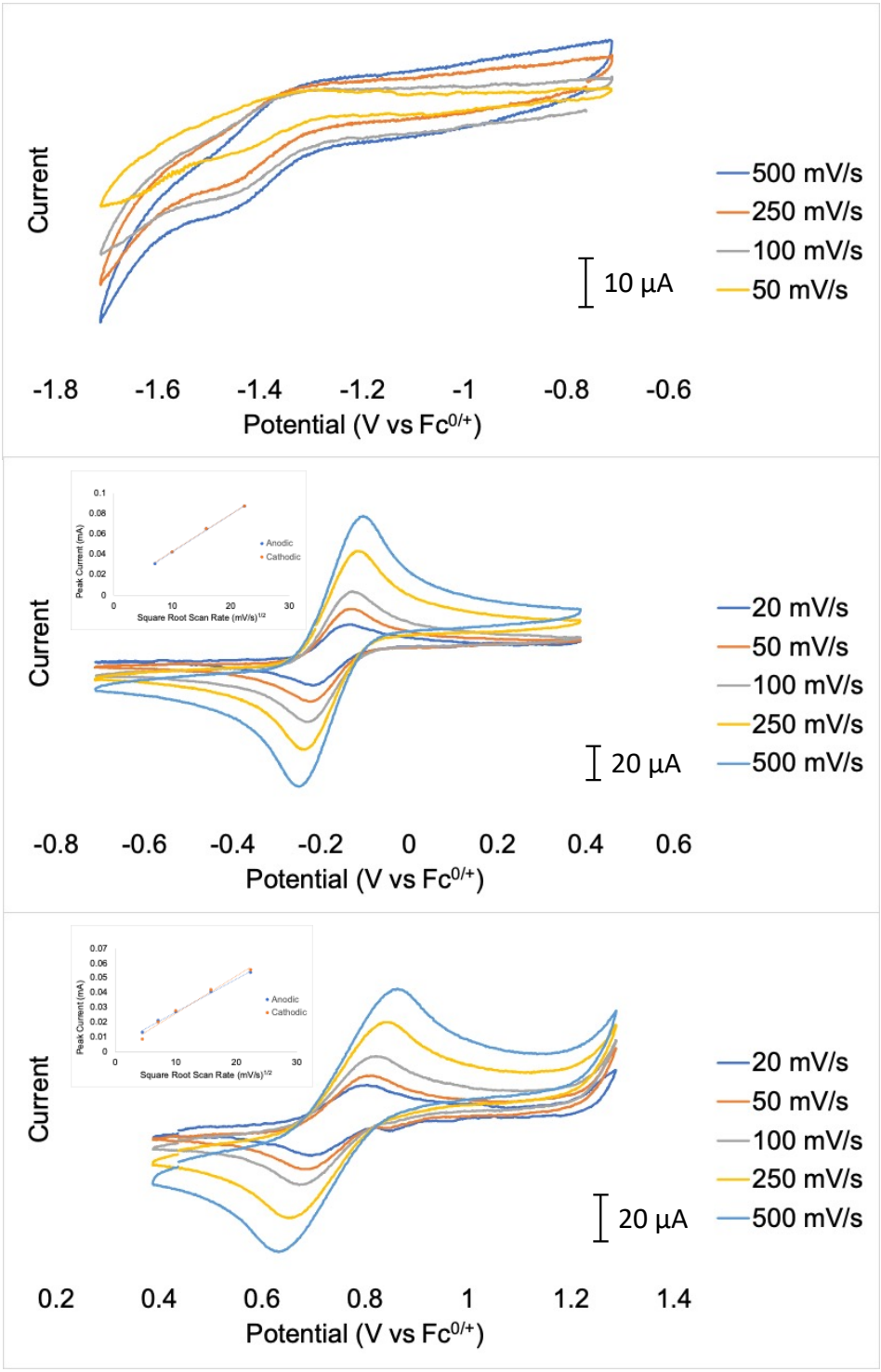


Figure 4.S8 Cyclic voltammograms of isolated redox events for [**3**][$PF_6$]. Top: $Ru_2^{4+/5+}$, middle: $Ru_2^{5+/6+}$, bottom: $Ru_2^{6+/7+}$. Insets: plots of peak current vs square root of scan rate.

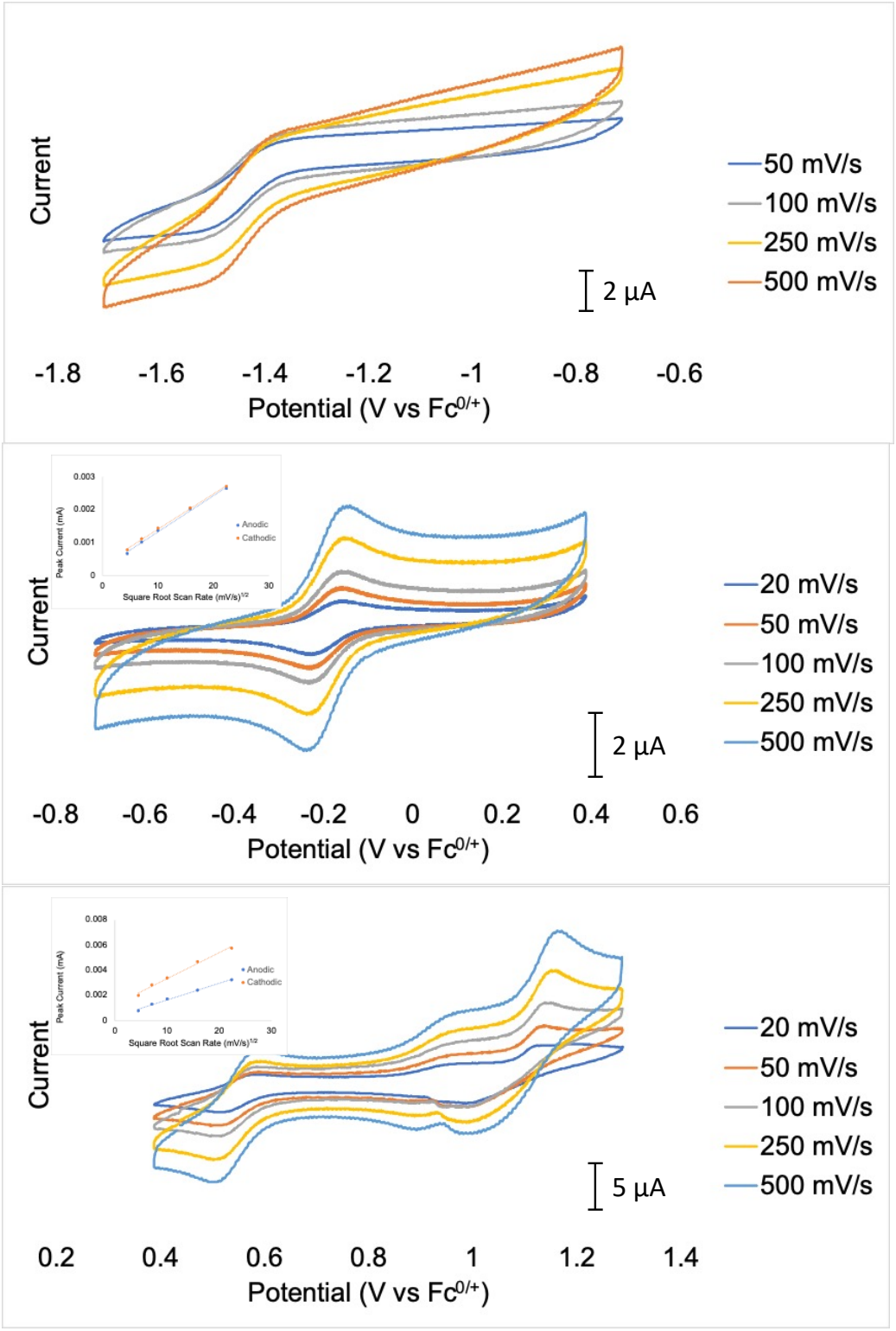


Figure 4.S9 Cyclic voltammograms of isolated redox events for [**4**][$PF_6$]. Top: $Ru_2^{4+/5+}$, middle: $Ru_2^{5+/6+}$, bottom: $Ru_2^{6+/7+}$. Insets: plots of peak current vs square root of scan rate.

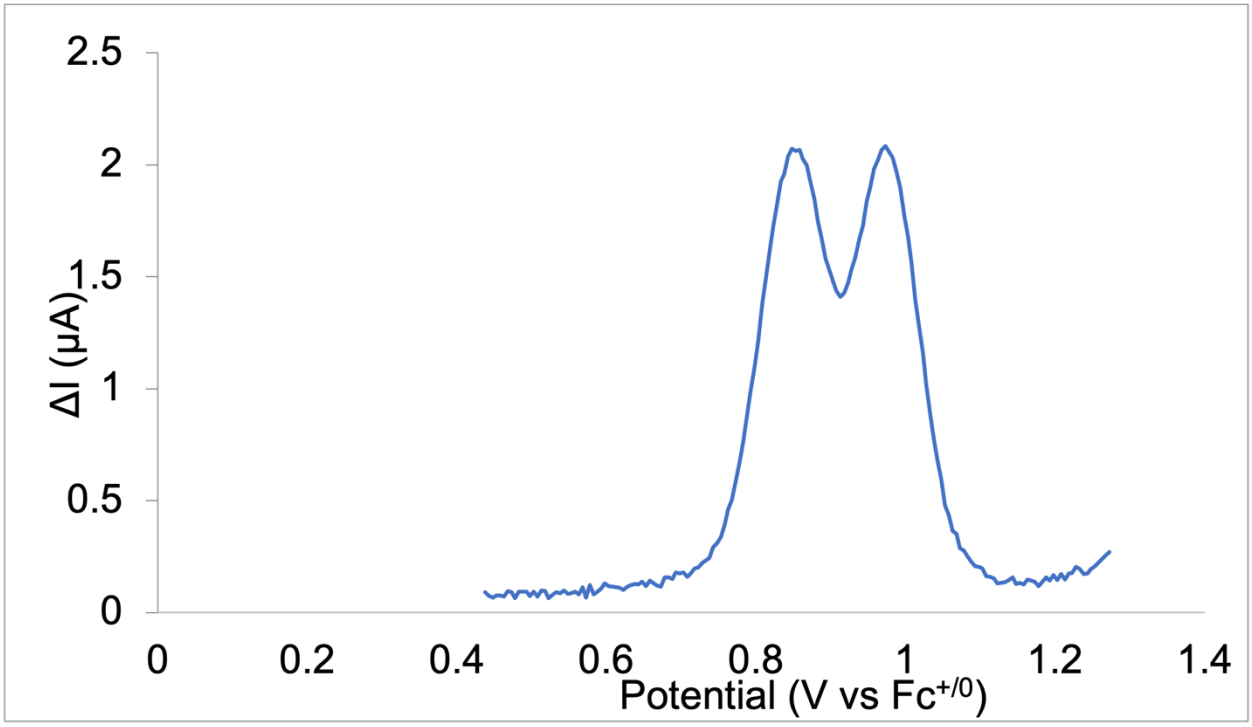


Figure 4.S10 Differential pulse voltammogram (DPV) of [**2**][$PF_6$] in the region of the $Ru_2^{6+/7+}$ redox event showing two distinct redox events.

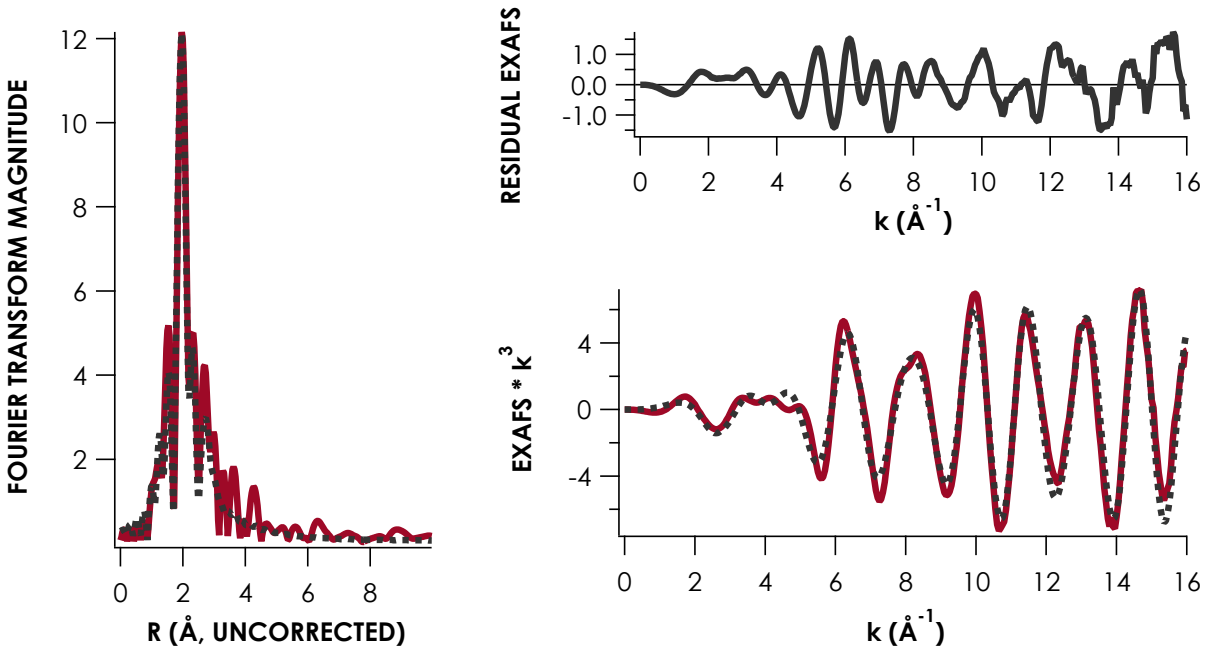


Figure 4.S11 Ru K-edge EXAFS of **1** obtained at 10 K. Experimental data is plotted as a solid red trace and fits are shown as dotted lines. Data were fit to the unsmoothed raw data and simulated over the range k = 2-16 Å$^{-1}$.

| Fit | Path | CN | R (Å) | ± | $\sigma^2$ | ± | $E_0$ (eV) | F factor |
|---|---|---|---|---|---|---|---|---|
| **1** | Ru–N (inner) | 4 | 2.082 | 0.048 | 0.0039 | 0.0031 | -13.993 | 73.14 |
| **2** | Ru–N (inner) | 4 | 2.104 | 0.027 | 0.0054 | 0.0023 | -16.658 | 14.91 |
| | Ru–Ru | 1 | 2.267 | 0.009 | 0.0009 | 0.0005 | | |
| **3** | Ru–N (inner) | 4 | 2.059 | 0.025 | 0.0062 | 0.0024 | -14.090 | 13.24 |
| | Ru–Ru | 1 | 2.271 | 0.008 | 0.0010 | 0.0005 | | |
| | Ru–Cl | 0.5 | 2.708 | 0.044 | 0.0007 | 0.0043 | | |
| **4** | Ru–N (inner) | 4 | 2.075 | 0.014 | 0.0065 | 0.0017 | -9.997 | 5.65 |
| | Ru–Ru | 1 | 2.278 | 0.005 | 0.0011 | 0.0004 | | |
| | Ru–Cl | 0.5 | 2.735 | 0.029 | 0.0002 | 0.0027 | | |
| | Ru–N (distal) | 4 | 3.004 | 0.018 | 0.0004 | 0.0015 | | |

Table 4.S4 EXAFS simulations for **1**. EXAFS were fit with Artemis using paths calculated by FEFF6. Distance (R) and Debye-Waller factors ($\sigma^2$) were allowed to float while coordination

numbers (CN) were held constant. Goodness of fit is determined by F, defined as $[(\sum_i^n[k_i^3(\mathrm{EXAFS_{obs}} - \mathrm{EXAFS_{calc}})_i])^2/n]^{1/2}$. Errors in distances are estimated to be 0.02-0.03 Å and 25% for coordination numbers.

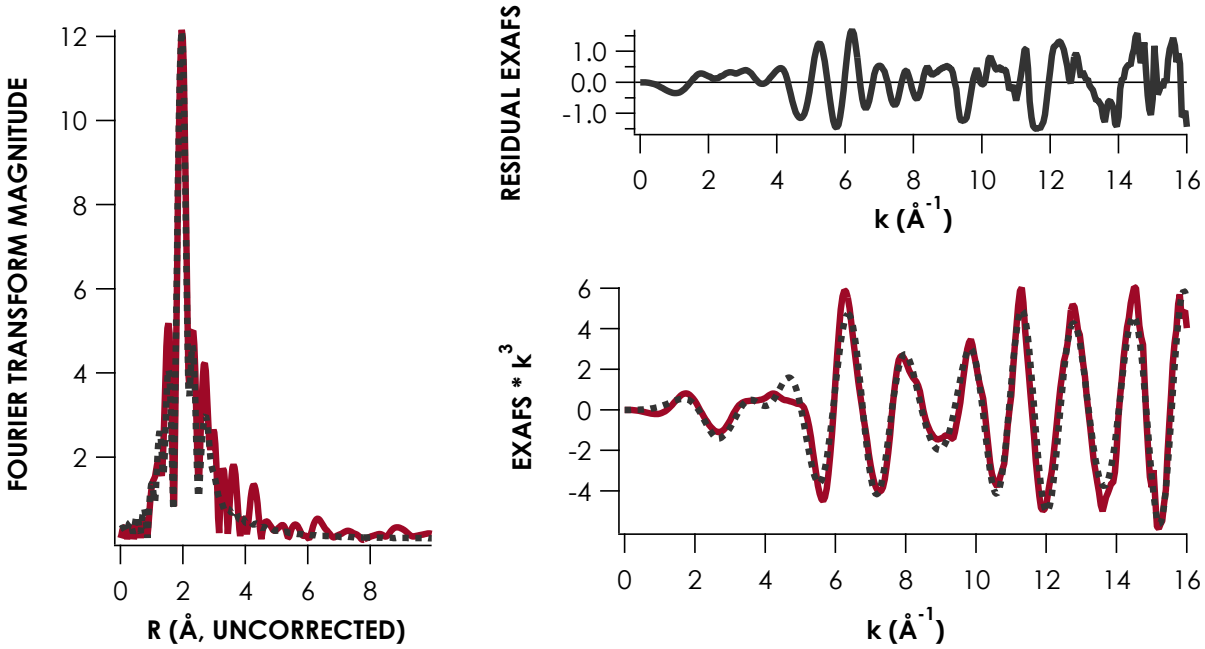


Figure 4.S12 Ru K-edge EXAFS of [**1**][$PF_6$] obtained at 10 K. Experimental data is plotted as a solid red trace and fits are shown as dotted lines. Data were fit to the unsmoothed raw data and simulated over the range k = 2-16 Å$^{-1}$.

| Fit | Path | CN | R (Å) | ± | $\sigma^2$ | ± | $E_0$ (eV) | F factor |
|---|---|---|---|---|---|---|---|---|
| **1** | Ru–N (inner) | 4 | 2.033 | 0.063 | 0.0070 | 0.0040 | -16.596 | 76.82 |
| **2** | Ru–N (inner) | 4 | 2.029 | 0.003 | 0.0059 | 0.0023 | -14.140 | 20.41 |
| | Ru–Ru | 1 | 2.303 | 0.011 | 0.0015 | 0.0007 | | |
| **3** | Ru–N (inner) | 4 | 2.044 | 0.025 | 0.0070 | 0.0023 | -12.005 | 18.00 |
| | Ru–Ru | 1 | 2.307 | 0.010 | 0.0016 | 0.0006 | | |
| | Ru–Cl | 0.5 | 2.696 | 0.044 | 0.0005 | 0.0039 | | |

| | | | | | | | | |
|---|---|---|---|---|---|---|---|---|
| **4** | Ru–N (inner) | 4 | 2.051 | 0.013 | 0.0065 | 0.0017 | -8.956 | 7.19 |
| | Ru–Ru | 1 | 2.313 | 0.006 | 0.0017 | 0.0005 | | |
| | Ru–Cl | 0.5 | 2.724 | 0.034 | 0.0010 | 0.0033 | | |
| | Ru–N (distal) | 4 | 2.993 | 0.018 | 0.0005 | 0.0014 | | |

Table 4.S5 EXAFS simulations for [**1**][$PF_6$]. EXAFS were fit with Artemis using paths calculated by FEFF6. Distance (R) and Debye-Waller factors ($\sigma^2$) were allowed to float while coordination numbers (CN) were held constant. Goodness of fit is determined by F, defined as $[(\sum_i^n[k_i^3(\mathrm{EXAFS_{obs}} - \mathrm{EXAFS_{calc}})_i])^2/n]^{1/2}$. Errors in distances are estimated to be 0.02-0.03 Å and 25% for coordination numbers.

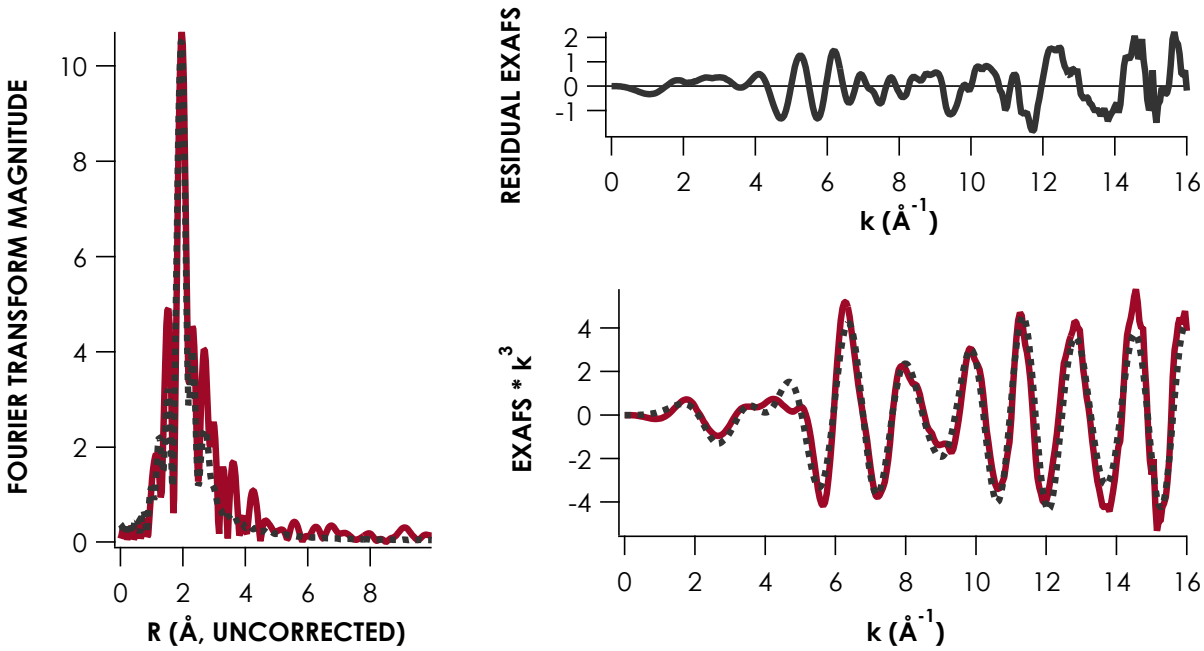

Figure 4.S13 Ru K-edge EXAFS of [**1**][$SbCl_6$] obtained at 10 K. Experimental data is plotted as a solid red trace and fits are shown as dotted lines. Data were fit to the unsmoothed raw data and simulated over the range k = 2-16 $Å^{-1}$.

| Fit | Path | CN | R (Å) | ± | $\sigma^2$ | ± | $E_0$ (eV) | F factor |
|---|---|---|---|---|---|---|---|---|
| **1** | Ru–N (near) | 4 | 2.030 | 0.066 | 0.0079 | 0.0041 | -17.190 | 76.55 |
| **2** | Ru–N (near) | 4 | 2.026 | 0.029 | 0.0076 | 0.0027 | -14.569 | 23.00 |
| | Ru–Ru | 1 | 2.297 | 0.012 | 0.0020 | 0.0007 | | |
| **3** | Ru–N (near) | 4 | 2.047 | 0.026 | 0.0087 | 0.0028 | -12.001 | 20.38 |
| | Ru–Ru | 1 | 2.302 | 0.011 | 0.0016 | 0.0007 | | |
| | Ru–Cl | 0.5 | 2.703 | 0.040 | 0.0004 | 0.0036 | | |
| **4** | Ru–N (near) | 4 | 2.048 | 0.015 | 0.0082 | 0.0021 | -9.287 | 10.16 |
| | Ru–Ru | 1 | 2.307 | 0.008 | 0.0021 | 0.0006 | | |
| | Ru–Cl | 0.5 | 2.730 | 0.045 | 0.0021 | 0.0047 | | |
| | Ru–N (far) | 4 | 2.991 | 0.024 | 0.0012 | 0.0018 | | |

Table 4.S6 EXAFS simulations for [**1**][$SbCl_6$]. EXAFS were fit with Artemis using paths calculated by FEFF6. Distance (R) and Debye-Waller factors ($\sigma^2$) were allowed to float while coordination numbers (CN) were held constant. Goodness of fit is determined by F, defined as $[(\sum_i^n[k_i^3(\mathrm{EXAFS_{obs}} - \mathrm{EXAFS_{calc}})_i])^2/n]^{1/2}$. Errors in distances are estimated to be 0.02-0.03 Å and 25% for coordination numbers.

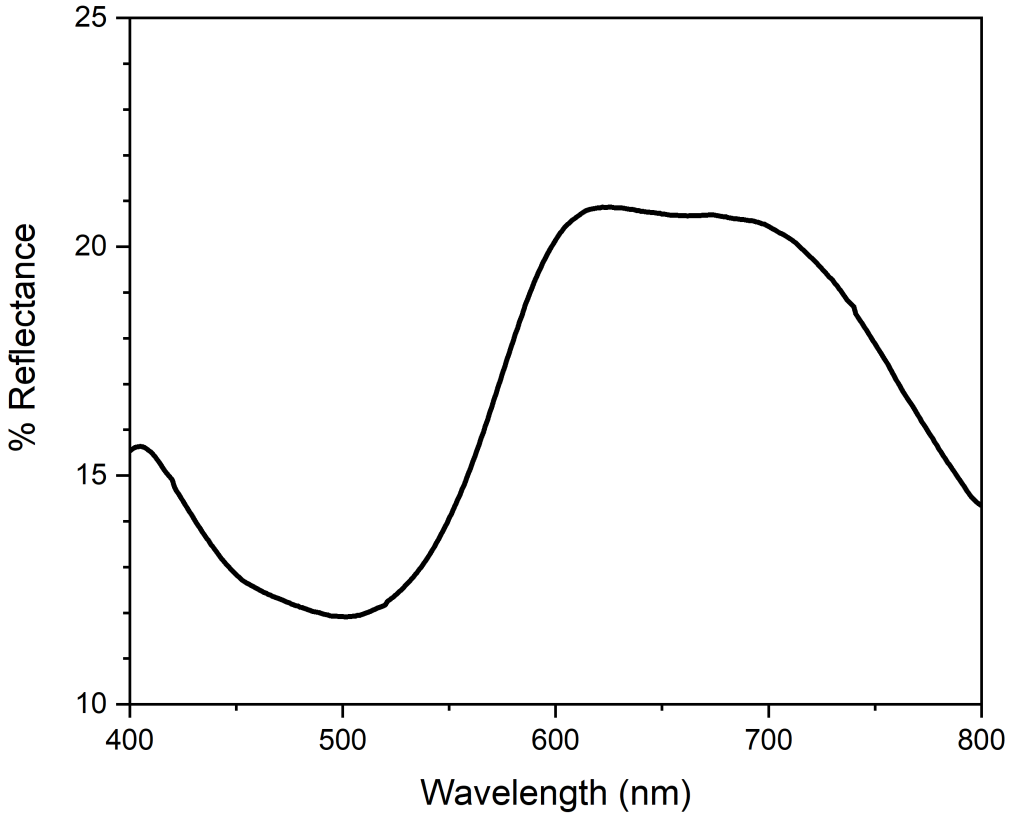


Figure 4.S14 Solid-state visible reflectance spectrum of **4**. The decreased reflectance around 500 and 800 nm correspond to the peaks in the solution-state absorption spectrum at ~400 and 800 nm, and the shift in the higher energy feature is responsible for the difference in color between solid and solution state.

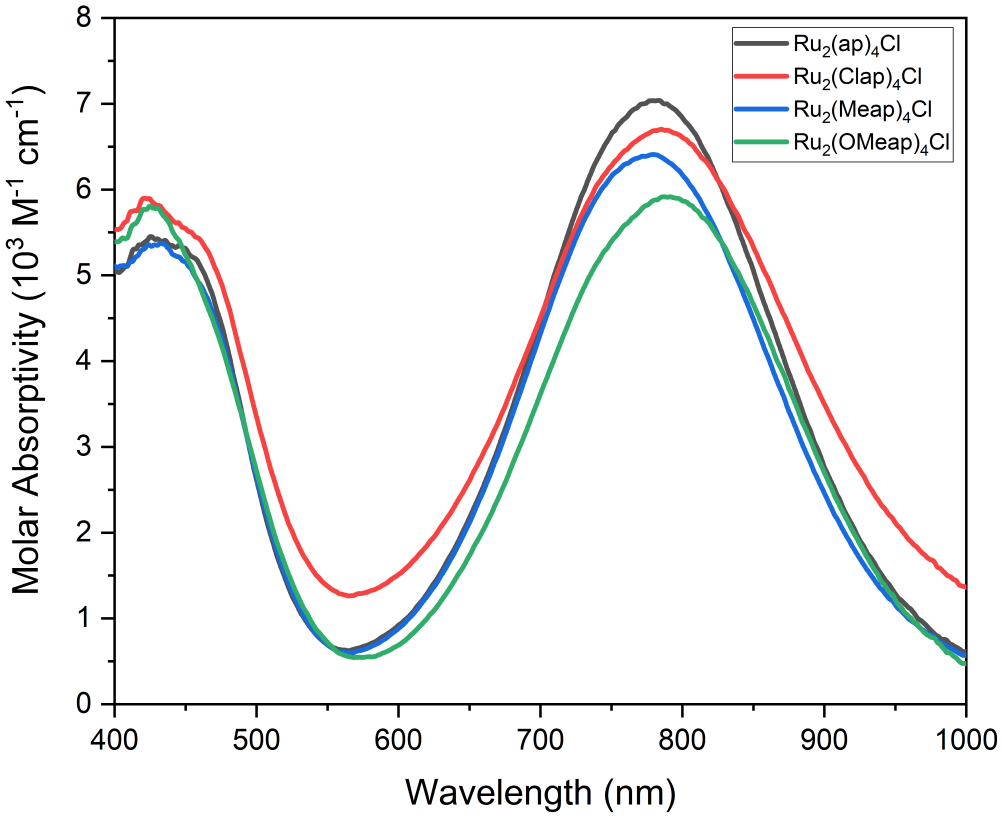


Figure 4.S15 Vis-NIR spectra of **1-4** in $CH_2Cl_2$.

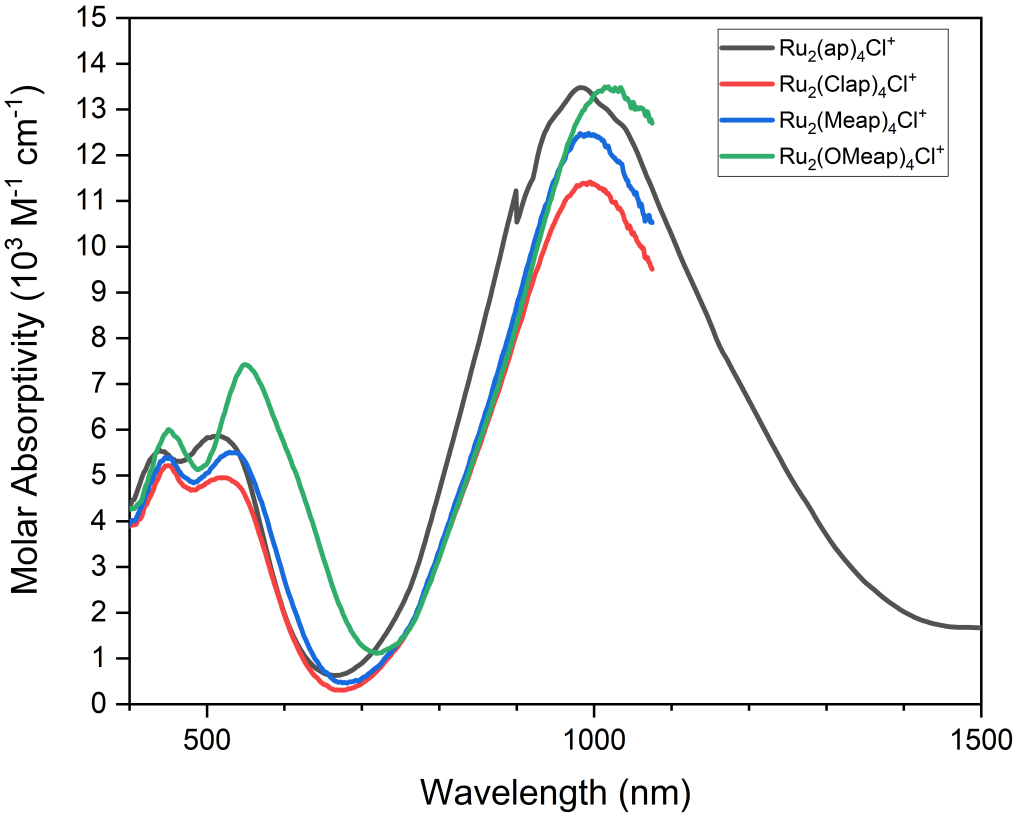


Figures 4.S16 Vis-NIR spectra of [**1**-**4**][$SbCl_6$] in $CH_2Cl_2$. The discontinuity in the spectrum of [**1**][$SbCl_6$] at 900 nm is due to a change from a UV-Vis to a NIR detector.

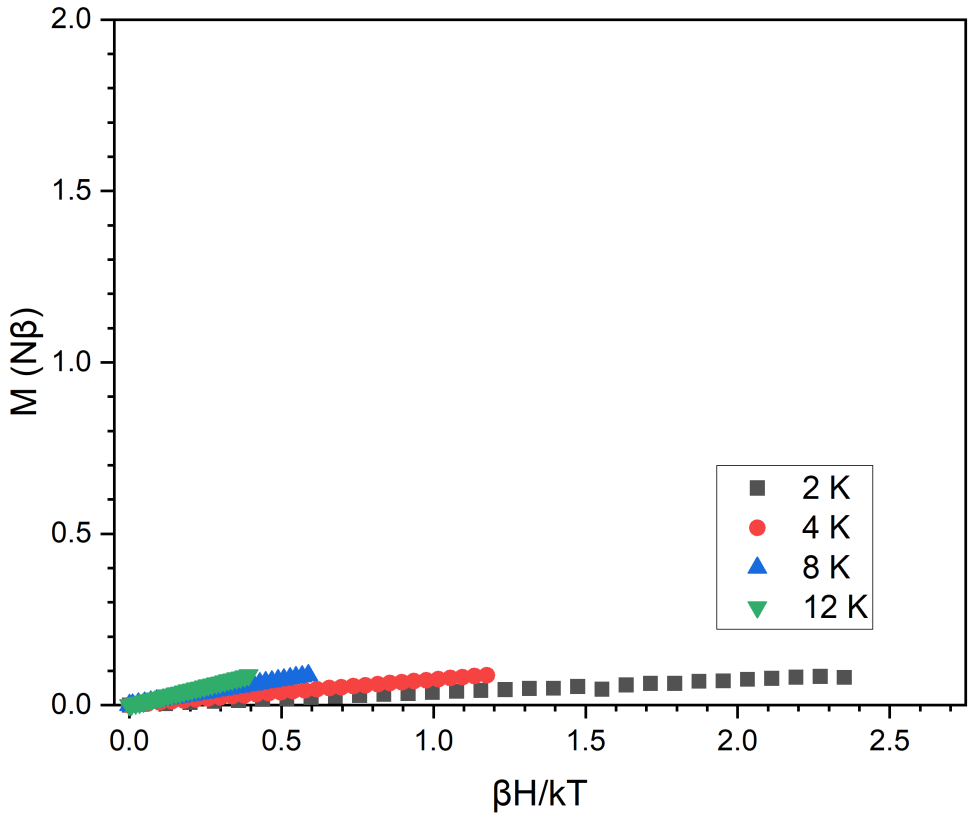


Figure 4.S17 Reduced magnetization data for [**1**][$SbCl_6$]. The low reduced magnetization values and lack of saturation at high field are consistent with an $m_s$ = 0 ground electronic state. The saturation value of M for $S$ = 1 is 2 (Nβ) for $g$ = 2.

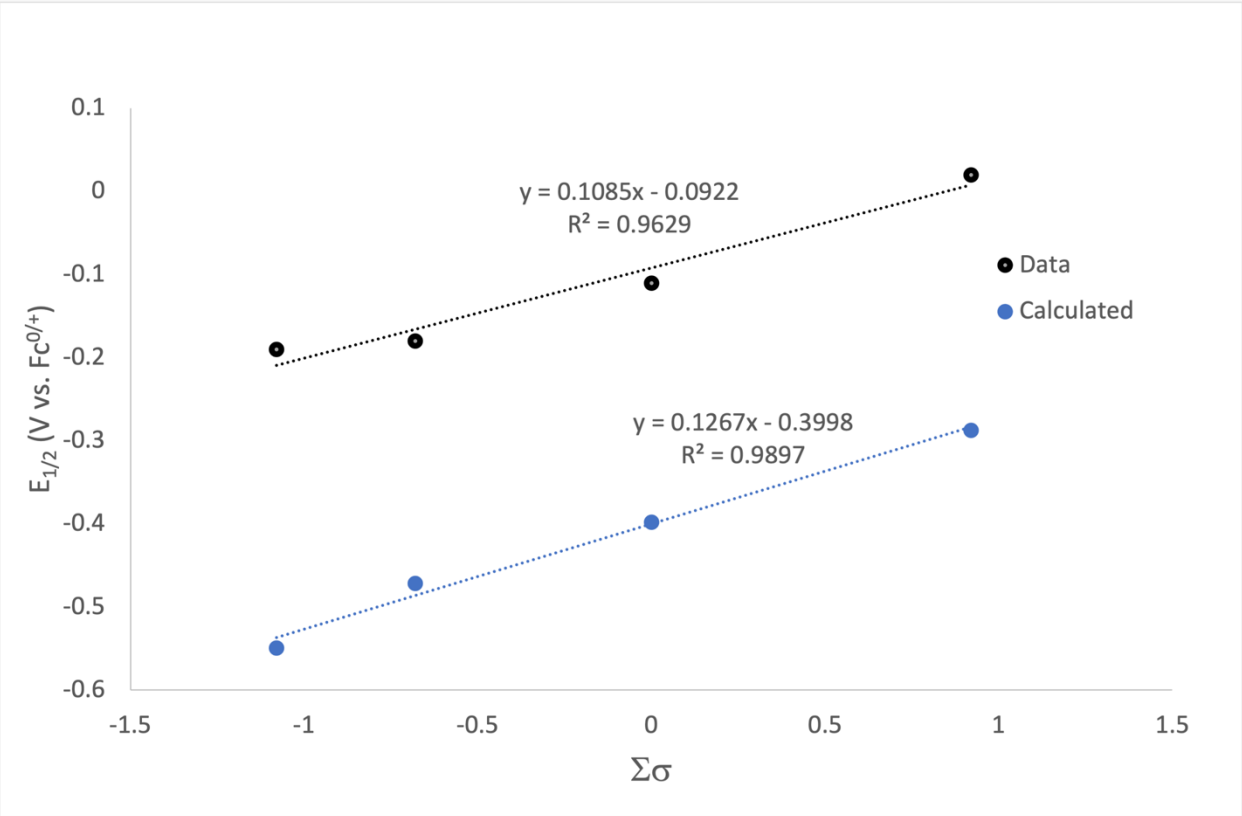


Figure 4.S18 Hammett plot showing the linear free energy relationship between ligand Hammett parameters and calculated $Ru_2^{5+/6+}$ redox potential.

B3LYP geometry-optimized coordinates for **1**

| | | | |
|---|---|---|---|
| Ru | 2.23843938050046 | 2.46984447865498 | 12.98701947255017 |
| Ru | 2.23851167909793 | 0.15679735547540 | 12.98693870677676 |
| Cl | 2.23884104466787 | 5.00863456496640 | 12.98738878991085 |
| N | 3.97511390726370 | 0.15194725112516 | 11.83683966059731 |
| N | 3.59860409733008 | 2.39803352265066 | 11.32734270994147 |
| N | 1.08805037740770 | 0.15179405795478 | 11.25053926976185 |
| N | 0.57899814542096 | 2.39814064900083 | 11.62657045830444 |
| C | 4.29156235474386 | 1.23815295722104 | 11.08996983100104 |
| C | 5.27073945075333 | 1.21424419384535 | 10.05058258284292 |
| C | 5.49552457951221 | 2.33653770387205 | 9.27721392586767 |
| C | 4.75070343125324 | 3.50573609954222 | 9.52015857048353 |
| C | 3.82117317874589 | 3.48006545334335 | 10.54683119012970 |
| C | 4.85921045983168 | -0.95419837377502 | 11.88982864818882 |
| C | 4.44245681591923 | -2.23221753639312 | 11.47241952525314 |
| C | 5.29969732421360 | -3.33380898968342 | 11.58528859150818 |
| C | 6.58835307918030 | -3.17930797016446 | 12.10725372088326 |
| C | 7.01374396957105 | -1.90902403135250 | 12.52037728742648 |
| C | 6.15930867845786 | -0.80901291181846 | 12.41820050494408 |
| C | 0.34124518653485 | 1.23808706192975 | 10.93405200603417 |
| C | -0.69834436573982 | 1.21413219908397 | 9.95512378646625 |
| C | -1.47099119345498 | 2.33673846599201 | 9.72944536935350 |
| C | -1.22718687072343 | 3.50631842933134 | 10.47331126440933 |
| C | -0.20074243734863 | 3.48054028190424 | 11.40307945927844 |
| C | 1.14072645168964 | -0.95435570358714 | 10.36648294342434 |
| C | 1.66766584754107 | -0.80893126507465 | 9.06580993443504 |
| C | 1.76933311592346 | -1.90883857844714 | 8.21117106873541 |
| C | 1.35723028361497 | -3.17932139331390 | 8.63698945915366 |
| C | 0.83687818060253 | -3.33408187698209 | 9.92627028755838 |
| C | 0.72441686742776 | -2.23258036170571 | 10.78367489631664 |
| N | 0.87810265056806 | 2.39781105721905 | 14.64665948650948 |
| N | 3.89813814154687 | 2.39785241838472 | 14.34733472951901 |
| N | 0.50205357060562 | 0.15153271877438 | 14.13735178222023 |
| N | 3.38876955907710 | 0.15167653470568 | 14.72353483773019 |
| C | 0.18566420419938 | 1.23768265648344 | 14.88437387698529 |
| C | 0.65496084541828 | 3.47995759834060 | 15.42684030867976 |
| C | 4.13570788521710 | 1.23784207255385 | 15.03998898597380 |
| C | 4.67836882162907 | 3.47997957537054 | 14.57037146658675 |
| C | -0.38187529653185 | -0.95473640435869 | 14.08473505311162 |
| C | 3.33583922097576 | -0.95448012135489 | 15.60754959490469 |
| C | -0.79300121667739 | 1.21347320328279 | 15.92421304349670 |
| C | -0.27433590913778 | 3.50539974089970 | 16.45373166085151 |
| C | 5.17535065010198 | 1.21378533432803 | 16.01891453592910 |
| C | 5.70502362474709 | 3.50565497618810 | 15.49991467785650 |
| C | 0.03527141999009 | -2.23282656188768 | 14.50158886760700 |
| C | -1.68245242323852 | -0.80963253997554 | 13.55747673310458 |

| | | | |
|---|---|---|---|
| C | 2.80865674686118 | -0.80910892606925 | 16.90811861406142 |
| C | 3.75199476746670 | -2.23277060055014 | 15.19039297556589 |
| C | -1.01823522749079 | 2.33581195660840 | 16.69738386415789 |
| C | 5.94843631480496 | 2.33619708358244 | 16.24416182154339 |
| C | -0.82204008604055 | -3.33442026757616 | 14.38930066469395 |
| C | -2.53696275489888 | -1.90963749920025 | 13.45592880451222 |
| C | 2.70654800690700 | -1.90899780071093 | 17.76269431437235 |
| C | 3.63914227110264 | -3.33428375656044 | 16.04773370726299 |
| C | -2.11117279099851 | -3.17995784372163 | 13.86853137080576 |
| C | 3.11848652079027 | -3.17950791726027 | 17.33687321616977 |
| H | 5.81133912929823 | 0.29215374300211 | 9.85940700344047 |
| H | 6.23294718709355 | 2.30434043326253 | 8.47519616864335 |
| H | 4.88451391989634 | 4.40867057467679 | 8.92916648210007 |
| H | 3.23079268273613 | 4.35855594790180 | 10.79194864938067 |
| H | 3.44860055435913 | -2.35362585856892 | 11.04850171783200 |
| H | 4.95815612014664 | -4.31445839116628 | 11.25423158002976 |
| H | 7.25499911891258 | -4.03687354635053 | 12.19161451086198 |
| H | 8.01295602345633 | -1.77637588551768 | 12.93489368266379 |
| H | 6.48694512463427 | 0.17229565398727 | 12.75829993143861 |
| H | -0.89017926387967 | 0.29182868225955 | 9.41512695213925 |
| H | -2.27287818338845 | 2.30449067355228 | 8.99190355188859 |
| H | -1.81728759229942 | 4.40968995157376 | 10.33852517186982 |
| H | 0.04500063830076 | 4.35930301660494 | 11.99276980446113 |
| H | 2.00693823435971 | 0.17255597239994 | 8.73785975361357 |
| H | 2.18260218859345 | -1.77587299837583 | 7.21149583711631 |
| H | 1.44099043799257 | -4.03680394927973 | 7.97014589299840 |
| H | 0.50679255629602 | -4.31497964274881 | 10.26805770703199 |
| H | 0.30146291122747 | -2.35418391442709 | 11.77791114183672 |
| H | 1.24458683321604 | 4.35878790348692 | 15.18120099888627 |
| H | 4.43292980899109 | 4.35859947160331 | 13.98031932333175 |
| H | -1.33297359872491 | 0.29112714978866 | 16.11590357719792 |
| H | -0.40859346162515 | 4.40848031842387 | 17.04439959961001 |
| H | 5.36689386669443 | 0.29155387349882 | 16.55916572506769 |
| H | 6.29552851067027 | 4.40882060203375 | 15.63428499859942 |
| H | 1.02941246355675 | -2.35430713294180 | 14.92477870875602 |
| H | -2.01048454182209 | 0.17172657663319 | 13.21792130909812 |
| H | 2.46963050222696 | 0.17244243525408 | 17.23608575184388 |
| H | 4.17502289715139 | -2.35445536832075 | 14.19619125130912 |
| H | -1.75529326874050 | 2.30331805977344 | 17.49972247436317 |
| H | 6.75038497849556 | 2.30390411269048 | 16.98163180055947 |
| H | -0.48031442236260 | -4.31514525028419 | 14.71995467615770 |
| H | -3.53656063333457 | -1.77695073936937 | 13.04235925543937 |
| H | 2.29302822534477 | -1.77598827028265 | 18.76225495750827 |
| H | 3.96909105543722 | -4.31522725030956 | 15.70594854702984 |
| H | -2.77786274634240 | -4.03753709671038 | 13.78471359114329 |
| H | 3.03432320649890 | -4.03703127884567 | 18.00361099900341 |

B3LYP geometry-optimized coordinates for **2**

| | | | |
|---|---|---|---|
| Ru | 9.17132576019061 | 5.32284635211075 | 4.24680060481234 |
| Ru | 9.17146791365722 | 3.00892956054143 | 4.24682606846300 |
| Cl | 9.17112750932167 | 7.85318092847107 | 4.24681878438260 |
| Cl | 14.57428882488213 | -1.67570100184308 | 5.16326689502650 |
| Cl | 8.25600004475932 | -1.67588127226711 | 9.64968768982269 |
| N | 10.46008405001091 | 5.24946228643091 | 5.96357428242893 |
| N | 10.86128061822802 | 3.00489044142964 | 5.46395785811280 |
| N | 7.45447219526961 | 5.24924996715707 | 5.53555145160084 |
| N | 7.95440811146859 | 3.00478520489477 | 5.93681912248261 |
| C | 10.64657390380193 | 6.32989885498192 | 6.75578358726406 |
| H | 10.06561307174601 | 7.20810248654088 | 6.48851007960383 |
| C | 11.53186577745763 | 6.35395230320241 | 7.82095412376510 |
| H | 11.63884775402207 | 7.25556255099302 | 8.41931477075644 |
| C | 12.26762040781149 | 5.18599018440033 | 8.09247608900827 |
| H | 12.97041030443613 | 5.15268742748019 | 8.92475581722722 |
| C | 12.07740526678608 | 4.06502606461850 | 7.30712715911747 |
| H | 12.61011704828920 | 3.14319080100980 | 7.52070290327382 |
| C | 11.14474810693393 | 4.09151790761673 | 6.22751432115087 |
| C | 11.75212968030556 | 1.90672102659658 | 5.43769897125483 |
| C | 13.07661138243263 | 2.06093131118175 | 4.97611598276649 |
| H | 13.42353940846440 | 3.04570674717234 | 4.66773035531405 |
| C | 13.94394444307550 | 0.97108511974437 | 4.89556268302583 |
| H | 14.96221423642583 | 1.10149090079453 | 4.53446802351926 |
| C | 13.48917325044542 | -0.29904238351184 | 5.26961265347477 |
| C | 12.18204827738554 | -0.48193553089989 | 5.72667190019132 |
| H | 11.83923250027467 | -1.47177193903360 | 6.02162770951412 |
| C | 11.32397166986151 | 0.61949657427975 | 5.81288267350873 |
| H | 10.31219496166216 | 0.48245230070169 | 6.18593095822052 |
| C | 6.66203686894072 | 6.32954007778153 | 5.72197179527467 |
| H | 6.92881743031989 | 7.20758197400875 | 5.14055322587580 |
| C | 5.59725221673515 | 6.35364075319376 | 6.60772666007852 |
| H | 4.99863218113980 | 7.25508321037478 | 6.71459531312668 |
| C | 5.32650459018573 | 5.18594215234060 | 7.34417919370148 |
| H | 4.49488368481197 | 5.15282476482995 | 8.04776543614768 |
| C | 6.11193475036415 | 4.06503632580586 | 7.15391834611877 |
| H | 5.89903430840918 | 3.14342351281006 | 7.68730266078640 |
| C | 7.19093571819859 | 4.09139721628225 | 6.22052089639468 |
| C | 7.98085552672950 | 1.90659740025555 | 6.82766333500578 |
| C | 8.44461873324122 | 2.06034216997639 | 8.15140628112644 |
| H | 8.75481257078032 | 3.04471128474820 | 8.49783998791498 |
| C | 8.52543731207500 | 0.97053917151727 | 9.01874824639468 |
| H | 8.88880366251662 | 1.10064732635489 | 10.03623731977367 |
| C | 8.14928986672604 | -0.29921004101394 | 8.56468683410402 |
| C | 7.68997592698188 | -0.48170615128670 | 7.25828532665174 |

| | | | |
|---|---|---|---|
| H | 7.39332188566521 | -1.47122547700775 | 6.91606104230012 |
| C | 7.60368409995069 | 0.61972214423708 | 6.40021266643198 |
| H | 7.22906966520600 | 0.48299971529760 | 5.38897333480127 |
| Cl | 3.76837589010599 | -1.67574810949779 | 3.33051582401420 |
| Cl | 10.08746559103056 | -1.67565585356546 | -1.15612677571493 |
| N | 7.88263502393257 | 5.24932111847279 | 2.52996603682160 |
| N | 7.48152927274070 | 3.00475822712631 | 3.02968414169801 |
| N | 10.88812045841640 | 5.24946482297896 | 2.95808039080114 |
| N | 10.38848321697737 | 3.00490227548337 | 2.55692675493826 |
| C | 7.69616642873948 | 6.32969827721646 | 1.73768004754027 |
| H | 8.27698187524774 | 7.20797707970444 | 2.00502255203960 |
| C | 6.81105773902828 | 6.35361751292254 | 0.67234841900378 |
| H | 6.70407736182699 | 7.25519513245874 | 0.07393933512253 |
| C | 6.07547408548014 | 5.18557397468713 | 0.40074213044403 |
| H | 5.37283732633039 | 5.15215354370167 | -0.43166080240280 |
| C | 6.26566701372725 | 4.06466869351212 | 1.18619731491621 |
| H | 5.73306689723115 | 3.14278600430577 | 0.97254144358947 |
| C | 7.19813178698231 | 4.09130195325762 | 2.26597208503458 |
| C | 6.59068062163612 | 1.90661974022038 | 3.05596141797880 |
| C | 5.26613808576190 | 2.06083446038826 | 3.51735330069872 |
| H | 4.91902928587403 | 3.04564106094565 | 3.82539569466158 |
| C | 4.39872580575244 | 0.97105524753228 | 3.59796655131632 |
| H | 3.38041440588093 | 1.10159373792449 | 3.95888571449617 |
| C | 4.85351245070530 | -0.29913372422399 | 3.22414092998611 |
| C | 6.16069149471684 | -0.48207649102012 | 2.76723268885146 |
| H | 6.50352885954390 | -1.47194985388962 | 2.47243404866708 |
| C | 7.01879576721777 | 0.61932000656655 | 2.68095721783445 |
| H | 8.03057053001874 | 0.48224915150884 | 2.30792535646298 |
| C | 11.68040454084562 | 6.32985497577071 | 2.77158642698165 |
| H | 11.41345595970710 | 7.20792182586936 | 3.35288970486126 |
| C | 12.74522500817036 | 6.35401010398534 | 1.88588945181545 |
| H | 13.34369176675748 | 7.25554466652954 | 1.77892355085074 |
| C | 13.01628422652077 | 5.18622084503788 | 1.14969110061367 |
| H | 13.84802739002185 | 5.15311621236012 | 0.44624634429272 |
| C | 12.23102760616945 | 4.06522496495127 | 1.34005945812775 |
| H | 12.44424253597209 | 3.14344773391214 | 0.80708024614723 |
| C | 11.15188095430336 | 4.09159383754531 | 2.27325774316837 |
| C | 10.36219434806453 | 1.90673618213959 | 1.66605469089781 |
| C | 9.89913882489174 | 2.06065756957164 | 0.34207368366777 |
| H | 9.58957144296840 | 3.04518425024672 | -0.00450179424196 |
| C | 9.81843829484151 | 0.97085752647196 | -0.52528750085669 |
| H | 9.45560531019548 | 1.10104505369582 | -1.54295987591282 |
| C | 10.19403549685465 | -0.29899938513365 | -0.07105313945983 |
| C | 10.65268161839155 | -0.48162297059707 | 1.23556149610132 |
| H | 10.94898511670852 | -1.47118967080086 | 1.57796105170141 |
| C | 10.73883277878788 | 0.61977436093119 | 2.09369449421688 |

| | | | |
|---|---|---|---|
| H | 11.11290402653877 | 0.48288522349461 | 3.10511162712886 |

B3LYP geometry-optimized coordinates for **3**

| | | | |
|---|---|---|---|
| Ru | 3.31096885380303 | 4.74430228149419 | 12.87339837479313 |
| Ru | 3.31096025269878 | 7.05692534536010 | 12.87332118679343 |
| Cl | 3.31100680122498 | 2.20025934560860 | 12.87338905608522 |
| N | 4.98991425459398 | 4.81549252079458 | 11.53616687023625 |
| N | 4.49330880637172 | 7.06411042974144 | 11.15927912409339 |
| N | 4.64801704375446 | 4.81564323737295 | 14.55228218227549 |
| N | 5.02475892486975 | 7.06428346106131 | 14.05591022403777 |
| C | 5.76866762556929 | 3.73127134995115 | 11.31887086018248 |
| H | 5.51207347041879 | 2.85154931904502 | 11.90256287227674 |
| C | 6.80675580805285 | 3.70426411164117 | 10.40211358486707 |
| H | 7.39490361340367 | 2.79895583278102 | 10.27175165725814 |
| C | 7.06379054679263 | 4.87526095699973 | 9.66452381037546 |
| H | 7.87409940094428 | 4.90634150067691 | 8.93613065163388 |
| C | 6.29255898920741 | 5.99987638043532 | 9.88375110291708 |
| H | 6.49304999117541 | 6.92276758871161 | 9.34796434761095 |
| C | 5.24064740945961 | 5.97753068023091 | 10.85031696457837 |
| C | 4.46407789391340 | 8.17808718162801 | 10.28281715629148 |
| C | 3.95316497177081 | 8.05339030708001 | 8.97384969621025 |
| H | 3.60730193936004 | 7.07973882739225 | 8.62933907193203 |
| C | 3.87109209668400 | 9.16080357470584 | 8.13007510710014 |
| H | 3.46596122436476 | 9.03364617625505 | 7.12520146830489 |
| C | 4.28376890673989 | 10.43910492371180 | 8.55287464840068 |
| C | 4.78528223750721 | 10.55783707268408 | 9.85774122201343 |
| H | 5.11555643421632 | 11.53280078688103 | 10.21832449402967 |
| C | 4.88099096241248 | 9.45041096281335 | 10.70966742694166 |
| H | 5.28926949348050 | 9.56834670520646 | 11.71050319246665 |
| C | 4.20382941974825 | 11.62891165606644 | 7.62469812267762 |
| H | 4.33581980320170 | 12.57108500543595 | 8.16957546421547 |
| H | 3.23743786957782 | 11.66708866047929 | 7.10482838554622 |
| H | 4.98341247999469 | 11.58109924937050 | 6.85001523954491 |
| C | 4.86498451129613 | 3.73137223879947 | 15.33104358198505 |
| H | 4.28145171028848 | 2.85167068734929 | 15.07392461542731 |
| C | 5.78104646272588 | 3.70443915990421 | 16.36975395652904 |
| H | 5.91125572983823 | 2.79907214142261 | 16.95785581662374 |
| C | 6.51798573213661 | 4.87566513179259 | 16.62761341073378 |
| H | 7.24535627890970 | 4.90695008033056 | 17.43881791959137 |
| C | 6.29907830334408 | 6.00030876254968 | 15.85630912591804 |
| H | 6.83418614458244 | 6.92341397394572 | 16.05765514438506 |
| C | 5.33354115283321 | 5.97776259126714 | 14.80349197373519 |
| C | 5.90010422064692 | 8.17891215553910 | 14.02704137229661 |
| C | 7.21145153379231 | 8.05440998055412 | 13.52207254167933 |
| H | 7.55884716721363 | 7.08013904454616 | 13.18088584784922 |
| C | 8.05414486620984 | 9.16262885997684 | 13.44024481619744 |

| | | | |
|---|---|---|---|
| H | 9.06115026589577 | 9.03541390407053 | 13.04042290460621 |
| C | 7.62776455120821 | 10.44182161259363 | 13.84662596160154 |
| C | 6.32057787227733 | 10.56039578478574 | 14.34195182659562 |
| H | 5.95711840988275 | 11.53595888322214 | 14.66725560418829 |
| C | 5.46983016250683 | 9.45206131729550 | 14.43790449483136 |
| H | 4.46729111267462 | 9.56999850686367 | 14.84199565972021 |
| C | 8.55457408563753 | 11.63262868304374 | 13.76576953719998 |
| H | 9.06720789472038 | 11.67596474360719 | 12.79567533452131 |
| H | 9.33516552033487 | 11.58141160970492 | 14.53912741702819 |
| H | 8.01004222228555 | 12.57374058567162 | 13.90623643769088 |
| N | 1.63195082753301 | 4.81546825013154 | 14.21056059788062 |
| N | 2.12845329295547 | 7.06412152153320 | 14.58733673665121 |
| N | 1.97377456758767 | 4.81551460810181 | 11.19459674682156 |
| N | 1.59706348125803 | 7.06415963518718 | 11.69087844745721 |
| C | 0.85324568218114 | 3.73122108506614 | 14.42787206953437 |
| H | 1.11002054352402 | 2.85143175690124 | 13.84436160673156 |
| C | -0.18501364865595 | 3.70426965287018 | 15.34444696917366 |
| H | -0.77310161520904 | 2.79892925099289 | 15.47484822592041 |
| C | -0.44230801771690 | 4.87536247328885 | 16.08177694883886 |
| H | -1.25278210079481 | 4.90649791327721 | 16.80998240042812 |
| C | 0.32888991250636 | 6.00000715157924 | 15.86253601815959 |
| H | 0.12818384610156 | 6.92297285887264 | 16.39814064177790 |
| C | 1.38103156589891 | 5.97755838399543 | 14.89622574807704 |
| C | 2.15755405584495 | 8.17802585908798 | 15.46379320647855 |
| C | 2.66750556238917 | 8.05310629306312 | 16.77311297677817 |
| H | 3.01271818174544 | 7.07930162355525 | 17.11785134493731 |
| C | 2.74922105341403 | 9.16037144124444 | 17.61712946485539 |
| H | 3.15343111720675 | 9.03294299260147 | 18.62233609896780 |
| C | 2.33732285028892 | 10.43886330968912 | 17.19410292836042 |
| C | 1.83691947614629 | 10.55787807852032 | 15.88883724944324 |
| H | 1.50728130359293 | 11.53298390345304 | 15.52807248116353 |
| C | 1.74143624123142 | 9.45055231000570 | 15.03674954358627 |
| H | 1.33389373870655 | 9.56870902931834 | 14.03563615262366 |
| C | 2.41689878261220 | 11.62854597662247 | 18.12246129780072 |
| H | 2.28512698759900 | 12.57077947759788 | 17.57763996171836 |
| H | 3.38309086642934 | 11.66665038153873 | 18.64270550103202 |
| H | 1.63701502773394 | 11.58062181030389 | 18.89682926936793 |
| C | 1.75670209004110 | 3.73118435702243 | 10.41595039972641 |
| H | 2.34029843784300 | 2.85151003027943 | 10.67303070396973 |
| C | 0.84050677487956 | 3.70418060233416 | 9.37734864913577 |
| H | 0.71022119960766 | 2.79877991842837 | 8.78932059575772 |
| C | 0.10354029068072 | 4.87541776462065 | 9.11948504740098 |
| H | -0.62389195168196 | 4.90665877837085 | 8.30833638637295 |
| C | 0.32261266419470 | 6.00013230388096 | 9.89063803999020 |
| H | -0.21240052277652 | 6.92327876363580 | 9.68923435686531 |
| C | 1.28821512847680 | 5.97762678571504 | 10.94341509908054 |

| | | | |
|---|---|---|---|
| C | 0.72176928314278 | 8.17884432152254 | 11.71975673008053 |
| C | -0.58940637069245 | 8.05452423202327 | 12.22522612300503 |
| H | -0.93672782304698 | 7.08035601032211 | 12.56678234106986 |
| C | -1.43202796751724 | 9.16280748594183 | 12.30700847792893 |
| H | -2.43891004586098 | 9.03575776939077 | 12.70719171518954 |
| C | -1.00571486445518 | 10.44185170246887 | 11.90009970256905 |
| C | 0.30131832567132 | 10.56022801281435 | 11.40430984587150 |
| H | 0.66472477089741 | 11.53568084198371 | 11.07861348178347 |
| C | 1.15199704007756 | 9.45183812486738 | 11.30839288492970 |
| H | 2.15435759387801 | 9.56954583879146 | 10.90378630076072 |
| C | -1.93246584713899 | 11.63271200753041 | 11.98087021418968 |
| H | -2.44466939968211 | 11.67645856988299 | 12.95117387651653 |
| H | -2.71340466455390 | 11.58118352360627 | 11.20788489478561 |
| H | -1.38798416064850 | 12.57375735571464 | 11.83976763182978 |

B3LYP geometry-optimized coordinates for **4**

| | | | |
|---|---|---|---|
| Ru | 8.00035350164610 | 7.99954640827230 | 7.33486583199768 |
| Ru | 8.00041749466084 | 7.99931777020826 | 5.02374439551932 |
| Cl | 8.00044970241273 | 7.99970209319972 | 9.87674351110178 |
| O | 13.25734876247068 | 8.04379936089713 | 0.63738921450329 |
| N | 9.57574125318582 | 6.54156723165219 | 7.25837608740334 |
| N | 9.88241910398522 | 7.11355392085899 | 5.01848613808529 |
| C | 9.90259791038245 | 5.79327250289584 | 8.33590244417346 |
| H | 9.28179919713478 | 5.94897859063785 | 9.21411680374595 |
| C | 10.96591885748414 | 4.90532593934228 | 8.35822499384110 |
| H | 11.17834597756435 | 4.33223304694976 | 9.25758475047122 |
| C | 11.74284151399038 | 4.77958991126993 | 7.19097047752529 |
| H | 12.58681559141938 | 4.09055195773236 | 7.15762266482478 |
| C | 11.41713578507964 | 5.52297347192951 | 6.07313753158524 |
| H | 11.98415831872802 | 5.42043882809393 | 5.15266065296961 |
| C | 10.29892574366728 | 6.41183130319619 | 6.09849430942962 |
| C | 10.74329581825258 | 7.28730927388570 | 3.90464191219442 |
| C | 10.40247430368730 | 6.79514075040758 | 2.63567389824928 |
| H | 9.49127172475449 | 6.21303624397566 | 2.52020393256765 |
| C | 11.21449727962752 | 7.02853515716536 | 1.51642474474771 |
| H | 10.91282306279238 | 6.62626722021606 | 0.55262708082640 |
| C | 12.40152574449898 | 7.76363463507078 | 1.65344533488811 |
| C | 12.75733886459372 | 8.25708282763223 | 2.92460614186750 |
| H | 13.67736688475317 | 8.83239490307619 | 3.02046248916053 |
| C | 11.94111507385743 | 8.02615242487455 | 4.02654628953085 |
| H | 12.22027481228264 | 8.43005711740919 | 4.99859665039483 |
| C | 12.96217289924351 | 7.57063521348278 | -0.66743340715816 |
| H | 12.00993693267513 | 7.97605421283615 | -1.03942942618294 |
| H | 12.91878411176286 | 6.47222452903323 | -0.69926219176416 |
| H | 13.77404062432373 | 7.91591602270310 | -1.31383890547937 |
| O | 7.95892699829428 | 13.25913555844842 | 0.63875833441811 |

| | | | |
|---|---|---|---|
| N | 9.45833449944367 | 9.57498112618944 | 7.25822052405406 |
| N | 8.88646586384250 | 9.88127186643256 | 5.01818517405847 |
| C | 10.20636075288432 | 9.90221743999493 | 8.33581770364743 |
| H | 10.04978272607632 | 9.28224592891234 | 9.21445080847788 |
| C | 11.09514458926902 | 10.96487233083908 | 8.35767451731938 |
| H | 11.66788955486873 | 11.17775369615648 | 9.25716035352153 |
| C | 11.22217298536509 | 11.74061420936347 | 7.18975976273807 |
| H | 11.91243042318373 | 12.58353060128505 | 7.15571922739444 |
| C | 10.47874901549670 | 11.41475969421573 | 6.07197897859723 |
| H | 10.58253504475838 | 11.98066710722138 | 5.15093547570734 |
| C | 9.58864640801909 | 10.29751974513447 | 6.09798745415880 |
| C | 8.71297033350469 | 10.74244959464762 | 3.90453269459833 |
| C | 9.20447611428322 | 10.40164845927174 | 2.63529978861944 |
| H | 9.78560795923589 | 9.48991167309011 | 2.51922790776544 |
| C | 8.97171307710446 | 11.21450575009450 | 1.51651347566769 |
| H | 9.37341335231600 | 10.91299043698756 | 0.55245222247551 |
| C | 8.23812647309395 | 12.40236866263246 | 1.65426983447207 |
| C | 7.74527800964495 | 12.75809092597021 | 2.92568967558146 |
| H | 7.17166341013522 | 13.67907582438095 | 3.02224256042752 |
| C | 7.97538139392760 | 11.94097539651496 | 4.02713733746805 |
| H | 7.57178513197330 | 12.21996051065581 | 4.99935635014680 |
| C | 8.43314701307095 | 12.96529112560382 | -0.66595658204117 |
| H | 8.02792646951097 | 12.01360564691467 | -1.03963260755068 |
| H | 9.53163317893670 | 12.92184037971766 | -0.69691365226630 |
| H | 8.08871123279792 | 13.77807869632956 | -1.31166135837182 |
| O | 2.73960650144219 | 7.96203451056589 | 0.63871822698476 |
| N | 6.42518429586142 | 9.45760002856406 | 7.25827363499859 |
| N | 6.11845864045491 | 8.88535394035755 | 5.01840183473888 |
| C | 6.09853300365311 | 10.20612264565784 | 8.33570363193160 |
| H | 6.71875571754086 | 10.04968931184800 | 9.21420200374073 |
| C | 5.03602789878703 | 11.09508481930233 | 8.35758696052461 |
| H | 4.82395707271724 | 11.66858399873175 | 9.25680962729117 |
| C | 4.25977439563661 | 11.22163224333444 | 7.18996040094762 |
| H | 3.41663600094301 | 11.91166380608276 | 7.15595248552974 |
| C | 4.58517081913024 | 10.47781973452244 | 6.07230884928552 |
| H | 4.01887876628719 | 10.58119477093737 | 5.15148073766148 |
| C | 5.70241874114162 | 9.58773949184687 | 6.09817525083649 |
| C | 5.25735488864648 | 8.71226190733018 | 3.90464607090877 |
| C | 5.59884986744771 | 9.20329337481890 | 2.63542219753135 |
| H | 6.51122852943967 | 9.78342940111368 | 2.51942013168677 |
| C | 4.78587001061146 | 8.97142848677357 | 1.51655540805950 |
| H | 5.08797970295357 | 9.37285105585738 | 0.55256389424520 |
| C | 3.59700445215471 | 8.23944831142991 | 1.65421032391236 |
| C | 3.24087484096420 | 7.74656218038284 | 2.92550778479579 |
| H | 2.31949838570223 | 7.17350048700126 | 3.02179521890581 |
| C | 4.05818954020453 | 7.97566167776810 | 4.02703516635099 |

| | | | |
|---|---|---|---|
| H | 3.77889831670351 | 7.57200688995790 | 4.99914302061445 |
| C | 3.03508240676665 | 8.43483652525103 | -0.66617304713536 |
| H | 3.98519217846928 | 8.02575224460779 | -1.03957687791259 |
| H | 3.08277329701176 | 9.53310023223493 | -0.69742319716175 |
| H | 2.22108878087261 | 8.09327559035524 | -1.31187203377191 |
| O | 8.04108094156898 | 2.73925278594819 | 0.63917026102974 |
| N | 6.54226877975750 | 6.42438814328561 | 7.25843606087015 |
| N | 7.11452356915580 | 6.11739689996569 | 5.01865936311337 |
| C | 5.79356129654909 | 6.09800191272537 | 8.33580947489714 |
| H | 5.94980286768386 | 6.71851542796893 | 9.21411935026970 |
| C | 4.90456655015398 | 5.03553324084737 | 8.35779144223042 |
| H | 4.33076885124524 | 4.82384878757999 | 9.25689564637183 |
| C | 4.77835016635270 | 4.25888771847467 | 7.19038745009072 |
| H | 4.08815124928551 | 3.41590387815777 | 7.15652587416970 |
| C | 5.52243600244740 | 4.58389770568076 | 6.07279863367907 |
| H | 5.41965431219215 | 4.01710006949225 | 5.15220531966133 |
| C | 6.41223692935688 | 5.70136827542944 | 6.09850182435506 |
| C | 7.28793151230264 | 5.25615771084804 | 3.90503518039349 |
| C | 6.79446990516627 | 5.59590079396192 | 2.63629252753398 |
| H | 6.21190870841304 | 6.50679149942070 | 2.52067962608121 |
| C | 7.02690550946383 | 4.78298303626307 | 1.51748794854488 |
| H | 6.62308369147025 | 5.08344300680201 | 0.55395478585929 |
| C | 7.76227363196589 | 3.59613050982111 | 1.65471325322496 |
| C | 8.25727512944742 | 3.24155820912828 | 2.92562864217272 |
| H | 8.83230886286216 | 2.32141799478654 | 3.02175662173240 |
| C | 8.02726983114593 | 4.05867968393079 | 4.02710124881971 |
| H | 8.43229795590439 | 3.78044553928164 | 4.99894071551859 |
| C | 7.56561125540870 | 3.03279540104338 | -0.66519817887791 |
| H | 7.96968846094228 | 3.98498454056014 | -1.03873959304092 |
| H | 6.46707359689977 | 3.07526188141756 | -0.69525446420555 |
| H | 7.91045451935951 | 2.22064242463490 | -1.31145903210022 |

B3LYP geometry-optimized coordinates for [**1**]$^{+}$

| | | | |
|---|---|---|---|
| Ru | 3.883901 | 4.689200 | 15.034615 |
| Ru | 3.883948 | 2.363346 | 15.034658 |
| Cl | 3.884265 | 7.179566 | 15.035054 |
| N | 5.995666 | 4.606891 | 14.716885 |
| N | 5.910727 | 2.353864 | 15.326307 |
| N | 3.566307 | 4.607321 | 12.923026 |
| N | 4.175846 | 2.354310 | 13.007707 |
| C | 6.696366 | 5.688431 | 14.305302 |
| H | 6.111236 | 6.581053 | 14.105884 |
| C | 8.074618 | 5.689339 | 14.157162 |
| H | 8.579492 | 6.590654 | 13.818524 |
| C | 8.777630 | 4.507226 | 14.443933 |
| H | 9.859541 | 4.461095 | 14.328075 |

| | | | |
|---|---|---|---|
| C | 8.077801 | 3.388053 | 14.855608 |
| H | 8.591840 | 2.452177 | 15.051328 |
| C | 6.661589 | 3.440043 | 14.987603 |
| C | 6.536215 | 1.242314 | 15.954509 |
| C | 7.156791 | 1.403735 | 17.210375 |
| H | 7.182343 | 2.389017 | 17.672980 |
| C | 7.718767 | 0.306185 | 17.865333 |
| H | 8.189798 | 0.445430 | 18.837647 |
| C | 7.670491 | -0.967900 | 17.283366 |
| H | 8.109290 | -1.822062 | 17.797112 |
| C | 7.056887 | -1.133497 | 16.037182 |
| H | 7.020568 | -2.117524 | 15.571093 |
| C | 6.492620 | -0.037687 | 15.373866 |
| H | 6.032785 | -0.166862 | 14.397937 |
| C | 3.155088 | 5.689052 | 12.222353 |
| H | 2.954901 | 6.581401 | 12.807631 |
| C | 3.008685 | 5.690558 | 10.843933 |
| H | 2.670606 | 6.592022 | 10.338959 |
| C | 3.296993 | 4.508905 | 10.140696 |
| H | 3.183511 | 4.463517 | 9.058509 |
| C | 3.707936 | 3.389446 | 10.840490 |
| H | 3.904967 | 2.453938 | 10.326289 |
| C | 3.837875 | 3.440736 | 12.256964 |
| C | 4.804255 | 1.242895 | 12.382151 |
| C | 6.061170 | 1.404026 | 11.763660 |
| H | 6.524275 | 2.389097 | 11.739304 |
| C | 6.716282 | 0.306538 | 11.201781 |
| H | 7.689525 | 0.445388 | 10.732550 |
| C | 6.133377 | -0.967202 | 11.248021 |
| H | 6.647194 | -1.821301 | 10.809183 |
| C | 4.886075 | -1.132484 | 11.859399 |
| H | 4.419298 | -2.116228 | 11.894167 |
| C | 4.222639 | -0.036700 | 12.423546 |
| H | 3.245840 | -0.165436 | 12.881630 |
| N | 1.772300 | 4.606939 | 15.352491 |
| N | 1.857289 | 2.353951 | 14.742753 |
| N | 4.201830 | 4.606705 | 17.146414 |
| N | 3.592197 | 2.353733 | 17.061392 |
| C | 1.071675 | 5.688424 | 15.764289 |
| H | 1.656746 | 6.581157 | 15.963411 |
| C | -0.306532 | 5.689112 | 15.913053 |
| H | -0.811465 | 6.590352 | 16.251803 |
| C | -1.009458 | 4.506842 | 15.626768 |
| H | -2.091304 | 4.460548 | 15.743135 |
| C | -0.309669 | 3.387772 | 15.214711 |
| H | -0.823630 | 2.451827 | 15.019201 |

| | | | |
|---|---|---|---|
| C | 1.106426 | 3.440020 | 15.081970 |
| C | 1.231717 | 1.242438 | 14.114633 |
| C | 0.609492 | 1.404271 | 12.859645 |
| H | 0.582300 | 2.389943 | 12.397963 |
| C | 0.047467 | 0.306850 | 12.204554 |
| H | -0.424837 | 0.446456 | 11.232885 |
| C | 0.097329 | -0.967596 | 12.785568 |
| H | -0.341498 | -1.821717 | 12.271776 |
| C | 0.712574 | -1.133621 | 14.030893 |
| H | 0.750079 | -2.118030 | 14.496066 |
| C | 1.276928 | -0.037948 | 14.694322 |
| H | 1.738161 | -0.167567 | 15.669533 |
| C | 4.613191 | 5.688249 | 17.847221 |
| H | 4.813317 | 6.580705 | 17.262082 |
| C | 4.759791 | 5.689511 | 19.225652 |
| H | 5.098000 | 6.590871 | 19.730710 |
| C | 4.471541 | 4.507757 | 19.928692 |
| H | 4.585188 | 4.462115 | 21.010849 |
| C | 4.060478 | 3.388477 | 19.228684 |
| H | 3.863723 | 2.452858 | 19.742754 |
| C | 3.930349 | 3.440017 | 17.812276 |
| C | 2.963778 | 1.242188 | 17.686785 |
| C | 1.706643 | 1.403192 | 18.304851 |
| H | 1.243325 | 2.388176 | 18.328755 |
| C | 1.051472 | 0.305639 | 18.866584 |
| H | 0.078029 | 0.444458 | 19.335401 |
| C | 1.634616 | -0.967987 | 18.820624 |
| H | 1.120732 | -1.822132 | 19.259283 |
| C | 2.882168 | -1.133128 | 18.209679 |
| H | 3.349015 | -2.116843 | 18.175124 |
| C | 3.545659 | -0.037318 | 17.645670 |
| H | 4.522542 | -0.166010 | 17.187757 |

B3LYP geometry-optimized coordinates for [**2**]$^{+}$

| | | | |
|---|---|---|---|
| Ru | 5.69724283310569 | 10.85836784586727 | 5.03183351680872 |
| Ru | 5.68084258250012 | 8.53136583704884 | 5.02085157904568 |
| Cl | 5.71354318934460 | 13.34320020096683 | 5.04245220192927 |
| Cl | 1.09382012171162 | 3.86510482483368 | 2.06870495867963 |
| Cl | 2.72705336077836 | 3.81837054232650 | 9.56363291716268 |
| N | 3.59098953957558 | 10.78956782618896 | 5.39285270059299 |
| N | 3.64732999176308 | 8.53647285713313 | 4.77839287241879 |
| N | 6.05772368863028 | 10.76436421995463 | 7.13689348969932 |
| N | 5.43860645844225 | 8.51323698668415 | 7.05475399409894 |
| C | 2.90774615805962 | 11.87503985526200 | 5.82311489258354 |
| H | 3.50265746810007 | 12.76403672793424 | 6.00891057241224 |
| C | 1.53366620789065 | 11.88387012093816 | 6.00680560635851 |

| | | | |
|---|---|---|---|
| H | 1.04317024068394 | 12.78800439100142 | 6.35873809387489 |
| C | 0.81666899267134 | 10.70638486751908 | 5.73888491206426 |
| H | -0.26195392563139 | 10.66614213256680 | 5.88330862095127 |
| C | 1.49928599798761 | 9.58305778369666 | 5.30863528848263 |
| H | 0.97384363942998 | 8.65043623789196 | 5.12790302902330 |
| C | 2.91086913994336 | 9.62802516007589 | 5.13846455408006 |
| C | 3.00016209637913 | 7.43157627701769 | 4.16667905816597 |
| C | 2.32796091889795 | 7.59583784790303 | 2.93793129086357 |
| H | 2.27612932212265 | 8.58141862195037 | 2.47887521153661 |
| C | 1.74238836098246 | 6.50661665552049 | 2.29346001015680 |
| H | 1.23113851531799 | 6.63974110445110 | 1.34243768828722 |
| C | 1.82717126150244 | 5.23496177125957 | 2.87414952269623 |
| C | 2.48875671826009 | 5.04824748387135 | 4.09068755809274 |
| H | 2.54278639964945 | 4.05821247833299 | 4.53843529942743 |
| C | 3.07083633385807 | 6.14566024321057 | 4.73132193023557 |
| H | 3.56985192901733 | 6.00457430349426 | 5.68568805979626 |
| C | 6.48974605905978 | 11.84121918230843 | 7.83261648777426 |
| H | 6.67662171494224 | 12.73676947409144 | 7.24792822766295 |
| C | 6.67387338856791 | 11.83385979068776 | 9.20663009503920 |
| H | 7.02709601385184 | 12.73179105619898 | 9.70744435076127 |
| C | 6.40470372162881 | 10.64842953174271 | 9.90997028036436 |
| H | 6.54912358700629 | 10.59548426689623 | 10.98803830795430 |
| C | 5.97249874082027 | 9.53380660993992 | 9.21445755174781 |
| H | 5.79085900137950 | 8.59528076548634 | 9.72893499222688 |
| C | 5.80152214584276 | 9.59539343284543 | 7.80355725176386 |
| C | 4.82572140429405 | 7.40198259002201 | 7.68997191739857 |
| C | 3.59773352700729 | 7.56034194789559 | 8.36497777996074 |
| H | 3.13964161808339 | 8.54573650874638 | 8.42772363270285 |
| C | 2.95287854750147 | 6.46594468700292 | 8.94039773630137 |
| H | 2.00259179592635 | 6.59487017818485 | 9.45405827394631 |
| C | 3.53240320480174 | 5.19471745582086 | 8.84233774086957 |
| C | 4.74783727828583 | 5.01359093215027 | 8.17718911685393 |
| H | 5.19458267269301 | 4.02373476807867 | 8.11256667967906 |
| C | 5.38879668760334 | 6.11620240348325 | 7.60535604444819 |
| H | 6.34252554776621 | 5.97919035460824 | 7.10402176180328 |
| Cl | 10.21509488331153 | 3.77452923147898 | 7.92043280174919 |
| Cl | 8.57787014388485 | 3.81869555663705 | 0.44499220691093 |
| N | 7.80225527211119 | 10.76357545221086 | 4.67042042377092 |
| N | 7.71487283018676 | 8.50554820437278 | 5.26343112297486 |
| N | 5.33614322433449 | 10.78848801177907 | 2.92534082430830 |
| N | 5.92353981643650 | 8.52825961317901 | 2.98731950182342 |
| C | 8.50054868608724 | 11.84373437560686 | 4.25107277244209 |
| H | 7.91795781381846 | 12.74267336203440 | 4.07423353619128 |
| C | 9.87459681290483 | 11.83549412165655 | 4.06733640294062 |
| H | 10.37749060921085 | 12.73628251033388 | 3.72447545087222 |
| C | 10.57520990731732 | 10.64550430517634 | 4.32318256078098 |

| | | | |
|---|---|---|---|
| H | 11.65312849996423 | 10.59167322368248 | 4.17800433580687 |
| C | 9.87700548255334 | 9.52759338700686 | 4.74226709087950 |
| H | 10.38956007600976 | 8.58601671868652 | 4.91307563303021 |
| C | 8.46617751077773 | 9.59022583161157 | 4.91343238708928 |
| C | 8.34780291494372 | 7.38591356820108 | 5.86362692646240 |
| C | 9.02141562409797 | 7.52838068752460 | 7.09434676223997 |
| H | 9.08478334059176 | 8.50810198992083 | 7.56436622535434 |
| C | 9.59483520878753 | 6.42552162852972 | 7.72650382780287 |
| H | 10.10756057750783 | 6.54232350543807 | 8.67885944575859 |
| C | 9.49627662766479 | 5.16158039330915 | 7.13129879004499 |
| C | 8.83263952286518 | 4.99622897320137 | 5.91281597585450 |
| H | 8.76797724100812 | 4.01205639703858 | 5.45366042006362 |
| C | 8.26277069466363 | 6.10722549537619 | 5.28470952576248 |
| H | 7.76258671332865 | 5.98242894048319 | 4.32876160532689 |
| C | 4.92044238845706 | 11.87771250374374 | 2.23903357023666 |
| H | 4.74537760240225 | 12.77041451443381 | 2.83167986030396 |
| C | 4.73843203536287 | 11.88568772887262 | 0.86471764928061 |
| H | 4.39866679969145 | 12.79308852561254 | 0.37169114099571 |
| C | 4.99227922653146 | 10.70326008234344 | 0.15075171770948 |
| H | 4.84903119095682 | 10.66238758332036 | -0.92800447380241 |
| C | 5.40754617765024 | 9.57621223676879 | 0.83649960076665 |
| H | 5.57719951962277 | 8.64018867688561 | 0.31340874479753 |
| C | 5.57692624594289 | 9.62233982664414 | 2.24814012618200 |
| C | 6.52234258423257 | 7.41461122264410 | 2.34279836580380 |
| C | 7.75448639728417 | 7.56200854680158 | 1.67291290128206 |
| H | 8.22652556653767 | 8.54142332154087 | 1.62082745528844 |
| C | 8.38607502753635 | 6.46387758512607 | 1.08988003488926 |
| H | 9.33982611353362 | 6.58417169670722 | 0.58055022689197 |
| C | 7.78878334007939 | 5.19992507139282 | 1.17488659852681 |
| C | 6.56849144702829 | 5.02988986681711 | 1.83403926725674 |
| H | 6.10775889813715 | 4.04585219048553 | 1.88830432080499 |
| C | 5.94096987249655 | 6.13617740343002 | 2.41359153874691 |
| H | 4.98391533411176 | 6.00798479086168 | 2.91080713901360 |

B3LYP geometry-optimized coordinates for [**3**]$^{+}$

| | | | |
|---|---|---|---|
| Ru | 3.70572830079739 | 5.65122274136237 | 16.03664091970736 |
| Ru | 3.70570889409758 | 3.32563412064503 | 16.03659472292610 |
| Cl | 3.70584766102213 | 8.14517705009601 | 16.03652317359082 |
| N | 5.78507907467321 | 5.56698307182592 | 15.55845039685877 |
| N | 5.74805116954413 | 3.31807343054194 | 16.18828213144112 |
| N | 3.22763249477832 | 5.56739744418487 | 13.95732204805585 |
| N | 3.85726178715194 | 3.31840416616844 | 13.99404288510112 |
| C | 6.44948997282169 | 6.64472240169635 | 15.08199590317984 |
| H | 5.84940847892241 | 7.53616770130418 | 14.92530619790307 |
| C | 7.81077008743764 | 6.64328249129512 | 14.82054255119248 |
| H | 8.28659910735227 | 7.54094961699087 | 14.43354102708176 |

| | | | |
|---|---|---|---|
| C | 8.53457695623459 | 5.46274399771004 | 15.05910021869108 |
| H | 9.60318957409183 | 5.41450314437663 | 14.85468776188395 |
| C | 7.87108960247926 | 4.34797577689285 | 15.53745607737805 |
| H | 8.39910950620626 | 3.41321811120259 | 15.69817104421178 |
| C | 6.46998725117819 | 4.40125546491363 | 15.78338656055199 |
| C | 6.42090159676039 | 2.21433913704428 | 16.77805244842154 |
| C | 7.15414655137863 | 2.38905796746460 | 17.97003802956344 |
| H | 7.22296493885654 | 3.37972436480530 | 18.41673511749340 |
| C | 7.77319328786578 | 1.30282853150995 | 18.58584777428636 |
| H | 8.32860271010419 | 1.46399382691736 | 19.51029341655675 |
| C | 7.68879316431775 | 0.00501656644056 | 18.04522983323294 |
| C | 6.94994183993274 | -0.15979762463289 | 16.86323484908136 |
| H | 6.86559421113874 | -1.15057454622801 | 16.41627448753623 |
| C | 6.32474391502864 | 0.92291201187342 | 16.23405492183410 |
| H | 5.77656064178774 | 0.77066821998375 | 15.30755930180891 |
| C | 8.39191762507313 | -1.15536141463302 | 18.70723914155286 |
| H | 8.03266905551713 | -2.11636467529586 | 18.32130969709612 |
| H | 8.24531479976534 | -1.14330532373024 | 19.79502115880300 |
| H | 9.47623005696251 | -1.10914507087840 | 18.52853431363431 |
| C | 2.75198923000959 | 6.64549581032144 | 13.29290835902591 |
| H | 2.59580706952569 | 7.53692599320348 | 13.89319150450933 |
| C | 2.49129965242597 | 6.64449017742036 | 11.93148113703628 |
| H | 2.10531155742478 | 7.54251482306407 | 11.45552399418707 |
| C | 2.72972390696168 | 5.46399261054812 | 11.20754412023996 |
| H | 2.52641976903251 | 5.41624304424505 | 10.13869622819426 |
| C | 3.20709895202282 | 4.34882229675969 | 11.87107773320673 |
| H | 3.36766716619043 | 3.41407808729979 | 11.34297532786025 |
| C | 3.45244655882103 | 4.40171677740595 | 13.27231200013445 |
| C | 4.44757543485344 | 2.21522796534023 | 13.32056973483761 |
| C | 5.64107776138902 | 2.39055946521939 | 12.58992473211164 |
| H | 6.08848039828777 | 3.38107338174460 | 12.52363278856231 |
| C | 6.25765120386571 | 1.30515791029504 | 11.97028298205584 |
| H | 7.18334468461969 | 1.46677117263061 | 11.41709895119464 |
| C | 5.71612589794337 | 0.00747624278848 | 12.05128847237394 |
| C | 4.53243885370672 | -0.15793811624038 | 12.78723301789217 |
| H | 4.08479704835735 | -1.14862701383062 | 12.86893835379990 |
| C | 3.90258959303026 | 0.92402929249125 | 13.41317744257095 |
| H | 2.97511103703427 | 0.77126107913455 | 13.95952646772193 |
| C | 6.37989020013870 | -1.15201222756813 | 11.34832086436937 |
| H | 6.21457093614373 | -1.09787106855929 | 10.26229981004076 |
| H | 5.98481359184220 | -2.11321277280005 | 11.69690148889791 |
| H | 7.46594080952072 | -1.14671637781681 | 11.50792219992663 |
| N | 1.62641963118592 | 5.56707506144967 | 16.51495823678023 |
| N | 1.66319437243621 | 3.31819580863490 | 15.88496188042955 |
| N | 4.18346656333282 | 5.56738790315822 | 18.11600350415335 |
| N | 3.55409850702479 | 3.31831876582691 | 18.07914239249295 |

| | | | |
|---|---|---|---|
| C | 0.96221598393597 | 6.64483251213835 | 16.99166617894673 |
| H | 1.56243062542481 | 7.53620276894994 | 17.14831469995969 |
| C | -0.39900674723929 | 6.64349895568462 | 17.25338755753463 |
| H | -0.87468744732419 | 7.54116966568285 | 17.64056017005992 |
| C | -1.12296412379285 | 5.46305379000414 | 17.01481547033626 |
| H | -2.19155295028359 | 5.41488733825898 | 17.21936098142742 |
| C | -0.45965171327766 | 4.34829443911639 | 16.53621117344855 |
| H | -0.98786938578678 | 3.41370757796183 | 16.37531664342208 |
| C | 0.94140906804807 | 4.40141398210382 | 16.29004968816689 |
| C | 0.99012269534108 | 2.21443737175676 | 15.29554298274792 |
| C | 0.25592549578677 | 2.38907607215770 | 14.10413392419277 |
| H | 0.18626392191903 | 3.37980866992334 | 13.65774297058400 |
| C | -0.36352435387114 | 1.30289303787351 | 13.48867638306228 |
| H | -0.91970477390185 | 1.46414293521649 | 12.56471332439036 |
| C | -0.27862989364108 | 0.00506064236879 | 14.02916347125890 |
| C | 0.46115012156056 | -0.15974921324475 | 15.21057242976964 |
| H | 0.54589289729352 | -1.15053177020388 | 15.65744659134341 |
| C | 1.08675805634212 | 0.92296090820384 | 15.83934819398013 |
| H | 1.63562759705723 | 0.77066818640279 | 16.76542855640035 |
| C | -0.98226184710064 | -1.15530673310791 | 13.36767882178824 |
| H | -0.62286130149437 | -2.11630877918144 | 13.75346782079607 |
| H | -0.83633253537480 | -1.14335654703966 | 12.27980607743295 |
| H | -2.06645607046411 | -1.10896660535371 | 13.54705639246064 |
| C | 4.65851565136547 | 6.64563249783647 | 18.78058866850305 |
| H | 4.81458183793257 | 7.53710999648443 | 18.18035900861315 |
| C | 4.91871104682268 | 6.64471731447788 | 20.14211000329484 |
| H | 5.30420541437232 | 7.54288033735646 | 20.61820618758843 |
| C | 4.68041504283762 | 5.46414129420138 | 20.86595647227719 |
| H | 4.88331482809632 | 5.41646889815651 | 21.93488458228810 |
| C | 4.20354158309472 | 4.34884719382412 | 20.20226989597874 |
| H | 4.04298192171958 | 3.41407810997832 | 20.73034045871957 |
| C | 3.95865331973736 | 4.40167353582325 | 18.80095454663731 |
| C | 2.96384834160109 | 2.21505940148085 | 18.75253591592919 |
| C | 1.77001415476143 | 2.39014653114374 | 19.48268234001820 |
| H | 1.32228754629927 | 3.38053490919711 | 19.54865079033228 |
| C | 1.15353078463071 | 1.30465940295465 | 20.10225974321005 |
| H | 0.22757453580478 | 1.46608712912545 | 20.65505828761773 |
| C | 1.69548060038006 | 0.00713226342150 | 20.02167376720916 |
| C | 2.87951931165454 | -0.15804857001586 | 19.28623754022651 |
| H | 3.32751805276422 | -1.14860488430156 | 19.20495064657025 |
| C | 3.50928043730600 | 0.92401693265185 | 18.66037770688544 |
| H | 4.43715870853449 | 0.77153562511646 | 18.11461638628169 |
| C | 1.03179396652655 | -1.15242539131718 | 20.72460235627595 |
| H | 1.19677986339988 | -1.09808435679909 | 21.81066381716120 |
| H | 1.42720908541107 | -2.11358101943479 | 20.37627844363350 |
| H | -0.05421005461479 | -1.14742215104903 | 20.56468509597604 |

B3LYP geometry-optimized coordinates for [**4**]$^{+}$

| | | | |
|---|---|---|---|
| Ru | 5.16410747853765 | 5.16503603789149 | 11.28710412605858 |
| Ru | 5.16365568356146 | 5.16548896204823 | 13.61113072456349 |
| Cl | 5.16448631124682 | 5.16502974084384 | 8.79227115406357 |
| O | 10.12183561408079 | 7.06546942600538 | 17.90586390209375 |
| N | 6.05134838555685 | 7.10507310948169 | 11.37485161428219 |
| N | 6.54561927226628 | 6.67714789055626 | 13.61668952205382 |
| C | 6.06776093787709 | 7.92972187257143 | 10.30307499840019 |
| H | 5.56328611893634 | 7.55836527863742 | 9.41589514463168 |
| C | 6.69791515515875 | 9.16452470969237 | 10.30451585804352 |
| H | 6.67147884138369 | 9.78503156917528 | 9.41210330168575 |
| C | 7.34999231086530 | 9.57857754142721 | 11.47855852205313 |
| H | 7.84850521874291 | 10.54559552374300 | 11.52615324435790 |
| C | 7.33486220501391 | 8.75360414189392 | 12.58803121176179 |
| H | 7.80046711284457 | 9.06399360587651 | 13.51818964455011 |
| C | 6.66300405538963 | 7.49990435887629 | 12.53654475988394 |
| C | 7.42838519730976 | 6.83570479847702 | 14.71737861292070 |
| C | 6.94786249804188 | 7.08698649544846 | 16.01132107998618 |
| H | 5.88178901152877 | 7.23607218131464 | 16.16524359890893 |
| C | 7.81740315266600 | 7.17051098952027 | 17.10625617805298 |
| H | 7.40663867168181 | 7.37492925447027 | 18.09139698789698 |
| C | 9.19955262392816 | 7.00330196672118 | 16.91976527850883 |
| C | 9.69026475713832 | 6.75389423501729 | 15.62104459530824 |
| H | 10.76275693957990 | 6.61986771191350 | 15.48696747029527 |
| C | 8.82131371578124 | 6.67177257028253 | 14.54099762263752 |
| H | 9.21576194262789 | 6.46326540561538 | 13.54775285617076 |
| C | 9.70150379357878 | 7.30802591281186 | 19.24211739445158 |
| H | 9.20528151137862 | 8.28426556411739 | 19.33602896613955 |
| H | 10.60649715510315 | 7.30458194206803 | 19.85534637219954 |
| H | 9.02060793932645 | 6.52192571508648 | 19.59797102841324 |
| O | 0.20563450385538 | 3.25983048819899 | 17.90531558567601 |
| N | 4.27736858686497 | 3.22489949964034 | 11.37500178585206 |
| N | 3.78179105371364 | 3.65368083678208 | 13.61639550537162 |
| C | 4.26254031165822 | 2.39942752781621 | 10.30381259687018 |
| H | 4.76710829665806 | 2.77070300277630 | 9.41667193162094 |
| C | 3.63398297725502 | 1.16380612161354 | 10.30590346098205 |
| H | 3.66257558255795 | 0.54230187380281 | 9.41423456185685 |
| C | 2.98161997881638 | 0.74994089270099 | 11.47985465366031 |
| H | 2.48451675382323 | -0.21777477853742 | 11.52815127888928 |
| C | 2.99487332224334 | 1.57589301404164 | 12.58862213074264 |
| H | 2.52914790027144 | 1.26576429505323 | 13.51876221183998 |
| C | 3.66555079488425 | 2.83020787758615 | 12.53665988248156 |
| C | 2.89906724892934 | 3.49450509728733 | 14.71702535859462 |
| C | 3.37970990326093 | 3.24305136627223 | 16.01087358627499 |
| H | 4.44587815486325 | 3.09472786047607 | 16.16478713073930 |

| | | | |
|---|---|---|---|
| C | 2.51020387978952 | 3.15822721870402 | 17.10570322639811 |
| H | 2.92118538615840 | 2.95317757365171 | 18.09062206037358 |
| C | 1.12789038433294 | 3.32407212913224 | 16.91926823723153 |
| C | 0.63702814097059 | 3.57405562113543 | 15.62071840461475 |
| H | -0.43552398832650 | 3.70749522956723 | 15.48667768262404 |
| C | 1.50602935363602 | 3.65753364495022 | 14.54080311175473 |
| H | 1.11135220282343 | 3.86637187184515 | 13.54772529098598 |
| C | 0.62675376550792 | 3.01900061934528 | 19.24165364378094 |
| H | 1.12619271446037 | 2.04442425970590 | 19.33592480620174 |
| H | -0.27805485287727 | 3.01981356147378 | 19.85512737632386 |
| H | 1.30510447432314 | 3.80748979105008 | 19.59705800559813 |
| O | 3.26334205678822 | 10.12277312394769 | 17.90613859865913 |
| N | 3.22422340129656 | 6.05250251825296 | 11.37426369112148 |
| N | 3.65207178025008 | 6.54770676234592 | 13.61584991713886 |
| C | 2.39970487740987 | 6.06867140841989 | 10.30238093907378 |
| H | 2.77070490277496 | 5.56299984750331 | 9.41572257924746 |
| C | 1.16555821653844 | 6.70010543123254 | 10.30303950547013 |
| H | 0.54502752240661 | 6.67315105515144 | 9.41066761945856 |
| C | 0.75215795266530 | 7.35394285611125 | 11.47634367084737 |
| H | -0.21399943834308 | 7.85421912759018 | 11.52314476920130 |
| C | 1.57679102191550 | 7.33876900079043 | 12.58606711155729 |
| H | 1.26678063652866 | 7.80550229549375 | 13.51577738193050 |
| C | 2.82967426552970 | 6.66524661906172 | 12.53550505706765 |
| C | 3.49342204997869 | 7.43038188817669 | 14.71666781608712 |
| C | 3.23975989139222 | 6.94972744756942 | 16.01007374145438 |
| H | 3.08898143213963 | 5.88381685462496 | 16.16337327061376 |
| C | 3.15615981862871 | 7.81889342913329 | 17.10528633535854 |
| H | 2.94970363957094 | 7.40780482583570 | 18.08990050877555 |
| C | 3.32570698872720 | 9.20087681416992 | 16.91967324115789 |
| C | 3.57773768891024 | 9.69177493434554 | 15.62154814501362 |
| H | 3.71458031905489 | 10.76397776459567 | 15.48820995918256 |
| C | 3.65982312129533 | 8.82311758542073 | 14.54125765531125 |
| H | 3.87038789332580 | 9.21796926982074 | 13.54859393244917 |
| C | 3.02126110113858 | 9.70155185794982 | 19.24221165374147 |
| H | 2.04560129026545 | 9.20421981826925 | 19.33606330621948 |
| H | 3.02408590848029 | 10.60608668281508 | 19.85610591118223 |
| H | 3.80817502718108 | 9.02121519972745 | 19.59733788809809 |
| O | 7.07241552548528 | 0.20756466963243 | 17.90599043803841 |
| N | 7.10407503196144 | 4.27788546310914 | 11.37540122558852 |
| N | 6.67543996775142 | 3.78362897428334 | 13.61718061080304 |
| C | 7.92899690874158 | 4.26136930882153 | 10.30382050687271 |
| H | 7.55760980155266 | 4.76538585863448 | 9.41639677722567 |
| C | 9.16396774332964 | 3.63152606096241 | 10.30577978559113 |
| H | 9.78470052884237 | 3.65790374815743 | 9.41349683239704 |
| C | 9.57798218537961 | 2.98009690209254 | 11.48018370575050 |
| H | 10.54495876874886 | 2.48154407659018 | 11.52821826342617 |

| | | | |
|---|---|---|---|
| C | 8.75275889345976 | 2.99538649135204 | 12.58947520993188 |
| H | 9.06322431102903 | 2.53067704803489 | 13.52005365197113 |
| C | 7.49877655042476 | 3.66667725894538 | 12.53738028500334 |
| C | 6.83451058310311 | 2.90104378687241 | 14.71799284464112 |
| C | 7.08672643714779 | 3.38174168734260 | 16.01167742140748 |
| H | 7.23524799048921 | 4.44789115939279 | 16.16544552578856 |
| C | 7.17217247532388 | 2.51231313969001 | 17.10653840323071 |
| H | 7.37750211643795 | 2.92340315884288 | 18.09135031868153 |
| C | 7.00654871278137 | 1.12994571234362 | 16.92020805374954 |
| C | 6.75503938131603 | 0.63909750505386 | 15.62195543156533 |
| H | 6.62099677594295 | -0.43340978031765 | 15.48817313767169 |
| C | 6.67078216804763 | 1.50804475328732 | 14.54206448749439 |
| H | 6.46070075101895 | 1.11325970701495 | 13.54928780052540 |
| C | 7.31753095484029 | 0.62807266488339 | 19.24170277499918 |
| H | 8.29114299033035 | 1.12996345765268 | 19.33262499691594 |
| H | 7.32156019431325 | -0.27734945813634 | 19.85428227741437 |
| H | 6.52873844476418 | 1.30403721945011 | 19.60099875018290 |

B3LYP geometry-optimized coordinates for ferrocene

| | | | |
|---|---|---|---|
| C | -0.76945523550120 | 2.81996607821413 | 6.24943295847664 |
| H | -1.58567633746328 | 3.09233471493339 | 6.91191152831060 |
| C | 0.55885792613260 | 3.35234941294881 | 6.28906621221367 |
| H | 0.92674011765715 | 4.09860857573562 | 6.98703489529712 |
| C | 1.30853238611404 | 2.75103610349191 | 5.22797564804273 |
| H | 2.34508032544070 | 2.95985633287830 | 4.98029042591961 |
| C | 0.44371879078311 | 1.84695479339282 | 4.53263056300916 |
| H | 0.70939559997460 | 1.25115981504864 | 3.66430188382057 |
| C | -0.84053183185068 | 1.88918587494601 | 5.16384552326433 |
| H | -1.71997064503727 | 1.33064530522920 | 4.85754971615852 |
| Fe | -0.32440187965020 | 3.76469614069036 | 4.46731965635276 |
| C | -0.42850953971302 | 5.81842948418870 | 4.26587918780569 |
| H | -0.10119425758968 | 6.53540662873756 | 5.01296672612587 |
| C | 0.38057175308405 | 5.25808174023211 | 3.22636381413050 |
| H | 1.42944754564057 | 5.47505856775954 | 3.04713896963893 |
| C | -1.73610770835724 | 5.24409047624676 | 4.16697334919006 |
| H | -2.57423984214084 | 5.44808022232518 | 4.82673281665791 |
| C | -0.42695506975912 | 4.33763718774745 | 2.48470384257837 |
| H | -0.09835217032173 | 3.73365182022402 | 1.64415694277634 |
| C | -1.73484510550009 | 4.32831865592421 | 3.06656477676035 |
| H | -2.57246882194248 | 3.71639506910525 | 2.74488156347026 |

B3LYP geometry-optimized coordinates for ferrocenium

| | | | |
|---|---|---|---|
| C | -0.76837147586943 | 2.80438380544478 | 6.25714304148064 |
| H | -1.59215264455255 | 3.08676249002272 | 6.90520242176008 |
| C | 0.55894608683806 | 3.34031958410229 | 6.30239172439617 |
| H | 0.91685402344878 | 4.09965313558654 | 6.99071217154859 |

| | | | |
|---|---|---|---|
| C | 1.31471492983598 | 2.74134311682773 | 5.24350708281343 |
| H | 2.34579250216793 | 2.96651252805782 | 4.98919834163371 |
| C | 0.45467152040349 | 1.83498597101136 | 4.54380261559066 |
| H | 0.71982262645951 | 1.25415342884436 | 3.66576603708422 |
| C | -0.83283115187954 | 1.87355553552538 | 5.17025170333225 |
| H | -1.71396244024474 | 1.32663453119094 | 4.84973223582084 |
| Fe | -0.32363303487698 | 3.76426752648056 | 4.46659732968574 |
| C | -0.42818835620754 | 5.83128386196293 | 4.25356656848660 |
| H | -0.09168079203120 | 6.53430371933399 | 5.00918869927157 |
| C | 0.37575098117917 | 5.26796133824666 | 3.21082189171721 |
| H | 1.42846441826558 | 5.46904967103932 | 3.03821641922407 |
| C | -1.73809001081853 | 5.25984581305524 | 4.16033214290816 |
| H | -2.56741743388563 | 5.45335212359406 | 4.83357365825527 |
| C | -0.43748798597751 | 4.34871558076241 | 2.47254094451155 |
| H | -0.10927480797428 | 3.73109495380428 | 1.64238434950786 |
| C | -1.74378038021042 | 4.34317708177379 | 3.05979386188781 |
| H | -2.57851057407014 | 3.72058720333284 | 2.75299775908352 |

**4.7 References**


1. Chiarella, G. M.; Cotton, F. A.; Murillo, C. A.; Ventura, K.; Villagrán, D.; Wang, X., Manipulating Magnetism: $Ru_2^{5+}$ Paddlewheels Devoid of Axial Interactions. *J. Am. Chem. Soc.* **2014,** *136* (27), 9580-9589.

2. Mikuriya, M.; Yoshioka, D.; Handa, M., Magnetic interactions in one-, two-, and three-dimensional assemblies of dinuclear ruthenium carboxylates. *Coord. Chem. Rev.* **2006,** *250* (17), 2194-2211.

3. Miyasaka, H.; Clérac, R.; Campos-Fernández, C. S.; Dunbar, K. R., The first crystal structure of a one-dimensional chain of linked $Ru^{II}$=$Ru^{II}$ units. *J. Chem. Soc. Dalton Trans.* **2001,** (6), 858-861.

4. O'Neal, K. R.; Liu, Z.; Miller, J. S.; Fishman, R. S.; Musfeldt, J. L., Pressure-driven high-to-low spin transition in the bimetallic quantum magnet $[Ru_2(O_2CMe)_4][Cr(CN)_6]$. *Phys. Rev. B* **2014,** *90* (10), 104301.

5. Su, S.-D.; Zhu, X.-Q.; Wen, Y.-H.; Zhang, L.-T.; Yang, Y.-Y.; Lin, C.-S.; Wu, X.-T.; Sheng, T.-L., A Diruthenium-Based Mixed Spin Complex $Ru_2^{5+}$(*S*=1/2)-CN-$Ru_2^{5+}$(*S*=3/2). *Angew. Chem. Int. Ed.* **2019,** *58* (43), 15344-15348.

6. Uemura, K.; Uesugi, N.; Matsuyama, A.; Ebihara, M.; Yoshikawa, H.; Awaga, K., Integration of Paramagnetic Diruthenium Complexes into an Extended Chain by Heterometallic Metal–Metal Bonds with Diplatinum Complexes. *Inorg. Chem.* **2016,** *55* (14), 7003-7011.

7. Yang, B.-B.; Feng, L.-N.; Fan, X.-M.; Zhang, K.-X.; Yang, J.-H.; Liu, B., Towards a new type of heterometallic system based on a paddle-wheel $Ru_2$ dimer: first results derived from the use of a high spin diruthenium(III,III) building block. *Inorg. Chem. Front.* **2017,** *4* (6), 1061-1065.

8. Raghavan, A.; Yuan, F.; Ren, T., Drastic Tuning of the Electronic Structures of Diruthenium Aryl Complexes by Isoelectronic Axial Ligands. *Inorg. Chem.* **2020,** *59* (13), 8663-8666.

9. Opperwall, S. R.; Liu, B.; Pilo, A. L.; Cao, Z.; Fanwick, P. E.; Ren, T., Synthesis and characterization of $Ru_2(\eta^2$-D*m*AniF$)_2$(μ-D*m*AniF$)_2$(μ-OAc)(μ-O). *Polyhedron* **2016,** *103*, 126-130.

10. Zhang, J.; Kosaka, W.; Sugimoto, K.; Miyasaka, H., Magnetic Sponge Behavior via Electronic State Modulations. *J. Am. Chem. Soc.* **2018,** *140* (16), 5644-5652.

11. Miyasaka, H., Control of Charge Transfer in Donor/Acceptor Metal–Organic Frameworks. *Acc. Chem. Res.* **2013,** *46* (2), 248-257.

12. Wang, C.-H.; Gao, W.-Y.; Powers, D. C., Measuring and Modulating Substrate Confinement during Nitrogen-Atom Transfer in a $Ru_2$-Based Metal-Organic Framework. *J. Am. Chem. Soc.* **2019,** *141* (49), 19203-19207.

13. Miyasaka, H.; Motokawa, N.; Matsunaga, S.; Yamashita, M.; Sugimoto, K.; Mori, T.; Toyota, N.; Dunbar, K. R., Control of Charge Transfer in a Series of $Ru_2^{II,II}$/TCNQ Two-Dimensional Networks by Tuning the Electron Affinity of TCNQ Units: A Route to Synergistic Magnetic/Conducting Materials. *J. Am. Chem. Soc.* **2010,** *132* (5), 1532-1544.

14. Alves Rico, S. R.; Abbasi, A. Z.; Ribeiro, G.; Ahmed, T.; Wu, X. Y.; de Oliveira Silva, D., Diruthenium(II,III) metallodrugs of ibuprofen and naproxen encapsulated in intravenously injectable polymer–lipid nanoparticles exhibit enhanced activity against breast and prostate cancer cells. *Nanoscale* **2017,** *9* (30), 10701-10714.

15. Benadiba, M.; de M. Costa, I.; Santos, R. L. S. R.; Serachi, F. O.; de Oliveira Silva, D.; Colquhoun, A., Growth inhibitory effects of the Diruthenium-Ibuprofen compound, $[Ru_2Cl(Ibp)_4]$, in human glioma cells in vitro and in the rat C6 orthotopic glioma in vivo. *J. Biol. Inorg. Chem.* **2014,** *19* (6), 1025-1035.

16. Hanif Ur, R.; Freitas, T. E.; Gomes, R. N.; Colquhoun, A.; de Oliveira Silva, D., Axially-modified paddlewheel diruthenium(II,III)-ibuprofenato metallodrugs and the influence of the structural modification on U87MG and A172 human glioma cell proliferation, apoptosis, mitosis and migration. *J. Inorg. Biochem.* **2016,** *165*, 181-191.

17. Johnpeter, J. P.; Schmitt, F.; Denoyelle-Di-Muro, E.; Wagnières, G.; Juillerat-Jeanneret, L.; Therrien, B., Photoactive sawhorse-type diruthenium tetracarbonyl complexes. *Inorg. Chim. Acta* **2012,** *393*, 246-251.

18. Koceva-Chyła, A.; Matczak, K.; Hikisz, M. P.; Durka, M. K.; Kochel, M. K.; Süss-Fink, G.; Furrer, J.; Kowalski, K., Insights into the in vitro Anticancer Effects of Diruthenium-1. *ChemMedChem* **2016,** *11* (19), 2171-2187.

19. Osterloh, W. R.; Galindo, G.; Yates, M. J.; Van Caemelbecke, E.; Kadish, K. M., Synthesis, Structural and Physicochemical Properties of Water-Soluble Mixed-Ligand Diruthenium Complexes Containing Anilinopyridinate Bridging Ligands. *Inorg. Chem.* **2020,** *59* (1), 584-594.

20. Ribeiro, G.; Benadiba, M.; de Oliveira Silva, D.; Colquhoun, A., The novel ruthenium—γ-linolenic complex [$Ru_2(aGLA)_4Cl$] inhibits C6 rat glioma cell proliferation and induces changes in mitochondrial membrane potential, increased reactive oxygen species generation and apoptosis in vitro. *Cell Biochem. Funct.* **2010,** *28* (1), 15-23.

21. Delgado-Martínez, P.; González-Prieto, R.; Gómez-García, C. J.; Jiménez-Aparicio, R.; Priego, J. L.; Torres, M. R., Structural, magnetic and electrical properties of one-dimensional tetraamidatodiruthenium compounds. *Dalton Trans.* **2014,** *43* (8), 3227-3237.

22. Jiang, K.; Pookpanratana, S. J.; Ren, T.; Natoli, S. N.; Sperling, B. A.; Robertson, J.; Richter, C. A.; Yu, S.; Li, Q., Nonvolatile memory based on redox-active ruthenium molecular monolayers. *Appl. Phys. Lett.* **2019,** *115* (16), 162102.

23. Pookpanratana, S.; Zhu, H.; Bittle, E. G.; Natoli, S. N.; Ren, T.; Richter, C. A.; Li, Q.; Hacker, C. A., Non-volatile memory devices with redox-active diruthenium molecular compound. *J. Phys. Condens. Matter* **2016,** *28* (9), 094009.

24. Ren, T.; Zou, G.; Alvarez, J. C., Facile electronic communication between bimetallic termini bridged by elemental carbon chains. *Chem. Commun.* **2000,** (13), 1197-1198.

25. Ren, T., Diruthenium *σ*-Alkynyl Compounds: A New Class of Conjugated Organometallics. *Organometallics* **2005,** *24* (21), 4854-4870.

26. Ying, J.-W.; Cao, Z.; Campana, C.; Song, Y.; Zuo, J.-L.; Tyler, S. F.; Ren, T., Linear trimers of diruthenium linked by polyyndiyl or phenylenediethynyl bridges: A family of unique electronic wires. *Polyhedron* **2015,** *86*, 76-80.

27. Cao, Z.; Xi, B.; Jodoin, D. S.; Zhang, L.; Cummings, S. P.; Gao, Y.; Tyler, S. F.; Fanwick, P. E.; Crutchley, R. J.; Ren, T., Diruthenium–Polyyn-diyl–Diruthenium Wires: Electronic Coupling in the Long Distance Regime. *J. Am. Chem. Soc.* **2014,** *136* (34), 12174-12183.

28. Das, A.; Reibenspies, J. H.; Chen, Y.-S.; Powers, D. C., Direct Characterization of a Reactive Lattice-Confined $Ru_2$ Nitride by Photocrystallography. *J. Am. Chem. Soc.* **2017,** *139* (8), 2912-2915.

29. Harvey, M. E.; Musaev, D. G.; Du Bois, J., A Diruthenium Catalyst for Selective, Intramolecular Allylic C–H Amination: Reaction Development and Mechanistic Insight Gained through Experiment and Theory. *J. Am. Chem. Soc.* **2011,** *133* (43), 17207-17216.

30. Musch Long, A. K.; Yu, R. P.; Timmer, G. H.; Berry, J. F., Aryl C−H Bond Amination by an Electrophilic Diruthenium Nitride. *J. Am. Chem. Soc.* **2010,** *132* (35), 12228-12230.

31. Musch Long, A. K.; Timmer, G. H.; Pap, J. S.; Snyder, J. L.; Yu, R. P.; Berry, J. F., Aryl C–H Amination by Diruthenium Nitrides in the Solid State and in Solution at Room Temperature: Experimental and Computational Study of the Reaction Mechanism. *J. Am. Chem. Soc.* **2011,** *133* (33), 13138-13150.

32. Corcos, A. R.; Long, A. K. M.; Guzei, I. A.; Berry, J. F., A Synthetic Cycle for Nitrogen Atom Transfer Featuring a Diruthenium Nitride Intermediate. *Eur. J. Inorg. Chem.* **2013,** *2013* (22-23), 3808-3811.

33. Corcos, A. R.; Berry, J. F., Anilinopyridinate-supported $Ru_2^{x+}$ (x = 5 or 6) paddlewheel complexes with labile axial ligands. *Dalton Trans.* **2017,** *46* (17), 5532-5539.

34. Angaridis, P., Ruthenium Compounds. In *Multiple Bonds Between Metal Atoms*, Cotton, F. A.; Murillo, C. A.; Walton, R. A., Eds. Springer: Boston, MA, 2005.

35. Corcos, A. R.; Roy, M. D.; Killian, M. M.; Dillon, S.; Brunold, T. C.; Berry, J. F., Electronic Structure of Anilinopyridinate-Supported $Ru_2^{5+}$ Paddlewheel Compounds. *Inorg. Chem.* **2017,** *56* (23), 14662-14670.

36. Corcos, A. R.; Pap, J. S.; Yang, T.; Berry, J. F., A Synthetic Oxygen Atom Transfer Photocycle from a Diruthenium Oxyanion Complex. *J. Am. Chem. Soc.* **2016,** *138* (31), 10032-10040.

37. Villalobos, L.; Barker Paredes, J. E.; Cao, Z.; Ren, T., *tert*-Butyl Hydroperoxide Oxygenation of Organic Sulfides Catalyzed by Diruthenium(II,III) Tetracarboxylates. *Inorg. Chem.* **2013,** *52* (21), 12545-12552.

38. Thompson, D. J.; Barker Paredes, J. E.; Villalobos, L.; Ciclosi, M.; Elsby, R. J.; Liu, B.; Fanwick, P. E.; Ren, T., Diruthenium(II,III) tetracarboxylates catalyzed $H_2O_2$ oxygenation of organic sulfides. *Inorg. Chim. Acta* **2015,** *424*, 150-155.

39. Goberna-Ferrón, S.; Peña, B.; Soriano-López, J.; Carbó, J. J.; Zhao, H.; Poblet, J. M.; Dunbar, K. R.; Galán-Mascarós, J. R., A fast metal–metal bonded water oxidation catalyst. *J. Catal.* **2014,** *315*, 25-32.

40. Raghavan, A.; Ren, T., Bisaryl Diruthenium(III) Paddlewheel Complexes: Synthesis and Characterization. *Organometallics* **2019,** *38* (19), 3888-3896.

41. Natoli, S. N.; Zeller, M.; Ren, T., Diruthenium-DMBA compounds bearing extended cross-conjugated ligands. *J. Organomet. Chem.* **2017,** *847*, 90-96.

42. Savchenko, J.; Cao, Z.; Natoli, S. N.; Cummings, S. P.; Prentice, B. M.; Fanwick, P. E.; Ren, T., New Diruthenium Bis-alkynyl Compounds as Potential Ditopic Linkers. *Organometallics* **2013,** *32* (21), 6461-6467.

43. Bear, J. L.; Li, Y.; Han, B.; Kadish, K. M., Synthesis, Molecular Structure, and Electrochemistry of a Paramagnetic Diruthenium(III) Complex. Characterization of $Ru_2(hpp)_4Cl_2$, Where hpp Is the 1,3,4,6,7,8- Hexahydro-2H-pyrimido[1,2-a]pyrimidinate Ion. *Inorg. Chem.* **1996,** *35* (5), 1395-1398.

44. Cotton, F. A.; Murillo, C. A.; Reibenspies, J. H.; Villagrán, D.; Wang, X.; Wilkinson, C. C., Paramagnetism at Ambient Temperature, Diamagnetism at Low Temperature in a Ru26+ Core: Structural Evidence for Zero-Field Splitting. *Inorg. Chem.* **2004,** *43* (26), 8373-8378.

45. Xu, G.-L.; Jablonski, C. G.; Ren, T., $Ru_2(DMBA)_4(BF_4)_2$ and $Ru_2(DMBA)_4(NO_3)_2$: the first examples of diruthenium compounds containing $BF_4^-$ and $NO_3^-$ as ligands. *Inorg. Chim. Acta* **2003,** *343*, 387-390.

46. Cotton, F. A.; Yokochi, A., Synthesis, Structure, and Magnetic Properties of New $Ru_2^{6+}$ Compounds. *Inorg. Chem.* **1997,** *36* (4), 567-570.

47. Chakravarty, A. R.; Cotton, F. A.; Tocher, D. A., Syntheses, molecular structures, and properties of two polar diruthenium(II,III) complexes of 2-hydroxypyridine and 2-anilinopyridine. *Inorg. Chem.* **1985,** *24* (2), 172-177.

48. Kadish, K. M.; Wang, L.-L.; Thuriere, A.; Van Caemelbecke, E.; Bear, J. L., Factors Affecting the Electrochemical and Spectroelectrochemical Properties of Diruthenium(III,II) Complexes Containing Four Identical Unsymmetrical Bridging Ligands. *Inorg. Chem.* **2003,** *42* (3), 834-843.

49. Kadish, K. M.; Phan, T. D.; Giribabu, L.; Shao, J.; Wang, L.-L.; Thuriere, A.; Van Caemelbecke, E.; Bear, J. L., Electrochemical and Spectroelectrochemical Characterization of $Ru_2^{4+}$ and $Ru_2^{3+}$ Complexes under a CO Atmosphere. *Inorg. Chem.* **2004,** *43* (3), 1012-1020.

50. Kadish, K. M.; Wang, L.-L.; Thuriere, A.; Giribabu, L.; Garcia, R.; Van Caemelbecke, E.; Bear, J. L., Solvent Effects on the Electrochemistry and Spectroelectrochemistry of Diruthenium Complexes. Studies of $Ru_2(L)_4Cl$ Where L = 2-$CH_3$ap, 2-Fap, and 2,4,6-$F_3$ap, and ap is the 2-Anilinopyridinate Anion. *Inorg. Chem.* **2003,** *42* (25), 8309-8319.

51. Van Caemelbecke, E.; Phan, T.; Osterloh, W. R.; Kadish, K. M., Electrochemistry of metal-metal bonded diruthenium complexes. *Coord. Chem. Rev.* **2021,** *434*, 213706.

52. Ito, A.; Fujino, H.; Ushiyama, K.; Yamanaka, E.; Yamasaki, R.; Okamoto, I., Acid-controlled switching of conformational preference of N,N-diarylamides bearing pyridine. *Tetrahedron Lett.* **2016,** *57* (42), 4737-4741.

53. Doyle, M. P.; Bagheri, V.; Wandless, T. J.; Harn, N. K.; Brinker, D. A.; Eagle, C. T.; Loh, K. L., Exceptionally high trans (anti) stereoselectivity in catalytic cyclopropanation reactions. *J. Am. Chem. Soc.* **1990,** *112* (5), 1906-1912.

54. Jahn, U.; Aussieker, S., Triarylaminium Salt Induced Oxidative Cyclizations of Tertiary Amines. Convenient Access to 2-Substituted Pyrrolidinium Salts. *Org. Lett.* **1999,** *1* (6), 849-852.

55. Nguyen, M.; Phan, T.; Caemelbecke, E. V.; Kajonkijya, W.; Bear, J. L.; Kadish, K. M., Interconversion between (3,1) and (4,0) Isomers of $Ru_2(L)_4X$ Complexes where L is 2-Anilinopyridinate or 2-(2,4,6-Trifluoroanilino)pyridinate Anion and X = $Cl^-$ or $C{\equiv}CC_5H_4N^-$. *Inorg. Chem.* **2008,** *47* (17), 7775-7783.

56. Bear and Kadish use the $\sigma_p$ Hammett parameter to describe the $Ru_2$(2-Meap)$_4$Cl complex, when the methyl group is actually ortho to the anilino nitrogen of the anilinopyridinate ligand.

Compound **3** considered in this work is more appropriately described by the given $\sigma_p$ Hammett parameter and exhibits redox potentials that more closely fit the overall data trends found for analogously substituted anilinopyridinate complexes.

57. The value of 0.089 V reported by the authors includes 8 compounds, only 4 of which are appropriately parameterized by para- sigma parameters. The value listed here, 0.085 V, was found by linear least squares fitting of the $E_{1/2}$ values for the unsubstituted diphenylformamidinate compounds and the three *para*- substituted ligand compounds, excluding the *meta*- and di-substituted ligand compounds.

58. Lin, C.; Ren, T.; Valente, E. J.; Zubkowski, J. D.; Smith, E. T., Continuous Spectroscopic and Redox Tuning of Dinuclear Compounds: Chlorotetrakis(μ-N,N′-diarylformamidinato)diruthenium(II,III). *Chemistry Letters* **1997,** *26* (8), 753-754.

59. Lin, C.; Protasiewicz, J. D.; Smith, E. T.; Ren, T., Redox tuning of the dimolybdenum compounds at the ligand periphery: a direct correlation with the Hammett constant of the substituents. *J. Chem. Soc. Chem. Commun.* **1995,** (22), 2257-2258.

60. Lin, C.; Protasiewicz, J. D.; Smith, E. T.; Ren, T., Linear Free Energy Relationships in Dinuclear Compounds. 2. Inductive Redox Tuning via Remote Substituents in Quadruply Bonded Dimolybdenum Compounds. *Inorg. Chem.* **1996,** *35* (22), 6422-6428.

61. Connelly, N. G.; Geiger, W. E., Chemical Redox Agents for Organometallic Chemistry. *Chem. Rev.* **1996,** *96* (2), 877-910.

62. Krause, M. O.; Oliver, J. H., Natural widths of atomic *K* and *L* levels, *K*α X-ray lines and several *KLL* Auger lines. *J. Phys. Chem. Ref. Data* **1979,** *8* (2), 329-338.

63. Hämäläinen, K.; Siddons, D. P.; Hastings, J. B.; Berman, L. E., Elimination of the inner-shell lifetime broadening in X-ray-absorption spectroscopy. *Phys. Rev. Lett.* **1991,** *67* (20), 2850-2853.

64. Lima, F. A.; Bjornsson, R.; Weyhermüller, T.; Chandrasekaran, P.; Glatzel, P.; Neese, F.; DeBeer, S., High-resolution molybdenum K-edge X-ray absorption spectroscopy analyzed with time-dependent density functional theory. *Phys. Chem. Chem. Phys.* **2013,** *15* (48), 20911-20920.

65. Pap, J. S.; DeBeer George, S.; Berry, J. F., Delocalized Metal–Metal and Metal–Ligand Multiple Bonding in a Linear Ru–Ru≡N Unit: Elongation of a Traditionally Short Ru≡N Bond. *Angew. Chem. Int. Ed.* **2008,** *47* (52), 10102-10105.

66. Chiarella, G. M.; Cotton, F. A.; Murillo, C. A.; Young, M. D.; Zhao, Q., Large Changes in Electronic Structures of $Ru_2^{6+}$ Species Caused by the Variations of the Bite Angle of Guanidinate Ligands: Tuning Magnetic Behavior. *Inorg. Chem.* **2010,** *49* (6), 3051-3056.

67. Wang, C.-F.; Zuo, J. L.; Ying, J.-W.; Ren, T.; You, X.-Z., Novel Heterometallic Fe−$Ru_2$−Fe Arrays via "Complex of Complexes" Approach. *Inorg. Chem.* **2008,** *47* (20), 9716-9722.

68. See Phi User Manual. http://www.molmag.manchester.ac.uk/software/phi_manual.pdf

69. Tait, C. D.; Garner, J. M.; Collman, J. P.; Sattelberger, A. P.; Woodruff, W. H., Vibrational study of multiply metal-metal bonded ruthenium porphyrin dimers. *J. Am. Chem. Soc.* **1989,** *111* (20), 7806-7811.

70. Roy, L. E.; Jakubikova, E.; Guthrie, M. G.; Batista, E. R., Calculation of One-Electron Redox Potentials Revisited. Is It Possible to Calculate Accurate Potentials with Density Functional Methods? *J. Phys. Chem. A* **2009,** *113* (24), 6745-6750.

71. Berry, J. F.; Bothe, E.; Cotton, F. A.; Ibragimov, S. A.; Murillo, C. A.; Villagrán, D.; Wang, X., Metal−Metal Bonding in Mixed Valence $Ni_2^{5+}$ Complexes and Spectroscopic Evidence for a $Ni_2^{6+}$ Species. *Inorg. Chem.* **2006,** *45* (11), 4396-4406.

72. Berry, J. F., Two-Center/Three-Electron Sigma Half-Bonds in Main Group and Transition Metal Chemistry. *Acc. Chem. Res.* **2016,** *49* (1), 27-34.

73. Berry, J. F.; Bill, E.; Bothe, E.; Cotton, F. A.; Dalal, N. S.; Ibragimov, S. A.; Kaur, N.; Liu, C. Y.; Murillo, C. A.; Nellutla, S.; North, J. M.; Villagrán, D., A Fractional Bond Order of 1/2 in $Pd_2^{5+}$−Formamidinate Species; The Value of Very High-Field EPR Spectra. *J. Am. Chem. Soc.* **2007,** *129* (5), 1393-1401.

74. Bruker-AXS (2016). APEX3. Version 2016.5-0. Madison, Wisconsin, USA.

75. Krause, L.; Herbst-Irmer, R.; Sheldrick, G. M.; Stalke, D., Comparison of silver and molybdenum microfocus X-ray sources for single-crystal structure determination. *J. Appl. Crystallogr.* **2015,** *48* (1), 3-10.

76. Spek, A., PLATON SQUEEZE: a tool for the calculation of the disordered solvent contribution to the calculated structure factors. *Acta Crystallogr. C* **2015,** *71* (1), 9-18.

77. Ravel, B.; Newville, M., ATHENA, ARTEMIS, HEPHAESTUS: data analysis for X-ray absorption spectroscopy using IFEFFIT. *J. Synchrotron Rad.* **2005,** *12* (4), 537-541.

78. Chilton, N. F.; Anderson, R. P.; Turner, L. D.; Soncini, A.; Murray, K. S., PHI: A powerful new program for the analysis of anisotropic monomeric and exchange-coupled polynuclear d- and f-block complexes. *J. Comput. Chem.* **2013,** *34* (13), 1164-1175.

79. Neese, F., Software update: the ORCA program system, version 4.0. *WIREs Computational Molecular Science* **2018,** *8* (1), e1327.

80. Neese, F.; Wennmohs, F.; Hansen, A.; Becker, U., Efficient, approximate and parallel Hartree–Fock and hybrid DFT calculations. A 'chain-of-spheres' algorithm for the Hartree–Fock exchange. *Chem. Phys.* **2009,** *356* (1), 98-109.

81. Grimme, S.; Antony, J.; Ehrlich, S.; Krieg, H., A consistent and accurate ab initio parametrization of density functional dispersion correction (DFT-D) for the 94 elements H-Pu. *J. Chem. Phys.* **2010,** *132* (15), 154104.

82. Becke, A. D., Density-functional thermochemistry. III. The role of exact exchange. *J. Chem. Phys.* **1993,** *98* (7), 5648-5652.

83. Lee, C.; Yang, W.; Parr, R. G., Development of the Colle-Salvetti correlation-energy formula into a functional of the electron density. *Phys. Rev. B* **1988,** *37* (2), 785-789.

84. Weigend, F.; Ahlrichs, R., Balanced basis sets of split valence, triple zeta valence and quadruple zeta valence quality for H to Rn: Design and assessment of accuracy. *Phys. Chem. Chem. Phys.* **2005,** *7* (18), 3297-3305.

85. Lenthe, E. v.; Baerends, E. J.; Snijders, J. G., Relativistic regular two-component Hamiltonians. *J. Chem. Phys.* **1993,** *99* (6), 4597-4610.

86. Pantazis, D. A.; Chen, X.-Y.; Landis, C. R.; Neese, F., All-Electron Scalar Relativistic Basis Sets for Third-Row Transition Metal Atoms. *J. Chem. Theory Comput.* **2008,** *4* (6), 908-919.

87. York, D. M.; Karplus, M., A Smooth Solvation Potential Based on the Conductor-Like Screening Model. *J. Phys. Chem. A* **1999,** *103* (50), 11060-11079.

88. Avogadro: an open-source molecular builder and visualization tool. Version 1.XX. http://avogadro.cc/ .

89. Hanwell, M. D.; Curtis, D. E.; Lonie, D. C.; Vandermeersch, T.; Zurek, E.; Hutchison, G. R., Avogadro: an advanced semantic chemical editor, visualization, and analysis platform. *J. Cheminformatics* **2012,** *4* (1), 17.

90. Jmol: an open-source Java viewer for chemical structures in 3D. http://www.jmol.org/ .

91. Lu, T.; Chen, F., Multiwfn: A multifunctional wavefunction analyzer. *J. Comput. Chem.* **2012,** *33* (5), 580-592.

92. Pettersen, E. F.; Goddard, T. D.; Huang, C. C.; Couch, G. S.; Greenblatt, D. M.; Meng, E. C.; Ferrin, T. E., UCSF Chimera—A visualization system for exploratory research and analysis. *J. Comput. Chem.* **2004,** *25* (13), 1605-1612.

93. Perdew, J. P., Density-functional approximation for the correlation energy of the inhomogeneous electron gas. *Phys. Rev. B* **1986,** *33* (12), 8822-8824.

94. Becke, A. D., Density-functional exchange-energy approximation with correct asymptotic behavior. *Phys. Rev. A* **1988,** *38* (6), 3098-3100.

95. Igor Pro 8: a product of WaveMetrics. https://www.wavemetrics.com/software/igor-pro-8

96. Stephenson, T. A.; Wilkinson, G., New ruthenium carboxylate complexes. *J. Inorg. Nuc. Chem.* **1966,** *28* (10), 2285-2291.

97. Brown, T. R.; Dolinar, B. S.; Hillard, E. A.; Clérac, R.; Berry, J. F., Electronic Structure of $Ru_2$(II,II) Oxypyridinates: Synthetic, Structural, and Theoretical Insights into Axial Ligand Binding. *Inorg. Chem.* **2015,** *54* (17), 8571-8589.

98. Nakamoto, K., Infrared and Raman Spectra of Inorganic and Coordination Compounds. *Handbook of Vibrational Spectroscopy* **2001**.

# Chapter 5

*Preliminary Evidence for a $Ru_2^{6+}$-Ligand Radical Complex.*

## 5.1 Abstract

The previous chapter describes the highest occupied orbitals of $Ru_2^{6+}$ *chloro* complexes supported by anilinopyridinate ligands as ligand-centered, derived from the *a* and *e* symmetry combinations of the N-atom *p* orbitals. If this description is accurate, this would revise the common assignment of the most anodic electrochemical features of these compounds. Oxidation beyond $Ru_2^{6+}$ is generally assigned as $Ru_2^{6+/7+}$, but we propose the anodic product to be a $Ru_2^{6+}$-ligand radical complex. This chapter presents preliminary evidence for this assignment.

## 5.2 Introduction

Since the initial report of a diruthenium paddlewheel complex in the 1980s,[1] a wide variety of these compounds have been extensively characterized.[2] By far the most well-known oxidation state is $Ru_2^{5+}$, with many $Ru_2^{4+}$ and a modest number of $Ru_2^{6+}$ compounds isolated and characterized as well. However, many electrochemically characterized $Ru_2$ compounds, particularly those supported by anilinopyridinate-type ligands, have a third redox couple, which is assigned as $Ru_2^{6+/7+}$.[3]

In previous work (Chapter 4), we describe how these $Ru_2(Xap)_4$ complexes have a set of three ligand-based orbitals, composed primarily of the *a* and *e* symmetry combinations of the amido N-atoms. When a chloro ligand occupies the axial site, these ligand orbitals are interposed between the singly-occupied $\delta^*$ and $\pi^*$ orbitals (for the $Ru_2^{5+}$ $S = 3/2$ state). Upon oxidation to a

triplet $Ru_2^{6+}$ state, these ligand orbitals become the HOMOs, and therefore subsequent oxidation is expected to be described as ligand-centered rather than metal-centered. This chapter describes preliminary efforts to confirm this hypothesis by accessing the $Ru_2^{6+}$-ligand radical complex resulting from oxidation of $Ru_2(Xap)_4Cl$ monocations.

### 5.3 Computational Predictions

As described in Chapter 4, DFT calculations for the electronic structure of $Ru_2(Xap)_4Cl^+$ complexes exhibit ligand-based HOMOs, as shown in Figure 5.1. With this knowledge, we calculated both doublet and quartet electronic configurations for the $Ru_2(ap)_4Cl^{2+}$ dication (**1**$^{2+}$). Both converged to broken symmetry solutions with a $Ru_2^{6+}$ $S = 1$ core and an $S = 1/2$ ligand radical, coupled either ferromagnetically or antiferromagnetically. Furthermore, both optimized geometries displayed weak Jahn-Teller distortion, consistent with the orbitally degenerate ground state resulting from removal of a single $\pi^*$ electron. Interestingly, the antiferromagnetic doublet displays less distortion, with nearly equal Ru-$N_{pyr}$ distances (2.14 Å) and only modest perturbation of the Ru-$N_{am}$ distances (2.04 and 2.07 Å for the *trans* ligand pairs). The quartet displays a complete loss in rotational symmetry, with unique bond distances ranging from 2.13-2.15 Å for the Ru-$N_{pyr}$ bond and 2.02-2.13 Å for the Ru-$N_{am}$ bond.

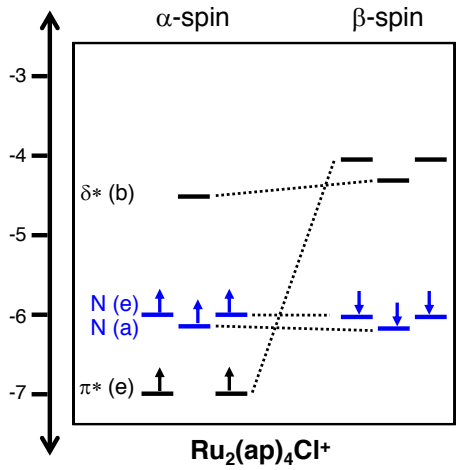


*Figure 5.1 DFT calculated molecular orbital energy level diagram for $Ru_2(ap)_4Cl^+$*

Vibrational calculations on both geometries resulted in a lower Gibbs free enthalpy (calculated at 298 K) for the low-spin configuration. Therefore, this geometry was used as the input for a broken symmetry calculation. The singly-occupied orbital is clearly a $Ru_2$ $\pi^*$ orbital, and the next lowest, with a calculated orbital magnetic overlap of 0.28, is the other $Ru_2$ $\pi^*$ orbital (Figure 5.2). The poor overlap with $Ru_2$ $\pi^*$ character is consistent with removal of a ligand-centered electron from the $Ru_2^{6+}$ configuration. A significant *J* coupling of –146 $cm^{-1}$ was calculated using the Yamaguchi formalism.[4, 5]

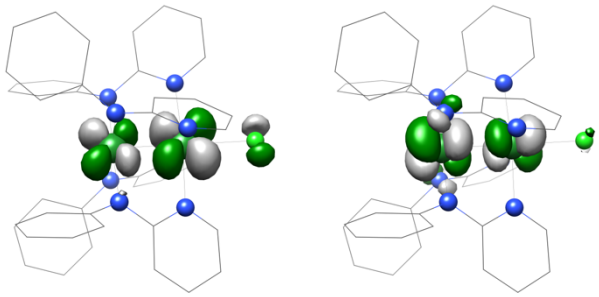

*Figure 5.2 Singly-occupied (left) and highest doubly-occupied (right) corresponding orbitals from the broken symmetry calculation.*

## 5.4 Experimental Results and Discussion

To validate predictions from DFT, we sought to synthetically prepare an $Ru_2^{6+}$-ligand radical complex. Based on the electrochemical data presented in Chapter 4, we initially selected $[Ru_2(OMeap)_4Cl][PF_6]$ ([**2**]$PF_6$) as a substrate and $NOPF_6$ as a one-electron oxidant. Titration of a solution of $NOPF_6$ in $CH_3CN$ to a solution of **2**$PF_6$ in $CH_2Cl_2$ was monitored by electronic absorption spectroscopy and showed an approximately isosbestic transition to a new product through at least 2.5 equivalents of oxidant (Figure 5.3). Moreover, the end product decays without isosbestic behavior, losing approximately one third of the peak intensity over 30 minutes. As multiple redox events occur between the $Ru_2^{5+/6+}$ potential and the potential of $NOPF_6$ in $CH_2Cl_2$ (1.0 V vs $Fc^{0/+}$), reaction stoichiometry and product determination are obscured.

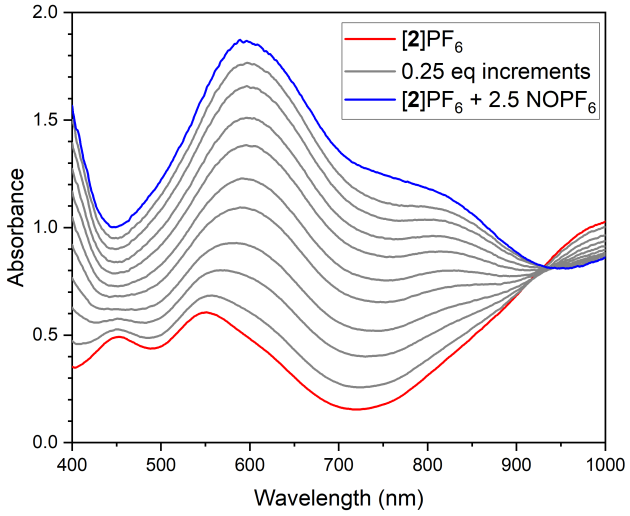


*Figure 5.3 Vis/NIR traces for the titration of [**2**]$PF_6$ in $CH_2Cl_2$ with $NOPF_6$ in $CH_3CN$. Gray traces represent 0.25 equivalent additions of $NOPF_6$. The titration was performed under $N_2$ at room temperature.*

An approximate titration, with one and two equivalents of oxidant, was performed and examined by EPR spectroscopy. Interestingly, only a trace $g = 2$ signal, consistent with an $S = 1/2$ system, was observed in samples frozen approximately 1 minute after mixing. This signal was

significantly stronger after the solution was allowed to sit for several days, indicating that the chemical change measured by electronic absorption spectroscopy is likely different from the redox event resulting in the $g = 2$ signal. It is yet unknown whether the final product measured by EPR spectroscopy is a $Ru_2^{6+}$ complex with a ligand radical or a decomposition product.

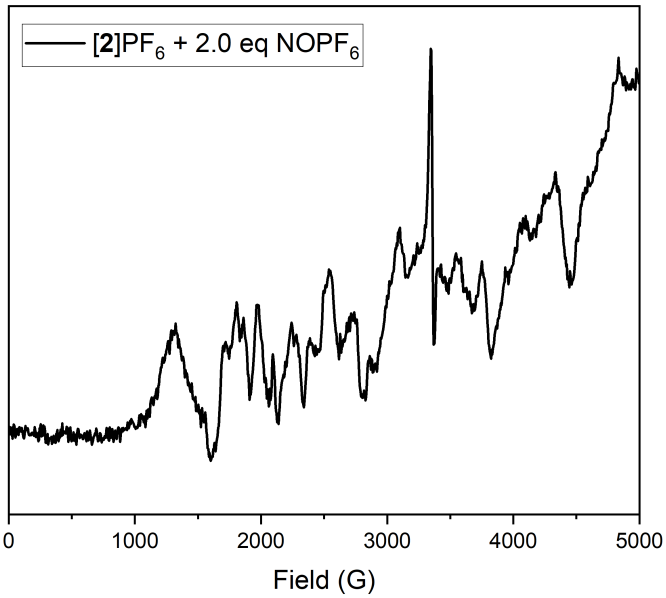


*Figure 5.4 X-band EPR spectrum of [**2**]$PF_6$ with 2.0 equivalents of $NOPF_6$ added. The sample was frozen approximately one minute following addition of the oxidant. The sharp derivative signal at ~3325 G is the only meaningful peak when compared to a background. The remaining features are noise due to the very low intensity of the signal.*

Given the unclear stoichiometry with [**2**]$PF_6$, the same titration and EPR experiments were conducted with $[Ru_2(Meap)_4Cl][PF_6]$ ([**3**]$PF_6$), which displayed a single isolated electrochemical oxidation wave within the potential of $NOPF_6$ (1.0 V vs $Fc^{0/+}$ in $CH_2Cl_2$). It is important to note that the peak current for this "$Ru_2^{6+/7+}$" feature is slightly below the peak currents for the $Ru_2^{5+/6+}$ feature at a given scan rate, meaning that a multi-electron event is highly unlikely. Titration under identical conditions indicated a stoichiometry of 2 $NOPF_6$ per [**3**]$PF_6$, while titration up to 4.5 equivalents with 0.5 equivalent increments indicates 2.5 equivalents of $NOPF_6$ are needed for full conversion (Figure 5.5). Compared to the reaction of [**2**]$PF_6$ with $NOPF_6$, the decay following titration occurred much more rapidly, with total conversion to a pale brown solution occurring in

under 10 minutes under an atmosphere of $N_2$ at room temperature. The incongruity between electrochemical peak currents and stoichiometry results in a wide variety of speculative explanations. However, given that $NOPF_6$ exhibits a broad, weak $g = 4$ signal by EPR, it is clear that the oxidant is not completely pure. Therefore, redox titration of this reagent is necessary before any meaningful conclusion can be drawn.

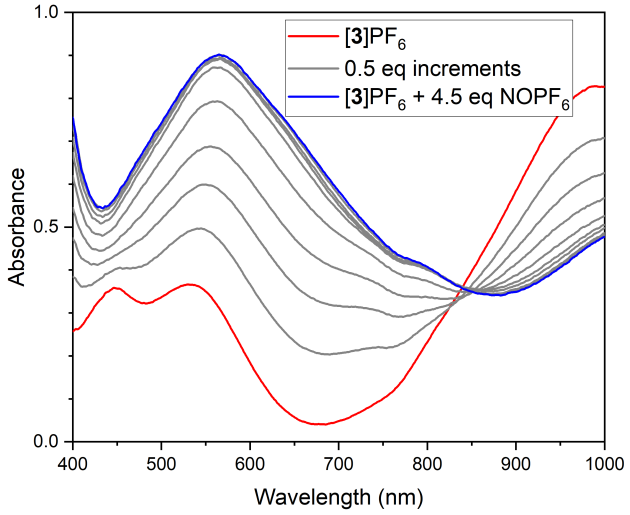


*Figure 5.5 Vis/NIR traces for the titration of [**3**]$PF_6$ in $CH_2Cl_2$ with $NOPF_6$ in $CH_3CN$. Gray traces represent 0.50 equivalent additions of $NOPF_6$. The titration was performed under $N_2$ at room temperature.*

EPR spectroscopy was again used to corroborate the titration data. As with the previous reaction, a $g = 2$ signal was observed following addition of oxidant, and the signal intensity grew substantially after several days compared to the initial sample frozen at approximately one minute of reaction time. Consistent with the faster decomposition as determined by electronic absorption spectroscopy, the initial signal detected by EPR spectroscopy was significantly stronger in the sample that was allowed to decay for several days. Moreover, the signal was stronger when two equivalents of $NOPF_6$ were added. A representative EPR spectrum is given in Figure 5.6. The EPR

signal is isotropic and does not exhibit shoulders characteristic of hyperfine interaction with a statistical mixture of two Ru atoms. This is particularly striking because the broken symmetry DFT results above indicate that the unpaired electron should be in an $Ru_2$ $\pi^*$ orbital, which should give a strongly axial or possibly rhombic EPR signal. If the Vis/NIR titration is accurate, the EPR spectrum could be explained by three-electron oxidation, resulting in a complex with antiferromagnetic coupling between two $Ru_2$ $\pi^*$ electrons and three ligand radical electrons. This would give the net spin primarily ligand character with an isotropic EPR signal broadened by superhyperfine interactions with $^{14}N$ and the ~30% abundant $I$ = 5/2 Ru nuclei. More accurate determination of the reaction stoichiometry is necessary to distinguish between the "$Ru_2^{7+}$" one-electron and the "$Ru_2^{9+}$" three-electron explanations.

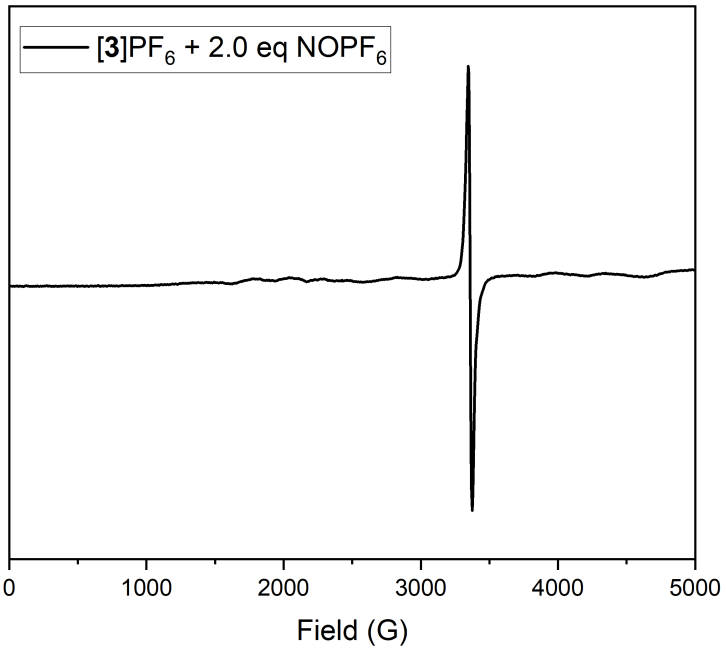


*Figure 5.6 X-band EPR spectrum of [**3**]$PF_6$ with 2.0 equivalents of $NOPF_6$ added. The sample was frozen approximately one minute following addition of the oxidant.*

**5.5 Initial Conclusions and Proposals for Future Work**

While isolation and structural characterization have thus far proven elusive due to the transient nature of the initial product of both reactions described, the EPR signal is consistent with the antiferromagnetically coupled $S = 1/2$ system predicted by DFT. Titration indicates either a more complex reaction stoichiometry or possible side reactions. I believe two experiments will be highly informative for determining the details of this reaction. First, because the byproduct of oxidation with $NOPF_6$ is NO, which is a strongly binding ligand, it is possible that the intermediate color is due to formation of a transient nitrosyl complex. This could be assessed by addition of NO to a solution of "decayed" reaction product. If the color is able to be cycled between addition and loss of NO, this would be strong evidence for this nitrosyl intermediate. Second, alternative oxidation via bulk electrolysis should be performed on [**3**]$PF_6$. ([**2**]$PF_6$ is less suitable due to low solubility.) By monitoring a constant potential electrolysis with electronic absorption spectroscopy, reaction stoichiometry in the absence of NO could be determined. If the intermediate color is indeed the result of a transient nitrosyl complex, then the rapid decay seen by chemical oxidation should be irrelevant and a stable electrochemical oxidation product should be obtained.

Given the presence of the $g = 2$ signal after several days, it is clear that there is a stable odd-electron product. As both [**2**]$PF_6$ and [**3**]$PF_6$ are $S = 1$ complexes and $NOPF_6$ is diamagnetic, this product is most likely the product of oxidation of the $Ru_2$ complex. Moreover, as the signal lacks $^{14}N$ hyperfine splitting, we can rule out lingering NO as the odd-electron product observed. Therefore, a preparatory scale reaction between [**2**]$PF_6$ or [**3**]$PF_6$ and $NOPF_6$ should yield an isolable product. This product can be purified and studied by X-ray single crystal diffraction to determine the structure, as well as $^1H$ NMR for comparison to other paramagnetic $Ru_2$ complexes.

The oxidation of these $Ru_2^{6+}$ complexes is clearly complex, but the presence of a stable odd-electron product is extremely promising.

## 5.6 Methods

### *5.6.1 Physical Measurements*

Vis/NIR spectroscopy was measured using a StellarNet tungsten halogen source and a BLACK-Comet UV/Vis spectrometer. EPR data were acquired on a Bruker ELEXSYS E500 EPR spectrometer equipped with a Varian E102 microwave bridge. An Oxford Instruments ESR-900 continuous-flow helium cryostat and an Oxford Instruments 503S temperature controller were used to control the sample temperature. Measurement conditions were: 9.38 GHz, 2 G modulation amplitude, 2500 G center field, 5000 G sweep width, 20.48 ms time constant, 40.96 ms conversion time, and 10 K.

### *5.6.2 Computational Methods*

Initial coordinates for $\mathbf{1}^+$ were obtained from the crystal structure of the hexachloroantimonate salt (Chapter 4). All calculations were carried out with the ORCA software package version 4.0.0.2.[6] Calculations were performed by unrestricted Kohn-Sham DFT using the B3LYP hybrid functional with the RIJCOSX chain of spheres approximation.[7-9] Ruthenium atoms were modeled with the TZVP basis set. All other atoms were modeled with the def2-SVP basis set.[10] Relativistic effects were treated using the zero-order relativistic approximation (ZORA) Hamiltonian with the SARC/J auxiliary basis set for coulomb fitting.[11, 12] These methods were used to perform geometry optimizations and numerical vibrational frequency analysis on relevant structures. The conductor-like polarizable continuum model (CPCM) was also implemented to model the solvent effects of dichloromethane in all calculations.[13]

*5.6.3 Synthetic Methods*

Standard Schlenk or glovebox techniques were used in all cases. [**2**]$PF_6$ and [**3**]$PF_6$ were prepared as described in Chapter 4. $NOPF_6$ (≥95%) was found to contain a paramagnetic impurity detectible as a broad $g = 4$ signal by EPR. Purification by dissolving $NOPF_6$ in minimal acetonitrile and precipitation with dichloromethane was unsatisfactory for removing this impurity. Inhibitor-free $CH_2Cl_2$ (Fisher Scientific) and $CH_3CN$ (Sigma Aldrich) were distilled from $CaH_2$ under $N_2$, stored over molecular sieves, and filtered before use. The purity of solvent was found to be particularly important for prolonging the lifetime of $NOPF_6$ stock solutions in $CH_3CN$. Poorly distilled solvent resulting in yellowing of the initially colorless solution within 48 hours, but exceptionally clean solvent gave a solution that remained colorless for over one week.

Titration measurements. Stock solutions of [**2**]$PF_6$ (~ 0.25 mM in $CH_2Cl_2$, saturated) and [**3**]$PF_6$ (~1.0 mM in $CH_2Cl_2$, not saturated) were diluted to ~ 0.1 mM for monitoring with a 10 mm path length Vis/NIR dip probe. $NOPF_6$ was prepared as a stock solution (~10 mM in $CH_3CN$). The diluted $Ru_2$ solution was mounted on a Schlenk line with the dip probe through a rubber septum. A gastight syringe was charged with $NOPF_6$ solution in a glovebox before bring brought to the flask with $Ru_2$. Aliquots of $NOPF_6$ were added through the septum with rapid stirring, and several seconds were given before each spectrum was recorded. The entire titration was complete in approximately 3 minutes.

EPR samples were prepared in a glovebox by adding 10 mM $NOPF_6$ in $CH_3CN$ to undiluted $Ru_2$ stock solutions (1 mL $Ru_2$ stock as prepared for titration measurements). Either one or two equivalents of $NOPF_6$ were added by gastight syringe and a pipet was used to bubble $N_2$ through the solution while mixing. An aliquot was added to an EPR tube, which was then sealed with

parafilm before being extracted from the glovebox and frozen in liquid nitrogen. Samples were frozen within approximately one minute of $NOPF_6$ addition.

### 5.7 Atomic Coordinates of Calculated Structures

B3LYP geometry-optimized coordinates for **1** (doublet)

| | | | |
|---|---|---|---|
| Ru | 3.88462423567106 | 4.62104480036544 | 15.03454544970930 |
| Ru | 3.88424399024391 | 2.26314165860843 | 15.03432833112097 |
| Cl | 3.88499722912141 | 7.08029527824371 | 15.03441805792365 |
| N | 5.98513760455064 | 4.52960498009791 | 14.64376012188133 |
| N | 5.93269217508005 | 2.29924331085767 | 15.34955306226877 |
| N | 3.52080481181517 | 4.51979559660152 | 12.92994360787953 |
| N | 4.20399231846719 | 2.28214229867424 | 13.01931410114395 |
| C | 6.65762775630881 | 5.58543467833395 | 14.15553979638810 |
| H | 6.07190220960585 | 6.48026480855824 | 13.96570166117166 |
| C | 8.03325738141589 | 5.56492209144891 | 13.91449324428848 |
| H | 8.51601974146205 | 6.45170161365212 | 13.51124821806930 |
| C | 8.74764431896241 | 4.39563452986040 | 14.18586563168530 |
| H | 9.81668281984740 | 4.33367218528883 | 13.99184076946446 |
| C | 8.06426934361018 | 3.29421488266054 | 14.68705484202115 |
| H | 8.57862698775213 | 2.35353629603525 | 14.85795576884774 |
| C | 6.67001779854484 | 3.37762781247373 | 14.92007858628010 |
| C | 6.56555288595799 | 1.28503279553092 | 16.08269599795483 |
| C | 7.40986884631074 | 1.60047743618792 | 17.17672936965232 |
| H | 7.57250608751849 | 2.64070740853452 | 17.45202145755020 |
| C | 7.98852175123358 | 0.57941355149191 | 17.92613915124157 |
| H | 8.61729765702650 | 0.83046722716902 | 18.77883985714818 |
| C | 7.75849817966213 | -0.76326867056915 | 17.59146910605345 |
| H | 8.22223925423486 | -1.55709897437832 | 18.17462124021916 |
| C | 6.93235910022496 | -1.08221220970873 | 16.50355469502516 |
| H | 6.76679897909102 | -2.12287781965983 | 16.22975748299145 |
| C | 6.32647552936161 | -0.07059778854913 | 15.76126990104168 |
| H | 5.71704442094949 | -0.31524305051254 | 14.89408215947325 |
| C | 3.06845543968033 | 5.58435768108102 | 12.23122304126005 |
| H | 2.86988770990031 | 6.48177512944766 | 12.80973223035993 |
| C | 2.87715979434237 | 5.56289729039966 | 10.85616768666341 |
| H | 2.50481125884860 | 6.45101591941266 | 10.35170107563744 |
| C | 3.16332256204681 | 4.38031867782707 | 10.15866732462071 |
| H | 3.01236108845748 | 4.31758375544988 | 9.08225432362054 |
| C | 3.62303063068721 | 3.27773085540200 | 10.86033904958031 |
| H | 3.82098570091493 | 2.33833446409846 | 10.35297999702904 |
| C | 3.79981446964259 | 3.35530467388998 | 12.26550385568534 |
| C | 4.95003406231684 | 1.24350617214991 | 12.39990291716596 |

| | | | |
|---|---|---|---|
| C | 6.14448241501468 | 1.54355782271031 | 11.71017982524795 |
| H | 6.46947929604513 | 2.57857449541528 | 11.61824087074241 |
| C | 6.91568338412490 | 0.51863434517110 | 11.16026063655299 |
| H | 7.83856915256780 | 0.76549535803473 | 10.63702236704015 |
| C | 6.51357894410948 | -0.81827094777058 | 11.28511472992370 |
| H | 7.11763813043215 | -1.61436673462294 | 10.85273067891030 |
| C | 5.32811010063472 | -1.12149466548129 | 11.96283687712191 |
| H | 4.99807067307439 | -2.15553195393876 | 12.05408816450907 |
| C | 4.54990482859213 | -0.09994718425166 | 12.51739561395981 |
| H | 3.61279135383818 | -0.33763692581902 | 13.01331473231616 |
| N | 1.78413789319733 | 4.53044722626857 | 15.42567750361729 |
| N | 1.83510485099465 | 2.30030741592639 | 14.71904066110672 |
| N | 4.24762146848641 | 4.51934392141569 | 17.13916697284664 |
| N | 3.56425887298318 | 2.28180469969863 | 17.04934154101661 |
| C | 1.11262822005648 | 5.58629507973751 | 15.91519793469030 |
| H | 1.69902934911243 | 6.48061180423685 | 16.10535404998055 |
| C | -0.26289844825288 | 5.56650935323555 | 16.15695475282341 |
| H | -0.74488760494771 | 6.45331379468526 | 16.56106554589057 |
| C | -0.97811577336937 | 4.39784251720934 | 15.88518911408423 |
| H | -2.04707900001541 | 4.33634722126877 | 16.07977468670000 |
| C | -0.29562361329866 | 3.29628738036541 | 15.38306138603214 |
| H | -0.81050410686453 | 2.35589200315611 | 15.21244100391371 |
| C | 1.09848330520314 | 3.37897856662641 | 15.14911387695831 |
| C | 1.20185160845337 | 1.28614582986277 | 13.98649702515578 |
| C | 0.35502769129699 | 1.60092410987069 | 12.89410004889272 |
| H | 0.19039588891140 | 2.64101336777433 | 12.61945234789519 |
| C | -0.22381785370579 | 0.57950536047672 | 12.14539035948315 |
| H | -0.85445581453786 | 0.83016301126907 | 11.29395286609922 |
| C | 0.00845394293453 | -0.76305070460442 | 12.47910696756794 |
| H | -0.45538614173806 | -1.55719342146379 | 11.89646196522595 |
| C | 0.83699390132092 | -1.08144028973122 | 13.56537093292921 |
| H | 1.00429307610779 | -2.12201437407456 | 13.83845516604216 |
| C | 1.44300638318338 | -0.06941767690646 | 14.30689918025325 |
| H | 2.05425167776001 | -0.31366082509011 | 15.17292042953546 |
| C | 4.69929224823681 | 5.58394044283978 | 17.83821608351594 |
| H | 4.89910908309683 | 6.48109016548173 | 17.25971525944804 |
| C | 4.88859793330642 | 5.56282068363813 | 19.21355251486797 |
| H | 5.26039373904508 | 6.45100524300622 | 19.71831373163814 |
| C | 4.60122440957647 | 4.38048524686932 | 19.91094608902216 |
| H | 4.75057923315958 | 4.31803216243509 | 20.98760169180423 |
| C | 4.14244721059959 | 3.27775684615954 | 19.20891280226336 |
| H | 3.94382333987068 | 2.33847493548343 | 19.71618414340761 |
| C | 3.96761590485724 | 3.35498543353418 | 17.80347504516480 |
| C | 2.81862681523549 | 1.24241852007300 | 17.66818305979588 |
| C | 1.62231200165079 | 1.54117274776016 | 18.35515923335667 |
| H | 1.29558742823967 | 2.57576862830510 | 18.44558839943706 |

| | | | |
|---|---|---|---|
| C | 0.85156590885556 | 0.51549427971571 | 18.90434949003838 |
| H | -0.07277631517655 | 0.76134190521920 | 19.42548251419242 |
| C | 1.25603918750437 | -0.82087156286367 | 18.78147442290290 |
| H | 0.65231685714918 | -1.61756403270895 | 19.21322693607722 |
| C | 2.44346361168712 | -1.12279737005932 | 18.10662382559616 |
| H | 2.77539703001419 | -2.15637367280592 | 18.01704870371750 |
| C | 3.22123635045206 | -0.10047468187784 | 17.55286900515771 |
| H | 4.16000384006634 | -0.33703624732139 | 17.05956306341308 |

B3LYP geometry-optimized coordinates for **1** (quartet)

| | | | |
|---|---|---|---|
| Ru | 3.90094695907565 | 4.60480265054009 | 15.00614590217112 |
| Ru | 3.94426146241930 | 2.24332537452589 | 15.04699040551016 |
| Cl | 3.89908663551475 | 7.05242610000196 | 14.99583297310566 |
| N | 5.98741367874517 | 4.50893580412663 | 14.58836543647969 |
| N | 5.94017194660580 | 2.30453491264731 | 15.36291697382903 |
| N | 3.50063665241852 | 4.48276244369681 | 12.91880439215370 |
| N | 4.22841388565771 | 2.26392046547550 | 13.02331724172257 |
| C | 6.65229693743516 | 5.55058648229877 | 14.04443750539292 |
| H | 6.05347031763957 | 6.42076650853743 | 13.79310036894126 |
| C | 8.02605328746675 | 5.54087329830213 | 13.83580190218843 |
| H | 8.50733658349709 | 6.40975907869019 | 13.39387033656811 |
| C | 8.75338950747826 | 4.39989271239782 | 14.20349935611049 |
| H | 9.82973635970379 | 4.35166088210315 | 14.04773699504597 |
| C | 8.08183535381066 | 3.31621271559356 | 14.74723582564854 |
| H | 8.61127116331243 | 2.40290975460464 | 15.00084244081948 |
| C | 6.67662278078581 | 3.37632042312138 | 14.92388631479636 |
| C | 6.56516810990876 | 1.29442186487808 | 16.13448712836290 |
| C | 7.25571757157453 | 1.62566326349234 | 17.32059174094063 |
| H | 7.33343250209286 | 2.66734749332088 | 17.62738210349671 |
| C | 7.81636589258111 | 0.61907793037665 | 18.10689541475479 |
| H | 8.33730572477432 | 0.88428825731412 | 19.02577564737609 |
| C | 7.70545165281643 | -0.72506808390599 | 17.72375178244010 |
| H | 8.14864070025525 | -1.50646568634851 | 18.33903219226286 |
| C | 7.02955309493863 | -1.05773204537028 | 16.54378943919520 |
| H | 6.95398110642586 | -2.09807983851606 | 16.23063667635298 |
| C | 6.45889393815144 | -0.05732620589905 | 15.75254036337371 |
| H | 5.96516147528045 | -0.31175916566258 | 14.81731704651729 |
| C | 2.99825720742369 | 5.52735257854095 | 12.22313756695440 |
| H | 2.78645954449386 | 6.42400450165753 | 12.79789826494686 |
| C | 2.77902792267020 | 5.48700605722587 | 10.85329610090328 |
| H | 2.37318463883588 | 6.35973090405100 | 10.34793164867714 |
| C | 3.08566598243028 | 4.30548163055308 | 10.16142904122562 |
| H | 2.91505119411051 | 4.22859263485584 | 9.08886704763764 |
| C | 3.58922412935944 | 3.22196414220621 | 10.86220815224646 |
| H | 3.80072280854489 | 2.28343942349220 | 10.35894314334864 |
| C | 3.79357049105292 | 3.31701008086774 | 12.26341841103062 |

| | | | |
|---|---|---|---|
| C | 4.97038655555463 | 1.22194107651652 | 12.40512045287362 |
| C | 6.14432194415641 | 1.52394156616526 | 11.68167469527494 |
| H | 6.45605762273195 | 2.56084835999572 | 11.56812640690693 |
| C | 6.91307336391340 | 0.49899061154435 | 11.12877648392497 |
| H | 7.82014142301098 | 0.74773049063871 | 10.57935516875215 |
| C | 6.52986099186910 | -0.84030040192626 | 11.28467253280962 |
| H | 7.13224605054787 | -1.63645629404623 | 10.85003754410825 |
| C | 5.36662564226108 | -1.14585625674374 | 11.99888802532895 |
| H | 5.05222476371683 | -2.18203032860985 | 12.11706799380304 |
| C | 4.59177954202883 | -0.12397172385793 | 12.55783805938830 |
| H | 3.67277157076454 | -0.36601604573421 | 13.08425312602745 |
| N | 1.80745014721703 | 4.52224252360088 | 15.43843245005295 |
| N | 1.83908578163011 | 2.29781759002207 | 14.70620037418245 |
| N | 4.26824230660446 | 4.51305050437854 | 17.12119015398771 |
| N | 3.57793208426165 | 2.27586286052800 | 17.06780124318798 |
| C | 1.15557800665526 | 5.56645582602811 | 15.97810181307951 |
| H | 1.75189154045144 | 6.45140304255906 | 16.18078798502227 |
| C | -0.21481943489511 | 5.54900068417570 | 16.24387162593848 |
| H | -0.68436124959877 | 6.42675298208373 | 16.68106770778686 |
| C | -0.94388206618568 | 4.39559663130309 | 15.94268459959337 |
| H | -2.01073180402014 | 4.33717961287613 | 16.14967096861147 |
| C | -0.28016534592794 | 3.30582821656895 | 15.39239949962978 |
| H | -0.80782200704228 | 2.37717385733158 | 15.19826719734755 |
| C | 1.11305136453010 | 3.38230796162440 | 15.14544370507348 |
| C | 1.19539710910519 | 1.32750481377662 | 13.93308807754422 |
| C | 0.34233597606046 | 1.69473974657836 | 12.85972838375637 |
| H | 0.19438542669509 | 2.74647672272700 | 12.62285336697381 |
| C | -0.26466351316876 | 0.71180199607741 | 12.08293951969329 |
| H | -0.89970831481118 | 1.00339147648265 | 11.24801857575834 |
| C | -0.05451423370461 | -0.64542682696948 | 12.36793809833135 |
| H | -0.53970552874401 | -1.41027271391056 | 11.76387880465534 |
| C | 0.78284337631297 | -1.01759790854541 | 13.43182975552574 |
| H | 0.93392275937359 | -2.07027101249577 | 13.66499696697768 |
| C | 1.41719884415156 | -0.04478638247584 | 14.19879708452753 |
| H | 2.03709203635378 | -0.33131866001216 | 15.04535296110368 |
| C | 4.73096209874750 | 5.57934330099903 | 17.80216389061620 |
| H | 4.94701042836467 | 6.46568729161375 | 17.21300051038685 |
| C | 4.91658090586554 | 5.57723690052665 | 19.18282335390284 |
| H | 5.30262954007625 | 6.46845918350097 | 19.67133504300331 |
| C | 4.61103773124220 | 4.41547970242537 | 19.90053204106975 |
| H | 4.75853437905219 | 4.36837025651969 | 20.97792399120368 |
| C | 4.13644843314891 | 3.30707642606745 | 19.21392168296670 |
| H | 3.93331311209775 | 2.37696942071210 | 19.73557102171760 |
| C | 3.96661927445488 | 3.36645633491234 | 17.80840921155617 |
| C | 2.84747938097996 | 1.23442394466061 | 17.67730863602259 |
| C | 1.70781600542353 | 1.51697672881689 | 18.46568725682684 |

| | | | |
|---|---|---|---|
| H | 1.40842882822856 | 2.54966487610904 | 18.63465080754676 |
| C | 0.94858448328374 | 0.47464243287854 | 18.99590779463475 |
| H | 0.06508034318650 | 0.70471395716605 | 19.58951636920927 |
| C | 1.31144084208281 | -0.85886580584461 | 18.76099794657971 |
| H | 0.71802808932765 | -1.66864940083277 | 19.18226055173717 |
| C | 2.44246496834585 | -1.14504319980370 | 17.98536843510762 |
| H | 2.73989741641220 | -2.17811095743357 | 17.81163462147726 |
| C | 3.20320778484466 | -0.10973374327540 | 17.43979788252022 |
| H | 4.10263502368711 | -0.33392759176706 | 16.87088126184782 |

**5.8 References**


1. Bennett, M. J.; Caulton, K. G.; Cotton, F. A., Structure of tetra-n-butyratodiruthenium chloride, a compound with a strong metal-metal bond. *Inorg. Chem.* **1969,** *8* (1), 1-6.
2. Angaridis, P., Ruthenium Compounds. In *Multiple Bonds Between Metal Atoms*, Cotton, F. A.; Murillo, C. A.; Walton, R. A., Eds. Springer: Boston, MA, 2005.
3. Van Caemelbecke, E.; Phan, T.; Osterloh, W. R.; Kadish, K. M., Electrochemistry of metal-metal bonded diruthenium complexes. *Coord. Chem. Rev.* **2021,** *434*, 213706.
4. Yamaguchi, K.; Takahara, Y.; Fueno, T. In *Ab-Initio Molecular Orbital Studies of Structure and Reactivity of Transition Metal-OXO Compounds*, Applied Quantum Chemistry, Dordrecht, 1986//; Smith, V. H.; Schaefer, H. F.; Morokuma, K., Eds. Springer Netherlands: Dordrecht, 1986; pp 155-184.
5. Soda, T.; Kitagawa, Y.; Onishi, T.; Takano, Y.; Shigeta, Y.; Nagao, H.; Yoshioka, Y.; Yamaguchi, K., Ab initio computations of effective exchange integrals for H-H, H-He-H and Mn <SUB>2</SUB>O <SUB>2</SUB> complex: comparison of broken-symmetry approaches. *Chemical Physics Letters* **2000,** *319*, 223-230.
6. Neese, F., Software update: the ORCA program system, version 4.0. *WIREs Computational Molecular Science* **2018,** *8* (1), e1327.
7. Becke, A. D., Density-functional thermochemistry. III. The role of exact exchange. *J. Chem. Phys.* **1993,** *98* (7), 5648-5652.
8. Grimme, S.; Antony, J.; Ehrlich, S.; Krieg, H., A consistent and accurate ab initio parametrization of density functional dispersion correction (DFT-D) for the 94 elements H-Pu. *J. Chem. Phys.* **2010,** *132* (15), 154104.
9. Neese, F.; Wennmohs, F.; Hansen, A.; Becker, U., Efficient, approximate and parallel Hartree–Fock and hybrid DFT calculations. A 'chain-of-spheres' algorithm for the Hartree–Fock exchange. *Chem. Phys.* **2009,** *356* (1), 98-109.
10. Weigend, F.; Ahlrichs, R., Balanced basis sets of split valence, triple zeta valence and quadruple zeta valence quality for H to Rn: Design and assessment of accuracy. *Phys. Chem. Chem. Phys.* **2005,** *7* (18), 3297-3305.
11. Lenthe, E. v.; Baerends, E. J.; Snijders, J. G., Relativistic regular two-component Hamiltonians. *J. Chem. Phys.* **1993,** *99* (6), 4597-4610.
12. Pantazis, D. A.; Chen, X.-Y.; Landis, C. R.; Neese, F., All-Electron Scalar Relativistic Basis Sets for Third-Row Transition Metal Atoms. *J. Chem. Theory Comput.* **2008,** *4* (6), 908-919.

13. York, D. M.; Karplus, M., A Smooth Solvation Potential Based on the Conductor-Like Screening Model. *J. Phys. Chem. A* **1999,** *103* (50), 11060-11079.

# Chapter 6

*Enhanced Redox Sensitivity of $Ru_2$ Complexes Supported by Carbolinate Ligands.*

## 6.1 Abstract

DFT calculations on diruthenium paddlewheel complexes supported by monoanionic carbolinate ligands indicate greater sensitivity of the $Ru_2^{5+/6+}$ redox couple to electron -withdrawing and -donating substituents compared to the same redox reaction for both diarylformamidinate and anilinopyridinate complexes. These calculations also show an analogous frontier orbital arrangement to anilinopyridinate complexes, with the one significant difference being the addition of four ligand aryl-centered orbitals below the energy of the ligand N-centered orbitals yet above the singly-occupied $Ru_2$ $\pi^*$ orbitals. Synthetic efforts to prepare $Ru_2(carb)_4Cl$ appear successful based on MALDI mass spectrometry, elemental analysis, and EPR spectroscopy, but the insolubility of the complex prevents crystallographic characterization or measurement of the targeted $Ru_2^{5+/6+}$ redox couple.

## 6.2 Introduction

As described extensively in previous chapters, we are keenly interested in the ability to prepare and isolate high-valent metal-metal bonded compounds to determine their viability as reactive intermediates for small molecule activation.[1-8] Chapter 4 of this thesis describes our success in accessing relatively high oxidation states at mild potentials through rational ligand design. Encouraged by the tunability of anilinopyridinate ligands (Figure 6.1, center), we sought to develop and evaluate a similar ligand that should be even more tunable.

While the molecule α-carboline (Hcarb, Figure 6.1, right) has been known for nearly a century,[9] it took until 2000 before it was employed as a ligand by Cotton and coworkers, and only to a very limited extent.[10, 11] While the geometric consequences of the constrained bite angle were explored, neither the derivatization of the ligand nor the spectroscopic properties of the resultant complexes were explored. By analogy to the anilinopyridinate ligand, we reason that substitution with electron donating or withdrawing groups at the position *para* to the *amido* nitrogen should result in ligands with substantially altered electron donating properties and, by extension, bimetallic complexes with highly tunable redox potentials. As established by the work presented in Chapter 4, anilinopyridinate complexes are more sensitive to electronic substituents than the well-studied diarylformamidinate (Figure 6.1, left) complexes. By tying the two 6-membered rings together and establishing a delocalized π system across the entire ligand, we increased electronic communication through the ligand to the bimetallic core.

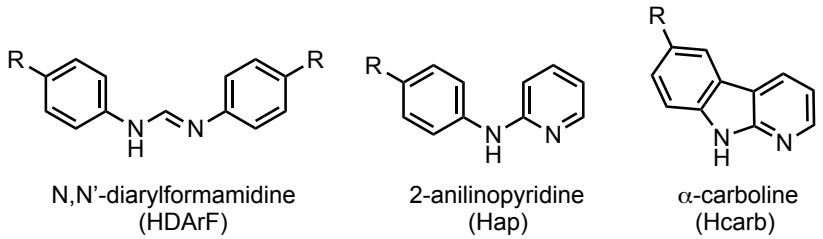


*Figure 6.1. N,N-donor ligands with* para-*aryl positions highlighted.*

## 6.3 Computational Predictions

Initial atomic coordinates for DFT were prepared by manually editing the coordinates from $Ru_2(ap)_4Cl$.[12] Removal of the appropriate 2 H-atoms from each ligand and adjustments to bond lengths, bond angles, and dihedral angles eventually yielded satisfactory starting coordinates. After a preliminary DFT geometry optimization, ligand substitution (Figure 6.2) was modeled by again manually adjusting the coordinates to add the desired atoms. The divergent bite angle of the

ligand,[11] caused by tethering the aryl and pyridyl rings, is reflected in the predicted bond distances. Compared to bond lengths calculated for $Ru_2(ap)_4Cl$ by identical computational methods, $Ru_2(carb)_4Cl$ has longer M–L (~0.01 Å longer) and M–M (~0.09 Å longer) bonds. Specifically, the Ru–Ru distance is 2.39 (2.30 for $Ru_2(ap)_4Cl$). The Ru–$N_{pyr}$ distance is 2.15 (c.f. 2.13) and the Ru–$N_{am}$ distance is 2.07 (c.f. 2.06). In contrast, the Ru–Cl distance is shorter (2.47 vs. 2.51), presumably because the tethered ligand offers less steric repulsion to the chloro ligand.

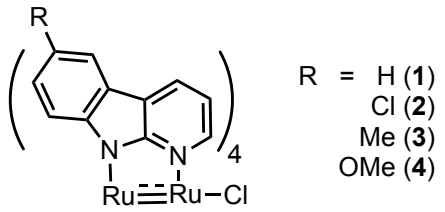


*Figure 6.2.$Ru_2(carb)_4Cl$ complexes considered computationally.*

Calculations on the quartet and doublet states for the neutral $Ru_2^{5+}$ compounds (**1**-**4**) uniformly identified the quartet state as lower energy, by a range of 15-27 kJ/mol. Calculations performed for cationic $Ru_2^{6+}$ complexes identified the intermediate spin triplet state as lower in energy than both the singlet and quintet states, with the singlet configurations being highest in energy. For $\mathbf{1}^+$-$\mathbf{3}^+$, the triplet was more stable by at least 11 kJ/mol; however, calculations on the triplet and quintet states for $\mathbf{4}^+$ were nearly equal in energy, with the triplet more stable by only 1.2 kJ/mol.

As with the anilinopyridinate counterparts, the *a* and *e* symmetry combinations of the amido N-atom *p* orbitals are present and have energies between the singly-occupied $\pi^*$ and singly- or un-occupied $\delta^*$ orbitals. In addition, there are four energetically equivalent ligand (aryl) orbitals below the N-atom *a* and *e* orbitals but again above the $\pi^*$ orbitals. See Figure 6.3 for a molecular orbital diagram of $\mathbf{1}^+$. Thus, subsequent oxidation beyond the $Ru_2^{6+}$ complexes is expected to be

ligand-centered unless the axial chloro ligand were replaced with a sufficiently π-donating ligand so as to raise the $\pi^*$ orbitals to higher energy than the ligand orbitals.

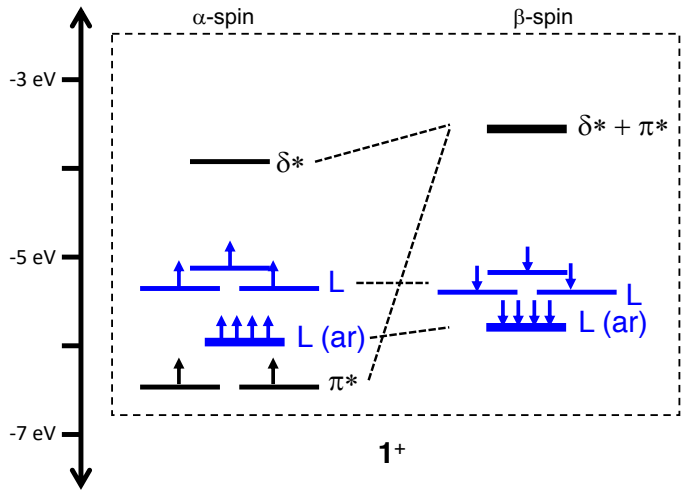


*Figure 6.3. Calculated orbital energy level diagram for **1**⁺. Ligand-based orbitals are highlighted in blue.*

DFT provides a relatively accurate and highly accessible platform for predicting the redox properties of transition metal compounds.[13] This is particularly the case when similar compounds have been benchmarked with experimental results. Thus, electronic and thermodynamic calculations were performed with identical methods used for the anilinopyridinate complexes described in Chapter 4. Therefore, direct comparisons of calculated redox potentials are straightforward (Figure 6.4). The $Ru_2^{5+/6+}$ couple for the carboline complexes is shifted ~400 mV cathodically, indicating more facile oxidation. This is consistent with the expectation that increased conjugation of the equatorial ligand would increase electron donation to the metal center. Moreover, there is a linear free energy relationship between $E_{1/2}$ and the sum of the Hammett parameters (Σσ),given by the slope ρ. For the carb complexes, ρ, is 186 mV/σ, nearly 50% greater than the 127 mV/σ calculated (116 mV/σ measured) for ap complexes and more than twice as large as values reported for DArF complexes of both Ru[14] and Mo[15, 16] (Table 6.1).

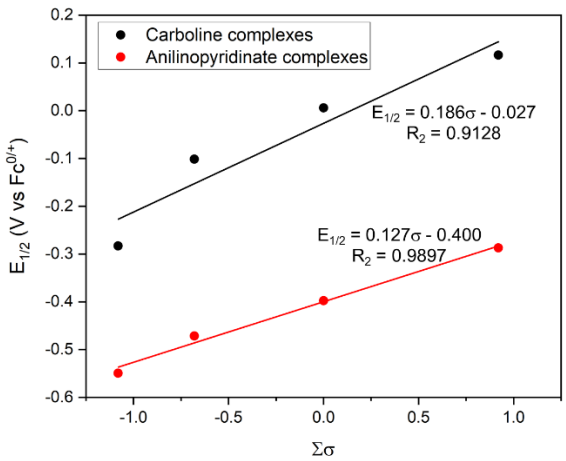


*Figure 6.4.DFT predicted linear free energy relationships for the redox reactions of **1-4** (black) and the anilinopyridinate complexes described in Chapter 3.*

| Complexes | ρ (mV/σ) |
|---|---|
| $Ru_2$(R-DArF)$_4$Cl | 85[14] |
| $Ru_2$(R-ap)$_4$Cl | 116 (127 calc.) |
| $Ru_2$(R-carb)$_4$Cl | (186 calc.) |

*Table 6.1. Measured (calculated) Hammett correlation, ρ, between redox potential of $Ru_2^{5+/6+}$ and the sum of Hammett σ parameters.*

## 6.4 Experimental Results

With promising predictions in hand, we set out to synthesize the desired complexes and measure their electrochemical properties. The α-carboline ligand was synthesized following a literature procedure.[17] Synthesis of the diruthenium carboline complex was attempted both by refluxing the ligand with diruthenium tetraacetate chloride in toluene with an excess of lithium chloride and a Soxhlet extractor containing a thimble charged with potassium carbonate, as well as a reaction in excess molten ligand. The solvent-phase reaction produced a range of unidentified

products with varying solubility, including an insoluble fraction that contains the desired product. Under molten ligand conditions, the desired product, as determined by MALDI mass spectrometry, is obtained in satisfactory yield

The reaction product is insoluble in nearly all standard solvents, including alcohols, acetonitrile, dichloromethane, THF, and water. It is sparingly soluble in DMSO and pyridine, DMF, and DMA, with a maximum concentration in DMF of 1.8 mg in 10.0 mL (0.20 mM). The insoluble nature of the product in most organic solvents is a barrier to study, and crystallographic determination of the structure has not been successful thus far. Furthermore, the compound relaxes too quickly for NMR analysis even at suitable concentrations in pyridine-d5. However, the mass envelope is readily detected by solid-phase MALDI mass spectrometry. EPR analysis of a pyridine solution of **1** further confirms the product assignment based on the characteristic $S = 3/2$ $Ru_2^{5+}$ signal (Figure 6.5). As with other $Ru_2^{5+}$ compounds, **1** exhibits an axial $S = 3/2$ signal with large zero-field splitting, such that only the $m_s = \pm 1/2$ transitions are observed with effective $g$-values of 2 and 4. While definitive isomeric assignment cannot be made, the lack of measurable rhombicity in the EPR signal leads us to predict that a (4,0) isomer is obtained. Initial attempts to measure the redox potential for **1** were unsuccessful due to the low solubility even in DMF.

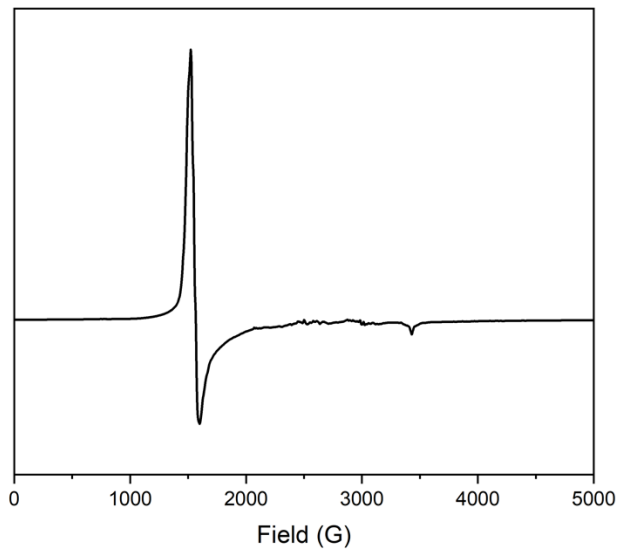


*Figure 6.5. X-band EPR spectrum of **1** in frozen pyridine solution at 10 K. Simulation is underway at the time of writing.*

## 6.5 Future work

Given the insolubility of **1**, we are currently attempting to prepare a more soluble analog before assessing strongly electron -withdrawing and -donating substituents. Installation of a *tert*-butyl group *para* to the *anilino* nitrogen gives 4-$^{t}$Butyl-α-carboline. Despite being obtained in low yield, this proteo-ligand is significantly more soluble than the parent compound. Attempts to prepare a soluble $Ru_2$ complex with this ligand are underway at the time of writing and appear initially successful. As the alkyl group is a relatively weak electron-donating group, both the 4-methoxy and 4-fluoro derivatives, the syntheses for which are reported, will be subsequently prepared. Pending successful electrochemical analysis, both experimental and calculated redox potentials will be compared to diarylformamidinate and anilinopyridinate complexes.

## 6.6 Methods

### *6.6.1 Physical Measurements*

MALDI mass spectrometry was performed with a Bruker Ultraflex™ III mass spectrometer equipped with a SmartBeam™ laser. IR spectroscopy was performed with a Bruker Tensor 27 spectrometer using an ATR adapter. Vis/NIR spectroscopy was measured using a StellarNet tungsten halogen source and a BLACK-Comet UV/Vis spectrometer. Elemental analysis was performed by Midwest Microlab, LLC in Indianapolis, IN, USA. EPR data were acquired on a Bruker ELEXSYS E500 EPR spectrometer equipped with a Varian E102 microwave bridge. An Oxford Instruments ESR-900 continuous-flow helium cryostat and an Oxford Instruments 503S temperature controller were used to control the sample temperature. Measurement conditions were: 9.38 GHz, 2 G modulation amplitude, 2500 G center field, 5000 G sweep width, 40.96 ms time constant, 20.48 ms conversion time, and 10 K.

### *6.6.2 Computational Methods*

Initial coordinates for **1** were prepared from the coordinates for $Ru_2(ap)_4Cl$ published by Cotton et al.[12] H-atoms were removed as necessary and bond distances, bond angles, and dihedral angles were modified using the Avogadro software program[18, 19] until satisfactory starting coordinates were obrtained. Coordinates for **2**-**4** and [**1**-**4**]$^+$ were generated by editing the optimized coordinates for **1**. All calculations were carried out with the ORCA version 4.2.1 software package.[20] Calculations were performed by unrestricted Kohn-Sham DFT using the B3LYP hybrid functional with the RIJCOSX chain of spheres approximation.[21-24] Ruthenium atoms were modeled with the TZVP basis set. All other atoms were modeled with the def2-SVP basis set.[25] Relativistic effects were treated using the zero-order relativistic approximation (ZORA) Hamiltonian with the SARC/J auxiliary basis set for coulomb fitting.[26, 27] These methods were used to perform geometry

optimizations and numerical vibrational frequency analysis on relevant structures. The conductor-like polarizable continuum model (CPCM) was also implemented to model the solvent effects of dichloromethane in all calculations.[28] The Avogadro program[18, 19] was used to edit .xyz files, the Jmol program[29] was used to visualize vibrational frequencies, and the MultiWFN program[30] was used to visualize molecular orbitals.

*6.6.3 Synthetic Methods*

α-carboline was prepared by literature methods.[17] Aniline was distilled before use and all other reagents were used as received. Purity was determined by $^1$H NMR, which matched the literature report. $Ru_2(OAc)_4Cl$ was prepared as described in the literature.[31, 32]

Synthesis of $Ru_2(carb)_4Cl$ (**1**). $Ru_2(OAc)_4Cl$ (228.1 mg, 0.4815 mmol, 1 eq.) and Hcarb (2191.6 mg, 13.030 mmol, 27.06 eq.) were added to a sublimator equipped with a stir bar and closed without a cold finger. The vessel was evacuated and refilled with $N_2$ three times and then heated in a sand bath to ~250 °C until molten. After two hours, the sublimator was opened, the stirbar removed, and the sides scraped down to remove accumulated Hcarb and HOAc. The sublimator was then equipped with a cold finger and excess Hcarb was removed by sublimation at 165 °C under a dynamic vacuum, yielding a blue/green solid left in the sublimator. Yield: 347.7 mg (0.3836 mmol, 80%). Analytically pure product was obtained by copious washing with $CH_2Cl_2$. MW: 906.35 g mol$^{-1}$. MALDI (*m*/*z*): ([M]$^+$) 903.3 (uncalibrated). IR (ATR): 3054, 1621, 1597, 1560, 1469, 1443, 1416, 1367, 1330, 1287, 1272, 1232, 1197, 1145, 1124, 1011, 943, 846, 774, 759, 736, 701, 633 cm$^{-1}$. [$C_{44}H_{28}ClN_8Ru_2$•$3CH_2Cl_2$]: Calcd C 48.62, H 2.95, N 9.65, found C 48.12, H 2.60, N 9.64.

## 6.7 Atomic Coordinates for Calculated Structures

B3LYP geometry-optimized coordinates for **1**

| | | | |
|---|---|---|---|
| Ru | 0.126333 | -0.065458 | -0.018448 |
| Ru | -1.961519 | 0.995481 | 0.446427 |
| N | -2.503508 | 0.844547 | -1.541398 |
| C | -1.705950 | 0.156350 | -2.397472 |
| N | -0.520406 | -0.380569 | -2.044653 |
| C | 0.155744 | -1.043993 | -3.009044 |
| C | -0.319520 | -1.179941 | -4.316258 |
| C | -1.549279 | -0.614285 | -4.688940 |
| C | -2.265141 | 0.072678 | -3.713070 |
| C | -3.518590 | 0.793908 | -3.628243 |
| C | -3.614163 | 1.249055 | -2.274749 |
| C | -4.721576 | 2.002097 | -1.853239 |
| C | -5.723106 | 2.286963 | -2.783513 |
| C | -5.637038 | 1.836971 | -4.117867 |
| C | -4.536717 | 1.091554 | -4.546737 |
| H | -4.469781 | 0.748844 | -5.579143 |
| H | -6.435264 | 2.077927 | -4.818653 |
| H | -6.587633 | 2.872007 | -2.470954 |
| H | -4.798713 | 2.365311 | -0.829875 |
| H | -1.921627 | -0.714252 | -5.707945 |
| H | 0.283540 | -1.729233 | -5.035847 |
| H | 1.109772 | -1.469680 | -2.712331 |
| N | -1.128425 | 2.849272 | 0.075474 |
| C | 0.141521 | 2.922096 | -0.397863 |
| N | 0.934772 | 1.846026 | -0.574761 |
| C | 2.173156 | 2.078901 | -1.063561 |
| C | 2.640727 | 3.358620 | -1.374085 |
| C | 1.820414 | 4.481910 | -1.183158 |
| C | 0.538884 | 4.267555 | -0.684331 |
| C | -0.613404 | 5.074548 | -0.338115 |
| C | -1.606859 | 4.154462 | 0.125539 |
| C | -2.861080 | 4.617048 | 0.554107 |
| C | -3.112182 | 5.989894 | 0.510872 |
| C | -2.138649 | 6.901301 | 0.050818 |
| C | -0.887263 | 6.450249 | -0.373932 |
| H | -0.135778 | 7.156202 | -0.726964 |
| H | -2.367080 | 7.966175 | 0.029535 |
| H | -4.080924 | 6.364113 | 0.840773 |
| H | -3.620742 | 3.927474 | 0.918439 |
| H | 2.182332 | 5.481785 | -1.420838 |
| H | 3.650950 | 3.464166 | -1.762850 |
| H | 2.801811 | 1.203776 | -1.200070 |
| N | -1.455852 | 1.166989 | 2.443000 |

| | | | |
|---|---|---|---|
| C | -0.204047 | 0.824441 | 2.840440 |
| N | 0.719313 | 0.286842 | 2.017489 |
| C | 1.926260 | 0.009509 | 2.558816 |
| C | 2.232230 | 0.249447 | 3.901136 |
| C | 1.270506 | 0.800886 | 4.762620 |
| C | 0.020570 | 1.098767 | 4.227777 |
| C | -1.230699 | 1.654050 | 4.701760 |
| C | -2.103064 | 1.669486 | 3.567213 |
| C | -3.418790 | 2.143879 | 3.687060 |
| C | -3.847312 | 2.603858 | 4.933705 |
| C | -2.989882 | 2.598395 | 6.053943 |
| C | -1.681200 | 2.123492 | 5.945016 |
| H | -1.021378 | 2.118263 | 6.812543 |
| H | -3.355183 | 2.966319 | 7.011879 |
| H | -4.866373 | 2.973792 | 5.042195 |
| H | -4.095471 | 2.146854 | 2.834003 |
| H | 1.503855 | 0.986588 | 5.810455 |
| H | 3.227229 | -0.001222 | 4.261994 |
| H | 2.660186 | -0.423301 | 1.885224 |
| N | -2.832829 | -0.838627 | 0.825151 |
| C | -2.056066 | -1.951835 | 0.843902 |
| N | -0.739299 | -1.948954 | 0.552662 |
| C | -0.098881 | -3.136964 | 0.627939 |
| C | -0.740617 | -4.327217 | 0.980995 |
| C | -2.113539 | -4.335322 | 1.274572 |
| C | -2.794596 | -3.123696 | 1.206190 |
| C | -4.149591 | -2.656789 | 1.415772 |
| C | -4.117854 | -1.247873 | 1.166612 |
| C | -5.287289 | -0.479139 | 1.277341 |
| C | -6.472240 | -1.122107 | 1.640934 |
| C | -6.508704 | -2.509839 | 1.891965 |
| C | -5.351334 | -3.282914 | 1.779508 |
| H | -5.382163 | -4.355516 | 1.970692 |
| H | -7.449571 | -2.980561 | 2.174048 |
| H | -7.387985 | -0.538419 | 1.731125 |
| H | -5.278133 | 0.591321 | 1.078750 |
| H | -2.619318 | -5.261091 | 1.546700 |
| H | -0.155593 | -5.243397 | 1.020408 |
| H | 0.960593 | -3.120676 | 0.389413 |
| Cl | 2.283859 | -1.166267 | -0.498490 |

B3LYP geometry-optimized coordinates for **1**$^{+}$

| | | | |
|---|---|---|---|
| Ru | 0.146706 | -0.076446 | -0.024700 |
| Ru | -1.950334 | 0.988663 | 0.441807 |
| N | -2.484845 | 0.839906 | -1.515025 |
| C | -1.694826 | 0.143096 | -2.381732 |

| | | | |
|---|---|---|---|
| N | -0.513685 | -0.400193 | -2.033292 |
| C | 0.153013 | -1.073105 | -3.001131 |
| C | -0.336670 | -1.206174 | -4.301282 |
| C | -1.565296 | -0.630501 | -4.667599 |
| C | -2.264167 | 0.063471 | -3.687318 |
| C | -3.513638 | 0.800093 | -3.594954 |
| C | -3.598591 | 1.259429 | -2.245371 |
| C | -4.688765 | 2.029357 | -1.817285 |
| C | -5.692733 | 2.325249 | -2.743489 |
| C | -5.617881 | 1.868821 | -4.073427 |
| C | -4.527908 | 1.105714 | -4.508564 |
| H | -4.471638 | 0.760247 | -5.540070 |
| H | -6.415452 | 2.117495 | -4.771734 |
| H | -6.546641 | 2.923637 | -2.428939 |
| H | -4.755682 | 2.400114 | -0.796364 |
| H | -1.945850 | -0.730218 | -5.683010 |
| H | 0.254860 | -1.762830 | -5.024483 |
| H | 1.105607 | -1.507617 | -2.714904 |
| N | -1.130360 | 2.814799 | 0.077268 |
| C | 0.141916 | 2.898814 | -0.406783 |
| N | 0.935468 | 1.827511 | -0.592579 |
| C | 2.170367 | 2.066813 | -1.093655 |
| C | 2.622502 | 3.350197 | -1.403455 |
| C | 1.797771 | 4.469857 | -1.200414 |
| C | 0.525098 | 4.243411 | -0.690140 |
| C | -0.631541 | 5.045134 | -0.326861 |
| C | -1.615440 | 4.122503 | 0.142826 |
| C | -2.863726 | 4.573082 | 0.593270 |
| C | -3.121437 | 5.946319 | 0.561092 |
| C | -2.157947 | 6.859812 | 0.092317 |
| C | -0.907159 | 6.416413 | -0.352771 |
| H | -0.163903 | 7.127582 | -0.710922 |
| H | -2.388968 | 7.923932 | 0.079450 |
| H | -4.085934 | 6.315219 | 0.907166 |
| H | -3.615327 | 3.880579 | 0.967335 |
| H | 2.151558 | 5.471967 | -1.438432 |
| H | 3.627472 | 3.464024 | -1.802775 |
| H | 2.805590 | 1.198918 | -1.240748 |
| N | -1.452735 | 1.159822 | 2.408107 |
| C | -0.194812 | 0.826952 | 2.816584 |
| N | 0.732906 | 0.295431 | 1.998492 |
| C | 1.943199 | 0.031091 | 2.544920 |
| C | 2.236704 | 0.282579 | 3.885963 |
| C | 1.265499 | 0.828710 | 4.742455 |
| C | 0.017653 | 1.109362 | 4.198799 |
| C | -1.246128 | 1.653513 | 4.666809 |

| | | | |
|---|---|---|---|
| C | -2.114686 | 1.656208 | 3.533013 |
| C | -3.436885 | 2.107325 | 3.643834 |
| C | -3.876881 | 2.564370 | 4.889000 |
| C | -3.021994 | 2.573835 | 6.007790 |
| C | -1.702841 | 2.117033 | 5.905311 |
| H | -1.046970 | 2.122972 | 6.775112 |
| H | -3.394120 | 2.937726 | 6.964255 |
| H | -4.901565 | 2.917746 | 4.994220 |
| H | -4.112902 | 2.095776 | 2.790873 |
| H | 1.492771 | 1.022026 | 5.789688 |
| H | 3.232423 | 0.044965 | 4.253026 |
| H | 2.686710 | -0.397636 | 1.880262 |
| N | -2.808571 | -0.816759 | 0.816744 |
| C | -2.035190 | -1.940152 | 0.847715 |
| N | -0.719463 | -1.942109 | 0.563077 |
| C | -0.081498 | -3.133238 | 0.652473 |
| C | -0.733534 | -4.312967 | 1.014410 |
| C | -2.109361 | -4.312949 | 1.301055 |
| C | -2.780587 | -3.099265 | 1.215954 |
| C | -4.139324 | -2.622737 | 1.411962 |
| C | -4.103504 | -1.219240 | 1.150378 |
| C | -5.267951 | -0.444189 | 1.237608 |
| C | -6.459535 | -1.079934 | 1.597163 |
| C | -6.499091 | -2.462107 | 1.862826 |
| C | -5.341028 | -3.242779 | 1.769919 |
| H | -5.377747 | -4.312647 | 1.971766 |
| H | -7.442929 | -2.928562 | 2.140745 |
| H | -7.374445 | -0.493637 | 1.670656 |
| H | -5.256249 | 0.623019 | 1.024523 |
| H | -2.620226 | -5.233323 | 1.579722 |
| H | -0.153976 | -5.231711 | 1.067104 |
| H | 0.978876 | -3.128584 | 0.420287 |
| Cl | 2.266196 | -1.157722 | -0.495390 |

B3LYP geometry-optimized coordinates for **2**

| | | | |
|---|---|---|---|
| Ru | -0.005068 | -0.002665 | 0.006632 |
| Ru | -2.100711 | 1.054901 | 0.443419 |
| N | -2.613757 | 0.902313 | -1.551705 |
| C | -1.819762 | 0.185086 | -2.387809 |
| N | -0.648634 | -0.367624 | -2.012162 |
| C | 0.022441 | -1.064550 | -2.955310 |
| C | -0.441258 | -1.215409 | -4.265648 |
| C | -1.651416 | -0.627503 | -4.664225 |
| C | -2.362599 | 0.092747 | -3.708596 |
| C | -3.597830 | 0.846641 | -3.651699 |
| C | -3.701264 | 1.323246 | -2.306446 |

| | | | |
|---|---|---|---|
| C | -4.794552 | 2.111968 | -1.915910 |
| C | -5.774299 | 2.416486 | -2.860728 |
| C | -5.663806 | 1.938885 | -4.181501 |
| C | -4.587288 | 1.155653 | -4.595794 |
| H | -4.523620 | 0.802738 | -5.623216 |
| Cl | -6.923168 | 2.352508 | -5.338803 |
| H | -6.629722 | 3.028820 | -2.583350 |
| H | -4.883636 | 2.494646 | -0.900960 |
| H | -2.013159 | -0.735660 | -5.686094 |
| H | 0.157166 | -1.792207 | -4.967256 |
| H | 0.964563 | -1.503903 | -2.640675 |
| N | -1.265166 | 2.908549 | 0.078527 |
| C | -0.000885 | 2.979104 | -0.411634 |
| N | 0.790380 | 1.902051 | -0.591136 |
| C | 2.020600 | 2.131735 | -1.100028 |
| C | 2.483499 | 3.409675 | -1.427039 |
| C | 1.666935 | 4.533862 | -1.231482 |
| C | 0.392734 | 4.321476 | -0.712443 |
| C | -0.754690 | 5.129527 | -0.355086 |
| C | -1.741419 | 4.212448 | 0.127669 |
| C | -2.987746 | 4.680911 | 0.571278 |
| C | -3.244786 | 6.051040 | 0.526251 |
| C | -2.267713 | 6.944059 | 0.043952 |
| C | -1.020560 | 6.505401 | -0.398536 |
| H | -0.282321 | 7.216427 | -0.764155 |
| Cl | -2.638089 | 8.663891 | 0.004679 |
| H | -4.202975 | 6.439203 | 0.865058 |
| H | -3.746135 | 3.999731 | 0.952875 |
| H | 2.024720 | 5.532217 | -1.480997 |
| H | 3.487625 | 3.512226 | -1.831753 |
| H | 2.648440 | 1.256355 | -1.238887 |
| N | -1.617180 | 1.230813 | 2.444743 |
| C | -0.358427 | 0.922132 | 2.849999 |
| N | 0.580643 | 0.400310 | 2.034822 |
| C | 1.792380 | 0.160410 | 2.581884 |
| C | 2.088464 | 0.420734 | 3.923244 |
| C | 1.110422 | 0.952627 | 4.777275 |
| C | -0.145153 | 1.212192 | 4.234829 |
| C | -1.412099 | 1.737146 | 4.699537 |
| C | -2.279967 | 1.723371 | 3.561934 |
| C | -3.607014 | 2.165235 | 3.677278 |
| C | -4.057276 | 2.621577 | 4.916008 |
| C | -3.191988 | 2.636041 | 6.027738 |
| C | -1.871198 | 2.198376 | 5.941290 |
| H | -1.224352 | 2.217790 | 6.816352 |
| Cl | -3.804098 | 3.220607 | 7.570403 |

| | | | |
|---|---|---|---|
| H | -5.081991 | 2.968200 | 5.031556 |
| H | -4.285314 | 2.148652 | 2.825854 |
| H | 1.334705 | 1.153383 | 5.824188 |
| H | 3.088850 | 0.200170 | 4.288568 |
| H | 2.539610 | -0.260275 | 1.915279 |
| N | -2.970666 | -0.782249 | 0.813302 |
| C | -2.183521 | -1.887394 | 0.876995 |
| N | -0.859975 | -1.877316 | 0.618973 |
| C | -0.209516 | -3.055305 | 0.740695 |
| C | -0.847604 | -4.244402 | 1.106191 |
| C | -2.227252 | -4.261557 | 1.361252 |
| C | -2.918020 | -3.058777 | 1.244765 |
| C | -4.282716 | -2.602408 | 1.403290 |
| C | -4.259042 | -1.199082 | 1.124758 |
| C | -5.441946 | -0.445840 | 1.183095 |
| C | -6.632361 | -1.089998 | 1.520600 |
| C | -6.642306 | -2.471624 | 1.796183 |
| C | -5.482506 | -3.243206 | 1.742149 |
| H | -5.517362 | -4.309622 | 1.956599 |
| Cl | -8.167456 | -3.242235 | 2.216380 |
| H | -7.562770 | -0.528210 | 1.570944 |
| H | -5.446472 | 0.620355 | 0.963846 |
| H | -2.731176 | -5.185942 | 1.641034 |
| H | -0.253746 | -5.152239 | 1.184464 |
| H | 0.855510 | -3.033974 | 0.528548 |
| Cl | 2.155143 | -1.095957 | -0.444572 |

B3LYP geometry-optimized coordinates for **2**$^{+}$

| | | | |
|---|---|---|---|
| Ru | 0.015388 | -0.012817 | 0.000152 |
| Ru | -2.089379 | 1.049194 | 0.438589 |
| N | -2.599514 | 0.894382 | -1.525765 |
| C | -1.808823 | 0.174457 | -2.373827 |
| N | -0.639666 | -0.379761 | -2.003726 |
| C | 0.025706 | -1.080110 | -2.952245 |
| C | -0.451216 | -1.227053 | -4.256023 |
| C | -1.663709 | -0.634780 | -4.646855 |
| C | -2.361508 | 0.086045 | -3.685112 |
| C | -3.597261 | 0.847863 | -3.618726 |
| C | -3.691824 | 1.324697 | -2.275710 |
| C | -4.773505 | 2.122060 | -1.876870 |
| C | -5.757342 | 2.432895 | -2.815934 |
| C | -5.657804 | 1.953053 | -4.135344 |
| C | -4.585157 | 1.160043 | -4.556251 |
| H | -4.529728 | 0.806717 | -5.583655 |
| Cl | -6.912942 | 2.369541 | -5.283516 |
| H | -6.605888 | 3.052049 | -2.533835 |

| | | | |
|---|---|---|---|
| H | -4.854412 | 2.508562 | -0.863099 |
| H | -2.033423 | -0.742269 | -5.665415 |
| H | 0.138692 | -1.806141 | -4.962666 |
| H | 0.968346 | -1.524597 | -2.648475 |
| N | -1.268646 | 2.876591 | 0.075137 |
| C | 0.001064 | 2.957999 | -0.418394 |
| N | 0.793557 | 1.885898 | -0.602559 |
| C | 2.023441 | 2.122284 | -1.116193 |
| C | 2.472932 | 3.403705 | -1.439339 |
| C | 1.650523 | 4.524346 | -1.236186 |
| C | 0.382458 | 4.299636 | -0.713373 |
| C | -0.771420 | 5.102454 | -0.345108 |
| C | -1.751343 | 4.181915 | 0.137198 |
| C | -2.994638 | 4.639575 | 0.594830 |
| C | -3.257359 | 6.009292 | 0.560269 |
| C | -2.287683 | 6.907171 | 0.075891 |
| C | -1.038414 | 6.473498 | -0.379441 |
| H | -0.305226 | 7.189162 | -0.745193 |
| Cl | -2.658031 | 8.618709 | 0.048479 |
| H | -4.213777 | 6.391474 | 0.909685 |
| H | -3.748018 | 3.955562 | 0.980233 |
| H | 2.001512 | 5.525109 | -1.483559 |
| H | 3.474145 | 3.514710 | -1.848539 |
| H | 2.658390 | 1.253895 | -1.262109 |
| N | -1.611950 | 1.229154 | 2.409992 |
| C | -0.349092 | 0.922911 | 2.827200 |
| N | 0.592055 | 0.402921 | 2.017633 |
| C | 1.805005 | 0.168716 | 2.571027 |
| C | 2.088466 | 0.437501 | 3.911291 |
| C | 1.102892 | 0.969046 | 4.759618 |
| C | -0.147856 | 1.218738 | 4.207229 |
| C | -1.424942 | 1.739083 | 4.664873 |
| C | -2.287113 | 1.717973 | 3.526346 |
| C | -3.618100 | 2.144199 | 3.632340 |
| C | -4.078562 | 2.598771 | 4.868354 |
| C | -3.218143 | 2.623587 | 5.981989 |
| C | -1.888950 | 2.195986 | 5.900990 |
| H | -1.246563 | 2.221795 | 6.778762 |
| Cl | -3.834870 | 3.201609 | 7.515780 |
| H | -5.107154 | 2.934433 | 4.978689 |
| H | -4.294427 | 2.117449 | 2.780172 |
| H | 1.320821 | 1.175389 | 5.806280 |
| H | 3.087576 | 0.224095 | 4.283775 |
| H | 2.560044 | -0.250893 | 1.913514 |
| N | -2.947114 | -0.759191 | 0.809059 |
| C | -2.164046 | -1.875402 | 0.878900 |

| | | | |
|---|---|---|---|
| N | -0.842620 | -1.870480 | 0.623760 |
| C | -0.195556 | -3.052392 | 0.754760 |
| C | -0.843979 | -4.231201 | 1.127354 |
| C | -2.225993 | -4.239771 | 1.379175 |
| C | -2.905603 | -3.034422 | 1.251163 |
| C | -4.273112 | -2.567684 | 1.400895 |
| C | -4.243648 | -1.168794 | 1.114111 |
| C | -5.421065 | -0.409110 | 1.154395 |
| C | -6.617008 | -1.045757 | 1.488185 |
| C | -6.633338 | -2.423636 | 1.775063 |
| C | -5.472009 | -3.201992 | 1.735056 |
| H | -5.512658 | -4.266386 | 1.956690 |
| Cl | -8.154851 | -3.186005 | 2.188323 |
| H | -7.545304 | -0.480071 | 1.525376 |
| H | -5.422496 | 0.654248 | 0.923369 |
| H | -2.735294 | -5.158934 | 1.664425 |
| H | -0.256450 | -5.142097 | 1.214858 |
| H | 0.869884 | -3.042526 | 0.546792 |
| Cl | 2.138953 | -1.088365 | -0.443442 |

B3LYP geometry-optimized coordinates for **3**

| | | | |
|---|---|---|---|
| Ru | 0.011586 | -0.031892 | -0.007795 |
| Ru | -2.091510 | 0.979079 | 0.493234 |
| N | -2.666894 | 0.808387 | -1.483328 |
| C | -1.877792 | 0.121137 | -2.346746 |
| N | -0.673492 | -0.387063 | -2.014814 |
| C | -0.008829 | -1.054881 | -2.983893 |
| C | -0.514191 | -1.223985 | -4.276079 |
| C | -1.764806 | -0.690576 | -4.626875 |
| C | -2.470146 | 0.000278 | -3.645938 |
| C | -3.737468 | 0.693850 | -3.539841 |
| C | -3.805679 | 1.172087 | -2.195892 |
| C | -4.922403 | 1.907270 | -1.767857 |
| C | -5.951452 | 2.143127 | -2.678508 |
| C | -5.909120 | 1.670276 | -4.014512 |
| C | -4.788357 | 0.945602 | -4.436282 |
| H | -4.733546 | 0.577685 | -5.461496 |
| C | -7.064385 | 1.946404 | -4.950493 |
| H | -7.285290 | 3.021271 | -5.008082 |
| H | -6.851317 | 1.590714 | -5.965281 |
| H | -7.982807 | 1.448186 | -4.607710 |
| H | -6.820834 | 2.714643 | -2.351313 |
| H | -4.986963 | 2.295214 | -0.752519 |
| H | -2.161346 | -0.818392 | -5.633625 |
| H | 0.081369 | -1.774475 | -5.001052 |
| H | 0.960381 | -1.456851 | -2.703554 |

| | | | |
|---|---|---|---|
| N | -1.309736 | 2.852413 | 0.106158 |
| C | -0.056291 | 2.952043 | -0.403345 |
| N | 0.755988 | 1.893759 | -0.601573 |
| C | 1.972964 | 2.152953 | -1.129011 |
| C | 2.402319 | 3.442079 | -1.455997 |
| C | 1.563844 | 4.547472 | -1.240860 |
| C | 0.303090 | 4.306272 | -0.702810 |
| C | -0.855386 | 5.088180 | -0.322565 |
| C | -1.812576 | 4.148937 | 0.168659 |
| C | -3.060243 | 4.596195 | 0.631489 |
| C | -3.332468 | 5.963378 | 0.594294 |
| C | -2.398187 | 6.912637 | 0.108238 |
| C | -1.155895 | 6.459200 | -0.349725 |
| H | -0.422289 | 7.172941 | -0.726145 |
| C | -2.749280 | 8.383671 | 0.093476 |
| H | -2.971190 | 8.752736 | 1.104868 |
| H | -3.640004 | 8.576508 | -0.521094 |
| H | -1.926749 | 8.985708 | -0.309923 |
| H | -4.300034 | 6.315944 | 0.953545 |
| H | -3.801246 | 3.898472 | 1.018658 |
| H | 1.896046 | 5.554701 | -1.490873 |
| H | 3.397290 | 3.568972 | -1.876500 |
| H | 2.616447 | 1.291662 | -1.283214 |
| N | -1.555158 | 1.164605 | 2.480480 |
| C | -0.286136 | 0.862065 | 2.852749 |
| N | 0.637907 | 0.353478 | 2.011927 |
| C | 1.863411 | 0.115141 | 2.529396 |
| C | 2.187850 | 0.365161 | 3.865688 |
| C | 1.225758 | 0.884826 | 4.746433 |
| C | -0.043605 | 1.142597 | 4.236840 |
| C | -1.303118 | 1.655483 | 4.735638 |
| C | -2.194735 | 1.644185 | 3.620080 |
| C | -3.520968 | 2.076694 | 3.777203 |
| C | -3.932240 | 2.516320 | 5.034912 |
| C | -3.062843 | 2.541236 | 6.154739 |
| C | -1.743130 | 2.104876 | 5.990922 |
| H | -1.058791 | 2.113607 | 6.840176 |
| C | -3.567512 | 3.028508 | 7.494733 |
| H | -3.914721 | 4.069960 | 7.437027 |
| H | -4.418393 | 2.426690 | 7.844334 |
| H | -2.783473 | 2.978085 | 8.259447 |
| H | -4.962182 | 2.851473 | 5.162731 |
| H | -4.221092 | 2.062460 | 2.942992 |
| H | 1.473631 | 1.077301 | 5.789745 |
| H | 3.197350 | 0.146783 | 4.206837 |
| H | 2.597106 | -0.294934 | 1.841500 |

| | | | |
|---|---|---|---|
| N | -2.911679 | -0.876089 | 0.885620 |
| C | -2.106392 | -1.967722 | 0.901457 |
| N | -0.792650 | -1.931787 | 0.598032 |
| C | -0.120173 | -3.101724 | 0.673741 |
| C | -0.727186 | -4.307038 | 1.037826 |
| C | -2.097759 | -4.350800 | 1.340085 |
| C | -2.812261 | -3.158422 | 1.271854 |
| C | -4.178247 | -2.726735 | 1.485859 |
| C | -4.183713 | -1.321063 | 1.234043 |
| C | -5.377861 | -0.592121 | 1.349225 |
| C | -6.539086 | -1.271956 | 1.714635 |
| C | -6.556120 | -2.666034 | 1.972856 |
| C | -5.362042 | -3.386263 | 1.853249 |
| H | -5.353723 | -4.459978 | 2.044581 |
| C | -7.848012 | -3.347345 | 2.366595 |
| H | -8.614487 | -3.233994 | 1.586743 |
| H | -8.262922 | -2.914572 | 3.288054 |
| H | -7.698037 | -4.419788 | 2.537174 |
| H | -7.469934 | -0.710549 | 1.803910 |
| H | -5.406312 | 0.478227 | 1.151091 |
| H | -2.576770 | -5.289014 | 1.618306 |
| H | -0.117511 | -5.207038 | 1.077506 |
| H | 0.936362 | -3.058609 | 0.425280 |
| Cl | 2.190093 | -1.079043 | -0.526749 |

B3LYP geometry-optimized coordinates for **3**$^{+}$

| | | | |
|---|---|---|---|
| Ru | 0.002377 | -0.003677 | 0.006335 |
| Ru | -2.109048 | 1.010255 | 0.510749 |
| N | -2.680637 | 0.839529 | -1.435800 |
| C | -1.897130 | 0.145838 | -2.310456 |
| N | -0.696814 | -0.367393 | -1.983132 |
| C | -0.040070 | -1.042635 | -2.956180 |
| C | -0.558674 | -1.207727 | -4.241343 |
| C | -1.808602 | -0.664731 | -4.585672 |
| C | -2.498245 | 0.031002 | -3.600038 |
| C | -3.762202 | 0.739395 | -3.486059 |
| C | -3.820777 | 1.218977 | -2.144529 |
| C | -4.921966 | 1.970666 | -1.710222 |
| C | -5.952168 | 2.219699 | -2.616597 |
| C | -5.920384 | 1.743465 | -3.949811 |
| C | -4.808076 | 1.001287 | -4.377706 |
| H | -4.762528 | 0.632985 | -5.402556 |
| C | -7.073740 | 2.029186 | -4.881529 |
| H | -7.309640 | 3.101638 | -4.905086 |
| H | -6.853494 | 1.705194 | -5.904839 |
| H | -7.983891 | 1.507334 | -4.552322 |

| | | | |
|---|---|---|---|
| H | -6.811042 | 2.804656 | -2.287408 |
| H | -4.976738 | 2.364075 | -0.696883 |
| H | -2.212580 | -0.790733 | -5.589106 |
| H | 0.026385 | -1.763963 | -4.970159 |
| H | 0.928100 | -1.452416 | -2.685946 |
| N | -1.344382 | 2.856825 | 0.123753 |
| C | -0.089114 | 2.967630 | -0.398494 |
| N | 0.725207 | 1.915099 | -0.599772 |
| C | 1.937753 | 2.180748 | -1.140791 |
| C | 2.347954 | 3.472035 | -1.474809 |
| C | 1.501611 | 4.572596 | -1.255953 |
| C | 0.251245 | 4.319295 | -0.704899 |
| C | -0.914711 | 5.094387 | -0.314626 |
| C | -1.858182 | 4.152341 | 0.190926 |
| C | -3.101182 | 4.587375 | 0.672832 |
| C | -3.386407 | 5.952136 | 0.632882 |
| C | -2.467980 | 6.903711 | 0.126774 |
| C | -1.223261 | 6.458442 | -0.345896 |
| H | -0.501276 | 7.176731 | -0.734104 |
| C | -2.833382 | 8.368649 | 0.096845 |
| H | -3.130249 | 8.725190 | 1.092675 |
| H | -3.683401 | 8.549936 | -0.576300 |
| H | -1.994591 | 8.983475 | -0.248209 |
| H | -4.350157 | 6.298677 | 1.006155 |
| H | -3.829389 | 3.887232 | 1.078398 |
| H | 1.822253 | 5.581053 | -1.513660 |
| H | 3.336930 | 3.607325 | -1.906158 |
| H | 2.589337 | 1.327258 | -1.300320 |
| N | -1.580065 | 1.197589 | 2.468198 |
| C | -0.304547 | 0.901796 | 2.850530 |
| N | 0.622237 | 0.399683 | 2.013448 |
| C | 1.850909 | 0.171837 | 2.535071 |
| C | 2.163382 | 0.429928 | 3.870490 |
| C | 1.192672 | 0.943400 | 4.747769 |
| C | -0.073878 | 1.186717 | 4.229935 |
| C | -1.345130 | 1.688970 | 4.723951 |
| C | -2.232487 | 1.668860 | 3.608050 |
| C | -3.564344 | 2.081206 | 3.757510 |
| C | -3.986121 | 2.515500 | 5.013950 |
| C | -3.119984 | 2.551176 | 6.133808 |
| C | -1.790106 | 2.130344 | 5.974771 |
| H | -1.109755 | 2.147103 | 6.826290 |
| C | -3.631277 | 3.031567 | 7.471156 |
| H | -3.980987 | 4.071814 | 7.410830 |
| H | -4.483848 | 2.426438 | 7.809720 |
| H | -2.852266 | 2.980639 | 8.240210 |

| | | | |
|---|---|---|---|
| H | -5.020509 | 2.835792 | 5.138847 |
| H | -4.262999 | 2.056294 | 2.922868 |
| H | 1.434557 | 1.140792 | 5.790998 |
| H | 3.173139 | 0.222684 | 4.217136 |
| H | 2.593169 | -0.233424 | 1.854490 |
| N | -2.917412 | -0.816980 | 0.901412 |
| C | -2.114171 | -1.918978 | 0.925883 |
| N | -0.801956 | -1.886532 | 0.627971 |
| C | -0.130873 | -3.059534 | 0.715053 |
| C | -0.747296 | -4.255540 | 1.085936 |
| C | -2.120937 | -4.292532 | 1.381991 |
| C | -2.826262 | -3.098036 | 1.300076 |
| C | -4.196321 | -2.657405 | 1.502578 |
| C | -4.197387 | -1.255649 | 1.241923 |
| C | -5.387698 | -0.520618 | 1.337888 |
| C | -6.554607 | -1.193919 | 1.698313 |
| C | -6.575510 | -2.584203 | 1.966985 |
| C | -5.379277 | -3.311617 | 1.863404 |
| H | -5.376276 | -4.383285 | 2.062558 |
| C | -7.869623 | -3.260525 | 2.353045 |
| H | -8.624176 | -3.154179 | 1.560985 |
| H | -8.294325 | -2.811818 | 3.261984 |
| H | -7.722721 | -4.330171 | 2.539748 |
| H | -7.484419 | -0.629922 | 1.773688 |
| H | -5.413683 | 0.547312 | 1.128792 |
| H | -2.604597 | -5.226285 | 1.665036 |
| H | -0.142461 | -5.157994 | 1.136735 |
| H | 0.926772 | -3.026351 | 0.472391 |
| Cl | 2.144175 | -1.031568 | -0.504981 |

B3LYP geometry-optimized coordinates for **4**

| | | | |
|---|---|---|---|
| Ru | -0.009012 | 0.011913 | 0.002767 |
| Ru | 2.161614 | 0.509901 | -0.856395 |
| N | 2.986551 | 0.295389 | 1.025809 |
| C | 2.184257 | -0.023353 | 2.069728 |
| N | 0.851820 | -0.209997 | 1.960622 |
| C | 0.187995 | -0.521601 | 3.095760 |
| C | 0.817026 | -0.653729 | 4.336929 |
| C | 2.203126 | -0.462200 | 4.454735 |
| C | 2.909776 | -0.140178 | 3.300825 |
| C | 4.286892 | 0.138079 | 2.946570 |
| C | 4.278551 | 0.399752 | 1.539667 |
| C | 5.474995 | 0.707544 | 0.882226 |
| C | 6.665267 | 0.752656 | 1.615553 |
| C | 6.674990 | 0.492832 | 3.005898 |
| C | 5.480369 | 0.185134 | 3.673981 |

| | | | |
|---|---|---|---|
| H | 5.510378 | -0.011080 | 4.744988 |
| O | 7.799820 | 0.519560 | 3.774124 |
| C | 9.048708 | 0.816002 | 3.172222 |
| H | 9.310656 | 0.082058 | 2.395934 |
| H | 9.057747 | 1.822508 | 2.728505 |
| H | 9.795981 | 0.772297 | 3.970044 |
| H | 7.589260 | 0.991657 | 1.095850 |
| H | 5.495105 | 0.911923 | -0.186945 |
| H | 2.699677 | -0.564455 | 5.419230 |
| H | 0.211620 | -0.906654 | 5.204301 |
| H | -0.883453 | -0.667557 | 2.992424 |
| N | 1.870157 | 2.522533 | -0.494026 |
| C | 0.702195 | 2.938956 | 0.051160 |
| N | -0.310841 | 2.107859 | 0.375315 |
| C | -1.413421 | 2.675998 | 0.911957 |
| C | -1.532256 | 4.050504 | 1.136280 |
| C | -0.479182 | 4.918219 | 0.804355 |
| C | 0.666734 | 4.358521 | 0.249072 |
| C | 1.951182 | 4.830565 | -0.227640 |
| C | 2.650526 | 3.664091 | -0.672220 |
| C | 3.943160 | 3.784440 | -1.194678 |
| C | 4.533303 | 5.050187 | -1.272417 |
| C | 3.843871 | 6.203865 | -0.831919 |
| C | 2.546639 | 6.093339 | -0.308997 |
| H | 2.033639 | 6.994343 | 0.024563 |
| O | 4.365182 | 7.461686 | -0.878021 |
| C | 5.672376 | 7.656393 | -1.391471 |
| H | 5.745531 | 7.347586 | -2.444813 |
| H | 6.425584 | 7.108590 | -0.806145 |
| H | 5.876815 | 8.728782 | -1.320300 |
| H | 5.537691 | 5.133436 | -1.678631 |
| H | 4.495893 | 2.912576 | -1.540130 |
| H | -0.564857 | 5.990365 | 0.979196 |
| H | -2.453108 | 4.430654 | 1.572914 |
| H | -2.220032 | 1.994824 | 1.167247 |
| N | 1.382753 | 0.734615 | -2.757938 |
| C | 0.054185 | 0.562177 | -2.957735 |
| N | -0.815558 | 0.246104 | -1.975240 |
| C | -2.111375 | 0.107958 | -2.332678 |
| C | -2.563972 | 0.276907 | -3.644211 |
| C | -1.662639 | 0.605587 | -4.669681 |
| C | -0.322473 | 0.753138 | -4.327777 |
| C | 0.915415 | 1.071700 | -5.010382 |
| C | 1.930053 | 1.047482 | -4.001578 |
| C | 3.259295 | 1.319185 | -4.344329 |
| C | 3.575142 | 1.610985 | -5.675211 |

| | | | |
|---|---|---|---|
| C | 2.573675 | 1.633971 | -6.673488 |
| C | 1.238198 | 1.363798 | -6.339261 |
| H | 0.482735 | 1.387968 | -7.123697 |
| O | 2.817799 | 1.908841 | -7.985107 |
| C | 4.142436 | 2.187022 | -8.406392 |
| H | 4.092529 | 2.369595 | -9.483884 |
| H | 4.548088 | 3.081231 | -7.910316 |
| H | 4.816617 | 1.338302 | -8.218569 |
| H | 4.610135 | 1.820395 | -5.932476 |
| H | 4.049361 | 1.305627 | -3.595219 |
| H | -2.008956 | 0.738782 | -5.694120 |
| H | -3.624106 | 0.148768 | -3.850909 |
| H | -2.798845 | -0.146479 | -1.531154 |
| N | 2.501515 | -1.492900 | -1.237591 |
| C | 1.534053 | -2.395984 | -0.948971 |
| N | 0.345632 | -2.070058 | -0.397745 |
| C | -0.515408 | -3.085971 | -0.168252 |
| C | -0.225473 | -4.417996 | -0.476156 |
| C | 1.006738 | -4.760709 | -1.055930 |
| C | 1.911654 | -3.733349 | -1.301425 |
| C | 3.241591 | -3.606480 | -1.862645 |
| C | 3.557007 | -2.212234 | -1.797115 |
| C | 4.794084 | -1.756462 | -2.266466 |
| C | 5.701883 | -2.675106 | -2.803872 |
| C | 5.387648 | -4.052167 | -2.877398 |
| C | 4.153643 | -4.519711 | -2.401241 |
| H | 3.933162 | -5.584531 | -2.464892 |
| O | 6.224148 | -4.994571 | -3.395739 |
| C | 7.483188 | -4.601739 | -3.915896 |
| H | 7.375667 | -3.892221 | -4.749692 |
| H | 7.964287 | -5.513010 | -4.283202 |
| H | 8.119845 | -4.148568 | -3.141826 |
| H | 6.659286 | -2.311012 | -3.167135 |
| H | 5.060453 | -0.701867 | -2.220987 |
| H | 1.237433 | -5.796871 | -1.301954 |
| H | -0.972568 | -5.178026 | -0.259006 |
| H | -1.466732 | -2.808291 | 0.276359 |
| Cl | -2.261075 | -0.507651 | 0.896385 |

B3LYP geometry-optimized coordinates for **4**$^{+}$

| | | | |
|---|---|---|---|
| Ru | -0.027142 | 0.007095 | 0.009328 |
| Ru | 2.149742 | 0.506112 | -0.852362 |
| N | 2.968940 | 0.292461 | 1.004833 |
| C | 2.167745 | -0.024630 | 2.060739 |
| N | 0.837884 | -0.209183 | 1.955652 |
| C | 0.176399 | -0.517358 | 3.096159 |

| | | | |
|---|---|---|---|
| C | 0.814490 | -0.645370 | 4.330826 |
| C | 2.202446 | -0.455009 | 4.441451 |
| C | 2.898944 | -0.137666 | 3.282240 |
| C | 4.278126 | 0.139291 | 2.917821 |
| C | 4.263832 | 0.397234 | 1.511102 |
| C | 5.456222 | 0.702425 | 0.844535 |
| C | 6.649509 | 0.748414 | 1.569624 |
| C | 6.664686 | 0.491659 | 2.960977 |
| C | 5.468490 | 0.185826 | 3.639080 |
| H | 5.504887 | -0.007490 | 4.709956 |
| O | 7.783181 | 0.517604 | 3.721089 |
| C | 9.038875 | 0.810843 | 3.122577 |
| H | 9.297170 | 0.073719 | 2.349412 |
| H | 9.047716 | 1.817013 | 2.680479 |
| H | 9.780099 | 0.764685 | 3.924968 |
| H | 7.571151 | 0.985222 | 1.045465 |
| H | 5.472512 | 0.903874 | -0.224935 |
| H | 2.704028 | -0.554841 | 5.403021 |
| H | 0.214557 | -0.894864 | 5.202748 |
| H | -0.895398 | -0.663170 | 3.002415 |
| N | 1.866705 | 2.495266 | -0.494530 |
| C | 0.693260 | 2.922267 | 0.051105 |
| N | -0.319447 | 2.095824 | 0.375115 |
| C | -1.422867 | 2.669655 | 0.910495 |
| C | -1.531654 | 4.043943 | 1.128562 |
| C | -0.474192 | 4.907006 | 0.793855 |
| C | 0.666210 | 4.337357 | 0.241819 |
| C | 1.956866 | 4.802426 | -0.237837 |
| C | 2.652051 | 3.632553 | -0.677348 |
| C | 3.945644 | 3.743269 | -1.200106 |
| C | 4.541417 | 5.004079 | -1.283491 |
| C | 3.855061 | 6.161903 | -0.847579 |
| C | 2.551954 | 6.058697 | -0.322343 |
| H | 2.043591 | 6.963424 | 0.006720 |
| O | 4.374234 | 7.409908 | -0.896838 |
| C | 5.684249 | 7.611214 | -1.411387 |
| H | 5.754080 | 7.300924 | -2.463526 |
| H | 6.435607 | 7.066410 | -0.822646 |
| H | 5.880518 | 8.684435 | -1.339986 |
| H | 5.545914 | 5.082358 | -1.689455 |
| H | 4.495607 | 2.868609 | -1.541710 |
| H | -0.554910 | 5.979685 | 0.964624 |
| H | -2.450305 | 4.430818 | 1.563444 |
| H | -2.234259 | 1.995994 | 1.168206 |
| N | 1.384655 | 0.732675 | -2.732074 |
| C | 0.049514 | 0.558358 | -2.941811 |

| | | | |
|---|---|---|---|
| N | -0.820596 | 0.240452 | -1.964524 |
| C | -2.117189 | 0.100509 | -2.328243 |
| C | -2.557920 | 0.271623 | -3.641372 |
| C | -1.650891 | 0.603454 | -4.662274 |
| C | -0.315581 | 0.751129 | -4.308921 |
| C | 0.929970 | 1.073505 | -4.984787 |
| C | 1.938991 | 1.048936 | -3.971568 |
| C | 3.270506 | 1.323413 | -4.303927 |
| C | 3.594648 | 1.618304 | -5.630286 |
| C | 2.597575 | 1.641221 | -6.633629 |
| C | 1.255055 | 1.367296 | -6.306606 |
| H | 0.505171 | 1.392292 | -7.095711 |
| O | 2.843141 | 1.916476 | -7.934755 |
| C | 4.168682 | 2.202267 | -8.361309 |
| H | 4.111474 | 2.384925 | -9.437741 |
| H | 4.566630 | 3.097884 | -7.863631 |
| H | 4.843028 | 1.354622 | -8.174703 |
| H | 4.630203 | 1.830180 | -5.881674 |
| H | 4.056559 | 1.310281 | -3.551128 |
| H | -1.990977 | 0.737902 | -5.688101 |
| H | -3.616265 | 0.142762 | -3.855672 |
| H | -2.811343 | -0.155749 | -1.533852 |
| N | 2.488298 | -1.471077 | -1.232927 |
| C | 1.521753 | -2.386202 | -0.940376 |
| N | 0.335836 | -2.064326 | -0.389208 |
| C | -0.521135 | -3.086070 | -0.155127 |
| C | -0.219582 | -4.413569 | -0.462189 |
| C | 1.014870 | -4.749929 | -1.043492 |
| C | 1.908665 | -3.715574 | -1.290147 |
| C | 3.241200 | -3.579471 | -1.853915 |
| C | 3.548674 | -2.184213 | -1.790837 |
| C | 4.782400 | -1.719060 | -2.260433 |
| C | 5.695288 | -2.630413 | -2.797138 |
| C | 5.387794 | -4.009582 | -2.869054 |
| C | 4.152206 | -4.486573 | -2.389393 |
| H | 3.939331 | -5.552528 | -2.452130 |
| O | 6.220363 | -4.943374 | -3.383527 |
| C | 7.484582 | -4.555922 | -3.905837 |
| H | 7.375048 | -3.849664 | -4.740882 |
| H | 7.959720 | -5.471230 | -4.268838 |
| H | 8.118167 | -4.103852 | -3.129938 |
| H | 6.650264 | -2.261659 | -3.161076 |
| H | 5.043388 | -0.663467 | -2.215575 |
| H | 1.252536 | -5.784389 | -1.287785 |
| H | -0.960347 | -5.178963 | -0.243143 |
| H | -1.474061 | -2.817554 | 0.290284 |

Cl -2.246071 -0.505095 0.888868

**6.8 References**

1. Corcos, A. R.; Long, A. K. M.; Guzei, I. A.; Berry, J. F., A Synthetic Cycle for Nitrogen Atom Transfer Featuring a Diruthenium Nitride Intermediate. *Eur. J. Inorg. Chem.* **2013,** *2013* (22-23), 3808-3811.

2. Corcos, A. R.; Pap, J. S.; Yang, T.; Berry, J. F., A Synthetic Oxygen Atom Transfer Photocycle from a Diruthenium Oxyanion Complex. *J. Am. Chem. Soc.* **2016,** *138* (31), 10032-10040.

3. Das, A.; Reibenspies, J. H.; Chen, Y.-S.; Powers, D. C., Direct Characterization of a Reactive Lattice-Confined $Ru_2$ Nitride by Photocrystallography. *J. Am. Chem. Soc.* **2017,** *139* (8), 2912-2915.

4. Goberna-Ferrón, S.; Peña, B.; Soriano-López, J.; Carbó, J. J.; Zhao, H.; Poblet, J. M.; Dunbar, K. R.; Galán-Mascarós, J. R., A fast metal–metal bonded water oxidation catalyst. *J. Catal.* **2014,** *315*, 25-32.

5. Harvey, M. E.; Musaev, D. G.; Du Bois, J., A Diruthenium Catalyst for Selective, Intramolecular Allylic C–H Amination: Reaction Development and Mechanistic Insight Gained through Experiment and Theory. *J. Am. Chem. Soc.* **2011,** *133* (43), 17207-17216.

6. Musch Long, A. K.; Timmer, G. H.; Pap, J. S.; Snyder, J. L.; Yu, R. P.; Berry, J. F., Aryl C–H Amination by Diruthenium Nitrides in the Solid State and in Solution at Room Temperature: Experimental and Computational Study of the Reaction Mechanism. *J. Am. Chem. Soc.* **2011,** *133* (33), 13138-13150.

7. Musch Long, A. K.; Yu, R. P.; Timmer, G. H.; Berry, J. F., Aryl C−H Bond Amination by an Electrophilic Diruthenium Nitride. *J. Am. Chem. Soc.* **2010,** *132* (35), 12228-12230.

8. Villalobos, L.; Barker Paredes, J. E.; Cao, Z.; Ren, T., *tert*-Butyl Hydroperoxide Oxygenation of Organic Sulfides Catalyzed by Diruthenium(II,III) Tetracarboxylates. *Inorg. Chem.* **2013,** *52* (21), 12545-12552.

9. Lawson, W.; Perkin, W. H.; Robinson, R., LXXVI.—Harmine and harmaline. Part VII. A synthesis of apoharmine and of certain carboline and copyrine derivatives. *Journal of the Chemical Society, Transactions* **1924,** *125* (0), 626-657.

10. Cotton, F. A.; Zhou, H.-C., Some interesting structural chemistry of lithium. *Inorg. Chim. Acta* **2000,** *298* (2), 216-220.

11. Cotton, F. A.; Daniels, L. M.; Murillo, C. A.; Zhou, H.-C., The effect of divergent-bite ligands on metal–metal bond distances in some paddlewheel complexes. *Inorg. Chim. Acta* **2000,** *300-302*, 319-327.

12. Chakravarty, A. R.; Cotton, F. A.; Tocher, D. A., Syntheses, molecular structures, and properties of two polar diruthenium(II,III) complexes of 2-hydroxypyridine and 2-anilinopyridine. *Inorg. Chem.* **1985,** *24* (2), 172-177.

13. Roy, L. E.; Jakubikova, E.; Guthrie, M. G.; Batista, E. R., Calculation of One-Electron Redox Potentials Revisited. Is It Possible to Calculate Accurate Potentials with Density Functional Methods? *J. Phys. Chem. A* **2009,** *113* (24), 6745-6750.

14. Lin, C.; Ren, T.; Valente, E. J.; Zubkowski, J. D.; Smith, E. T., Continuous Spectroscopic and Redox Tuning of Dinuclear Compounds: Chlorotetrakis(μ-N,N′-diarylformamidinato)diruthenium(II,III). *Chemistry Letters* **1997,** *26* (8), 753-754.

15. Lin, C.; Protasiewicz, J. D.; Smith, E. T.; Ren, T., Redox tuning of the dimolybdenum compounds at the ligand periphery: a direct correlation with the Hammett constant of the substituents. *J. Chem. Soc. Chem. Commun.* **1995,** (22), 2257-2258.

16. Lin, C.; Protasiewicz, J. D.; Smith, E. T.; Ren, T., Linear Free Energy Relationships in Dinuclear Compounds. 2. Inductive Redox Tuning via Remote Substituents in Quadruply Bonded Dimolybdenum Compounds. *Inorg. Chem.* **1996,** *35* (22), 6422-6428.

17. He, L.; Allwein, S. P.; Dugan, B. J.; Knouse, K. W.; Ott, G. R.; Zificsak, C. A., Synthesis of α-Carboline. *Organic Synthesis* **2016,** *93*, 272-285.

18. Avogadro: an open-source molecular builder and vizualization tool. Version 1.2. http://avogadro.cc/ .

19. Hanwell, M. D.; Curtis, D. E.; Lonie, D. C.; Vandermeersch, T.; Zurek, E.; Hutchison, G. R., Avogadro: an advanced semantic chemical editor, visualization, and analysis platform. *J. Cheminformatics* **2012,** *4* (1), 17.

20. Neese, F., Software update: the ORCA program system, version 4.0. *WIREs Computational Molecular Science* **2018,** *8* (1), e1327.

21. Neese, F.; Wennmohs, F.; Hansen, A.; Becker, U., Efficient, approximate and parallel Hartree–Fock and hybrid DFT calculations. A 'chain-of-spheres' algorithm for the Hartree–Fock exchange. *Chem. Phys.* **2009,** *356* (1), 98-109.

22. Grimme, S.; Antony, J.; Ehrlich, S.; Krieg, H., A consistent and accurate ab initio parametrization of density functional dispersion correction (DFT-D) for the 94 elements H-Pu. *J. Chem. Phys.* **2010,** *132* (15), 154104.

23. Becke, A. D., Density-functional thermochemistry. III. The role of exact exchange. *J. Chem. Phys.* **1993,** *98* (7), 5648-5652.

24. Lee, C.; Yang, W.; Parr, R. G., Development of the Colle-Salvetti correlation-energy formula into a functional of the electron density. *Phys. Rev. B* **1988,** *37* (2), 785-789.

25. Weigend, F.; Ahlrichs, R., Balanced basis sets of split valence, triple zeta valence and quadruple zeta valence quality for H to Rn: Design and assessment of accuracy. *Phys. Chem. Chem. Phys.* **2005,** *7* (18), 3297-3305.

26. Lenthe, E. v.; Baerends, E. J.; Snijders, J. G., Relativistic regular two-component Hamiltonians. *J. Chem. Phys.* **1993,** *99* (6), 4597-4610.

27. Pantazis, D. A.; Chen, X.-Y.; Landis, C. R.; Neese, F., All-Electron Scalar Relativistic Basis Sets for Third-Row Transition Metal Atoms. *J. Chem. Theory Comput.* **2008,** *4* (6), 908-919.

28. York, D. M.; Karplus, M., A Smooth Solvation Potential Based on the Conductor-Like Screening Model. *J. Phys. Chem. A* **1999,** *103* (50), 11060-11079.

29. Jmol: an open-source Java viewer for chemical stuctures in 3D. http://www.jmol.org/ .

30. Lu, T.; Chen, F., Multiwfn: A multifunctional wavefunction analyzer. *J. Comput. Chem.* **2012,** *33* (5), 580-592.

31. Stephenson, T. A.; Wilkinson, G., New ruthenium carboxylate complexes. *J. Inorg. Nuc. Chem.* **1966,** *28* (10), 2285-2291.

32. Brown, T. R.; Dolinar, B. S.; Hillard, E. A.; Clérac, R.; Berry, J. F., Electronic Structure of $Ru_2$(II,II) Oxypyridinates: Synthetic, Structural, and Theoretical Insights into Axial Ligand Binding. *Inorg. Chem.* **2015,** *54* (17), 8571-8589.

# Chapter 7

*A New Route to Diruthenium Oxo Complexes: Activation of $O_2$*

## 7.1 Abstract

Initial attempts to prepare a $Ru_2^{7+}$ terminal oxo compound were described previously in the thesis of Dr. Amanda Corcos. This chapter offers additional insight into the synthesis of such a reactive compound. First, the use of a soluble iodosylbenzene derivative, 2-(*tert*-butylsulfonyl)iodosylbenzene, facilitates a stoichiometric reaction with improved conversion compared to a suspension of iodosylbenzene. Second, changes to the ligand supporting the $Ru_2$ core are explored and alternative routes to Ru–O bond formation are presented. Third, the reactivity of $Ru_2^{5+}$ precursors with $O_2$ is presented as a route to generating $Ru_2$ oxo and hydroxo species under mild conditions.

## 7.2 Introduction

As discussed extensively in previous chapters, diruthenium oxo complexes have been invoked several times as reactive intermediates,[1-4] but there is no definitive characterization of these complexes. The Berry group has dedicated considerable effort to demonstrating the existence of these complexes, and the most extensive work is described in the dissertation of Dr. Amanda Corcos. To briefly summarize these efforts, $Ru_2(ap)_4X$, where X is a labile axial ligand such as $^-$OTf or $^-FBF_3$, were subject to O-atom transfer using either *m*CPBA (*meta*-chloroperoxybenzoic acid) or PhIO (iodosylbenzene) to replace the axial ligand with O and oxidize the complex by two electrons, resulting in a $Ru_2^{7+}$ terminal oxo complex. The products of these reactions were most

effectively characterized by mass spectrometry, showing the [$M^+$] mass envelope, and EPR spectroscopy, which features a signal consistent with an $S$ = 1/2 $Ru_2^{7+}$ complex. Unfortunately, *m*CPBA yields a mixture of products as determined by EPR. This is attributed to an acid/base equilibrium between the resulting *m*CBA and the oxo complex, giving a mixture of oxo and hydroxo $Ru_2^{7+}$ species. PhIO, on the other hand, only gives one EPR active product, but conversion is not complete. This is attributed to the insoluble nature of PhIO due to the polymeric I–O interaction.

My initial efforts focused on continuing this approach. Based on the selectivity of PhIO, the soluble, monomeric analog $^tBuSO_2PhIO$ (2-(*tert*-butylsulfonyl)iodosylbenzene) was employed.[5] However, complete conversion was never observed by EPR spectroscopy. Moreover, the Vis/NIR trace measured immediately after addition of the oxidant was nearly identical to previously reported triplet $Ru_2^{6+}$ species. This led to the investigation of the electronic structure of $Ru_2^{6+}$ complexes with weak σ-donor ligands (Chapter 4).

While $Ru_2(ap)_4Cl$ and other $Ru_2^{5+}$ chloro compounds are indefinitely air stable, the triflate and tetrafluoroborate complexes used a precursors to oxo complexes are actually air sensitive.[6] Particularly telling is the color change from green, indicative of $Ru_2^{5+}$ anilinopyridinate complexes, to red, which is indicative of the $Ru_2^{6+}$ analogs. Therefore, investigation of $Ru_2(ap)_4X$ (X = $^-OTf$, $^-FBF_3$) with both water and oxygen was pursued. Below, I describe evidence for the activation of $O_2$ by these $Ru_2^{5+}$ complexes to a putative $Ru_2^{6+}$ hydroxo complex. Critically, this is not the only $Ru_2$ complex capable of reacting directly with $O_2$, indicating that a wide variety of oxidative chemistry is possible with this class of compounds.

## 7.3 Methods

### *7.3.1 Physical Measurements*

Vis/NIR spectra were obtained using a StellarNet tungsten halogen source, a BLACK-Comet UV/Vis spectrometer, and a DWARF-Star NIR spectrometer equipped with a 10 mm path length dip probe tip. Elemental analysis was performed by Midwest Microlab, LLC in Indianapolis, IN, USA. $^{1}$H NMR spectra were recorded on 400 MHz and 500 MHz Bruker Avance III spectrometers. EPR data were acquired on a Bruker ELEXSYS E500 EPR spectrometer equipped with a Varian E102 microwave bridge. An Oxford Instruments ESR-900 continuous-flow helium cryostat and an Oxford Instruments 503S temperature controller were used to control the sample temperature. Measurement conditions were: 9.38 GHz, 4 G modulation amplitude, 2500 G center field, 5000 G sweep width, 20.48 ms time constant, 20.48 ms conversion time, and 10 K.

### *7.3.2 Synthetic Methods*

$^{*}$PhIO was prepared according to literature methods.[5, 7] NOTE: Preparing hypervalent iodine species can be hazardous. Use of acetic anhydride and hydrogen peroxide should be avoided due to the possible formation of diacetyl peroxide, which forms shock-sensitive crystals when not dissolved.[8] **1** ($Ru_2(ap)_4OTf$, ap = 2-anilinopyridinate) and **2** ($Ru_2(ap)_4FBF_3$) were prepared as described in the literature,[6] and **3** ($Ru_2(Meap)_4Cl$, Meap = 2-(4'-methylanilino)pyridinate) and **4** ($Ru_2(OMeap)_4Cl$, OMeap = 2-(4'-methoxyylanilino)pyridinate) were prepared as described earlier (Chapter 4). Oxidations performed with PhIO, *m*CPBA, and $^{*}$PhIO used $CH_2Cl_2$ that was distilled from $CaH_2$ but contained amylene as an inhibitor. We have recently switched to inhibitor-free $CH_2Cl_2$ (Fisher Scientific), which is expected to reduce complications with this chemistry.

*Synthesis of $Ru_2(Meap)_4OTf$ (**6**).* This compound was prepared in an analogous manner to **1**, affording a bright green solid in 64-72% yield. Upon dissolution, the product rapidly discolors in air.

*Synthesis of $[Ru_2(OMeap)_4OTf][OTf]$ (**7**).* In a glovebox, a 50 mL Schlenk flask was charged with $Ru_2(OMeap)_4Cl$ (104 mg, 101 μmol) and AgOTf (51.7 mg, 201 μmol, 2.00 eq.). 25 mL of $CH_2Cl_2$ (inhibitor-free, distilled from $CaH_2$, stored over 3 Å molecular sieves under $N_2$ and filtered before use) was added, and the solution immediate became a dark blue. The reaction mixture was stirred for three days, over which time a white precipitate (AgCl) formed. The mixture was then filtered through a pad of celite, and extracted with an additional 75 mL $CH_2Cl_2$. The solvent was removed *in vacuo* to afford 122.8 mg (94%) of the title compound as a dark blue, air stable product. Preliminary $^1$H NMR ($CDCl_3$): 20.17 (1H), 9.57 (1H), 5.20 (2H), 2.78 (3H), 1.86 (2H), -2.35 (1H), -13.55 (1H). [$C_{50}H_{44}N_8F_6O_{10}Ru_2S_2$] Calcd C 46.30, H 3.42, N 8.64, found C 46.04, H 3.53, N 8.33.

Reactions with $^*$PhIO for EPR analysis: A Schlenk flask was charged with a 1.7 mM solution of **1** in $CH_2Cl_2$, which was prepared in a glovebox, and transferred to a Schlenk line, where it was cooled to –78 °C in a dry ice / acetone bath. 1.1 equivalents of a 14.7 mM solution of $^*$PhIO in $CH_2Cl_2$ was drawn into a gastight syringe in a glovebox before being taken to the flask and injected through a rubber septum. Aliquots were transferred to quartz EPR tubes via cannula and rapidly frozen in liquid nitrogen.

Reactions with $^*$PhIO for Vis/NIR analysis were performed as above with two differences: the reaction was performed at room temperature and the $Ru_2$ concentration was reduced to approximately 0.45 mM, suitable for measurement with a 10 mm path length.

Preparation of **1** + $O_2$ for single crystal X-ray analysis: in a glovebox, 20 mg of **1** was dissolved in a minimum quantity of $CH_2Cl_2$ in a Schlenk flask. The flask was removed from the glovebox and the solution sparged with $O_2$ (dried through a column of $CaSO_4$) for 30 minutes, during which time the solution changed from green to red. The solution was left to stand under $O_2$ overnight and was subsequently layered with dry pentane and left until small crystals grew. Due to the presence of unreacted **1**, definitive yield and characterization was not obtained.

Preparation of **1/2** + $O_2$ for $^1$H NMR spectral analysis. In a glovebox, a small quantity of **1** or **2** (~ 1 mg) was washed into a J. Young tube with $CD_2Cl_2$ (~ 500 µL, distilled from $CaH_2$). A balloon attached to a small segment of Tygon tubing was filled with $O_2$ and emptied 3x before being filled and pinched closed. The tubing was then connect to a glass J. Young adaptor and fixed to the top of the J. Young tube. the adaptor was loosened enough to allow a small amount of $O_2$ out to "burp" the system before the J. Young tube was opened. For **2**, ~ 1 minute of shaking the tube was sufficient for a color change from green to red. For **1**, no color change occurred after several minutes, so the tube and balloon system was left overnight. The following day, the solution had changed completely to red.

## 7.4 Results and Discussion

### *7.4.1 Selection of a more effective oxidant*

PhIO is a commonly employed O-atom source and two electron oxidant. However, the insolubility of the compound is often detrimental. The monomeric, soluble analog $^t$BuSO$_2$PhIO (hereafter $^*$PhIO) is therefore an excellent alternative for stoichiometrically sensitive studies.[5] While addition of a suspension of PhIO to a $CH_2Cl_2$ solution of $Ru_2(ap)_4OTf$ (**1**) did not result in

full conversion based on residual $S$ = 3/2 signal in the EPR spectrum, addition of a solution of $^{*}$PhIO to **1** shows complete consumption of **1** within two minutes. Unfortunately, the $S$ = 1/2 signal decays significantly within 30 minutes even at –78 °C (Figure 7.1). It is important to note that the line shape for the product of **1** with $^{*}$PhIO does not match the line shape reported by Dr. Corcos. Moreover, $Ru_2(ap)_4FBF_3$ (**2**) typically reacts much more quickly than **1** due to the more labile axial ligand. However, full consumption of **2** is not observed upon addition of $^{*}$PhIO.

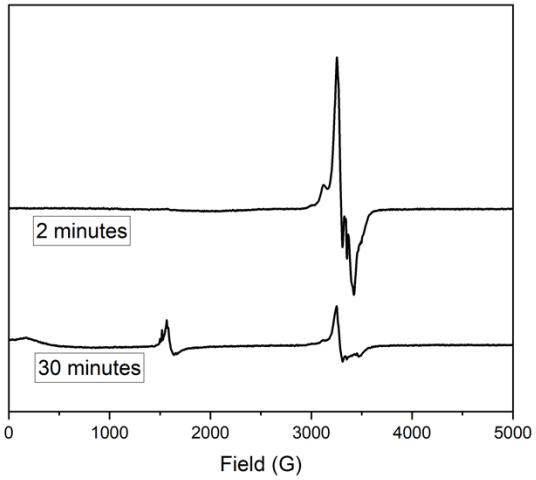


*Figure7.1. X-band EPR spectra for the reaction of **1** with $^{*}$PhIO in $CH_2Cl_2$. Due to the rate of reaction and decomposition, reproducing a spectrum with no signal at g = 4 (~1500 G) is difficult.*

The only other readily accessible spectroscopic technique for measuring these unstable reaction products is electronic absorption spectroscopy. When comparing Vis/NIR spectra of reaction mixtures that produce the above EPR signals, the Vis/NIR spectrum of the product is nearly identical to $Ru_2^{6+}$ anilinopyridinate complexes (Figure 7.2). There are no spectroscopic reports of complexes unambiguously described as $Ru_2^{7+}$. Thus, it is impossible to say whether a $Ru_2^{7+}$ oxo or hydroxo compound would have a similar electronic absorption spectrum to the $Ru_2^{6+}$

compounds previously reported. Therefore, determining the concentration of the $S = 1/2$ product(s) by EPR spin quantitation is a critical future step, as the signal may be due to a minor product.

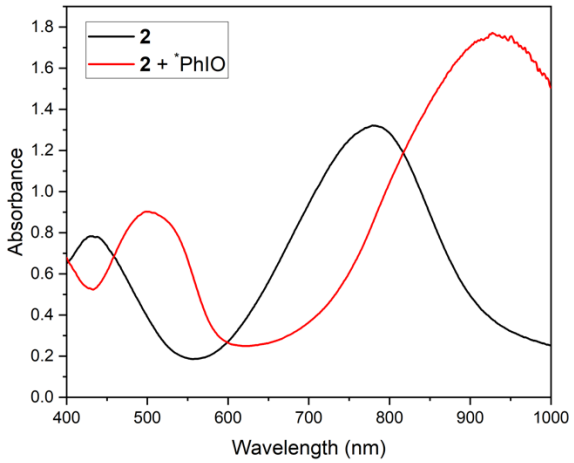


*Figure 7.2. Vis/NIR spectra of **2** and **2** + *PhIO in $CH_2Cl_2$. The latter is consistent with the spectra of $Ru_2^{6+}$ compounds reported earlier (Chapter 4).*

### *7.4.2 Optimization of the $Ru_2L_4$ core*

Due to the apparent instability of $Ru_2(ap)_4O^+$ based on the above data, it is worth considering alternative $Ru_2$ complexes and routes for generating the reactive oxo species. Stemming from work described in Chapter 4, there are two accessible and promising candidates for future study. Initial work with these $Ru_2$ systems is described, followed by proposals for future experiments.

$Ru_2(Meap)_4Cl$ (**3**) is a more electron-rich analog of $Ru_2(ap)_4Cl$ with otherwise similar properties. **3** undergoes metathesis with TlOTf to afford $Ru_2(Meap)_4OTf$ (**6**) under the same conditions used to prepare **1**. As with **1**, **6** is air stable as a solid, but solutions discolor rapidly when exposed to the atmosphere. As reported in Chapter 4, the $Ru_2^{5+/6+}$ redox couple for the corresponding chloro complexes is shifted 60 mV cathodically for **3** compared to $Ru_2(ap)_4Cl$. This

increased electron richness provided by the substituted ligand is expected to increase the stability of a highly oxidized oxo complex.

$Ru_2(OMeap)_4Cl$ (**4**) may also prove a fruitful starting material, though not in the same manner. While more electron rich than **3**, the insolubility of **4** prevents axial ligand metathesis with TlOTF. However, reaction with two equivalents of AgOTf produces the $Ru_2^{6+}$ complex $[Ru_2(OMeap)_4OTf][OTf]$ (**7**) in good yield. This dark blue salt is modestly soluble in $CH_2Cl_2$ and displays a $^1H$ NMR spectrum consistent with a triplet $Ru_2^{6+}$ electron configuration (Figure 7.3).

I propose that **3** and the corresponding $^-$OTf complex can serve as replacements for **1** in the direct method of using $^*$PhIO to achieve O-atom transfer and afford an $Ru_2^{7+}$ complex. Moreover, I propose **4** and the corresponding ditriflate salt as a starting material for a more stepwise synthesis of a $Ru_2$ oxo species. Axial ligand metathesis with a soluble hydroxide salt is expected to afford the $[Ru_2(OMeap)_4OH]^+$ cation. Critically, deprotonation would give a neutral $Ru_2^{6+}$ oxo. This would permit analysis of the acid/base equilibrium between oxo and hydroxo complexes, as well as providing a spectroscopic basis for studying both protonation and oxidation state. Separate one-electron oxidation would make accessible both the $[Ru_2(OMeap)_4OH]^{2+}$ dication and the $[Ru_2(OMeap)_4O]^+$ cation. Spectroscopic and structural characterization of these four complexes, as well as electrochemical analysis and pKa measurement, would allow for a square scheme to be constructed, giving insight into the modes of reactivity available for $Ru_2$ oxo compounds.

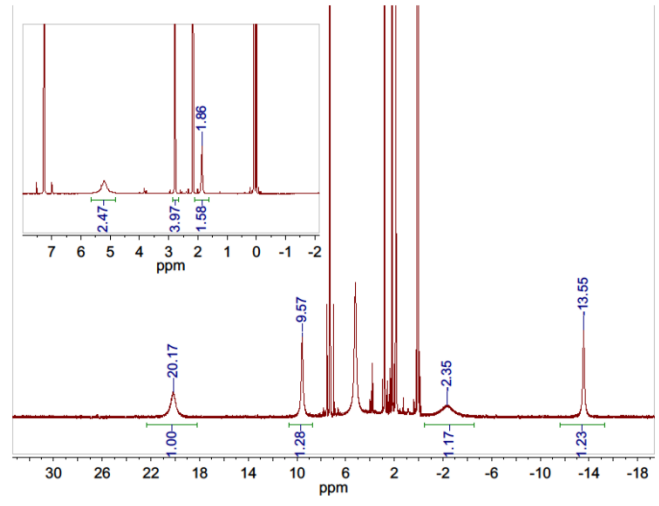


*Figure 7.3. $^1$H NMR spectrum of $[Ru_2(OMeap)_4OTf][OTf]$ in $CDCl_3$. While the peaks are sufficiently different from the chloride analog (Chapter 4), the paramagnetic shifts of the peaks at 20.17, 9.57, and 13.55 are consistent with an oxidation state of $Ru_2^{6+}$.*

### *7.4.3 Reactivity with $O_2$*

$Ru_2^{5+}$ complexes are generally regarded as stable to oxidation by $O_2$. However, the anilinopyridinate ligand is particularly electron donating, significantly decreasing the potential of the $Ru_2^{5+/6+}$ redox couple. While the parent $Ru_2(ap)_4Cl$, **5**, is indefinitely stable in air in both solid and solution forms, **1** changes color from green to red over several hours when dissolved. **2** changes color rapidly in solution when exposed to air, turning red in a matter of minutes, and it even changes color as a solid over the course of several hours. This indicates that the labile axial ligand facilitates reaction with either $H_2O$ or $O_2$. While one report describes $Ru_2(ap)_4(OH_2)^+$ as a red crystal, the X-ray crystallographic data do not provide unambiguous determination of the protonation of the Ru-bound O atom.[9] Based on the known spectroscopic features of $S = 1$ $Ru_2^{6+}$ compounds and the excess of oxidant used to prepare the compound, I propose that it is instead a hydroxo compound with a $Ru_2^{6+}$ oxidation state.

As further evidence for assignment of the red material as an $Ru_2^{6+}$ hydroxo complex, a solution of **1** in $CH_2Cl_2$ undergoes no color change upon addition of degassed $H_2O$. However, sparging an equivalent solution with dry $O_2$ prompts a rapid (~ 30 minutes) color change from green to red. Reaction of **2** in $CH_2Cl_2$ with an atmosphere of $O_2$ results in a much faster color change (~ 1 minute), consistent with a more labile axial ligand and an inner sphere electron transfer reaction. However, **2** ultimately affords a variety of unidentifiable side products, likely due to the relative instability of $^{-}BF_4$ compared to $^{-}OTf$. $^1H$ NMR spectral analysis of **1** + $O_2$ and **2** + $O_2$ in $CD_2Cl_2$ shows clear conversion to $S = 1$ $Ru_2^{6+}$ products, although **1** + $O_2$ still shows significant $Ru_2^{5+}$ signal despite complete color change. Full conversion of **1** requires several days under a static $O_2$ atmosphere following the initial mixing and color change.

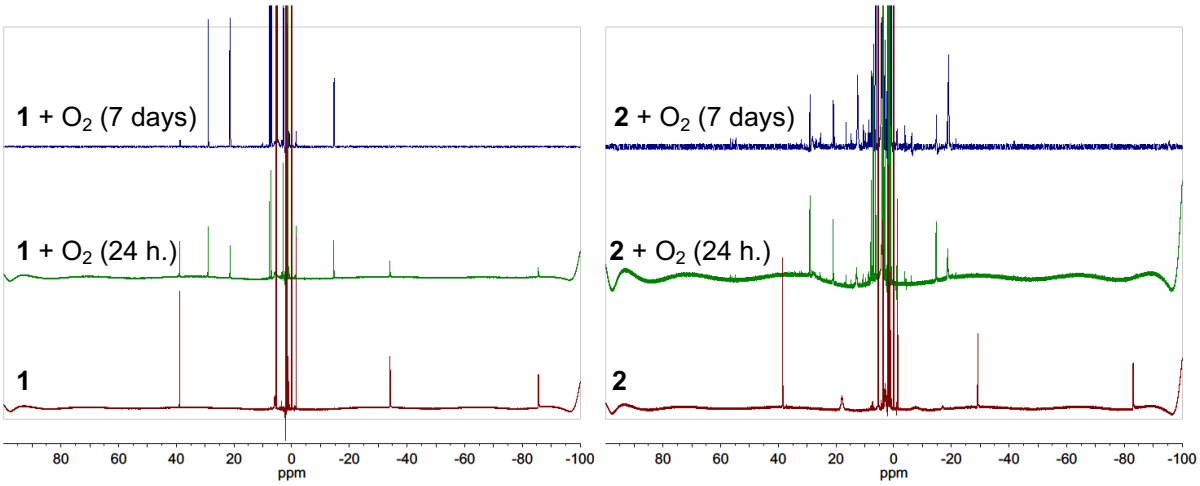


*Figure 7.4. $^1H$ NMR analysis of the reaction of **1** (left) and **2** (right) with $O_2$. Bottom spectra are the initial $Ru_2^{5+}$ complexes. Middle spectra were acquired ~ 1 day after exposure to a dry $O_2$ atmosphere. Top spectra were acquired after an additional week under a the static $O_2$ atmosphere.*

Finally, the product of **1** with $O_2$ was characterized structurally with single crystal X-ray diffraction. Unfortunately, the only crystals obtained were small and of poor quality. However, a solvable dataset was collected using a synchrotron light source. While the quality of the data and resulting model is poor, it is clear that the triflate ion is outer sphere and a light atom occupies the

axial site. Based on the assignment of $S = 1$ $Ru_2^{6+}$ by $^1$H NMR, we infer that the product is a hydroxo complex. However, high quality X-ray crystallographic data and corroborating experiments are needed to confirm this assignment.

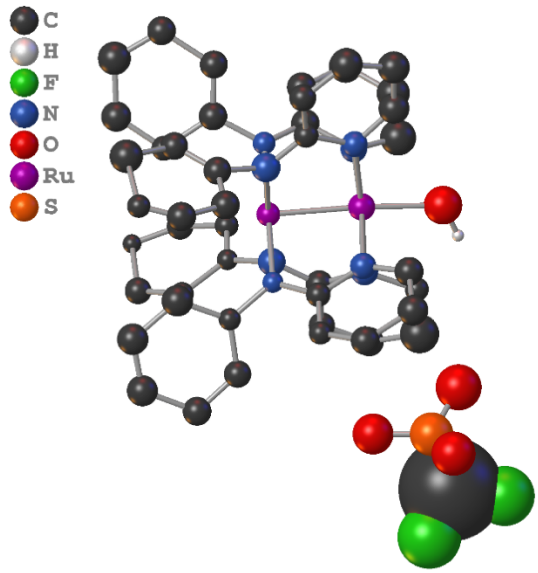


*Figure 7.5. Preliminary structure of the product of **1** with $O^2$. $P\bar{1}$ Unit cell dimensions (Å): a = 9.853(2); b = 14.776(3); 19.1919(4). α = 109.30(3)°; β = 104.64(3)°, γ = 95.47(3)°. Z = 2, Z' = 1, V = 2501.9(1) Å$^3$. Asymmetric unit contents: $C_{45}H_{37}F_3N_8O_4Ru_2S$.* $R_1$ *= 30.59%.* $wR_2$ *= 64.75%.*

If the end product of the reaction of **1** or **2** with $O_2$ is a hydroxo compound, the OH hydrogen is expected to be derived from solvent. If H atom transfer is a rate determining step, kinetic analysis of the reaction should show a kinetic isotope effect between $CH_2Cl_2$ and $CD_2Cl_2$. This experiment, as well as additional characterization of the reaction product, are important future steps to determine the nature of $O_2$ reactivity for $Ru_2$ compounds.

**7.5 References**

1. Corcos, A. R.; Pap, J. S.; Yang, T.; Berry, J. F., A Synthetic Oxygen Atom Transfer Photocycle from a Diruthenium Oxyanion Complex. *J. Am. Chem. Soc.* **2016,** *138* (31), 10032-10040.

2. Goberna-Ferrón, S.; Peña, B.; Soriano-López, J.; Carbó, J. J.; Zhao, H.; Poblet, J. M.; Dunbar, K. R.; Galán-Mascarós, J. R., A fast metal–metal bonded water oxidation catalyst. *J. Catal.* **2014,** *315*, 25-32.

3. Thompson, D. J.; Barker Paredes, J. E.; Villalobos, L.; Ciclosi, M.; Elsby, R. J.; Liu, B.; Fanwick, P. E.; Ren, T., Diruthenium(II,III) tetracarboxylates catalyzed $H_2O_2$ oxygenation of organic sulfides. *Inorg. Chim. Acta* **2015,** *424*, 150-155.

4. Villalobos, L.; Barker Paredes, J. E.; Cao, Z.; Ren, T., *tert*-Butyl Hydroperoxide Oxygenation of Organic Sulfides Catalyzed by Diruthenium(II,III) Tetracarboxylates. *Inorg. Chem.* **2013,** *52* (21), 12545-12552.

5. Macikenas, D.; Skrzypczak-Jankun, E.; Protasiewicz, J. D., A New Class of Iodonium Ylides Engineered as Soluble Primary Oxo and Nitrene Sources. *J. Am. Chem. Soc.* **2011,** *133* (11), 4151-4151.

6. Corcos, A. R.; Berry, J. F., Anilinopyridinate-supported $Ru_2^{x+}$ (x = 5 or 6) paddlewheel complexes with labile axial ligands. *Dalton Trans.* **2017,** *46* (17), 5532-5539.

7. Song, F.; Wang, C.; Falkowski, J. M.; Ma, L.; Lin, W., Isoreticular Chiral Metal−Organic Frameworks for Asymmetric Alkene Epoxidation: Tuning Catalytic Activity by Controlling Framework Catenation and Varying Open Channel Sizes. *J. Am. Chem. Soc.* **2010,** *132* (43), 15390-15398.

8. See correction notice for ref 5 as well as the report in Chemical and Engineering News: http://pubsapp.acs.org/cen/letters/89/8902letters.html? .

9. Gao, L.; Zhang, L.; Chen, Z., Tetrakis(2-anilinopyridinato)aquadiruthenium(II,III) hexafluoroantimonate diethyl ether solvate. *Acta Crys.* **2003,** *E59*, m419-m420.